THE EXPRESSION OF TWO-PORE DOMAIN POTASSIUM CHANNELS IN OSTEOBLASTIC CELLS

Thesis submitted in accordance with the requirements of the University of Liverpool for the degree of Doctor of Philosophy

by

Anne Wendy Gallagher

15th March 2010

Acknowledgements

Firstly, I would like to thank my supervisors Dr John Quayle and Prof Jim Gallagher for their help and support over the last 4 years, and for giving me the opportunity to undertake this research. I would like to express my appreciation for the help of Dr Tomoko Kamishima for her considerable assistance with the antibody work. The electrophysiology chapter was made possible with a great deal of patient practical and theoretical help from John & Tomoko. Thanks must also go to Ms Jane Dillon and Dr Peter Wilson for their continued help in the lab and some fantastic cups of tea! I would like to gratefully acknowledge the support my future husband Michael has given to me over the duration of my PhD. I have no doubt that I would have perpetually struggled without his words of encouragement and faith in me: this work is dedicated to him. Finally, thanks must go to William and Finlay who never failed to put a smile on my face when I needed it the most.

Table of Contents

Abbreviations

8-pCPT – 8-pCPT-2'-O-Me-cAMP
AA – Arachidonic acid
AC – Adenylyl cyclase
ALP – Alkaline phosphatase
ALS – Amyotropic lateral sclerosis
ANOVA – Analysis of variance
APS – Ammonium persulphate
ATP – Adenosine triphosphate
BK – Large-conductance K^+ channel
BL-1249 – ((5,6,7,8-tetrahydro-naphthalen-1-yl)-[2-(1H-tetrazol-5-yl)-phenyl]-amine)
BLAST – Basic local alignment search tool
BMPs – Bone morphogenic proteins
BSA – Bovine serum albumin
CCB – Calcium channel blocker
CCD – Cleidocranial dysplasia
CCE – Capacitative calcium entry
CRE – cAMP response element
CREB – cAMP response element binding protein
cDNA – Complementary DNA
CGRP – Calcitonin gene related peptide
DAG – Diacylglycerol
DAPI – 4',6-diamidino-2-phenylindole
DMEM – Dulbecco's modified Eagle's medium
DNA – Deoxyribonucleic acid
DNase – Deoxyribonuclease
dNTPs - Deoxynucleotide triphosphates
ECL – Electrochemiluminesence
EDTA – Ethylene diamine tetraacetic acid
EGTA – Ethylene glycol tetraacetic acid
Epac – Exchange protein activated by cAMP
ER – Oestrogen receptor
ERK – Extracellular signal-related kinase
GAPDH – Glyceraldehyde 3-phosphate dehydrogenase
GC – Glucocorticoid
GPCR – G-protein coupled receptor
GRK – G protein-coupled receptor kinase
GSK – Glycogen synthase kinase
HEPES – 4-(2-Hydroxyethyl)piperazine-1-ethanesulfonic acid
hERG – human ether-a-go-go-related gene
IC_{50} – Concentration that produces 50% inhibition of response
IP_3 – Inositol triphosphate
IV – Current-voltage
K_{2P} – Two-pore domain K^+ channel
KCB – K^+ channel blocker

KCO – K^+ channel opener

K_{ir} – Inward rectifier K^+ channel

KT5720 – (9S,10S,12S)-2,3,9,10,11,12-Hexahydro-10-hydroxy-9-methyl-1-oxo-9,12-epoxy-1H-diindolo[1,2,3-fg:3',2',1'-kl]pyrrolo[3,4-i][1,6]benzodiazocine-10-carboxylic acid, hexyl ester

K_v – Voltage gated K^+ channel

LPC – lipophosphtidylcholine

LRP5 – Low-density lipoprotein (LDL)-receptor-related protein 5

MAPK – Mitogen-activated protein kinase

MEM – Minimum essential medium

mRNA - Messenger ribonucleic acid

MSCs – Mesenchymal stem cells

NMDA – N-methyl-D-aspartate

NO – Nitric oxide

nVDR – Nuclear vitamin D receptor

OPG – Osteoprotegrin

P1NP – Ntelopeptide of type 1 collagen

PBS – Phosphate buffered saline

PCR – Polymerase chain reaction

PDEs – Phosphodiesterases

PDL – Peridontal ligament

PGE_2 – Prostaglandin E_2

PGI_2 – Prostacyclin

PIP_2 – Phophatidylinositol 4,5-biphosphate

PKA – Protein kinase A

PKC – Protein kinase C

PKG – Protein kinase G

PLC – Phospholipase C

PNPP – P-nitrophenyl phosphate

PTH – Parathyroid hormone

PTHrP – PTH-related protein

RANK – Receptor activator of NF-κB

RANKL – Receptor activator of NF-κB ligand

RLU – Relative light units

RNA – Ribonucleic acid

RT-PCR – Reverse transcriptase polymerase chain reaction

Runx2 – Runt-related transcription factor 2

S.E.M – Standard error of the mean

SERMs – Selective oestrogen receptor modulators

S.D – Standard deviation

SDS – Sodium dodecyl sulphate

SDS-PAGE – Sodium dodecyl sulphate polyacrylamide gel

siRNA – Small interfering RNA

Sox9 – Sex determining region Y-box 9

SRE – Serum response element

TALK – TWIK-related alkaline activated K^+ channel

TASK – TWIK-related Acid-sensitive K^+ channel

TBE – Tris/Borate/EDTA

TBST – Tris-Buffered Saline Tween-20

TEA – Tetraethylammonium

TEMED – Tetramethylethylenediamine

TGF-β – Transforming growth factor-β

THIK – Tandem pore domain Halothane Inhibited K^+ channel

TMD – Transmembrane domain

TRAAK – TWIK-related Arachidonic Acid-stimulated K^+ channel

TREK – TWIK-Related K^+ channel

TRESK – TWIK-Related Spinal cord K^+ channel

TRP – Transient receptor potential

TWIK – Tandem pore domain Weak Inward rectifier K^+ channel

VDCCs – Voltage-dependent Ca^{2+} channels

$\mathbf{V_m}$ – Membrane potential

Abstract

The aim of this project was to characterize the expression of members of the K_{2P} channel family in osteoblastic cells. Recent studies in the literature had indicated the presence of members of the TREK sub-family in human and rodent osteoblasts, but no examination of the other sub-families had been reported. Primers were designed against all functional members of the K_{2P} family and RT-PCR was used to screen cDNA from primary osteoblasts and a number of osteosarcoma cell lines. The results revealed the expression of TASK-1, -2, -3 & -5, TWIK-1 & -2, TRAAK and TREK-1 in human osteoblastic cells. Results that were particularly consistent and strong across the cells studied included those for TASK-2, TWIK-1 & 2, TRAAK and TREK-1. Immunocytochemistry confirmed the RT-PCR findings, with TREK-1 displaying one of the most convincing examples of localising to the plasma membrane. Western blotting with the same set of antibodies also confirmed protein expression of K_{2P} channels over a range of osteoblastic cells. The evidence for mRNA and protein expression provided a basis for the design of some functional assays. SaOS-2 reporter cells transfected with the c-fos promoter were used to screen the effects of a variety of K^+ and Ca^{2+} channel agents. PTH was used as a c-fos stimulant to compare with the effects of the channel agents on basal expression levels. The putative TREK-1 activators riluzole and BL-1249 produced significant changes to the PTH-induced rise in c-fos. Riluzole enhanced the PTH-induced stimulation ($P<0.001$) but had no effect on its own. Conversely, BL-1249 reduced both basal and PTH-induced c-fos expression ($P<0.001$ for PTH stimulated cells). The difference between these results was explained through the known effects of riluzole on other proteins; particularly the inhibition of phosphodiesterases. The generic KCBs Ba^{2+} and TEA failed to show any significant effects, whereas modulators of K_{ATP} channels (glibenclamide and pinacidil) produced limited changes in c-fos expression. Activation and inhibition of VDCCs did not consistently affect the expression of c-fos or the production of ALP. Investigation into the mechanism behind PTH stimulation appeared to support the involvement of PKA in the second messenger pathway. Electrophysiological observations revealed an increase in whole-cell current following the addition of BL-1249 to SaOS-2 cells ($P<0.05$ at +80mV). AA was used as a positive control and also increased whole cell current in the same cell type. TE-85 cells displayed broad variation in their response to BL-1249, and whole-cell currents were inhibited upon application of AA. Recordings of membrane potential were taken from SaOS-2 cells and revealed the resting membrane potential to be -22.9mV ($n=6$). A significant hyperpolarization was seen after exposure to BL-1249, which brought the membrane potential down to -31.6mV ($P<0.001$). The effects on membrane potential and whole-cell current were reversed following wash-out of BL-1249. This work has demonstrated the expression of various K_{2P} channels in several types of osteoblastic cell including primary human osteoblasts. If BL-1249 can be shown to solely activate TREK-1, then the results contained here suggest that the currents produced by this channel may play a role in normal osteoblast functions.

1.0 Introduction

1.1 Bone

1.1.1 Skeletal tissue

The mammalian skeleton exists to provide mechanical and metabolic support. The skeleton enables mechanical movement and gives protection to the major organs. It also provides a calcium store which can be utilised when serum Ca^{2+} levels drop. Bone tissue is able to release OH^- in order to balance low blood pH, and houses the process of haematopoiesis. Bone is a dynamic tissue that constantly undergoes remodelling based upon the input of various endocrine, autocrine and paracrine signals.

Two structural formations of bone exist; cortical and trabecular. Cortical bone is extremely compact and constitutes the majority of an individuals bone mass. It covers the outer part of bony structures, providing strength and protection. Trabecular bone is less dense, but contains most of the surface area within the skeleton. As such, it is often targeted when metabolic needs override mechanical function. It is found within the metaphyseal and epiphyseal regions of the long bones.

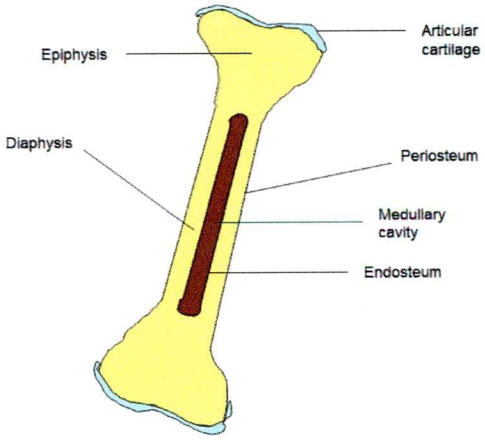

Figure 1.1. Cross-sectional diagram showing the gross anatomical features of a long bone.

Bone is covered by the periosteum, a layer of fibroblastic and osteogenic cells. The fibrous outermost surface is highly innervated and vascularised. The innermost part is the cambium layer which contains mesenchymal progenitors (Allen *et al.*, 2004). Breaks and fractures can damage the periosteum causing pain and bleeding. During embryonic development the bone collar derives from the periosteal bud to initiate vascularisation and osteogenesis.

Osteoblasts are the cells responsible for creating bone. They secrete an extracellular matrix which becomes mineralized. Osteoclasts are large cells derived from haematopoietic precursors that are able to resorb bone. They are easily recognisable due to their large size and multinucleated appearance. Osteoclasts possess a ruffled border in contact with the resorbing substrate. The clear zone forms an effective seal to allow acidification and secretion of lysosomal enzymes onto the resorbing surface. Bone formation and resorption are coupled in the process of bone remodelling. Remodelling by osteoblasts and osteoclasts is a tightly controlled process; an imbalance in bone remodelling can lead to conditions such as osteoporosis and osteopetrosis. The remodelling process starts with resorption and is followed by bone formation. The resorption period is brief, lasting around 3 weeks but formation takes several months to complete. Osteoblast stimulatory factors such as insulin-like growth factor and Transforming growth factor-β (TGF-β) are released through degradation of the matrix thereby helping to ensure that formation follows resorption (Heberden *et al.*, 1998).

Mineralization of the skeleton occurs through the deposition of hydroxyapatite crystals ($Ca_5(PO_4)_3OH$) onto a collagenous matrix, making bone a valuable reservoir of calcium ions. Bone resorption can be increased to facilitate homeostasis during bouts of low plasma Ca^{2+}. The two key hormones that control this process are parathyroid hormone (PTH) and $1,25(OH)_2D_3$. The thyroid hormone calcitonin is also involved in calcium regulation; it lowers plasma Ca^{2+} by inhibiting osteoclast activity and decreasing resorption of calcium and phosphate from the renal proximal tubule (Miller, 2008).

Despite the variety and prevalence of bone disorders, there are relatively few pharmacological compounds available for their treatment. Bisphosphonates are the most commonly used drugs, and are used to inhibit bone resorption in osteoporotic patients. The inhibition of resorption helps to restore bone mass homeostasis (Rodan, 1997). Despite its resorptive effects, PTH can also stimulate bone formation. Low-dose intermittent PTH administration in the form of teriparitide is an effective anabolic tool in the treatment of osteoporosis. Oestrogen replacement may be also used as a therapy for post-menopausal

osteoporosis as can selective oestrogen receptor modulators (SERMs) such as tamoxifen and raloxifene. The SERMs are thought to have a positive effect on bone formation due to an upregulation in TGF-β (Grainger and Metcalf, 1996). Other therapies in clinical use include strontium ranelate, dietary calcium supplementation and calcitonin administration (Miller, 2008). A recent and welcome addition to the field has been a monoclonal antibody known as denosumab, which targets the RANKL pathway (Lewiecki, 2008). This therapy has the potential to be effective in a number of bone disorders including osteoporosis and myeloma. Drugs in development for the treatment of osteoporosis include cathepsin K inhibitors and osteoprotegerin.

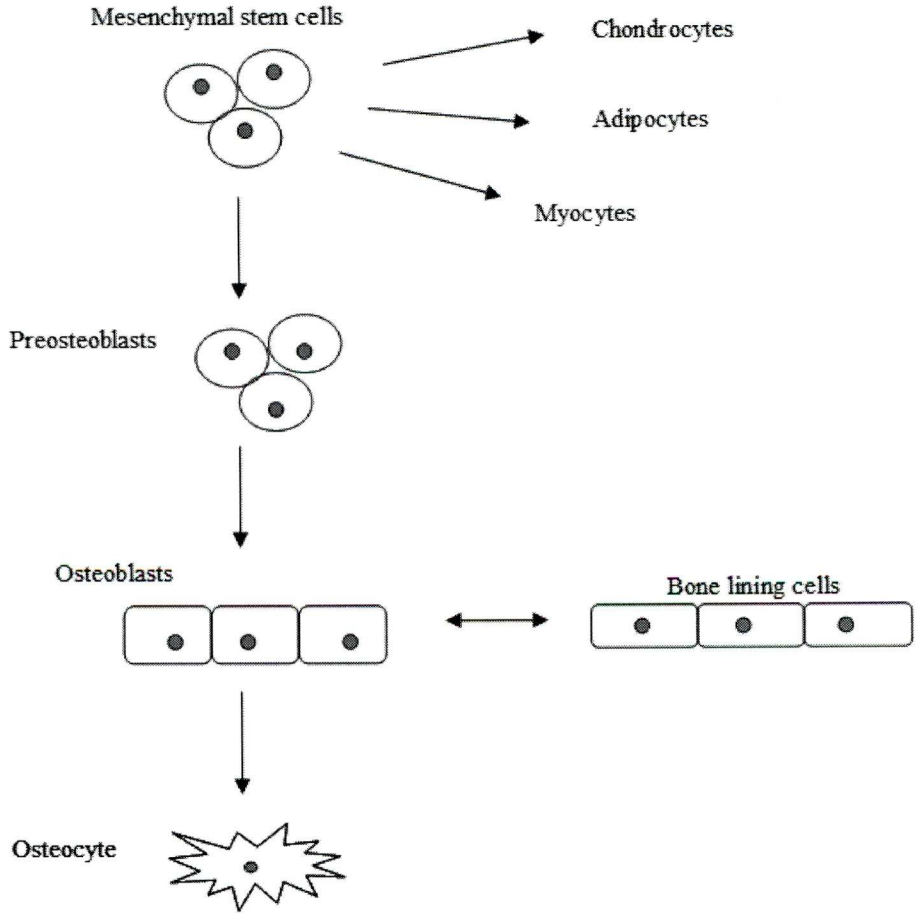

Figure 1.2. Osteoblasts, chondrocytes, myocytes and adipocytes are all derived from mesenchymal stem cells (MSCs). Bone lining cells are quiescent osteoblasts that can be reactivated by stimulatory factors such as PTH. Osteocytes are cells of the osteoblast lineage which become embedded in the bone matrix. These cells play an important role in mediating the response to mechanical loading.

1.1.2 Osteoblasts

Osteoblasts are primarily secretory cells that synthesize and deliver the organic components of bone matrix, which can be divided into collagenous and non-collagenous proteins. Collagen I is the predominant substrate for the mineralization process. Many of the various non-collagenous proteins facilitate the deposition of calcium and phosphate onto the collagen fibrils. Stimulatory factors such as bone morphogenic proteins (BMPs) encourage the osteoblasts multipotent precursors to differentiate along the osteoblastic pathway. The early cells produced by progression along this route are known as preosteoblasts. Osteoblast development can be divided into three sequential stages; proliferation, extracellular matrix maturation and matrix mineralization (Franceschi, 1999). Traditionally, osteoblast differentiation has been measured by the expression of certain marker proteins. Collagen I is an early stage marker secreted by pre-osteoblasts and osteoblasts. Collagen I binds to the $\alpha_2\beta_1$ integrin expressed on the osteoblast cell surface which encourages further differentiation (Xiao *et al.*, 1998, Damsky, 1999). Mid-stage marker proteins are numerous and include alkaline phosphatase (ALP), osteonectin and osteopontin (Dworetzky *et al.*, 1990, Sommer *et al.*, 1996). An osteoblast is considered mature by the time it begins to express osteocalcin. This event marks the transition from matrix maturation to mineralization. Osteoblasts can express the proteins osteoprotegerin (OPG) and receptor activator of NF-κB ligand (RANKL). RANKL encourages osteoclastic precursors to differentiate and fuse, forming cells capable of bone resorption. OPG acts as a decoy receptor for RANKL, and subsequently can inhibit osteoclast activity through reduced signalling at the receptor activator of NF-κB (RANK) (Boyce and Xing, 2008).

1.1.3 Genetics and the development of bone

There are two ways in which bone can be created: endochondral and intramembranous ossification. Endochondral bone formation occurs when a cartilage model recruits osteoblasts to convert it into bone. When the developing bone becomes vascularized, the chondrocytes undergo apoptosis and the bone structure becomes mineralized by osteoblasts. Intramembranous ossification does not require a cartilage intermediary and bone is formed in the first instance by osteoblasts. Most bones are formed through the process of endochondral ossification, but the clavicles and some cranial bones are created by intramembranous ossification.

Patterning of the skeleton must occur before the differentiation of tissue specific cell-types. Many genes are required to successfully complete this process and Sox-9 is one of the earliest to be expressed. It is required for the formation of mesenchymal condensations, the first stage in both methods of ossification (Lefebvre *et al.*, 2001). Cbfa1 or Runx2 is one of the most studied transcription factors in skeletal genetics. Cbfa1 coordinates the early and late stages of osteoblast and chondrocyte differentiation respectively (Karsenty, 2001 and Wagner and Karsenty, 2001, Ducy *et al.*, 2000b). In Cbfa1-deficient mice, chondrocytes fail to hypertrophy and osteoblast differentiation does not occur (Otto *et al.*, 1997). Heterozygous knockout mice appear to mimic the human disorder cleidocranial dysplasia (CCD). This condition results in hypoplastic clavicles and delayed fusion of some cranial sutures due to a defect in intramembranous ossification. Osterix acts downstream of Cbfa1 during osteoblast differentiation. Osterix -/- mice display a similar phenotype to the Cbfa1-null mice, although chondrocyte hypertrophy is enabled and consequently vascular invasion occurs. Osteoblast differentiation is completely abolished in both these mutants (Nakashima *et al.*, 2002). Although the use of mouse models can present difficulties due to species variation, the genes controlling skeletal development are extremely conserved (Karsenty, 2003). This fortuitous detail has resulted in a huge advance in our understanding of bone biology over the two decades.

1.1.4 Mechanical stimulation

Mechanical force has a well-documented anabolic effect on bone. In support of this observation, bone unloading which may occur during periods of immobility has a catabolic effect on bone mass. Mechanical strain is transferred into shear stress in the extracellular fluid surrounding bone matrix. Osteocytes embedded in the matrix are perfectly placed to respond to these variations in shear stress. Mechanical stimulation results in nitric oxide (NO) and prostaglandin E_2 (PGE_2) release from these cells (Nomura and Takano-Yamamoto, 2000). NO release inhibits the activity of osteoclasts (Mancini *et al.*, 1998) but encourages the differentiation of osteoblasts (Vezeridis *et al.*, 2006).

1.1.5 Wnt Signalling

Wnts are a family of around 20 proteins secreted at various stages of development that have a potent anabolic effect on bone tissue. Their expression promotes osteoblast differentiation, proliferation and mineralization and also inhibits osteoblast and osteocyte apoptosis. The anabolic effects of Wnts on bone are due to their ability to stabilize the intracellular protein β-catenin. Phosphorylation of β-catenin by glycogen synthase kinase 3 (GSK3), results in its proteosomal degradation. Unphosphorylated β-catenin translocates to the nucleus and activates gene transcription (Novak and Dedhar, 1999). This is commonly referred to as the canonical pathway. LRP5 forms a complex with the Frizzled G-protein coupled receptor (GPCR) which when activated by Wnt binding inhibits GSK3 activity. Mutations in the LRP5 gene can result in loss or gain of function and therefore produce either high or low bone mass phenotypes (Balemans and Van Hul, 2007). Canonical Wnt signalling is tightly controlled by several inhibitory factors, including Dickkopf-1 (Dkk1), sclerostin (SOST), WIF-1 and sFRP (Krishnan *et al.*, 2006). Wnt proteins are upregulated during the early stages of fracture repair (Zhong *et al.*, 2006). The canonical Wnt signalling pathway represents an exciting potential target for pharmacological interventions in bone disease.

1.2 Hormonal modulation of bone

1.2.1 Parathyroid hormone

PTH is secreted by the parathyroid glands in response to low serum Ca^{2+}. PTH is 84 amino acids in length, although amino acids 1-34 are sufficient to evoke most of its biological activity. The effects of parathyroid hormone on bone can often be difficult to review due to its wide ranging influence over the remodelling process. Fundamentally, PTH can stimulate bone formation and resorption but both of these effects are somewhat dose-dependent; making comparisons between studies awkward. Given the hormones' role in calcium homeostasis it would seem that high levels of PTH or continuous administration will result in net resorption so as to release Ca^{2+}. Lower concentrations of PTH or intermittent administration appear to support bone formation. At high doses PTH inhibits the proliferation of osteoblastic cells, but at low doses can stimulate their proliferation (Partridge *et al.*, 1985, MacDonald *et al.*, 1986).

The effects of continuous PTH on the skeleton were first observed in patients with hyperparathyroidism. These patients often suffer from osteitis fibrosa, symptoms of which include osteomalacia, peritrabecular fibrosis and increased osteoclastic resorption (Lotinun *et al.*, 2002). The anabolic effect of intermittent PTH *in vivo* is largely due to the activation of quiescent bone lining cells rather than an increase in osteoblastic progenitors (Dobnig and Turner, 1995). Stimulation of osteoblasts by PTH increases expression of RANKL and decreases expression of OPG; encouraging osteoclastogenesis and consequently an increase in bone resorption. (Huang *et al.*, 2004). PTH can potentiate the Ca^{2+} response induced by nucleotide binding to P2 receptors (Buckley *et al.*, 2001).

Parathyroid hormone related peptide (PTHrP) has a similar biological role to PTH. It has been shown to be important in early bone development and is involved in hypercalcemia of malignancy. PTH can induce rapid up-regulation of PTHrP mRNA in osteoblasts (Walsh *et al.*, 1997). PTH and PTHrP share a GPCR known as PTHR1. PTHR1 has been reported to couple both $G\alpha_s$ and $G\alpha_q$. This results in a dual signal transduction pathway leading to cAMP formation and/or release of Ca^{2+} from intracellular stores (Abou-Samra *et al.*, 1992). The

cAMP signalling pathway is induced following $G\alpha_s$ stimulation of adenylyl cyclase (AC) and results in the phosphorylation of proteins and transcription factors by PKA. $G\alpha_q$ activates phospholipase C (PLC) which hydrolyses PIP_2 to produce IP_3 and DAG. IP_3 mediates store-operated Ca^{2+} release from the endoplasmic reticulum while DAG activates PKC.

The investigation into downstream signalling occurring from PTHR1 in osteoblasts is contentious. In the rat osteoblast cell line UMR-106, c-fos induction was reported to be mediated mainly by PKC (Kano *et al.*, 1994a) but the same group suggest PKA is responsible for the positive effects of PTH on ALP expression (Kano *et al.*, 1994b). Ca^{2+} and cAMP responses to PTH have been reported in UMR-106 cells (Reid *et al.*, 1987, Yamaguchi *et al.*, 1987). Bizzarri and Civitelli (1994) observed that PTH induced rises in $[Ca^{2+}]_i$ were cell cycle dependent in UMR-106 cells. Boland *et al*, (1986) failed to find any changes in $[Ca^{2+}]_i$ after PTH administration to various osteoblastic cells. PTH results in cAMP generation in the SaOS-2 cell line (Rodan *et al.*, 1987). PKA was shown to be almost solely responsible for c-fos induction in SaOS-2 cells (Evans *et al.*, 1996). Few genes have been shown to be regulated via PKC activation in osteoblasts (Qin *et al.*, 2004) and AC activity is necessary for anabolic effects in vivo (Golzman, 1999). Both PKA and PKC stimulation by PTH can lead to an increase in MAPK activity (Cole, 1999).

Adding complexity to the role of PTH in bone and other tissues is the desensitization and down-regulation of PTHR1. As is common with receptors coupled to AC, PTHR1 undergoes homologous desensitization when challenged and subsequently rechallenged with PTH. This process is complex and appears to involve multiple pathways (Fukayama *et al.*, 1992). Activated PTHR1 is rapidly phosphorylated by G protein-coupled receptor kinases (GRKs), resulting in β-arrestin recruitment. This mediates the inactivation of the receptor through internalization. Both G protein and β-arrestin interaction with PTHR1 can stimulate extracellular signal-related kinase (ERK)-1 and -2 activity (Gesty-Palmer *et al.*, 2006).

PTH plays an important role in the response to mechanical loading. In thyroparathyroidectomized rats no osteogenic response is seen in loaded vertebrae. This effect was reversed by administration of PTH prior to mechanical stimulation (Chow *et al.*, 1998). The presence of PTH during bone loading appears to increase levels of c-fos mRNA in osteocytes. PTH was shown to inhibit eNOS activity produced by mechanical strain (Bakker *et al.*, 2003). These observations demonstrate the dual effects of PTH on increasing bone formation and resorption even in a mechanically stimulated bone environment.

1.2.2 Vitamin D_3

Vitamin D_3 is formed by the exposure of 7-dehydro-cholesterol to UV light. It must undergo hydroxylation to become metabolically active. Firstly, it is hydroxylated in the liver to give $25(OH)D_3$. The renal enzyme 1α-hydroxylase catalyses the final stage of the process to produce $1,25(OH)_2D_3$, also known as calcitriol. $1,25(OH)_2D_3$ is produced during bouts of hypocalcemia to increase calcium absorption from the small intestine and re-absorption from the kidneys (Lips, 2006). In preosteoblasts, $1,25(OH)_2D_3$ arrests differentiation and proliferation but in more mature osteoblasts it increases matrix protein expression (Mulkins *et al.*, 1983, Owen *et al.*, 1991, St-Arnaud, 2008, Beresford *et al.*, 1986). $1,25(OH)_2D_3$ is crucial for normal longitudinal bone growth as it is required by proliferating and hypertrophic chondrocytes at the epiphyseal growth plates. $1,25(OH)_2D_3$ exerts its genomic effects via the nVDR while ion channels and other membrane proteins mediate the rapid non-genomic effects. $1,25(OH)_2D_3$ administration produces wide-ranging effects on osteoblast ion channels. A study by Zanello and Norman (2003) shows the activation of three different types of ion channel in response to physiological levels of $1,25(OH)_2D_3$.

The effect of $1,25(OH)_2D_3$ on calcium channels in osteoblasts has been investigated by several groups. $1,25(OH)_2D_3$ increases the mean opening time of L-type Ca^{2+} channels and shifts the threshold of activation towards the resting potential (Caffrey and Farach-Carson 1989). The effect of $1,25(OH)_2D_3$ can be mimicked by the addition of a cAMP analog, indicating that it may play a role in channel phosphorylation (Zanello and Norman, 2003). $1,25(OH)_2D_3$ treatment of

primary osteoblasts results in an increase in Ca^{2+} entry and release from intracellular stores (Lieberherr, 1987, Civitelli *et al.*, 1990). Transcriptional changes eg. downregulation of Cav1.2 (α_{1C}) require the nuclear vitamin D receptor (nVDR) (Meszaros *et al.*, 1996). Liu *et al.*, (1999) demonstrated that the α_{1C} subunit was responsible for $1,25(OH)_2D_3$ and depolarization induced calcium influx in ROS 17/2.8 osteoblastic cells via ribozyme ablation. The downregulation of α_{1C} in response to $1,25(OH)_2D_3$ treatment may be a preventative measure against Ca^{2+} toxicity and subsequent cell damage (Bergh *et al.*, 2006).

1.2.3 Sex steroids and leptin

Circulation of sex steroids, particularly oestrogen, helps to maintain bone mass. Both osteoblasts and osteoclasts express receptors for oestrogen. Both types of oestrogen receptor (ERα and ERβ) are found in bone, indicating the importance of the hormone in bone homeostasis. Signalling through these receptors in osteoblasts causes secretion of OPG. The effect of oestrogen on osteoclasts is more complex, involving cytokine expression and the immune system (Zallone, 2006). Following the menopause oestrogen levels decline and this can trigger the onset of osteoporosis.

Leptin is a hormone produced by adipocytes. Leptin-deficient mice were observed to be obese, suffer from hypogonadism, hypercortisolism and increased bone mass. This hormonal interaction with bone is not direct – it requires leptin signalling in the hypothalamus (Ducy *et al.*, 2000a). Leptin acts on the sympathetic nervous system to induce noradrenaline signalling. Subsequent activation of β-adrenoceptors in bone results in an inhibition of bone formation (Harada and Rodan, 2003).

1.2.4 Non-hormonal influences on bone homeostasis

Glucocorticoid (GC) administration is known to result in rapid bone loss and osteoporosis (Alesci *et al.*, 2005). GCs appear to stabilise the cytosolic $1,25(OH)_2D_3$ receptor in bone, and so have a synergistic effect on resorption (Manolagas *et al.*, 1979). Another GC effect on bone is to repress Wnt signalling by increasing the expression of Dkk1 and sFRP1 (Ohnaka *et al.*, 2005). Low pH potentiates the activity of RANKL, $1,25(OH)_2D_3$, PTH and ATP/ADP on osteoclasts (Arnett, 2008). Osteoclast stimulation may require initial acid activation, followed by the addition of pro-resorptive agents. Acidosis reduces matrix mineralization by osteoblasts. Both these actions serve to increase available hydroxyl ions to provide a buffer for excess $[H^+]$.

1.3 Potassium Channels

1.3.1 Three families of K^+ channel

More than 70 genes encoding potassium channels have been cloned from humans. All K^+ channels contain a conserved motif in the pore-forming region, called the P domain. This is a repeated sequence of GXG which ultimately confers K^+ selectivity on these channels. They can be placed into one of three classes dependent upon their basic structure; those that have two, four or six transmembrane domains (TMD). Two and six TMD classes form tetramers of pore-forming subunits, while the four TMD class are likely to form dimers (Patel and Honoré, 2002). This is because four pore forming domains per functional unit are necessary to confer K^+ selectivity (Doyle *et al.*, 1998).

Table 1.3. The three families of potassium channel and their basic characteristics

Transmembrane domains	Channel type	Pore domains	Nomenclature
6	Voltage-gated	1	K_v
4	Two-pore domain	2	K_{2P}
2	Inward rectifier	1	K_{ir}

Potassium channels are required for cell proliferation and progression of the cell cycle, particularly into the G_1 phase (Pardo, 2004, Wonderlin and Strobl, 1996). They are also important in the maintenance of membrane potential. Opening of potassium channels leads to an increase in K^+ efflux from the cells which results in membrane hyperpolarisation. K^+ channel closure can lead to depolarization, showing that regulation of these channels is important in controlling excitability.

1.3.2 K_v channels

Voltage-gated K^+ channels are activated by depolarization, and help to restore resting membrane potential (Shieh *et al.*, 2000). This family includes KCNQ, *Shaker*-related, *ether-a-go-go*-related (hERG) and Ca^{2+}-activated K^+ channels. The positively charged residues contained within the S4 TMD are considered to be important in voltage-sensing (Shieh *et al.*, 2000). Conformational changes induced by alterations in membrane potential result in pore opening or closing.

1.3.3 K_{ir} channels

K_{ir} channels help to stabilise resting membrane potential and control K^+ transport. (Reimann and Ashcroft, 1999). 15 genes encoding the α subunit of the K_{ir} channel have been observed in human DNA (Kubo *et al.*, 2005). This family of channels can conduct K^+ in an inward direction at negative membrane potentials, due to a partial blockade in the internal part of the pore by Mg^{2+} and polyamines (Shieh *et al.*, 2000). K_{ATP} channels are K_{ir} channels that open when $[ATP]_i$ decreases and $[ADP]_i$ increases i.e. during metabolic stress (Amoroso *et al.*, 1990). All K_{ir} channels are modulated by PIP_2 and several are modulated by G-proteins.

1.3.4 K_{2P} Channels

Two-pore domain potassium channels are responsible for the background "leak" of K^+ ions first described by Hodgkin and Huxley (1952). They are able to modulate the membrane potential of cells by passing K^+ currents and therefore they help to regulate excitability. Initially thought to be present within the CNS, over the last few years many K_{2P} channels have also been observed in other areas of the body (Medhurst *et al.* 2001). K_{2P} channels are relatively insensitive to a number of broad spectrum KCBs and display little time- or voltage-dependence (Lesage, 2003).

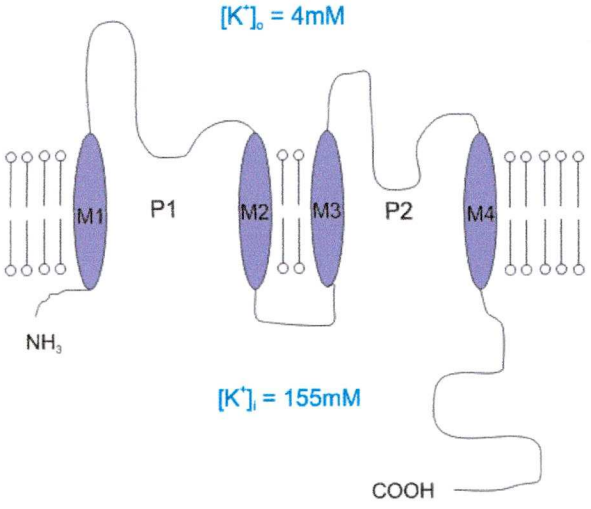

Figure 1.3. Diagram showing the membrane topology of a K_{2P} channel subunit, and the potassium ion gradient across a typical cell membrane. P1 represents the first pore-domain and P2 the second. M1-4 represent the TMDs.

K_{2P} channels contain two pore (P) domains and have 4 transmembrane domains (TMDs). This family of 15 channels can be subdivided into 6 subgroups.

1. Acid-sensitive outward rectifiers. TASK-1, -3 and 5
2. Weak inward rectifiers. TWIK-1, -2 and KCNK7 (non-functional)
3. Halothane-inhibited K_{2P} channels. THIK-1 and -2 (non-functional)
4. Alkaline-activated background K^+ channels. TASK-2, TALK-1 and -2
5. Calcium activated. TRESK
6. Lipid and thermosensitive, mechano-gated K^+ channels. TREK-1, -2 and TRAAK

Many K_{2P} channels have a phenylalanine (F) residue instead of a tyrosine (Y) in the GXG motif of the selectivity filter in the second pore domain. In homomeric channels this would result in a loss of K^+ selectivity. Interaction between the X in the GXG motif and a conserved aspartate (D) in the 2nd P domain immediately following the GXG motif, allows for variation in ion-selectivity and gating properties of K_{2P} channels (O'Connell *et al.*, 2002). TWIK-1 and -2 contain a GLG motif in the second pore domain (Chavez *et al.*, 1999). K_{2P} channels are conserved between M1 and M4, but the N- and C-termini show much more diversity (Shieh *et al.*, 2000).

The modulation of K_{2P} channels by GPCRs is reviewed by Mathie (2007). Activation of $G\alpha_q$ inhibits activity of TASK channels. The mechanism behind this effect has not been defined and is proposed to be direct, or via the breakdown of PIP_2. TRESK channels are enhanced by the action of $G\alpha_q$ on calcineurin. TREK channels exhibit the most complex relationship with GPCRs. Consistent with its actions on the TASK family $G\alpha_q$ and also $G\alpha_S$ inhibit TREK activity but $G\alpha_i$ activation results in channel stimulation.

Recent advances in the understanding of K_{2P} channel activity have been gained from the use of knockout mice, reviewed by Sabbadini and Yost (2009). So far, the most exciting results have been obtained by using TASK and TREK knockout animals. TREK-1 knockout mice require longer exposure to higher concentrations of volatile anaesthetics than their wild-type counterparts, to produce the same plane of anaesthesia (Heurteaux *et al.*, 2006). Neuroprotection is reduced in TREK-1 but not TRAAK knockout mice, in response to drug-induced seizures and ischemia (Heurteaux *et al.*, 2006). The removal of TASK channel genes produces physiological effects on the adrenal gland and in respiratory control (Heitzmann *et al.*, 2008, Mulkey *et al.*, 2007).

1.4 K_{2P} channel families

1.4.1 TASK

TASK channels are thought to be important in neuroprotection and chemoreception. TASK channels are expressed in brainstem respiratory neurons and rat arterial chemoreceptors (Bayliss *et al.*, 2001, Buckler *et al.*, 2000). TASK channels are thought to have a role in oxygen sensing in the carotid body (Buckler, 2007). TASK-1, -2, and -3 over-expression inhibited apoptosis in neuronal cells cultured in reduced serum and hypoxic conditions. TASK-3 over-expression conferred protective effects on oxygen and glucose deprived cultured rat hippocampal slices. This effect was potentiated by incubating slices with isoflurane. TASK-3 may be more effective at protecting cells from insults due to its relative insensitivity to low pH when compared with TASK-1 and -2 (Liu *et al.*, 2005). The pH sensing mechanism in TASK-1 and -3 involves a histidine (H) residue distal to the first pore domain. If this amino acid is mutated to aspartate (D) or neutrally charged asparagine (N) there is a reduction in pH sensitivity, but not total abolition of the response (O'Connell *et al.*, 2002). Dibasic sites on TASK-1 and -3 interact with coatamer proteins, specifically β-COP to retain channels in the endoplasmic reticulum. Escape from the ER is regulated by a phosphorylation site on the C-terminus of TASK-1 and -3. A phosphorylated channel binds 14-3-3β, which suppresses β-COP binding – allowing forward trafficking of channels to the plasma membrane. The protein p11 has been observed in some tissues to be involved in release of TASK-1 and -3 to the plasma membrane (Plant *et al.*, 2005).

1.4.2 TWIK

TWIK-1 was the first of the K_{2P} channels to be cloned. It is a weak inward-rectifier activated by PKC and inhibited by intracellular acidification (Lesage *et al.*, 1996a). TWIK-1 channels form dimers via a disulphide bridge in order to produce functional currents (Lesage *et al.*, 1996b). TWIK-1 activity is silenced by covalent modification with SUMO. If K274 (lysine) is mutated, TWIK-1 becomes active, as SUMO is unable to covalently modify the channel (Plant *et al.*, 2005). There is 53.8% sequence homology between TWIK-1 and -2 (Chavez

et al., 1999). Little information is available on TWIK-2, and to date the only papers characterising the electrophysiology of this channel are contradictory. Chavez *et al.* (1999) propose that TWIK-2 currents from transfected *Xenopus* oocytes are non-inactivating and display weak inward rectification. Channel activity was inhibited by intracellular acidification. Patel *et al.* (2000) report that TWIK-2 is an outwardly-rectifying, inactivating K_{2P} channel. This study also demonstrates that rat TWIK-2 currents are around 15 times larger than human TWIK-2 currents. Little is known about the biological role of TWIK-2 channels despite their seemingly broad expression in peripheral tissues (Medhurst *et al.*, 2001). KCNK7 is a member of the TWIK family, but no functional currents have been recorded from this channel. It is thought to be a silent subunit which may regulate the properties of other channels.

1.4.3 THIK

THIK-1 channels are widely expressed in rat tissue and are inhibited by halothane (Rajan *et al.*, 2001). THIK-2 displays no functional activity and its expression does not appear to influence THIK-1 currents, indicating that members of this family do not form heterodimers (Rajan *et al.*, 2001). THIK-1 is strongly inhibited by the halothane and weakly inhibited by extracellular acidification.

1.4.4 TALK

TALK-1 and TASK-2 are sensitive to pH in the range of 6 – 10 whereas TALK-2 is sensitive to more alkaline pH in the range of 7 – 10 (Kang and Kim, 2004). Lu *et al.*, (2007) propose that TALK-1 and -2 are modulated by the NO pathway, and therefore are involved in the response to metabolic ischaemia. TALK-1 and -2 are expressed in the exocrine pancreas and are activated by NO (Duprat *et al.*, 2004). TASK-2 is also a member of this sub-family and is activated by several general anaesthetics and is sensitive to both intracellular and extracellular pH, with channel inhibition seen upon intracellular acidification (Gray *et al.*, 2000). Changes in cell volume can also regulate the activity of this channel. TASK-2 channels are downregulated by chronic hypoxia. The downstream signalling for

this modulation occurs through Elk-1 binding to the promoter region (Brazier et al, 2005).

1.4.5 TRESK

TRESK channels are highly localised to the dorsal root ganglia of human spinal cord, and display low homology with other members of the K_{2P} channel family (Sano *et al.*, 2003). TRESK currents are outwardly-rectifying and are activated by anaesthetics, but the properties of this channel are subject to large inter-species variation (Keshavaprasad *et al.*, 2005). TRESK channels are highly sensitive to volatile anaesthetics and activate rapidly upon exposure to these agents (Kindler and Yost, 2005).

1.4.6 TREK

The TREK family consists of TREK-1 (KCNK2), TREK-2 (KCNK10) and TRAAK (KCNK4). They have the highest sequence identity among K_{2P} channels at 63 – 78%. Human TREK channels are highly expressed in both the central and peripheral nervous systems (Medhurst *et al.*, 2001). Of all the K_{2P} channels, TREK-1 has been particularly well studied with respect to regulatory aspects of its C-terminal domain. TREK channels are activated by membrane stretch and therefore changes in cell volume. Intracellular acidosis constitutively activates TREK channels, and heat stimulates the opening of TREK-1. Anionic polyunsaturated fatty acids, such as arachidonic acid are stimulators of TREK activity. Inhalational general anaesthetics such as halothane and isoflurane are also known to activate this family of channels. The carboxy terminus and the M1P1 loop are vital for the activation of TREK channels. TREK channel activity is negatively regulated by protein kinases. PKA-mediated phosphorylation of the carboxy terminal Ser333 results in the closure of TREK-1. PKC also has an inhibitory effect on TREK-1, although its target amino acid has yet to be determined. The actin cytoskeleton tonically represses the mechanosensitivity of TREK-1 (Lauritzen *et al.*, 2005). TREK channels are functionally similar to the *Aplysia* S-type K^+ channel. The S channel controls presynaptic facilitation of neurotransmitter release which is needed for behavioural sensitization. TREK

channels are expressed at high levels in the cerebral cortex and the hippocampus, which suggests they are important in higher brain processes in humans (Patel and Honoré 2002).

Membrane stretch reversibly opens the TREK channels. Increasing steps of negative pressure give increasingly larger currents in TREK-1 transfected COS cells. TRAAK displays faster desensitization than TREK-1. TREK-2 shows a high basal current but virtually no desensitization (Patel and Honoré 2002). TREK-1 is also opened by intracellular acidosis. This property is dependent on the negative charge of a glutamate (E) residue at position 306 in the proximal C-terminal domain (Honoré *et al.*, 2002). Desensitization aids signal plasticity, and helps protect cells from harmful overstimulation. A channel may desensitize via inactivation or adaptation. Inactivation is the process whereby the channel is prevented from activating whereas adaptation refers to an uncoupling of the stimulus from the channel (Patel *et al.*, 2001). AA is able to inhibit TREK-1 desensitization. When the brain becomes ischemic, neurons swell, and AA is released. Intracellular acidosis occurs – activating the TREK channels and reducing their desensitization. Resultant hyperpolarisation prevents a rise in $[Ca^{2+}]_i$ and therefore reduces excitotoxicity (Honoré *et al.*, 2006).

TRAAK currents are instantaneous and non-inactivating. Channel activity is potentiated by arachidonic acid and docosahexaenoate. This is a direct action and does not involve protein kinase C. When whole cells are subjected to negative pressures, TRAAK channels are opened in a dose-dependent fashion (Lesage *et al.*, 2000). In an inside-out patch configuration, TRAAK is opened by negative pressure, but positive pressure is able to produce activation of TRAAK in the outside-out patch configuration. This suggests TRAAK is activated by convex curvature of the plasma membrane (Maingret *et al.*, 1999). Cell depolarisation lowers the threshold for mechanical activation and also increases the maximal channel activity.

TREK-2 was the first K_{2P} channel to be identified in bone, specifically in the rat UMR-201-10B osteoblastic cell line (Chen *et al.,* 2005). This channel was shown to have a role in the induction of PTHrP in response to mechanical strain independent of calcium signalling. Other mechanosensitive channels are required, as siRNA knockdown of TREK-2 results in a 30% decrease in PTHrP expression. TREK-2 has also been identified in another peripheral secretory cell type: the pancreatic β cell line, MIN6 (Kang *et al.*, 2004).

1.5 Ion channels in bone

1.5.1 Expression of various ion channels in osteoblasts

Early osteoblastic cells have been shown to express both L- and T-type Ca^{2+} channels (Bergh *et al.*, 2003, Zahanich *et al.*, 2005). These are voltage-dependent Ca^{2+} channels (VDCCs) which allow Ca^{2+} influx at depolarized potentials. Their involvement in the response to $1,25(OH)D_3$ has been particularly well-documented (Caffrey and Farach-Carson 1989, Lieberherr, 1987, Civitelli *et al.*, 1990, Meszaros *et al.*, 1996 and Zanello and Norman, 2003). Many ion channels have mechanosensitive properties, which has drawn interest into the possibility that they may play a role in bone homeostasis. A study by Rawlinson *et al.* (1996) noted that gadolinium chloride, a traditionally used blocker of stretch-sensitive cation channels abolished loading induced PGI_2 (prostacyclin) and NO release and also reduced PGE_2 levels in rat ulnae. Nifedipine-sensitive channels were also shown to be important in the osteoblast response to strain (Rawlinson *et al.*, 1996). P2 receptors mediate nucleotide-induced signalling in many cell types. The family is divided into two subclasses; P2X are ligand-gated ion channels and P2Y are GPCRs. P2 receptors are abundant in bone cells and are important in localising systemic hormone responses (Gallagher, 2004). N-methyl-D-aspartate (NMDA) receptors are another ligand-gated ion channel present in osteoblasts (Gu *et al.*, 2002). Upon glutamate binding, these channels allow the influx Ca^{2+} and other cations. Recently, osteoblastic cells have been shown to express several members of the transient receptor potential (TRP) family of cation channels (Abed *et al.*, 2009). TRPs are a large family of channels which have the ability to form homo- or hetero-tetramers. Various TRP

channels have already been assigned roles in capacitative calcium entry (CCE), proliferation and mechanotransduction in murine and human osteosarcoma cells (Baldi *et al.*, 2003, Labelle *et al.*, 2007).

1.5.2 Potassium channels in bone

Two types of potassium currents were observed by Yellowley et al, (1998) in the MG-63 cell-line. One displayed characteristics of a K_{ir} channel, i.e. an inward current sensitive to barium, membrane voltage and external [K^+] and the other appeared to be produced by a K_{Ca} channel. Ca^{2+}-activated K^+ channels have also been observed in chick osteoblasts (Ravesloot *et al.*, 1990). Moreau *et al.* (1997) found that blockade of Ca^{2+}-activated and ATP-dependent K^+ channels potentiated $1,25(OH)_2D_3$-induced osteocalcin secretion in MG-63 cells. Large-conductance K^+ (BK) channels have also been reported to have effects on mineralization and proliferation in human osteoblasts (Henney *et al.*, 2009). Recordings from voltage-gated K^+ channels have been made from articular chondrocytes and several K^+ channels have been observed in murine osteocytes (Wilson *et al.*, 2004, Gu *et al.*, 2001). Osteoclasts have also been shown to express various types of K^+ channels (Komarova *et al.*, 2001, Ypey *et al.*, 1992, Weidema *et al.*, 1997).

1.5.3 K_{2P} channels in bone

Investigations into the expression of K_{2P} channels in skeletal tissue have been recent and brief. To date, only two publications have described the presence of these channels in bone. TREK-1 expression was reported in primary human osteoblasts and MG-63 cells (Hughes *et al.*, 2006). TREK-2 channels were found to be a key element in the production of PTHrP following mechanical loading of rat osteoblastic UMR-201-10b cells (Chen *et al.*, 2005). Chesnoy-Marchais and Fritsch (1994), used arachidonic acid to modulate ion channel currents in neonatal rat calvarial osteoblasts. One of the potassium currents they describe seems to fit the profile of a TREK channel, although the authors do not suggest a K_{2P} channel as a possible candidate, this may be due to the very limited knowledge regarding the K_{2P} channels at the time the paper was published.

TREK-1 expression has been observed in human tenocytes cultured from human patellar tendon samples. Recordings from the tenocytes showed an increase in the TREK-1 current when the cells were exposed to lipophosphtidylcholine (LPC), a distinguishing characteristic of TREK channels (Magra *et al.*, 2007). TREK-1 currents have also been reported in human periodontal ligament (PDL) fibroblasts (Saeki *et al.*, 2007).

1.6 Aims of the project

K_{2P} channels are a large and diverse family of ion channel that were initially found in the nervous system but are increasingly being observed in the periphery. As previously mentioned, K_{2P} channels are present in bone but their exact profile is unknown. The hypothesis behind this project is that K_{2P} channels are expressed in bone and their presence is a requirement for normal osteoblastic function. Osteoblasts are subject to various tightly controlled processes in an environment which is physiologically unique. Osteoblasts are conceivably exposed to mechanical strain, elevated extracellular Ca^{2+}, low pH and hypoxia and yet are still expected to fulfil their bone-forming duties. This project will determine whether channels other than TREK are present in osteoblasts by creating an expression profile of the functional members of the K_{2P} family in this cell type. Further experiments will attempt to characterize the channels shown to be present and propose an explanation of their existence in osteoblasts.

2.0 Methods

2.1 Tissue culture

2.1.1 Osteosarcoma and primary osteoblast cell culture

All bone-derived cells were cultured in Dulbecco's modified Eagle's medium (DMEM) (Sigma) supplemented with penicillin and streptomycin (Sigma), L-glutamine (Gibco) and 10% FCS (Biosera). SK-N-AS neuroblastoma cells were kindly provided by Dr Kate Haddley from the School of Biomedical Sciences, University of Liverpool. They were cultured in DMEM with high glucose (Sigma) and supplemented with 1% non-essential amino acids in minimal essential medium (MEM) (Gibco). 9cm Petri dishes were used for general stock culture and cells were incubated at 37°C with 5% CO_2. Cells were routinely passaged upon reaching confluence using 0.25% trypsin/EDTA (ethylenediaminetetraacetic acid) (Sigma) in a class II microbiological safety cabinet. A primary osteoblast sample named MA16 was obtained from Dr. B. Mwaura Kimani. Ethical committee approval was obtained for the use of bone tissue from patients undergoing primary knee replacement surgery in Wrightington Hospital from the Wrightington, Wigan and Leigh Local Research Ethics Committee (REC reference number 05/Q1410/13 Date: 21 March 2005). Only patients with osteoarthritis were included and informed consent was obtained prior to collection of the tissue. Patients with other arthropathies and those on steroids and diabetics were excluded. Bone shavings from the tibial and femoral cuts of a patient with osteoarthritis undergoing total knee replacement were collected and an explant culture was performed to grow the osteoblasts *in vitro*. The cells were frozen down in liquid nitrogen at passage 1 until they were required for use in experiments. MA16 cells were used to passage number eight before being discarded. Passage numbers of the human osteosarcoma cell lines MG-63, TE-85 and SaOS-2 were unrecorded.

2.2 Reverse transcriptase polymerase chain reaction (RT-PCR)

2.2.1 mRNA (Messenger ribonucleic acid) extraction

Medium was removed from a confluent petri dish of cells. Cells were rinsed with 1X phosphate buffered saline (PBS) and 0.5ml of TRI Reagent® (Sigma) was added over the surface of the dish. A cell scraper was used to collect the lysate, which was removed to an eppendorf tube and incubated at RT for 5 minutes. 100µl of chloroform was added to the lysate and the tube gently shaken. This was then left at RT for a further 15 minutes, before being spun at 12,000g for 15 minutes at 4°C (Megafuge 1.0R, Heraeus Instruments). This process causes the lysate to separate into three phases containing RNA (ribonucleic acid), DNA (deoxyribonucleic acid) and protein. The colourless phase at the top of the tube contains the RNA and so this was carefully removed to a fresh eppendorf. 0.25ml of isopropanol was added to the aqueous RNA. This mixture was briefly vortexed and incubated at RT for 10 minutes, then spun at 12,000g for 10 minutes at 4°C. This step precipitates the RNA into a pellet. Supernatant was discarded and 1ml 100% ethanol was added to the eppendorf. The pellet was gently loosened by inversion, and the tube spun at 10,000g for 5 minutes at 4°C. Supernatant was removed and the pellet was air dried for 5 -10 minutes, without being allowed to dry out completely. 30µl of molecular biology grade H_2O (Sigma) was added to the pellet which consequently dissolved.

2.2.2 DNAse (deoxyribonuclease) treatment

2µl DNAse I and 3µl of 10 x PCR buffer (both Qiagen) were added to the aqueous RNA. The tube was then incubated in a water bath for 1 hour at 37°C . The DNAse I was inactivated by heating the mixture to 70°C for 15 minutes, directly after incubation. 3µl of 3M sodium acetate, and 90µl of 100% ethanol were added to re-precipitate the RNA. The tube was centrifuged at 12,000g for 5 minutes at 4°C. Supernatant was removed and the pellet air dried and resuspended in 30µl H_2O (Sigma).

2.2.3 Reverse transcription of mRNA

The concentration of mRNA present in each sample was analysed using a GeneQuant II machine (Pharmacia Biotech). The 260/280 ratio was calculated for each sample, and any mRNA with a value lower than 1.8 was discarded. 5µg of total RNA was taken for each cDNA preparation. The appropriate volume of aqueous RNA was added to 1µl of oligo-dT primers (Qiagen) and the total volume made up to 12µl with H_2O. This was incubated in a Peltier Thermal Cycler, or PTC-200 (MJ Reaseach) for 10 minutes at 70°C. At this point two reactions were performed per RNA sample, to allow for a non-reverse transcribed (-RT) control. After incubation 4µl of 5 x first strand buffer, 2µl 0.1M DTT (both Invitrogen) and 1µl dNTPs (deoxynucleotide triphosphates) were added to the initial mix. Tubes were incubated for 2 minutes at 70°C before 1µl SuperScript® II (Invitrogen) reverse-transcriptase was added to the +RT tube and 1µl H_2O was added to the –RT control. After a brief flick to mix the sample, tubes were again placed in the PTC-200 and heated at 42°C for 50 minutes, then 70°C for 15 minutes. After the reaction was complete a test PCR was performed using Glyceraldehyde 3-phosphate dehydrogenase (GAPDH) primers and the cDNA was stored at -20°C.

2.2.4 PCR sample preparation and reaction conditions

PCR reaction mix

1µl 10 x PCR buffer (Qiagen)

8.1µl H_2O (Sigma)

0.2µl dNTPs (Amersham)

0.1µl 50µM forward primer (0.5µM final)

0.1µl 50µM reverse primer (0.5µM final)

0.1µl HotStarTaq (Qiagen)

0.4µl cDNA

Stock solutions were made up containing the 10 x buffer, water, dNTPs, primers and Taq polymerase. 9.6µl of this solution was added to a PCR tube (Sigma) followed by 0.4µl of cDNA. This allowed increased pipetting volume and therefore ensured a greater degree of accuracy. All reactions were performed in a PTC-200. Volumes were kept at 10µl total. When a fresh batch of cDNA was made, the first primers to be run through a PCR were always GAPDH to test the presence and quality of the cDNA on a gel.

Table 2.1. A description of the conditions used for RT-PCR reactions.

Step	Temperature (°C)	Time	Reaction phase
1	95	15 minutes	Required for activation of the DNA polymerase.
2	94	30 seconds	Denaturation phase.
3	60	30 seconds	Annealing phase.
4	72	40 seconds	Extension phase. Then back to step 2 (x 35)
5	72	5 minutes	Final extension.

2.2.5 Gel electrophoresis

PCR reactions were run out on 1.1% agarose gels consisting of 0.66g agarose (GIBCO BRL) added to 60mls of 1 x TBE (Tris/Borate/EDTA) buffer This solution was microwaved for approximately 50 seconds, until it began to boil. Once removed from the microwave and allowed to cool for around 5 minutes, 5µl of SYBR® Safe DNA gel stain (Invitrogen) was added and the gel was cast in a tray (Appligene). 2µl of type I gel-loading buffer (0.25% bromphenol blue, 0.25% xylene cyanol FF, 40% w/v sucrose made up in distilled water) was added to each 10µl completed PCR reaction to aid the addition of samples to the gel. The mixture was vortexed and briefly spun, then loaded into the gel. 2 lanes on each gel were loaded with 5µl of 50bp DirectLoad™ step ladder (Sigma) to enable the products to be accurately sized (See figure 2.1 below). The gel was run at 110V for approximately 50 minutes. The gel was allowed to cool in the tank for 10 minutes and was viewed using Safe Imager™ transilluminator (Invitrogen).

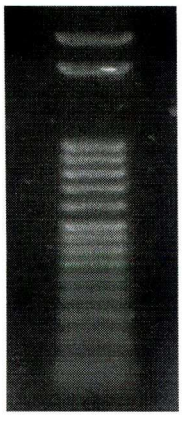

Figure 2.1. An image of DirectLoad™ step ladder taken from a 1.1% agarose gel. This product contains 17 bands ranging from 50 bp to 3000 bp.

2.2.6 Sequencing

A PCR reaction was performed with a larger than normal final volume of 50µl. The PCR product was extracted using QIAquick PCR purification kit (Qiagen) according to manufactured instructions. 1µl of the eluted 50µl final volume was taken to run on an agarose gel, to confirm the presence of the amplified cDNA. The concentration of the purified product was determined using the GeneQuant II, prior to sending the sample off to be sequenced. The samples were accompanied by 10µl of 10µM forward and reverse primers. The purified PCR product was sequenced with the chain-termination method, using the ABI 373 automated DNA sequencer (Applied Biosystems). The samples were processed by Mr Tadge Szestak in the School of Tropical Medicine, Liverpool University. Sequencing results were opened in Chromas 2.33 (Technelysium Pty Ltd). The sequence was then run through a nucleotide BLAST search (http://blast.ncbi.nlm.nih.gov/Blast.cgi) where a percentage value was obtained for the sequence similarity with the published mRNA.

2.2.7 Primer design and sequences

Primers were designed and then ordered through Oligo Perfect^{TM} Designer on the Invitrogen website. Primers all spanned intron/exon boundaries to distinguish any genomic amplification. Upon arrival, they were reconstituted using molecular biology grade H_2O (Sigma) to make a stock concentration of 50µM. T_m for all primers was set at 60°C during the design process and all reactions were run at this temperature.

Table 2.2. Primer sequences and predicted product sizes.

Primer set		Sequence	Product Size (bp)
GAPDH	fwd	5' TGCCTGCTCTTTGTCCTCAC 3'	182
	rev	3'CTGGTGTGGTTCTGGATCCT 5'	
TASK-1	fwd	5' CCTTCTACTTCGCCATCACC 3'	451
	rev	3' GTGAGGCCCGTAAGGATGTA 5'	
TASK-2	fwd	5' TGCCAAGAGACTAGGGCAGT 3'	503
	rev	3' TCTGCTTGATGAGGTCGTTG 5'	
TASK-3	fwd	5' CGGATCAAGGGGAAGTACAA 3'	310
	rev	3' GCATGCCACAGCACTTCTTA 5'	
TASK-5	fwd	5' TCCTGTGCACCCTGTGTTAC 3'	560
	rev	3' GGTGAGGGTGATGAAGCAGT 5'	
TWIK-1	fwd	5' GCCCTTGTCAGATGGAGGTA 3'	502
	rev	3' CACCTGATCCTCGTCCTTGT 5'	
TWIK-2	fwd	5' GTGACCGTCTGCTTTCTGGT 3'	393
	rev	3' GATGGAAGCGTAGTCGGTGT 5'	
THIK-1	fwd	5' TCATCGTGCTCTACCTGCTG 3'	596
	rev	3' GTAGCTCCAGCCTTCAATGG 5'	
THIK-2	fwd	5' CACCGTGGTGTCAACCATAG 3'	488
	rev	3'CGAGCAGGATGAAGAGGAAG 5'	
TALK-1	fwd	5' CAGACCCCAGCAAGCATTAT 3'	235
	rev	3' AAGTCCTGGGGTGTGACTTG 5'	
TALK-2	fwd	5' AGGGCTTCTACTTCGCCTTC 3'	344
	rev	3' GAGCAGAAGGTTCCAGATGC 5'	
TRESK	fwd	5' AGCTCGCTCTTTTTCTGCTG 3'	530
	rev	3' ATGTCCAACCTCTCCACCTG 5'	
TRAAK	fwd	5' CAGCGCCTTCTTTTTCTCAG 3'	447
	rev	3' AGGATCCAGAACCACACCAG 5'	
TREK-1	fwd	5' CCGTTAGGAAACACCTCCAA 3'	591
	rev	3' TGCTCTGAACTCTCCCACCT 5'	
TREK-2	fwd	5' TTGGAGACCAACTTGGAACC 3'	364
	rev	3' CGTAGCCAATCTCCGATCAT 5'	

2.3 Immunocytochemistry

2.3.1 Fixation, quenching and permeabilisation

Cells were counted using a haemocytometer (Incyto) and seeded at a concentration of approximately 1 x 10^5cells/ml. Cell suspension was placed onto 38mm glass coverslips (thickness 1) and cultured in 24-well plates overnight in medium containing 10% FCS. This allowed the cells time to adhere to the coverslips. The next morning medium was removed from the plate and the cells were fixed using freshly made 2% paraformaldehyde in PBS, pH 7.4. Following removal of the fixative after 10 minutes at room temperature, any unbound paraformaldehyde was quenched with the addition of 100mM glycine, pH 7.4. The glycine solution was left on for 10 minutes before being replaced by a permeabilisation solution of 0.1% Triton-X 100 in PBS, pH 7.4 for a further 10 minutes. This allowed the antibodies to gain access to intracellular epitopes.

2.3.2 Addition of primary and secondary antibodies

Cells were then washed three times in PBS and left at room temperature for a period of 10 minutes per wash. ~200µl of antibody buffer (2% v/v goat serum, 0.05% v/v Triton-X 100 and 1% w/v bovine serum albumin (BSA) made up in 1 x SSC, final pH was 7.2) was then added to each well and kept at room temperature for 30 minutes. After the non-specific binding sites had been blocked, the anti-rabbit primary antibody (Alomone Labs) could be added. Antibodies were reconstituted according to manufacturers instructions and resulted in final concentrations of 0.8mg/ml for TASK-1, TRAAK, TREK-1. TASK-2 gave a final concentration of 0.3mg/ml and TWIK-2 was used at 0.6mg/ml. All antibodies underwent a 1:200 dilution in antibody buffer prior to their addition to the cells. The coverslips were incubated with the antibody solution at 4°C overnight.

After the primary antibody was removed the cells were washed for 10 minutes, three times using antibody wash solution (0.05% v/v Triton-X 100, made up in 1x SSC and pH adjusted to 7.2). Alexa Fluor-488 goat anti-rabbit IgG secondary antibody (Invitrogen) was then added to the coverslips at a 1:500 dilution. The

plate was covered in foil, to prevent bleaching of the fluorophore. Cells were exposed to the secondary antibody for 1 hour at room temperature. After this the 3 x 10 minute washes were repeated with antibody wash solution. Prior to mounting, the coverslips were immersed twice in MilliQ water, covered in foil and air dried for 2-3 hours.

2.3.3 Mounting

Coverslips were mounted onto a labelled slide using VECTASHEILD® Hard-set mounting medium with 4',6-diamidino-2-phenylindole (DAPI) (Vector Labs). 20µl mounting medium was applied to each coverslip to give a final concentration of 1.5µg/ml DAPI. DAPI excites at 360nm and emits at about 460nm when bound to DNA. It is a useful tool in localising the staining of the primary/secondary antibody complex.

2.3.4 Control experiments

Antibody specificity was tested by using primary antibodies that had been pre-incubated for 1 hour at 37°C with the corresponding control peptide, at a protein ratio of 1:1. The control antigen/antibody complex was added to cells at the same dilution as primary antibody. Negative controls were produced by omitting the primary antibody, and incubating with secondary antibody as normal.

2.3.5 Confocal microscopy

Cells were imaged using the 40x oil immersion objective on a Leica confocal microscope. LCS software was used to operate the microscope and save images to disk. Alexa Fluor-488 absorbs light at 495nm and emits at 519nm which gives a green colour to the staining.

2.4 Western Blotting

2.4.1 Protein Extraction

Lysis buffer

1M Trizma HCl was made up and the pH adjusted to 8.8.

2ml of 1M Trizma HCl (20mM)

1.46g NaCl (250mM)

0.09g EDTA (3mM)

0.11g EGTA (3mM)

500µl Triton X 100 (0.5%)

The solution was made up to 100ml with distilled and de-ionised water. The pH was adjusted to 7.6 and the buffer was stored at 4°C. 10µl of protease inhibitors were added to every 1ml of lysis buffer immediately prior to the protein extraction.

Confluent petri dishes of cells were placed on ice and their culture medium removed. 500µl of lysis buffer with protease inhibitors was added to each dish and left over the ice for 5 minutes. A cell scraper was used to dislodge the cells from the dish which were then collected into a labelled 1.5ml eppendorf tube. The lysate was spun in a Megafuge 1.0R (Heraeus) pre-cooled to 4°C at 13,000rpm for 10 minutes. The supernatant was carefully removed to a fresh tube and an equal volume of Laemmli 2x sample buffer added (~500µl). The solution was gently mixed and placed in a heat block at 98 °C for 10 minutes. The protein extract was then stored at -20 °C.

2.4.2 SDS-PAGE (Sodium dodecyl sulphate-polyacrylamide gel)

A 10% resolving gel was made up using 3.3ml of 30% acrylamide, 2.5ml of resolving buffer, 100µl of 10% SDS, 3.97ml H_2O, 100µl of 10% ammonium persulfate (APS) and 5µl TEMED (tetramethylethylenediamine). The solution was vortexed and immediately loaded between 2 glass plates assembled in the casting tray. Enough room was left for the stacking gel to sit on top. Isopranolol was added to make a clean line between the two gels, and prevent the resolving gel from drying out. The 4% stacking gel consisted of, 1.3ml of 30% acrylamide,

2.5ml stacking buffer, 100µl of 10% SDS, 6ml H_2O, 100µl of 10% APS and 10µl TEMED. Isopranolol was poured off the resolving gel once set, which was then rinsed once with water. The stacking gel was then loaded in the remaining space between the two glass plates and the comb placed at the top. Once the stacking gel was set, the plates were transferred to a clamp which was placed into a gel tank. The 1x SDS running buffer (60g trizma base, 288g glycine and 20g SDS, made up into 2L water) was poured into the tank, making sure the inner cell was completely full and the electrode was fully immersed. The combs were removed and the Rainbow™ molecular weight markers (GE Healthcare) and protein extracts were loaded. A charge of 120V was applied for 1 hour.

2.4.3 Protein transfer

The nitrocellulose membranes and filter paper were cut to the size of the gel and the membranes soaked in H_2O then transfer buffer. The plates were removed from the tank and gently prised apart. The 4% stacking gel was removed using a scalpel and the 10% resolving gel was carefully removed from the plate. A nitrocellulose membrane was placed on top of the gel and smoothed out to ensure good contact. The gel and membrane were then sandwiched between two damp filter papers and gauze on either side and placed into a clamp. Once the clamp had been gently shut, it was put into the gel tank in the appropriate orientation for transfer. The transfer buffer was poured into the tank and ice packed around the outside, before 110V were applied for 1hr. Transfer buffer was made using, 4.5g trizma base (25mM), 21.6g glycine (192mM) and 300ml of 100% Methanol (20%). It was made up to 1.5L and covered to prevent evaporation of the methanol.

2.4.4 Addition of primary and secondary antibodies

Tris-Buffered Saline Tween-20 (TBST) was created using 2.42g Trizma base (20mM), 8.0g NaCl (127mM) and 1ml Tween-20 (0.1%) and made up to 1L using H_2O. The pH was then adjusted to 7.6. Once removed from the clamp, the membrane was placed in TBST and trimmed to size using the coloured ladders on either side of the protein extract as a guide. The membrane was then incubated in 1% or 5% skimmed milk (Marvel) TBST for a minimum of 1-2 hours prior to the addition of rabbit primary antibodies (Alomone Labs). Primary antibodies were used as a 1:200 dilution in milk TBST, and incubated with the membrane at 4 ^{o}C overnight. Three 10 minute washes were performed in TBST following the removal of the antibody. The goat anti-rabbit horseradish peroxidase-linked secondary antibody (Sigma) was used at a 1:5000 dilution in 1% milk TBST, and incubated at RT with the membrane for 90 minutes. Three 10 minute washes were repeated, and ECL reagent made up using equal parts of detection reagents 1 and 2. The ECL was kept in the dark until it was applied to the membrane for one minute. The ECL was then removed and the membrane wrapped in cling film. Small amounts of tape were used secure the covered membrane in a Hypercassette^{TM} (Amersham Biosciences).

2.4.5 Development

Once in a dark room, a safe light was used to apply Hyperfilm^{TM} ECL (Amersham Biosciences) to the front of the blot. The film was exposed in the Hypercassette^{TM} for 5 minutes and then a fresh film applied, this time for 10 minutes. The film was developed and then rinsed in water before being fixed and given a final rinse. Once dry the film could then be overlaid onto the membrane which was still secured in the Hypercassette^{TM}. The location of the molecular weight markers was then added to the film to aid the sizing of the bands.

2.5 C-fos reporter assay

2.5.1 Cell culture

Stably transfected SaOS-2 cells were cultured as normal in DMEM supplemented with penicillin, streptomycin, L-glutamine and 10% FCS. G-418 disulphate salt solution (Sigma) was added to this medium at a final concentration of 50μg/ml. This provides cells transfected with the c-fos reporter gene a survival advantage over wild-type cells. The plasmid used here is described in the paper by Bowler *et al.*, (1999), where various cells are transfected with different versions of the c-fos promoter. Briefly, the fragment containing the c-fos promoter (spanning positions -721 to -1, accession number M16287) linked to the luciferase gene was subcloned from pUC19fosluc1 (obtained from Dr L. Runkel) into pSV2neo, to create pfoslucneo1. The SaOS-2 reporter cells used in this Thesis were created by performing a transfection with pfoslucneo1 using Lipofectin (Invitrogen). Cells were frozen in liquid nitrogen by Ms Jane Dillon, and stored until they were required for use in experiments.

2.5.2 Assay technique

Cells were seeded into luminometric (white) 96-well plates and allowed to settle for 24hrs. Cells were then serum starved overnight in DMEM with penicillin, streptomycin and L-glutamine. The following morning, solutions were made up according to manufacturer's instructions (Sigma) and diluted in serum-free supplemented DMEM. After 4 hours exposure to the agents, medium was removed and the cells were washed with PBS. 5x cell culture lysis reagent (Promega) was diluted in MilliQ H_2O. 20μl of 1x lysis reagent was then added to each well and left at RT for 15 minutes before the plate was stored at -80°C overnight. Plates were fully defrosted at RT before being placed in the luminometer (LUCY 1, Labtech Int). Reagents were added to the plate by injection, one well at a time. RLU recordings were transferred to a PC using the Stingray program, and saved in Microsoft excel format.

2.6 Intracellular calcium imaging

2.6.1 Preparation and loading of cells

Cells were counted using a haemocytometer and seeded at a concentration of approximately 1 x 10^5cells/ml. The cell suspension was placed onto 22mm glass coverslips (thickness 1) and cultured in 12-well plates overnight in medium containing 10% FCS, to allow the cells time to adhere to the coverslips. The following morning medium was removed from the wells and cells were washed with HEPES incubation buffer. The wash solution was removed and replaced with 1ml HEPES loading buffer containing 2µl of 1mM Fura2-AM (Molecular Probes), 1µl sulphinpyrazone and 1µl pluronic F-127. Cells were then placed back into the incubator and left to load at 37°C for 20 minutes. HEPES (4-(2-Hydroxyethyl)piperazine-1-ethanesulfonic acid) buffer stock solution comprised of; HEPES (10mM), NaCl (121mM), KCl (4.7mM), KH_2PO_4 (1.2mM), 1M $CaCl_2$ (2mM), $NaHCO_3$ (5mM), $MgSO_4$ (1.2mM). Reagents were dissolved in sterile MilliQ water. HEPES incubation buffer was made using 100ml of HEPES buffer stock solution, stored at 4°C. The following reagents were added; 0.18g Glucose (10mM) and 0.2g BSA (0.2%). HEPES loading buffer was made by adding 0.18g BSA to 10ml of HEPES incubation buffer to bring the final BSA content to 2%.

2.6.2 Recording from cells

After loading was complete, the coverslip was carefully extracted from the plate using forceps and placed in the incubated chamber kept at 30°C above the oil immersion lens. 1ml HEPES incubation buffer was added to the chamber. The cells were brought into focus and a small group of around 5 cells were selected to record from using the imaging software, although results from individual cells could be displayed. Recording was initiated and 1 minute was allowed to record background Ca^{2+} levels before any compounds were added to the bath. Changes in fluorescence were monitored with a PTI Deltascan imaging system coupled to a Nikon Diaphot inverted microscope and Photon Science Ltd. (Robertsbridge, UK) Extended ISIS camera. The data were analyzed using PTI ImageMaster

software. Rises in $[Ca^{2+}]_i$ could be observed by calculating the ratio of emitted light from Fura-2 (measured at 520 nm), after excitation at 340 and 380 nm.

2.7 Alkaline phosphatase assay

2.7.1 Preparation and treatment of cells

SaOS-2 cells were seeded into 24-well plates and incubated at 37°C overnight. The following day, the medium on the cells was changed to include various treatments. The cells were incubated for a further 24 hours. The medium was removed from the well into pre-labelled 1.5ml eppendorf tubes, and spun at 13000rpm for 10 minutes (Galaxy 16DH mini microfuge, VWR) to remove any cell debris. The medium was carefully decanted into a fresh eppendorf tube and frozen at -20°C. The cell layer was briefly washed with PBS. 500µl of 1% TritonX 100 in PBS was added to each well. Plates were then stored at -80°C overnight. The cell layer underwent a freeze-thaw cycle before analysis.

2.7.2 Assay technique

The cell layer was defrosted at room temperature. The bottom of the wells was scraped with a pipette tip and then a 20µl sample was taken and placed into a clear 96-well plate. 2 PNPP tablets were added to 2ml diethanolamine substrate buffer (5x) (both Pierce) and 8ml distilled H_2O. 80µl of the resulting solution was added to the cell lysate by a multichannel pipette (Rainin). The reaction was left to run at room temperature for 15 minutes. The reaction was stopped by the addition of 100µl of 3M NaOH. The absorbance of the sample was then read in a spectrophotometer (Anthos Lucy 1, Labtech International) at a wavelength of 405nm.

2.8 Electrophysiology

2.8.1 Preparation of cells

Cells were trypsinised as in a routine passage. About 1ml of the cell suspension was added to a bijou containing 4ml of fresh medium with 10% FCS. Cells were best when left to recover for at least 2hrs after passage. Following the recovery period, 200µl of the cell suspension was added into the recording chamber. After the cells were added to the chamber they were left for 15mins to settle on the bottom before the bathing solution was circulated. This short delay was to try and prevent cells being washed away upon activation of the perfusion system.

2.8.2 Recording from cells

Single osteoblast cells in solution were placed in an experimental chamber through which control and treatment solutions were perfused. Seals were formed using a small amount of negative pressure in an extracellular solution containing (mM): 6 KCl, 134 NaCl, 1 MgCl2, 2 CaCl2, 10 HEPES, 10 glucose (pH adjusted to 7.4 with NaOH). The standard pipette (intracellular) solution contained (mM): 107 KCl, 33 KOH, 10 HEPES, 10 EGTA, 3 MgCl2, 3 Na2ATP, pH 7.2. Membrane current and voltage were amplified using an EPC-8 amplifier (List Instruments), digitised via a Digidata 1200 analogue to digital interface (Axon Instruments), and recorded on computer using pCLAMP8 software (Axon Instruments). Data were analysed using pCLAMP8 and SigmaPlot. Experiments were conducted at room temperature (18-22°C). A fresh glass microelectrode was used for each cell patch. Arachidonic acid (AA) and BL-1249 were obtained from Sigma Chemicals. AA was made up as 100mM stock solution in ethanol. Due to the short half-life of this compound in solution, the stock was prepared immediately before the addition into the recording chamber. BL-1249 was made up as a 10 mM stock solution in DMSO. Stock solutions were added to the extracellular solution to give the desired concentration.

After the cells were patched, a voltage-step protocol was performed which recorded current at voltages between -120mV and +100mV in 10mV increments.

Two control recording were taken from a single cell whilst cells were perfused in the extracellular solution described above. Then either 20μM AA or 10μM BL-1249 were perfused through the recording chamber and after three minutes, two further recordings were taken from the cell. Immediately after the second recording with the treatment, the recording chamber was washed out. After a further three minutes two washout recordings were taken to determine if the response was reversible. Vehicles were not added to the control recordings, due to experiments involving the different compounds being performed on the same day whilst using the same perfusion system i.e. there was one extracellular solution (containing 6mM K^+) which was used to perform all the initial recordings and the wash-out step. For recordings of membrane potential, current was clamped and voltage was recorded continuously over a period of approximately 10 minutes. Initially, the cell was perfused with the extracellular solution, and after a suitable baseline was recorded 10μM BL-1249 was circulated through the recording chamber. After several minutes, BL-1249 was washed out and the recovery of the membrane potential was observed.

2.9 Statistics

All statistics were produced using the InStat® 3.0 program (GraphPad Software, Inc). On samples which were not matched, a one-way analysis of variance (ANOVA) was performed on the data. On results obtained from matched groups, such as membrane potential recordings, a one-way ANOVA with repeated measures was used to compare the means. Data which was not normally distributed was analysed using a Kruskal-Wallis Test (non-parametric ANOVA) to test for significance (see Chapter 5).

3.0 Detection of K_{2P} Channel mRNA in Osteoblastic Cells Using RT-PCR

3.1 Introduction

The aim of the experiments performed in this chapter was to catalogue the expression of members of the K_{2P} channel family in osteoblastic cells using RT-PCR. A range of osteoblastic cell lines were chosen to try and build a comprehensive and reliable set of data. Included in the study were commonly used osteosarcoma cell lines (MG-63, TE-85 and SaOS-2), primary osteoblasts obtained from a routine joint replacement operation (MA16) and a neuronal cell line was utilised as a positive control (SK-N-AS). All of these cells were human in origin, meaning that the same set of primers could be used for all reverse-transcribed DNA. Previous studies have identified mRNA encoding members of the TREK K_{2P} channel family in rodent and human osteoblastic cells (Chen *et al.*, 2005, Hughes *et al.*, 2006). To date there have been no published investigations into the expression of other K_{2P} channel families in bone cells. It was felt necessary to initiate a thorough investigation into the expression profile of K_{2P} channels in osteoblasts.

PCR was chosen as a technique to screen for K_{2P} channels as it is a relatively quick and cost-efficient method and can be performed on multiple cell types. PCR amplifies a DNA sequence using oligonucleotide primers which correspond to the ends of the target sequence. A PCR cycle consists of three main stages. The first is carried out at 94°C to denature the double stranded DNA present in the reaction mix. The second step is the annealing of the primers to the target DNA sequence which occurs at approximately 55-60°C. Both these phases last for around 30 seconds. Finally, a slightly longer step allows extension or polymerisation of the primer-template complex. This cycle is repeated between 30 and 40 times to amplify the template cDNA (complementary DNA) to amounts detectable on an agarose gel with SYBR® safe. Primers were designed to be 20bp in length and have a GC content of 45-55%.

3.2 Methods

Primers were designed against functional human K_{2P} channels using the Oligo Perfect™ Designer on the Invitrogen website. The primers used in this study were designed to span intron/exon boundaries within the target gene so that amplification of genomic DNA would yield a separate band of a higher weight and therefore be clearly distinguishable from cDNA on a gel. After the design process, all primers were screened using a nucleotide basic local alignment search tool (BLAST) to confirm they targeted the mRNA for the appropriate K_{2P} channel, and that there was no cross-reaction with any other K_{2P} mRNA sequence. RNA was extracted from confluent cell cultures using TRI reagent® (Sigma) and treated with DNAse I (Qiagen) before being reverse transcribed. PCR reactions were run using HotStarTaq and its appropriate buffer (Qiagen). Each experiment included the sample mRNA to be tested, a negative reverse-transcribed control and a blank reaction containing no mRNA. This was to eliminate the possibility of genomic or environmental contamination giving a false positive result. Only the sample mRNA results are shown in Section 3.3, as no bands were observed in any of the negative controls or blanks. Reactions were run on 1.1% agarose gels in 1x TBE buffer. Included on the gel was a marker (50bp DirectLoad™ step ladder, Sigma) to enable the products to be accurately sized. Accurate sizing of the bands close to their expected weight was an early indicator that the primers were detecting K_{2P} mRNA. To confirm this was the case, PCR products were sequenced at the School of Tropical Medicine, Liverpool University. The resulting sequence was viewed in Chromas 2.33 (Technelysium Pty Ltd) and then entered into the nucleotide BLAST database (http://blast.ncbi.nlm.nih.gov/Blast.cgi) to compare with published mRNA sequences. A percentage value of similarity between the observed and the published sequences was recorded.

3.3 Results

Each row represents a separate experiment performed on mRNA which was extracted freshly each time another PCR screen began. The columns are headed by the cell type from which the mRNA was taken from.

3.3.1 TASK-1

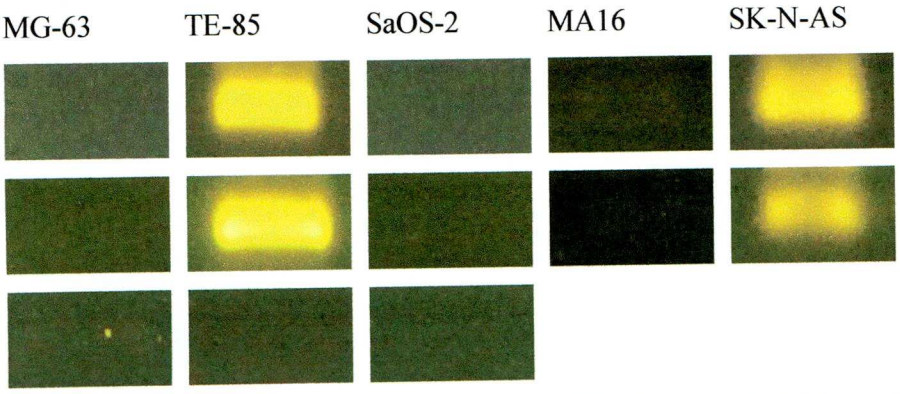

Figure 3.1. TASK-1 mRNA expression in MG-63, TE-85, MA16, SaOS-2 and SK-N-AS cells. The expected band size was 451bp.

Strongly positive bands can be clearly seen when TE-85 and SK-N-AS cDNA were run with primers for TASK-1. What appear to be very faint bands can be observed in the column for MA16 cells. In the third experiment using MG-63 cells a very faint band can just be seen. No positive signals were obtained for TASK-1 in SaOS-2 cells. A sequencing reaction was performed on the PCR product from the TE-85 cell line. The product was shown to have 100% sequence identity with TASK-1 mRNA when a BLAST was used to compare the product sequence with published sequences (http://blast.ncbi.nlm.nih.gov/Blast.cgi).

gi|11093519|gb|AF065163.1| Homo sapiens Kcnk3 channel mRNA, complete cds
Length=2590

GENE ID: 3777 KCNK3 | potassium channel, subfamily K, member 3 [Homo sapiens]
(Over 10 PubMed links)

Score = 821 bits (414), Expect = 0.0
Identities = 414/414 (100%), Gaps = 0/414 (0%)
Strand=Plus/Minus

```
Query  1    AGGCCACGTACTGCGGCTGCGTCTGCAGGGCCTGGTCCTTCTGCAGCGCCACGTAGTCGC  60
            ||||||||||||||||||||||||||||||||||||||||||||||||||||||||||||
Sbjct  792  AGGCCACGTACTGCGGCTGCGTCTGCAGGGCCTGGTCCTTCTGCAGCGCCACGTAGTCGC  733

Query  61   CGAAGCCGATGGTGGTGAGGGTGATGAAGCAGTAGTAGTAGGCCTGGAAGAAGGTCCAGT  120
            ||||||||||||||||||||||||||||||||||||||||||||||||||||||||||||
Sbjct  732  CGAAGCCGATGGTGGTGAGGGTGATGAAGCAGTAGTAGTAGGCCTGGAAGAAGGTCCAGT  673

Query  121  GCTCGTAGTGGGAGAAGGCGGCGGCGCCGATGCACAGCGTGCTGATGCACGAGAAGAAGC  180
            ||||||||||||||||||||||||||||||||||||||||||||||||||||||||||||
Sbjct  672  GCTCGTAGTGGGAGAAGGCGGCGGCGCCGATGCACAGCGTGCTGATGCACGAGAAGAAGC  613

Query  181  CGATGAGCACCATGTTGGCCATGGACACGTCGGCGCGCCGCATGCCCAGCCCCTTCTTGG  240
            ||||||||||||||||||||||||||||||||||||||||||||||||||||||||||||
Sbjct  612  CGATGAGCACCATGTTGGCCATGGACACGTCGGCGCGCCGCATGCCCAGCCCCTTCTTGG  553

Query  241  CGCGGTGCAGCAGGTACCTCACCAAGGTGTTGATGCGCTCGCCCAGGCTCTGGAACATGA  300
            ||||||||||||||||||||||||||||||||||||||||||||||||||||||||||||
Sbjct  552  CGCGGTGCAGCAGGTACCTCACCAAGGTGTTGATGCGCTCGCCCAGGCTCTGGAACATGA  493

Query  301  CGAGCGTGAGCGGGATGCCCAGCAGCGCGTAGAACATGCAGAACACCTTGCCGCCATCCG  360
            ||||||||||||||||||||||||||||||||||||||||||||||||||||||||||||
Sbjct  492  CGAGCGTGAGCGGGATGCCCAGCAGCGCGTAGAACATGCAGAACACCTTGCCGCCATCCG  433

Query  361  TGCTGGGTGCCGCGTGCCCGTAGCCGATGGTGGTGATGACGGTGATGGCGAAGT  414
            |||||||||||||||||||||||||||||||||||||||||||||||||||||
Sbjct  432  TGCTGGGTGCCGCGTGCCCGTAGCCGATGGTGGTGATGACGGTGATGGCGAAGT  379
```

Figure 3.2. TASK-1 PCR product sequence obtained using cDNA from TE-85 cells aligned with a published TASK-1 sequence using nucleotide BLAST (http://blast.ncbi.nlm.nih.gov/Blast.cgi).

3.3.2 TASK-2

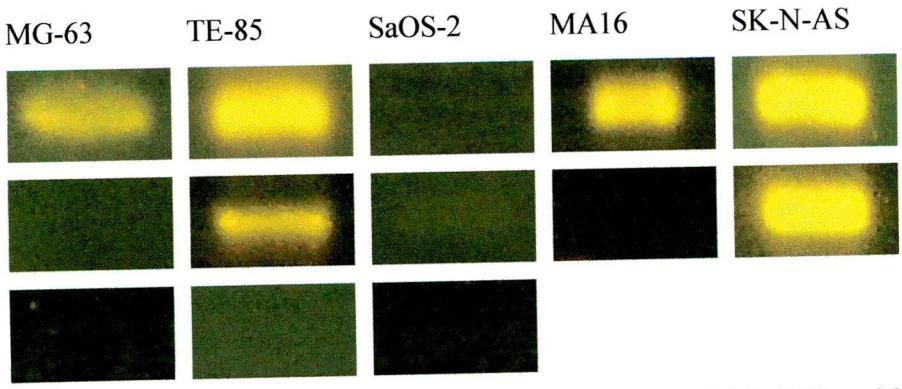

Figure 3.3. TASK-2 mRNA expression in MG-63, TE-85, MA16, SaOS-2 and SK-N-AS cells. The expected band size was 503bp.

TASK-2 expression was strong in TE-85 and SK-N-AS cells. Strong expression was seen in MA16 and MG-63 cells in one experiment, and was negative on

other occasions. A weak band can be observed in the second row for SaOS-2 cells, but this result was not repeated. TASK-2 was observed in all cell lines studied, although its expression was not seen consistently. A BLAST search on the PCR product from TE-85 cells was performed and revealed 98% homology between the product and published TASK-2 sequences.

```
gi|88999598|ref|NM_003740.3| Homo sapiens potassium channel, subfamily K, member
5 (KCNK5),
mRNA
Length=3800

 GENE ID: 8645 KCNK5 | potassium channel, subfamily K, member 5 [Homo sapiens]
(Over 10 PubMed links)

 Score =  831 bits (419),  Expect = 0.0
 Identities = 464/473 (98%), Gaps = 7/473 (1%)
 Strand=Plus/Plus

Query  1     AGAGGTGTGAGTCTGCGTGAAGGCACAGATCACGTTGGCACAGTCATCTTGCATCGTGTG  60
             |||||||||||||||| |||||| |||||||||  |||||||||||| |||||||||
Sbjct  815   AGAGGTGTGAGTCTGCG-GAAGGCGCAGATCACGT--GCACAGTCATCTT-CATCGTGTG  870

Query  61    GGGCGTGCCTAGTCCACCTGGTGATCCCACCCTTCGTATTGTCATGGTGACTGAGGGGTG  120
             |||||| ||||||||||||||||||||||||||||||  ||||||||||||||||||
Sbjct  871   GGGCGT-CCTAGTCCACCTGGTGATCCCACCCTTCGTATT--CATGGTGACTGAGGGGTG  927

Query  121   GAACTACATCGAGGGCCTCTACTACTCCTTCATCACCATCTCCACCATCGGCTTCGGTGA  180
             ||||||||||||||||||||||||||||||||||||||||||||||||||||||||||||
Sbjct  928   GAACTACATCGAGGGCCTCTACTACTCCTTCATCACCATCTCCACCATCGGCTTCGGTGA  987

Query  181   CTTTGTGGCCGGTGTGAACCCCAGCGCCAACTACCACGCCCTGTACCGCTACTTCGTGGA  240
             ||||||||||||||||||||||||||||||||||||||||||||||||||||||||||||
Sbjct  988   CTTTGTGGCCGGTGTGAACCCCAGCGCCAACTACCACGCCCTGTACCGCTACTTCGTGGA  1047

Query  241   GCTCTGGATCTACTTGGGGCTGGCCTGGCTGTCCCTTTTTGTCAACTGGAAGGTGAGCAT  300
             ||||||||||||||||||||||||||||||||||||||||||||||||||||||||||||
Sbjct  1048  GCTCTGGATCTACTTGGGGCTGGCCTGGCTGTCCCTTTTTGTCAACTGGAAGGTGAGCAT  1107

Query  301   GTTTGTGGAAGTCCACAAAGCCATTAAGAAGCGGCGGCGGCGACGGAAGGAGTCCTTTGA  360
             ||||||||||||||||||||||||||||||||||||||||||||||||||||||||||||
Sbjct  1108  GTTTGTGGAAGTCCACAAAGCCATTAAGAAGCGGCGGCGGCGACGGAAGGAGTCCTTTGA  1167

Query  361   GAGCTCCCCACACTCCCGGAAGGCCCTGCAGGTGAAGGGGAGCACAGCCTCCAATGACGT  420
             |||||||||||||||||||||||||||||||||||||||||||||||||||| |||||
Sbjct  1168  GAGCTCCCCACACTCCCGGAAGGCCCTGCAGGTGAAGGGGAGCACAGCCTCCAAGGACGT  1227

Query  421   CAACATCTTCAGCTTTCTTTCCAAGAAGGAAGAGACCTACAACGACCTCATCA  473
             |||||||||||||||||||||||||||||||||||||||||||||||||||||
Sbjct  1228  CAACATCTTCAGCTTTCTTTCCAAGAAGGAAGAGACCTACAACGACCTCATCA  1280
```

Figure 3.4. TASK-2 PCR product sequence obtained using cDNA from TE-85 cells aligned with a published TASK-2 sequence using nucleotide BLAST (http://blast.ncbi.nlm.nih.gov/Blast.cgi).

3.3.3 TASK-3

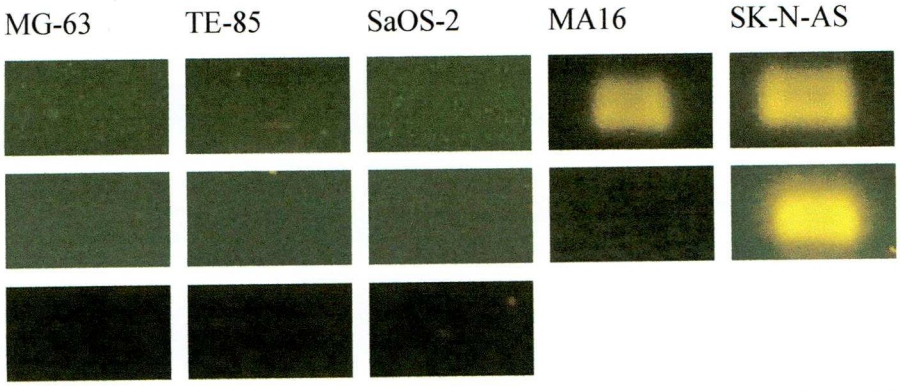

Figure 3.5. TASK-3 mRNA expression in MG-63, TE-85, MA16, SaOS-2 and SK-N-AS cells. The expected band size was 310bp.

SK-N-AS cells gave a strongly positive signal for TASK-3 on two occasions. The other positive signal came from MA16 cDNA. All bands obtained with TASK-3 primers appear to be very thick and in the two bands in the first row look like two bands very closely related in size.

3.3.4 TASK-5

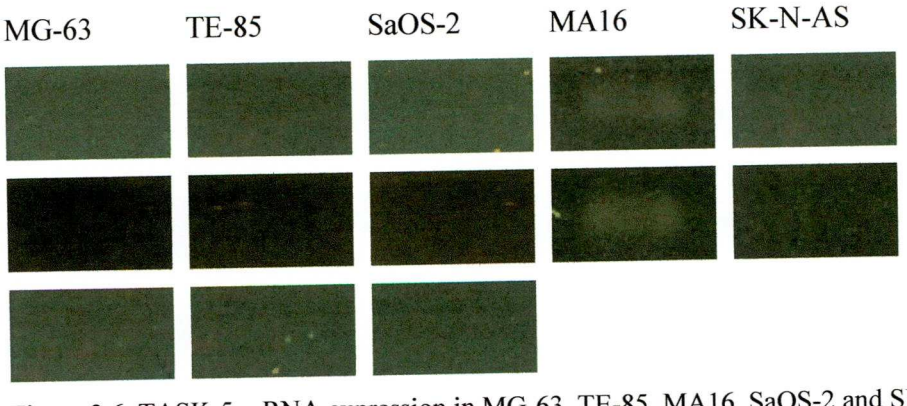

Figure 3.6. TASK-5 mRNA expression in MG-63, TE-85, MA16, SaOS-2 and SK-N-AS cells. The expected band size was 560bp.

TASK-5 signal was only faintly detected in cDNA from MA16 cells. The bands are faint but appeared on both occasions the experiment was run. No signal was observed in any of the other cell types.

3.3.5 TWIK-1

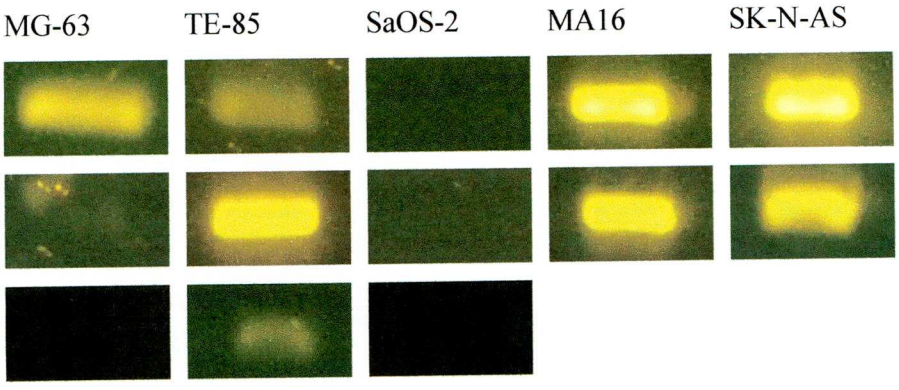

Figure 3.7. TWIK-1 mRNA expression in MG-63, TE-85, MA16, SaOS-2 and SK-N-AS cells. The expected band size was 502bp.

gi|15451900|ref|NM_002245.2| Homo sapiens potassium channel, subfamily K, member 1 (KCNK1),
mRNA
Length=1901

GENE ID: 3775 KCNK1 | potassium channel, subfamily K, member 1 [Homo sapiens]
(Over 10 PubMed links)

Score = 926 bits (467), Expect = 0.0
Identities = 467/467 (100%), Gaps = 0/467 (0%)
Strand=Plus/Plus

```
Query  1     TCTACTCCGTCATTGGCATTCCCTTCACCCTCCTGTTCCTGACGGCTGTGGTCCAGCGCA  60
             ||||||||||||||||||||||||||||||||||||||||||||||||||||||||||||
Sbjct  589   TCTACTCCGTCATTGGCATTCCCTTCACCCTCCTGTTCCTGACGGCTGTGGTCCAGCGCA  648

Query  61    TCACCGTGCACGTCACCCGCAGGCCGGTCCTCTACTTCCACATCCGCTGGGGCTTCTCCA  120
             ||||||||||||||||||||||||||||||||||||||||||||||||||||||||||||
Sbjct  649   TCACCGTGCACGTCACCCGCAGGCCGGTCCTCTACTTCCACATCCGCTGGGGCTTCTCCA  708

Query  121   AGCAGGTGGTGGCCATCGTCCATGCCGTGCTCCTTGGGTTTGTCACTGTGTCCTGCTTCT  180
             ||||||||||||||||||||||||||||||||||||||||||||||||||||||||||||
Sbjct  709   AGCAGGTGGTGGCCATCGTCCATGCCGTGCTCCTTGGGTTTGTCACTGTGTCCTGCTTCT  768

Query  181   TCTTCATCCCGGCCGCTGTCTTCTCAGTCCTGGAGGATGACTGGAACTTCCTGGAATCCT  240
             ||||||||||||||||||||||||||||||||||||||||||||||||||||||||||||
Sbjct  769   TCTTCATCCCGGCCGCTGTCTTCTCAGTCCTGGAGGATGACTGGAACTTCCTGGAATCCT  828

Query  241   TTTATTTTTGTTTTATTTCCCTGAGCACCATTGGCCTGGGGGGATTATGTGCCTGGGGAAG  300
             ||||||||||||||||||||||||||||||||||||||||||||||||||||||||||||
Sbjct  829   TTTATTTTTGTTTTATTTCCCTGAGCACCATTGGCCTGGGGGGATTATGTGCCTGGGGAAG  888

Query  301   GCTACAATCAAAAATTCAGAGAGCTCTATAAGATTGGGATCACGTGTTACCTGCTACTTG  360
             ||||||||||||||||||||||||||||||||||||||||||||||||||||||||||||
Sbjct  889   GCTACAATCAAAAATTCAGAGAGCTCTATAAGATTGGGATCACGTGTTACCTGCTACTTG  948

Query  361   GCCTTATTGCCATGTTGGTAGTTCTGGAAACCTTCTGTGAACTCCATGAGCTGAAAAAAT  420
             ||||||||||||||||||||||||||||||||||||||||||||||||||||||||||||
Sbjct  949   GCCTTATTGCCATGTTGGTAGTTCTGGAAACCTTCTGTGAACTCCATGAGCTGAAAAAAT  1008

Query  421   TCAGAAAAATGTTCTATGTGAAGAAGGACAAGGACGAGGATCAGGTG  467
             |||||||||||||||||||||||||||||||||||||||||||||||
Sbjct  1009  TCAGAAAAATGTTCTATGTGAAGAAGGACAAGGACGAGGATCAGGTG  1055
```

Figure 3.8. TWIK-1 PCR product sequence obtained using cDNA from MG-63 cells aligned with a published TWIK-1 sequence using nucleotide BLAST (http://blast.ncbi.nlm.nih.gov/Blast.cgi).

TWIK-1 primers gave positive results in all of the cells lines studied with the exception of SaOS-2. The signal was variable in MG-63 cells but was nonetheless detected on two occasions. PCR product from MG-63 cDNA was purified and sequenced. A BLAST search on the product revealed 100% homology with the published sequence for TWIK-1 mRNA.

3.3.6 TWIK-2

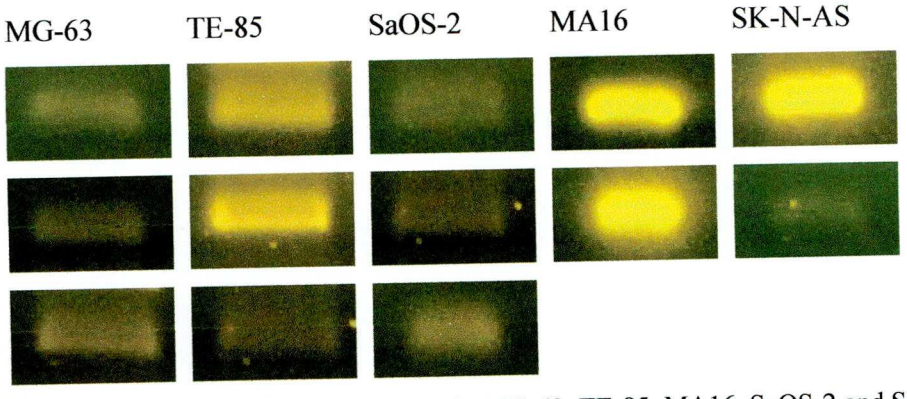

Figure 3.9. TWIK-2 mRNA expression in MG-63, TE-85, MA16, SaOS-2 and SK-N-AS cells. The expected band size was 393bp.

Remarkably, TWIK-2 was present in all of the samples studied in each experiment. Signals appeared stronger in TE-85 and MA16 cells when compared with MG-63 and SaOS-2. A sequencing reaction was performed on purified PCR product which originated from MG-63 cDNA. A BLAST search showed the PCR product had 97% homology with a published sequence for TWIK-2.

gi|13325107|gb|BC004367.1| Homo sapiens potassium channel, subfamily K, member 6, mRNA (cDNA
clone MGC:10363 IMAGE:3639657), complete cds
Length=2604

GENE ID: 9424 KCNK6 | potassium channel, subfamily K, member 6 [Homo sapiens]
(Over 10 PubMed links)

Score = 444 bits (224), Expect = 2e-121
Identities = 264/272 (97%), Gaps = 4/272 (1%)
Strand=Plus/Minus

```
Query  5    GAGAGTTGCTGGTGCGACTCCGGCTGGGGGCCCATGGATGTCCACCCGATCGTCCTCATC  64
            ||||||||||||||||||||||||||||||||| ||||||||||||||||||||||||
Sbjct  942  GAGAGTTGCTGGTGCGACTCCGGCTGGGGGCCCA-GGATGTCCACCCGATCGTCCTCATC  884

Query  65   CGCATTGAAACTGGCAGGGCACGGAGGGGGCAGCAGGATGAGCTCCGTGAGGCCGTGGAG  124
            ||||||||||||||||||||||||||||||||||||||||||||||||||||||||||||
Sbjct  883  CGCATTGAAACTGGCAGGGCACGGAGGGGGCAGCAGGATGAGCTCCGTGAGGCCGTGGAG  824

Query  125  GTCGGACATCGTGGCGGAAGGTCTGCAGCACCAGCACCATGGCCACCAGGCCCAGGAAGA  184
            |||||||| ||||||||||||||||||||||||||||||||||||||||||||||||||||
Sbjct  823  GTCGGACA-CGTGGCGGAAGGTCTGCAGCACCAGCACCATGGCCACCAGGCCCAGGAAGA  765

Query  185  GGTAGACTGTGACCGCCGCCTTGGTAGAGGGCCCGGTACGGCTGGCCAGGGGCCTCCCGC  244
            |||||||||||||  | |||| |||||||||||||| |||||||||||||||||| |
Sbjct  764  GGTAGACTGTGACCAGCACCTT-GTAGAGGGCCCGGTAGGGCTGGCCAGGGGCCTCCC-C  707

Query  245  GGGCACGTAGTCGCCCAGGCCGATGGTGGACA  276
            ||||||||||||||||||||||||||||||||
Sbjct  706  GGGCACGTAGTCGCCCAGGCCGATGGTGGACA  675
```

Figure 3.10. TWIK-2 PCR product sequence obtained using cDNA from MG-63 cells aligned with a published TWIK-2 sequence using nucleotide BLAST (http://blast.ncbi.nlm.nih.gov/Blast.cgi).

3.3.7 THIK-2

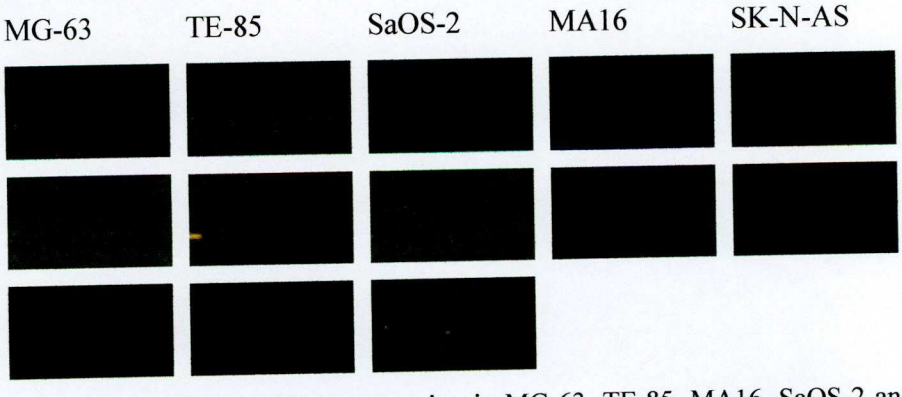

Figure 3.11. THIK-2 mRNA expression in MG-63, TE-85, MA16, SaOS-2 and SK-N-AS cells. The expected band size was 488bp.

THIK-2 mRNA was not detected in any of the osteoblastic samples despite multiple experiments using cDNA extracted on different occasions. It was also undetected in the neuronal cell line SK-N-AS.

3.3.8 TALK-1

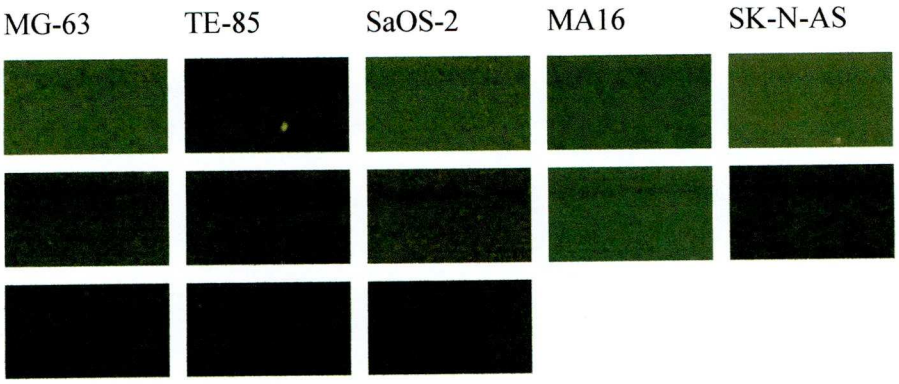

Figure 3.12. TALK-1 mRNA expression in MG-63, TE-85, MA16, SaOS-2 and SK-N-AS cells. The expected band size was 235bp.

No positive results were observed when any of the cell lines were screened with primers targeted at TALK-1 cDNA.

3.3.9 TALK-2

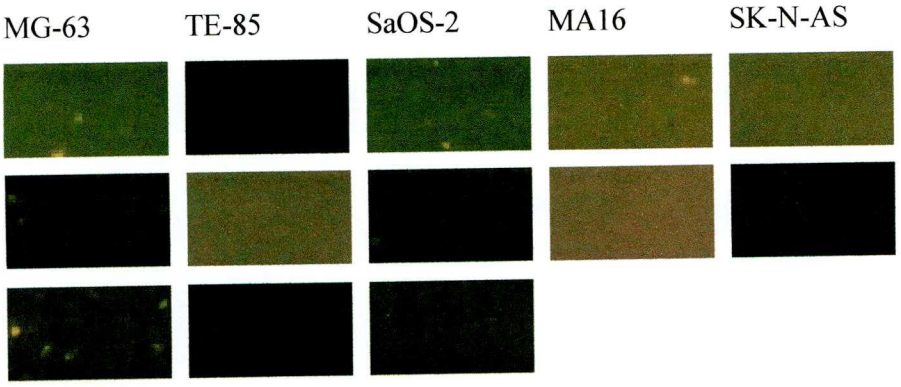

Figure 3.13. TALK-2 mRNA expression in MG-63, TE-85, MA16, SaOS-2 and SK-N-AS cells. The expected band size was 344bp.

TALK-2 mRNA was not detected in any of the samples despite multiple attempts at running the reaction.

3.3.10 THIK-1

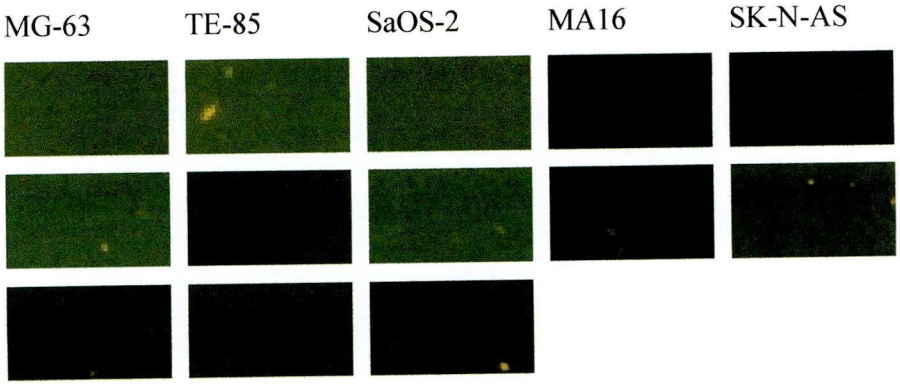

Figure 3.14. THIK-1 mRNA expression in MG-63, TE-85, MA16, SaOS-2 and SK-N-AS cells. The expected band size was 451bp.

No THIK-1 mRNA was detected in any of the cell lines.

3.3.11 TRESK

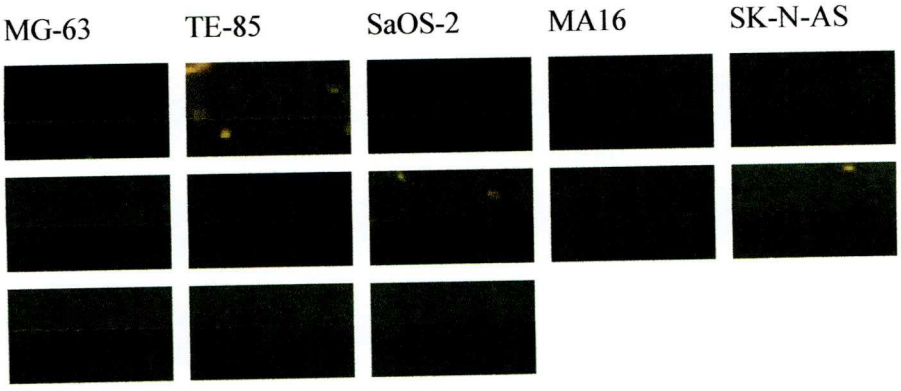

Figure 3.15. TRESK mRNA expression in MG-63, TE-85, MA16, SaOS-2 and SK-N-AS cells. The expected band size was 530bp.

TRESK-1 product was not detected in any of the experiments.

3.3.12 TRAAK

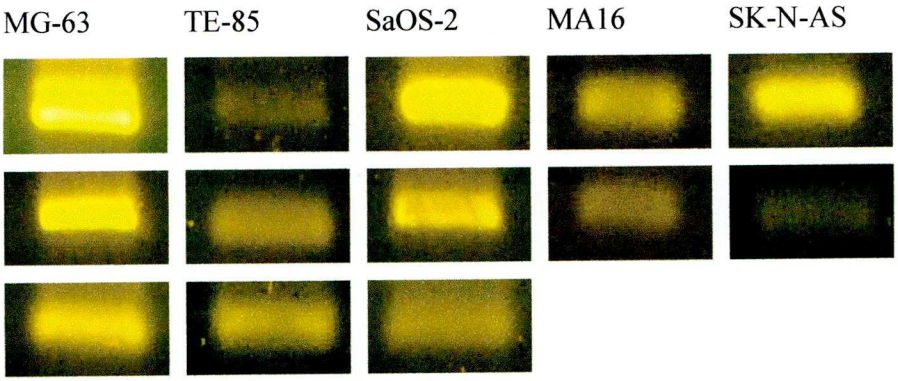

Figure 3.16. TRAAK mRNA expression in MG-63, TE-85, MA16, SaOS-2 and SK-N-AS cells. The expected band size was 447bp.

```
gi|7576934|gb|AF247042.1|AF247042 Homo sapiens tandem pore domain potassium
channel TRAAK (KCNK4)
mRNA, complete cds
Length=2772

 Score =  283 bits (143),  Expect = 6e-73
 Identities = 318/371 (85%), Gaps = 4/371 (1%)
 Strand=Plus/Minus

Query  33   ACATAATCGCCAAAGCCTACAGTGGTGAGTGTCACTATAACAAAGTAGATGGCTTCCAGC  92
            ||||| |||||||||||| || ||||| || |||||||| ||||||||||||||| ||||||
Sbjct  797  ACATAGTCGCCAAAGCCCACGGTGGTAAGCGTCACTATGACAAAGTAGATGGCCTCCAGC  738

Query  93   TTGCTCCAGACTCTCCATGTAGGAGAACACGAAGGTAGGAGTGAGGACAAAGAGCAGGCA  152
            ||||||||| | |||||| ||| |||||||||| || || ||||||||||||||||||||
Sbjct  737  TTGCTCCAGTC-CTCCATATAGCAGAACACGAACGTGGGCGTGAGGACAAAGAGCAGGCA  679

Query  153  GCCAATCAACAGGAAGAGCACCGCAGACAGCATATCTCACCAGCCCTGGTGGCACATGCC  212
            ||| |||| |||||| |||| ||| |||||||  ||| || ||| | |||||||| ||||
Sbjct  678  GCCGATCAGCAGGAAAAGCATCGCCGACAGCAC-TCTTACTAGCTCCGGTGGCACGTGCC  620

Query  213  ACTTCAAGAAAACTGCTTCGATGTGACCGATGCCCCGGCGCAGAGAGGAGCCCAGCCGGT  272
            |||||||||| |  ||||| ||||||||||||||  ||||||| ||||||||||||||||
Sbjct  619  ACTTCAAGAAGATGGCTTCAATGTGACCGATGCCATGGCGCAGGGAGGAGCCCAGCCGGT  560

Query  273  CCCCGACTCCAGCCAGCAGGCATCCCGAACAGTGGGATCCCCACCAGTGCATAGTAAGAT  332
            ||||||| || ||||| ||| ||||| ||||| || |||||||||| |||||| |||||
Sbjct  559  CCCCGACCCCTGCCAGTAGG-ATCCCAAACAGCGGAATCCCCACCAGCGCATAG-AAGAT  502

Query  333  ACAAAAGAGACGCCCAGCATCTGTGTGTAAGGCTATATTGCCGTAGCCGATGGTAGTGAT  392
             || ||||| ||||| |||||||||| | | ||| | |||||| |||||||||| |||||
Sbjct  501  GCAGAAGAGGCGCCCGGCATCTGTGCGCAGGGCCACATTGCCATAGCCGATGGTGGTGAT  442

Query  393  GATGGTCCCTG  403
            ||||||||||
Sbjct  441  GATGGTCCCTG  431
```

Figure 3.17. TRAAK PCR product sequence obtained using cDNA from MG-63 cells aligned with a published TRAAK sequence using nucleotide BLAST (http://blast.ncbi.nlm.nih.gov/Blast.cgi).

TRAAK mRNA was detected in all cell lines, for each experiment. The osteoblastic cell lines MG-63 and SaOS-2 appear to express TRAAK more strongly than the neuronal cell line. In the first band in the MG-63 column and the second experiment for SaOS-2 it appears there are two bands very close in size and almost overlapping. Purified product from a PCR reaction using MG-63 cDNA showed 85% homology with a published human TRAAK sequence. Although this was a lower value than some of the other sequences achieved, it was still the best match against all human mRNA in the PubMed database.

3.3.13 TREK-1

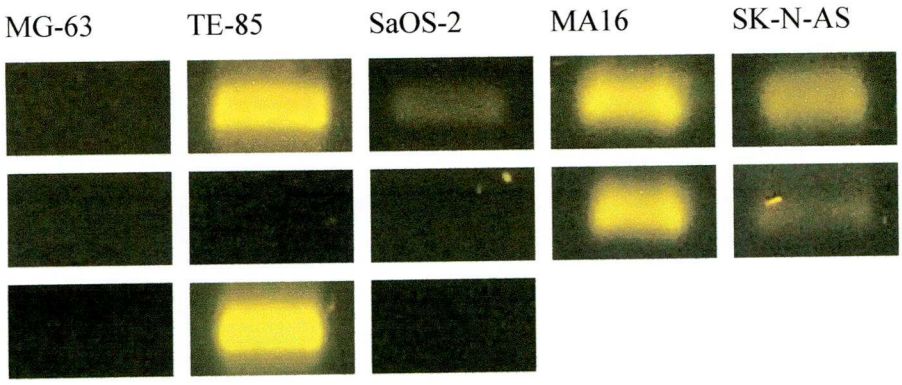

Figure 3.18. TREK-1 mRNA expression in MG-63, TE-85, MA16, SaOS-2 and SK-N-AS cells. The expected band size was 591bp.

TREK-1 was detected in TE-85, SaOS-2, MA16 and SK-N-AS. As with the TRAAK results, TREK-1 expression appears stronger in the osteoblastic cells than in the neuronal cell line. TREK-1 mRNA was absent from the MG-63 cells studied. A sequencing reaction was performed against purified PCR product originating from TE-85 cDNA. There was 99% homology between the product and published sequences for TREK-1.

gi|126723760|ref|NM_014217.3| Homo sapiens potassium channel, subfamily K, member 2 (KCNK2), transcript variant 2, mRNA
Length=3274

GENE ID: 3776 KCNK2 | potassium channel, subfamily K, member 2 [Homo sapiens] (Over 10 PubMed links)

Score = 1072 bits (541), Expect = 0.0
Identities = 551/553 (99%), Gaps = 1/553 (0%)
Strand=Plus/Plus

```
Query  5     ACTGGGATTTGGGAAGTTCCTTCTTCTTTGCTGGCACTGTTATTACAACCATAGGATTTG  64
             ||||||||||||||||||||||||||||||||||||||||||||||||||||||||||||
Sbjct  467   ACTGGGATTTGGGAAGTTCCTTCTTCTTTGCTGGCACTGTTATTACAACCATAGGATTTG  526

Query  65    GAAACATCTCACCACGCACAGAAGGCGGCAAAATATTCTGTATCATCTATGCCTTACTGG  124
             ||||||||||||||||||||||||||||||||||||||||||||||||||||||||||||
Sbjct  527   GAAACATCTCACCACGCACAGAAGGCGGCAAAATATTCTGTATCATCTATGCCTTACTGG  586

Query  125   GAATTCCCCTCTTTGGTTTTCTCTTGGCTGGAGTTGGAGATCAGCTAGGCACCATATTTG  184
             ||||||||||||||||||||||||||||||||||||||||||||||||||||||||||||
Sbjct  587   GAATTCCCCTCTTTGGTTTTCTCTTGGCTGGAGTTGGAGATCAGCTAGGCACCATATTTG  646

Query  185   GAAAAGGAATTGCCAAAGTGGAAGATACGTTTATTAAGTGGAATGTTAGTCAGACCAAGA  244
             ||||||||||||||||||||||||||||||||||||||||||||||||||||||||||||
Sbjct  647   GAAAAGGAATTGCCAAAGTGGAAGATACGTTTATTAAGTGGAATGTTAGTCAGACCAAGA  706

Query  245   TTCGCATCATCTCAACAATCATATTTATACTATTTGGCTGTGTACTCTTTGTGGCTCTGC  304
             ||||||||||||||||||||||||||||||||||||||||||||||||||||||||||||
Sbjct  707   TTCGCATCATCTCAACAATCATATTTATACTATTTGGCTGTGTACTCTTTGTGGCTCTGC  766

Query  305   CTGCGATCATATTCAAACACATAGAAGGCTGGAGTGCCCTGGACGCCATTTATTTTGTGG  364
             ||||||||||||||||||||||||||||||||||||||||||||||||||||||||||||
Sbjct  767   CTGCGATCATATTCAAACACATAGAAGGCTGGAGTGCCCTGGACGCCATTTATTTTGTGG  826

Query  365   TTATCACTCTAACAACTATTGGATTTGGTGACTACGTTGCAGGTGGATCCGATATTGAAT  424
             ||||||||||||||||||||||||||||||||||||||||||||||||||||||||||||
Sbjct  827   TTATCACTCTAACAACTATTGGATTTGGTGACTACGTTGCAGGTGGATCCGATATTGAAT  886

Query  425   ATCTGGACTTCTATAAGCCTGTCGTGTGGTTCTGGATCCTTGTAGGGCTTGCTTACTTTG  484
             ||||||||||||||||||||||||||||||||||||||||||||||||||||||||||||
Sbjct  887   ATCTGGACTTCTATAAGCCTGTCGTGTGGTTCTGGATCCTTGTAGGGCTTGCTTACTTTG  946

Query  485   CTGCTGTCCTGAGCATGATTGGAGATTGGCTCCGAGTGATATCTAAAAAGAACAAAAGAG  544
             |||||||||||||||||||||||||||||||||||||||||||||||| ||||||||
Sbjct  947   CTGCTGTCCTGAGCATGATTGGAGATTGGCTCCGAGTGATATCTAAAAAG-ACAAAAGAA  1005

Query  545   GAGGTGGGAGAGT  557
             |||||||||||||
Sbjct  1006  GAGGTGGGAGAGT  1018
```

Figure 3.19. TREK-1 PCR product sequence obtained using cDNA from TE-85 cells aligned with a published TREK-1 sequence using nucleotide BLAST (http://blast.ncbi.nlm.nih.gov/Blast.cgi).

3.3.14 TREK-2

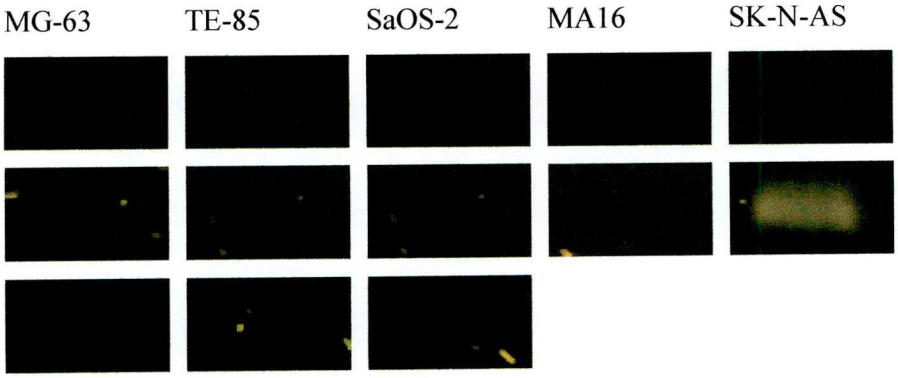

Figure 3.20. TREK-2 mRNA expression in MG-63, TE-85, MA16, SaOS-2 and SK-N-AS cells. The expected band size was 364bp.

TREK-2 mRNA was detected once in a sample from SK-N-AS cells. It was not detected in any of the osteoblastic cell lines or primary osteoblasts. TREK-2 primers were designed to target all three transcript variants described for products of this gene.

Table 3.1. Summary of PCR results for all primer sets screened in MG-63, TE-85, MA16, SaOS-2 and SK-N-AS cells.

	TE-85	MG-63	SaOS-2	MA16	SK-N-AS
TASK-1	++	~	-	+	++
TASK-2	++	+	~	++	++
TASK-3	-	-	-	+	++
TASK-5	-	-	-	+	-
TWIK-1	++	+	-	++	++
TWIK-2	+	++	+	++	++
THIK-2	-	-	-	-	-
TALK-1	-	-	-	-	-
TALK-2	-	-	-	-	-
THIK-1	-	-	-	-	-
TRESK	-	-	-	-	-
TRAAK	+	++	++	+	+
TREK-1	++	-	+	++	+
TREK-2	-	-	-	-	+

- no expression detected ~ possible weak expression

+ weak expression ++ strong expression

3.4 Discussion

The screening of primary osteoblasts and osteoblast cell lines for all functional members of the K_{2P} family of channels gave a number of repeatable positive and negative outcomes. These results are summarized in Figure 3.1. Out of 14 primer sets used, 9 of these gave positive results in at least one of the cell lines used. Of the 9 positive results, 6 were sequenced and all of these samples were found to match the published sequences to an acceptable degree. Members of the TASK, TWIK and TREK sub-families dominated the expression profile of K_{2P} channels in osteoblastic cells. TASK-2 was the sole representative of the alkaline-activated, or TALK sub-family. THIK and TRESK channels were absent from the various osteoblastic cells studied and the neuronally derived cell line SK-N-AS.

Previous work has described the expression of members of the TREK family of K_{2P} channels in osteoblastic cells (Chen *et al.*, 2005, Hughes *et al.*, 2006). Hughes *et al.*, (2006) reported the expression of TREK-1 in three out of three primary human osteoblast samples and in MG-63 cells. The expression of TRAAK and TREK-2 variant c was observed in some of the primary osteoblasts and appeared to vary between passage numbers. MG-63 cells expressed TRAAK but not TREK-2c. The above results confirm the finding that primary osteoblasts strongly express TREK-1 mRNA, but we did not observe TREK-1 mRNA in MG-63 cells. Hughes and co-workers reported the expression of TRAAK in most of the primary human osteoblasts and in MG-63 cells which these results also agree with. Chen *et al.* (2005) reported the expression of TREK-2 mRNA in the rat osteoblastic cell line UMR201. TREK-2 expression was not seen in the human osteoblastic cells studied here, but it was detected in SK-N-AS cells. The TREK-2 primers in this Chapter were designed to target all three splice variants of the TREK-2 gene. Hughes *et al.*, (2006) detected TREK-2c mRNA in an early passage of one of the primary osteoblast samples but all other experiments proved negative. Because Chen *et al.* (2005) did not report on the expression of TRAAK or TREK-1, it is not possible to directly compare the expression of TREK channels between human and rat osteoblastic cells. It seems possible that

there is some species variation in the expression of this sub-family of K_{2P} channels in osteoblasts.

To date, no other reports have been published on the expression of the remaining sub-groups in the K_{2P} channel family in bone. However, a small number of studies have observed K_{2P} channels in other skeletal tissues. Magra *et al.* (2007) described the expression of TREK-1 in tenocytes from human patellar tendon and a study by Saeki *et al.* (2007) looked into the expression of several K_{2P} channels in PDL fibroblasts. The PDL acts as a cushion between bone and tooth and is exposed to large forces during mastication. The fibroblasts revealed a strikingly similar pattern to that seen in the data for osteoblastic cells above. They described the mRNA present by order of its relative expression level as follows: TWIK-2 $\geq$ TREK-1 > TWIK-1 >> TASK-1> TRAAK $\geq$ TASK-2. They did not detect any TREK-2 mRNA in their sample which also complements the findings reported here.

The studies mentioned above claim that the mechanosensitive, and to an extent, AA-sensitivity of the TREK channels explains their presence in skeletal tissue (Chen *et al.*, 2005, Hughes *et al.*, 2006, Magra *et al.*, 2007 & Saeki *et al.*, 2007). Bone is an organ which is subjected to large mechanical stimuli on a regular basis. This is a necessary duty and one which is in fact required to maintain bone health. The presence and subsequent activation of a TREK K_{2P} channel in response to mechanical force may have a number of advantageous effects. The first major benefit may be transduction of the stimulus into an intracellular signal via a change in the membrane potential. The second benefit may come simply from change in the membrane potential to a more negative value. This would confer a protective effect in an environment where repeated stimulation may lead to excitotoxicity. Finally, the release of AA from membrane lipids in response to stretch would also activate a TREK channel which could lead to either or both of the above scenarios.

TASK channels are sensitive to external influences such as pH, glucose concentration and hypoxia (Duprat *et al.*, 2007). They are inhibited by extracellular protons prompting the possibility they may act as an acid sensor for

osteoblasts. TASK-3 is less sensitive to low pH than TASK-1 & -2 channels (Liu *et al.*, 2005). This simple fact may help to explain the presence of TASK-3 in primary osteoblasts and its absence in osteosarcoma cell lines. TASK-1 displays a relatively even pattern of expression between the CNS and the periphery whereas TASK-2 channels are mainly found in the periphery and TASK-3 is highly expressed in the CNS, (Goldstein *et al.*, 2005, Medhurst *et al.*, 2001).

The presence of TWIK-1 & -2 channels is more difficult to explain, given the poor functional data available for these channels in the literature. TWIK-1 & -2 expression has been documented in the nervous system and in peripheral tissues such as pancreas, spleen and stomach (Goldstein *et al.*, 2005, Medhurst *et al.*, 2001). Given that TWIK-1 & -2 have been shown in this chapter to be expressed very consistently across a number of different osteoblastic cells and considering the data published by Saeki *et al.*, (2007), a functional role is likely to exist for them in osteoblasts. The other member of the TWIK family not mentioned is this chapter is KCNK7. This was not included in the initial primer design due to its lack of functional activity. Perhaps in retrospect, it would have been interesting to look at the expression of this silent subunit in comparison to its close relations TWIK-1 &-2.

The lack of THIK-1 & -2, TALK-1 & -2 and TRESK may be explained by the limited expression and functional activity of these channels. THIK-1 is widely expressed in rat but not human tissues and no functional activity has been observed from THIK-2 (Rajan *et al.*, 2001). TALK-1 & -2 are sensitive to alkaline pH and are activated by NO (Duprat *et al.*, 2005, Kang & Kim, 2004). The latter property of TALK channels may be useful in a mechanically stimulated bone environment, although it is possible that they are present in other skeletal cell types. TRESK is highly localised to dorsal root ganglia, and does not posses any specific properties which might aid osteoblast function.

As yet there are no investigations which have focussed on K_{2P} expression in osteoclasts or osteocytes. It would be interesting to see if the profile of channel expression seen in osteoblasts is similar to, or complementary to that which may be seen in osteoclasts and osteocytes. Given that an osteoclast performs its duties in acidic and basic conditions, it may be expected that members of the TASK family are present in this cell type. By the same logic, one might expect the mechanosensitive osteocytes to express some members of the TREK family.

3.5 Conclusion

Screening of human osteoblasts and osteosarcoma cell lines revealed mRNA expression of TASK-1, -2, -3 & -5, TWIK-1 & -2, TREK-1 and TRAAK. mRNA for TALK-1 & -2, TRESK, THIK-1 & -2 and TREK-2 was not observed in osteoblastic cells. Further experiments are necessary to determine if protein expression matches that of the transcript and to characterise the functional role of these proteins in bone. The data in this Chapter reveals that K_{2P} channel expression in osteoblasts is not confined to members of the TREK family. Although no published studies have stated that K_{2P} expression in osteoblasts is limited to TREK channels, the lack of discussion and experimentation regarding the other sub-families needs to be addressed. It is perhaps surprising that so many members of the K_{2P} family are expressed in osteoblasts. The volume of channels that gave positive results in the RT-PCR indicate that there may be more than one functional role for these proteins in bone.

4.0 Detection of K_{2P} Channel Proteins in Osteoblastic Cells Using Immunocytochemistry & Western Blotting

4.1 Introduction

The aim of these experiments was to utilise commercially developed antibodies targeting K_{2P} channels, to screen for the presence of these proteins in human osteoblastic cell lines and primary osteoblasts. The mRNA expression profile for this family of channels is detailed in the previous Chapter and summarised in Table 3.1. Antibodies were chosen based on both the probability of finding the protein when taking into account the PCR data, and their availability at the time of performing the experiments. Two commonly used techniques were chosen to investigate K_{2P} protein expression; immunocytochemistry and western blotting. Immunocytochemistry gives an indication of the location of the protein within the cell, whereas western blotting can reveal the rough quantity of the protein present and any discrepancies in band sizing. As is the case throughout this Thesis, it is difficult to directly compare these results to published data. Relatively few studies have looked at K^+ channel protein expression in this cell type using immunocytochemistry and western blotting (Butler *et al.*, 2010, Hughes *et al.*, 2006, Moreau *et al.*, 1997, Hernandez *et al.*, 2007).

Immunoglobulin G (IgG) is the one of the simplest and most common types of antibody. IgG antibodies contain 3 segments that form a "Y" shape; two "Fragments having the Antigen Binding site" (fab) connected by a hinge to one "Fragment that Crystallizes" (fc). The fc section allows other proteins involved in the immune response to recognise the antibody and complete the removal of the antigen. The hinge is a small peptide sequence which allows lateral and rotational movements of the fab fragments. This increases the chance of an antibody binding site gaining access to its antigen.

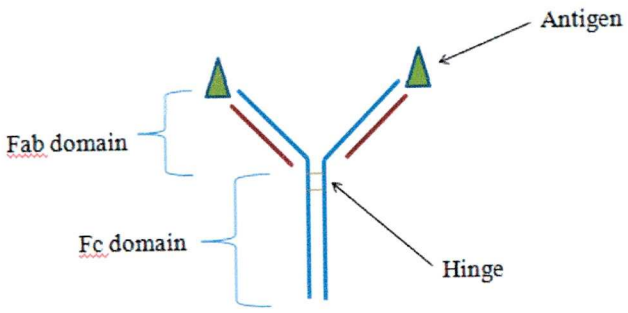

Figure 4.1. Schematic representation of an IgG antibody. The blue lines represent the heavy chain fragments and the brown lines the light chain fragments.

Amino acids are charged molecules, so the overall charge of a protein is dependant on the composition and number of amino acids it contains. The detergent sodium dodecyl sulphate (SDS) binds to hydrophobic regions within proteins. Roughly one molecule of SDS binds for every pair of amino acids. This causes a protein to revert to its secondary structure and eliminates any protein-protein interactions. SDS is added to protein samples in addition to the reducing agent β-mercaptoethanol which breaks any disulphide bonds. Protein/SDS complexes are negatively charged. This means that any protein, regardless of whether it is initially positively or negatively charged can be analysed using the charge-to-mass ratio conferred by SDS binding. When the complex is run out on an SDS polyacrylamide gel (SDS-PAGE), protein migrates towards the positive electrode and the porous polyacrylamide slows down the migration of the larger proteins, allowing size separation. The addition of ammonium persulphate (APS) and TEMED into the acrylamide solution assists in the polymerization of the acrylamide monomer by respectively releasing and stabilising free radicals.

If using a whole-cell extract, or tissue preparation, many proteins will be present on the SDS-PAGE gel. Individual proteins within the sample may be identified by antibodies coupled to a detectable dye or enzyme. This is usually done after transfer of proteins from the gel to a nitrocellulose membrane using a strong electrical field. The membrane can be incubated with primary and then secondary antibodies to confirm the presence of a specific protein using enhanced chemiluminescence (ECL). In a western blot, the secondary antibody is usually linked to a horseradish peroxidise (HRP) enzyme which catalyses the oxidation of luminol, a cyclic diacylhydrazide. After oxidation, the luminol emits light in a bid to return to its ground state. The location of the secondary antibody can therefore be revealed by exposing the membrane to a light-sensitive film. The weight of the protein of interest can be determined by comparing its band with molecular weight protein markers also run on the SDS-PAGE gel.

4.2 Methods

For immunocytochemistry, cells were seeded onto glass coverslips at approximately 1 x 10^5cells/ml. The following day, cells were fixed using 2% paraformaldehyde before being quenched and permeabilised. After washing, non-specific binding sites were blocked and primary antibodies were added. The cells were incubated with the antibody solution overnight at 4°C. The following morning, the primary antibody solution was removed, cells were washed and the secondary antibody was added and incubated at RT for one hour. During this time, the coverslips were covered in foil to prevent bleaching of the fluorophore. Cells were washed again and the coverslips immersed in MilliQ water to remove the final traces of unbound secondary antibody. Coverslips were mounted onto a labelled slide using VECTASHEILD® Hard-set mounting medium with 4',6-diamidino-2-phenylindole (DAPI) (Vector Labs).

For western blotting experiments, one lot of protein was extracted from each of the three cell lines and two western blots were performed using this sample. Confluent petri dishes of cells were lysed and the sample was centrifuged. Protein extract was obtained from the supernatant fraction and equal volume of Laemmli 2x sample buffer added (~500µl). Protein extracts were run on SDS-PAGE gels, before being transferred to a nitrocellulose membrane. The membrane was then incubated in 1% or 5% skimmed milk (Marvel) TBST for a minimum of 1-2 hours prior to the addition of rabbit primary antibodies (Alomone Labs). Primary antibodies were incubated with the membrane at 4°C overnight. The goat anti-rabbit horseradish peroxidase-linked secondary antibody (Sigma) was incubated at RT with the membrane for 90 minutes. ECL was freshly made up and applied to the membrane for one minute. The ECL was then removed and the membrane wrapped in cling film. Small amounts of tape were used secure the covered membrane in a Hypercassette™ (Amersham Biosciences). Once in a dark room, a safe light was used to apply Hyperfilm™ ECL (Amersham Biosciences) to the front of the blot. The film was exposed in the Hypercassette™ for 5 or 10 minutes. The film was developed and then rinsed in water before being fixed and given a final rinse. Once dry the film could then be overlaid onto the membrane which was still secured in the Hypercassette™.

The location of the molecular weight markers was then added to the film to aid the sizing of the bands.

Table 4.1. Epitopes of the primary antibodies used for immunocytochemistry and western blotting in this chapter (Alomone Labs).

Antibody	Epitope location	Residues	Epitope
Anti-TASK-1	C-terminus	252 - 269	(C)EDEKRDAEHRALLTRNGQ
Anti-TASK-2	C-terminus	483 - 499	(C)YEQLMNEYNKANSPKGT
Anti-TWIK-2	C-terminus	295 - 313	(C)ESHQQLSASSHTDYASIPR
Anti-TRAAK	C-terminus	343 - 359	(C)NLAFIDESSDTQSERGC
Anti-TREK-1	N-terminus	8 - 25	DPKSAAQNSKPRLSFSTK(C)

4.3 Results: Immunocytochemistry

4.3.1 TASK-1

Staining for TASK-1 was weak in all cell lines studied. In MG-63 cells it is diffuse and faint, prompting the possibility that TASK-1 protein is present in these cells in small quantities. In MA16 and TE-85 cells staining is concentrated close to the nucleus but is not seen elsewhere, which the image analysis confirms (see section E of figures 4.2 – 4.4).

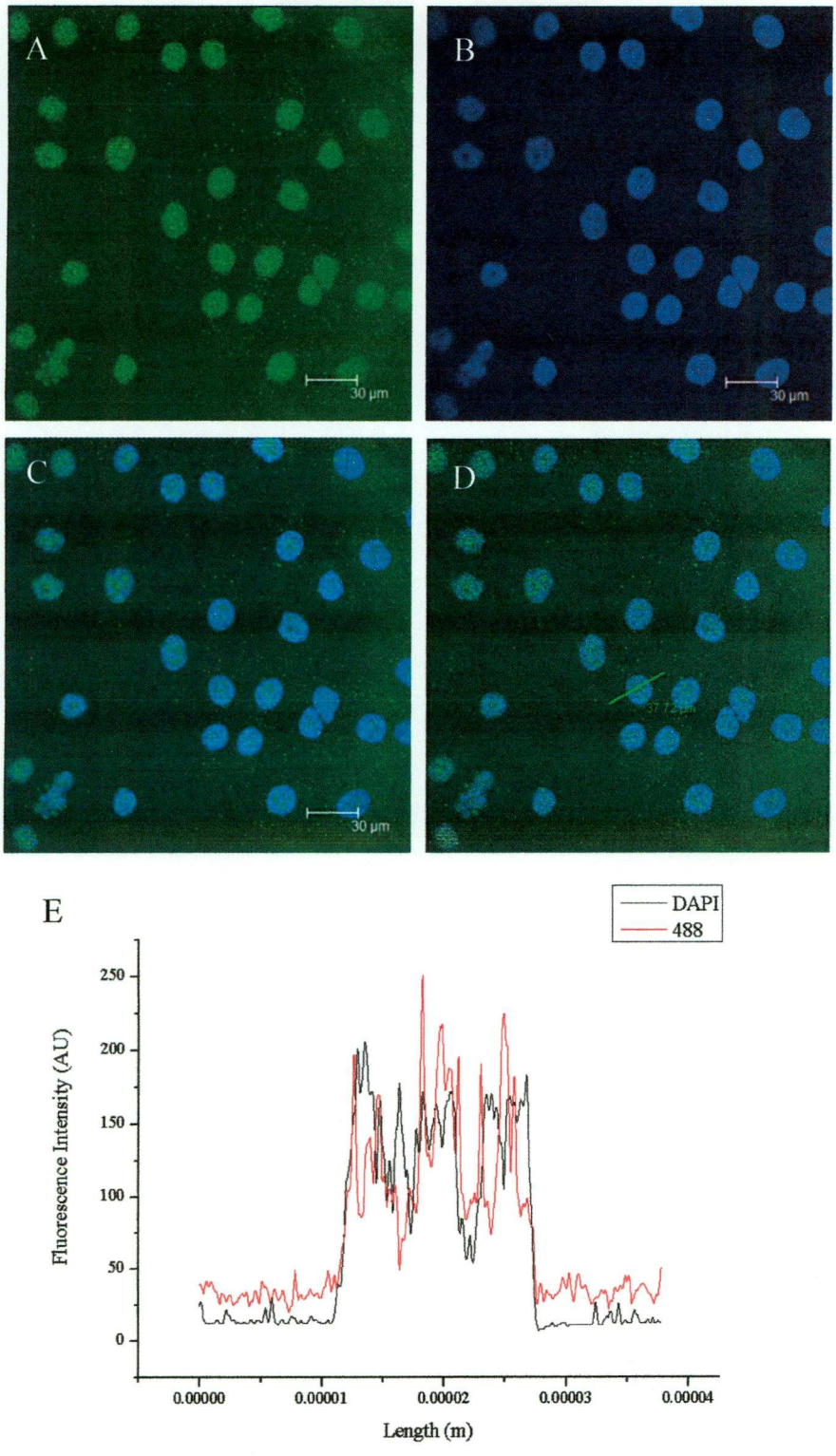

Figure 4.2. MG-63 cells stained with primary antibodies against TASK-1. A) Alexa Fluor-488. B) DAPI. C) Overlaid image of Alexa Fluor-488 & DAPI. D) Sample taken for image anaylsis. E) Graph showing the intensity of staining along the sample line through the cell selected in D.

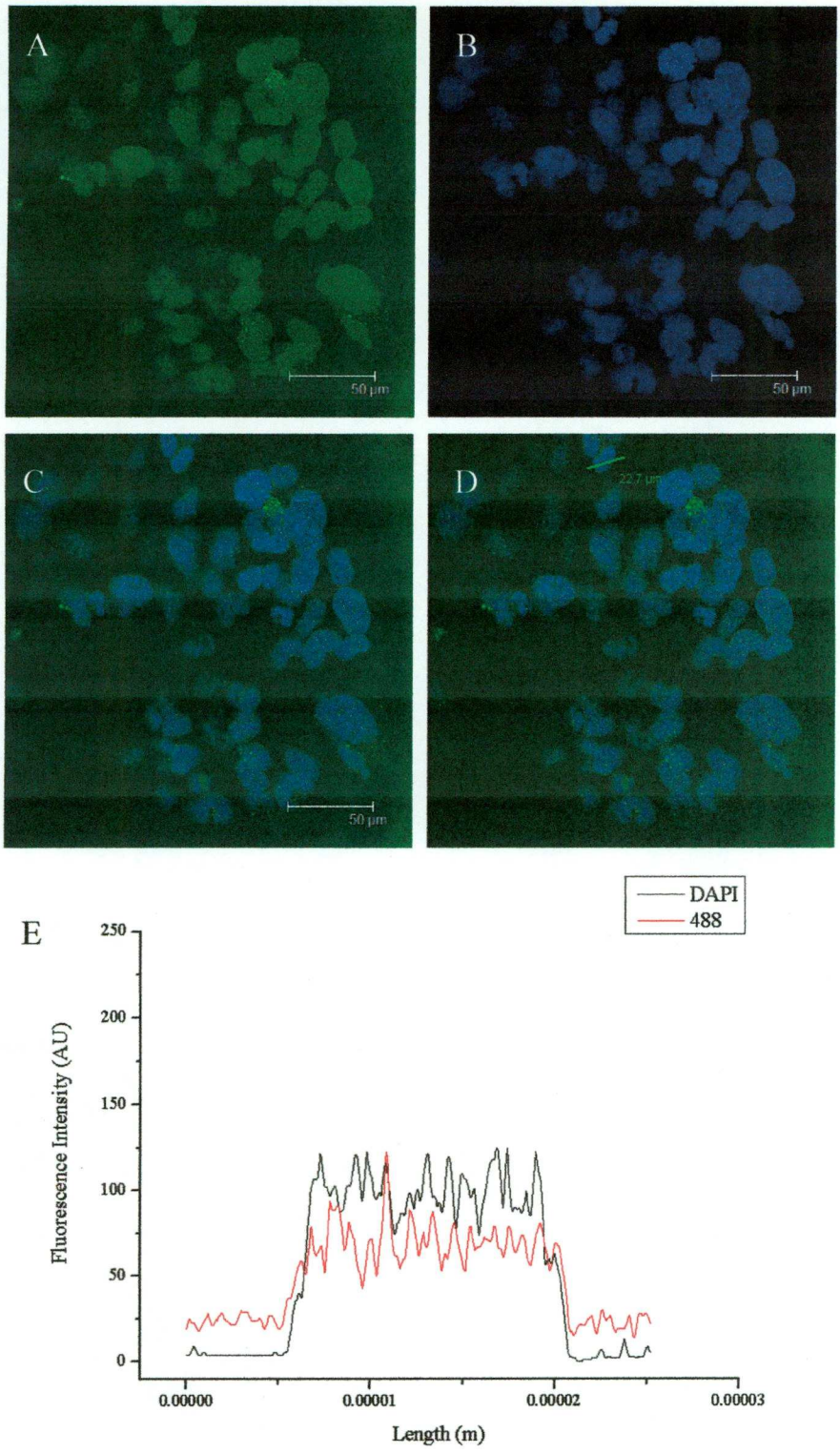

Figure 4.3. MA16 cells stained with primary antibodies against TASK-1. A) Alexa Fluor-488. B) DAPI. C) Overlaid image of Alexa Fluor-488 & DAPI. D) Sample taken for image analysis. E) Graph showing the intensity of staining along the sample line through the cell selected in D.

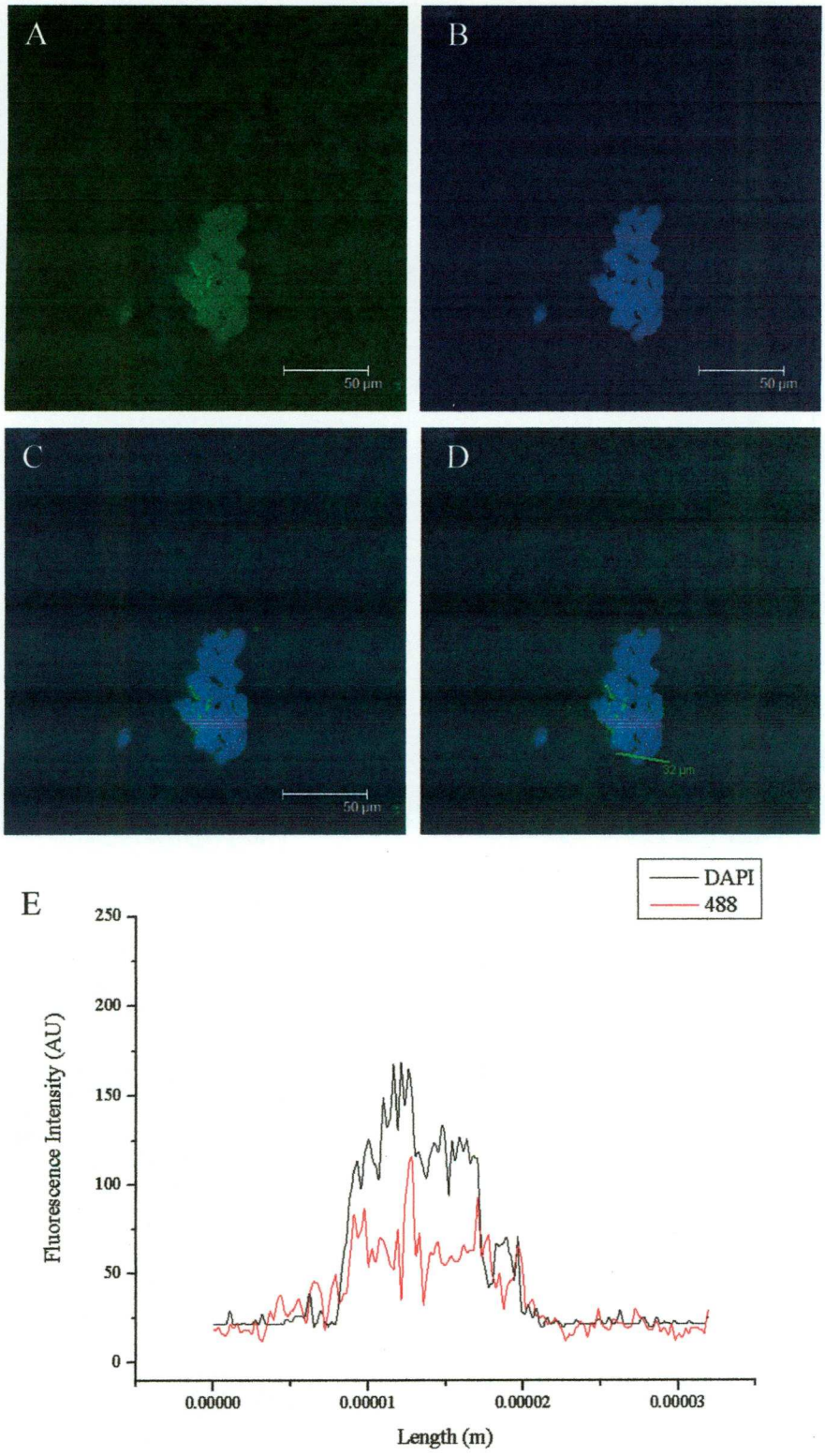

Figure 4.4. TE-85 cells stained with primary antibodies against TASK-1. A) Alexa Fluor-488. B) DAPI. C) Overlaid image of Alexa Fluor-488 & DAPI. D) Sample taken for image analysis. E) Graph showing the intensity of staining along the sample line through the cell selected in D.

4.3.2 TASK-2

TASK-2 staining is variable across cell lines. In MG-63 cells, it appears to be membranous as well as perinuclear. In MA16 cells staining can only be observed in the perinuclear region, although the confluence of these cells makes it difficult to see if any other cellular locations are stained. TE-85 cells display a similar pattern to MG-63 cells but the staining not associated with the nucleus is slightly weaker.

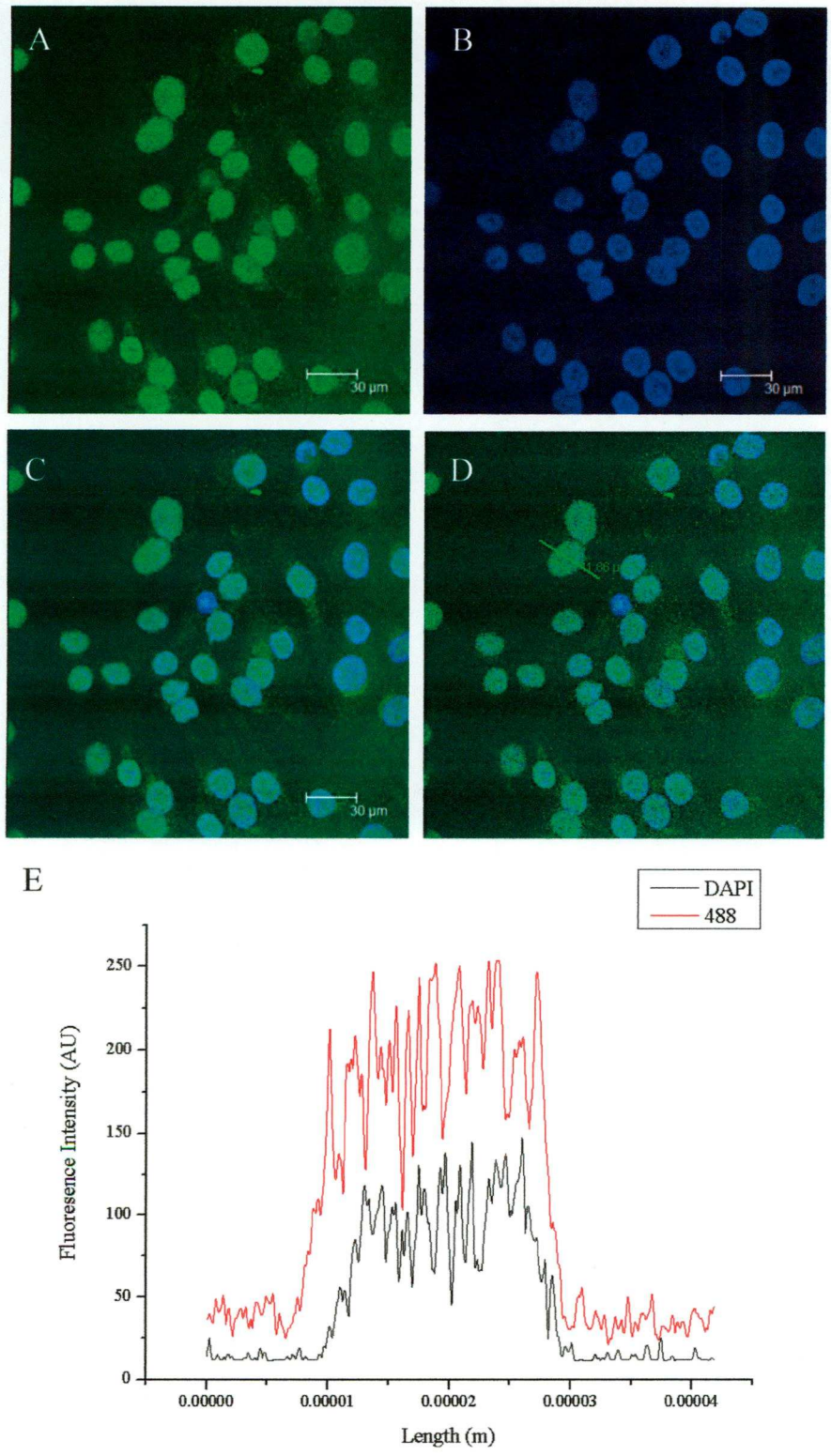

Figure 4.5. MG-63 cells stained with primary antibodies against TASK-2. A) Alexa Fluor-488. B) DAPI. C) Overlaid image of Alexa Fluor-488 & DAPI. D) Sample taken for image analysis. E) Graph showing the intensity of staining along the sample line through the cell selected in D.

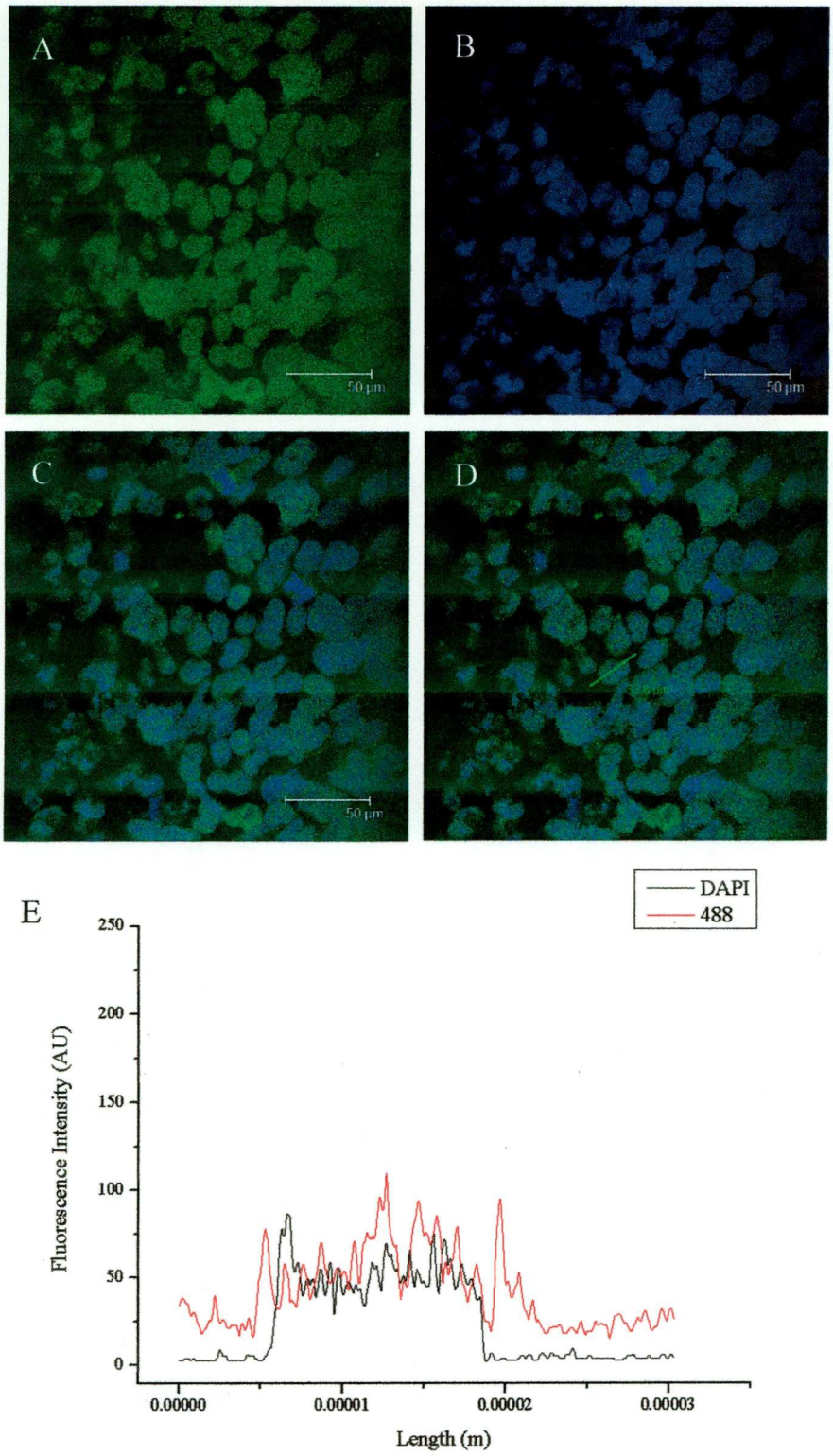

Figure 4.6. MA16 cells stained with primary antibodies against TASK-2. A) Alexa Fluor-488. B) DAPI. C) Overlaid image of Alexa Fluor-488 & DAPI. D) Sample taken for image analysis. E) Graph showing the intensity of staining along the sample line through the cell selected in D.

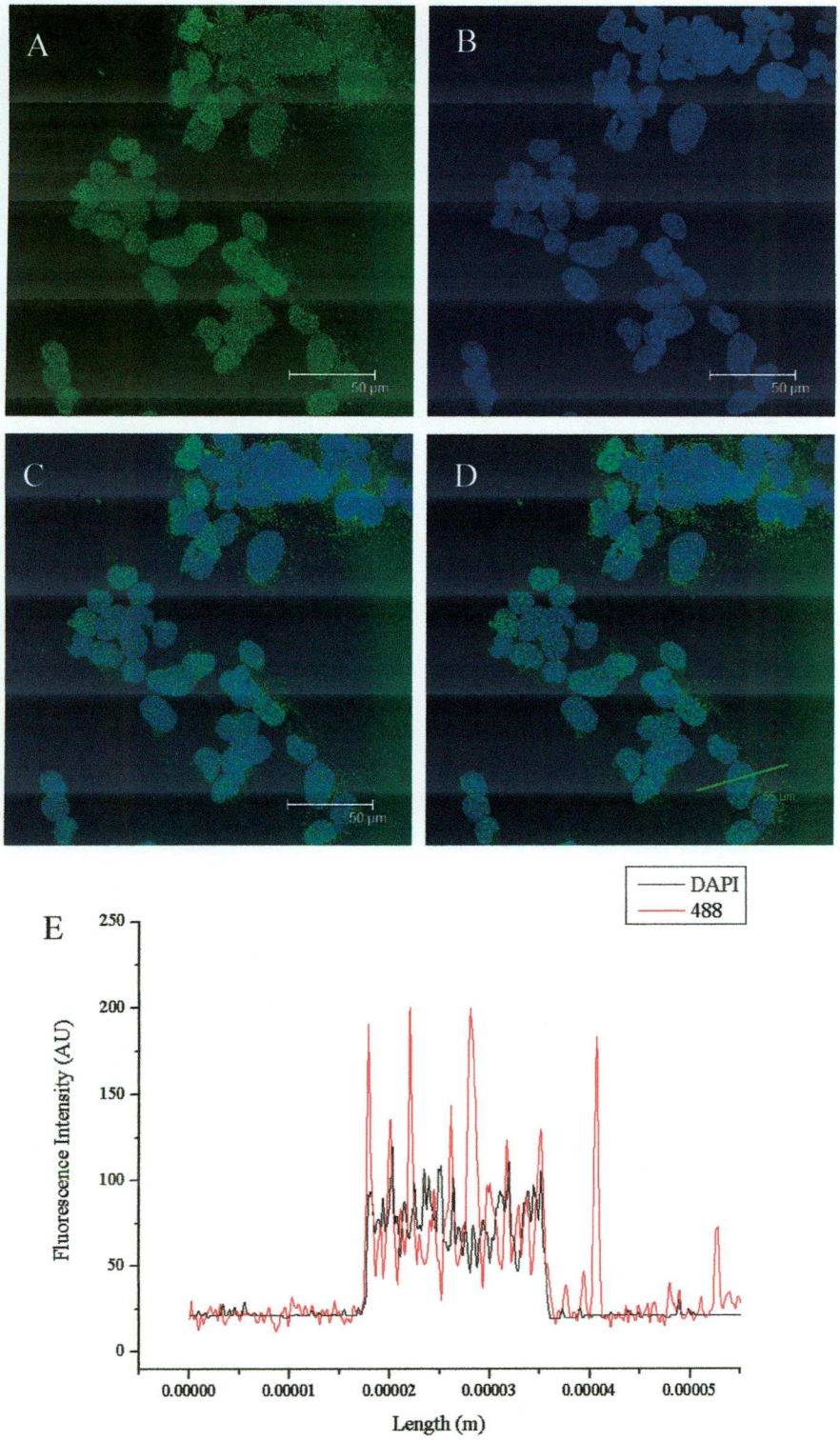

Figure 4.7. TE-85 cells stained with primary antibodies against TASK-2. A) Alexa Fluor-488. B) DAPI. C) Overlaid image of Alexa Fluor-488 & DAPI. D) Sample taken for image analysis. E) Graph showing the intensity of staining along the sample line through the cell selected in D.

4.3.3 TWIK-2

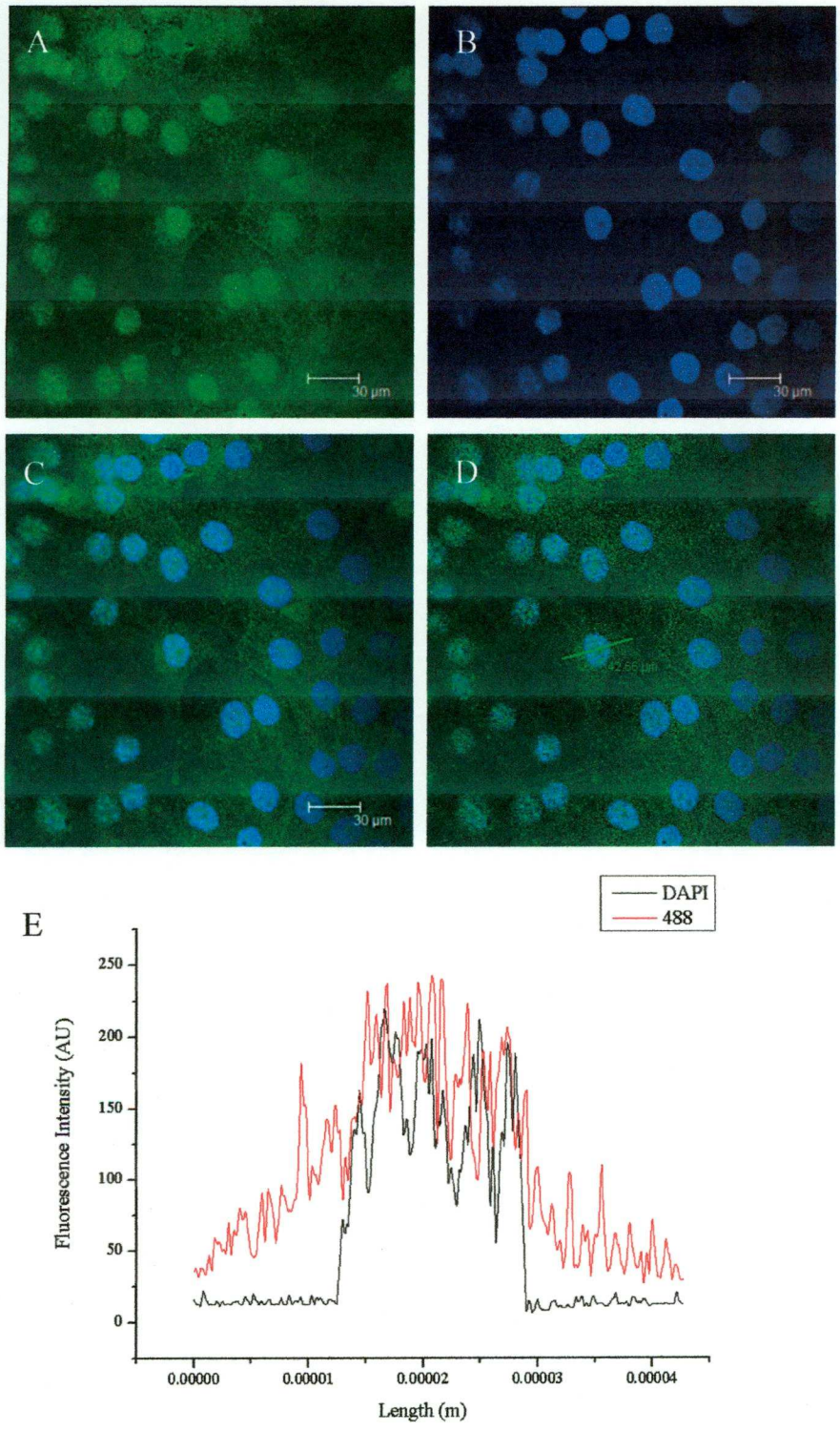

Figure 4.8. MG-63 cells stained with primary antibodies against TWIK-2. A) Alexa Fluor-488. B) DAPI. C) Overlaid image of Alexa Fluor-488 & DAPI. D) Sample taken for image analysis. E) Graph showing the intensity of staining along the sample line through the cell selected in D.

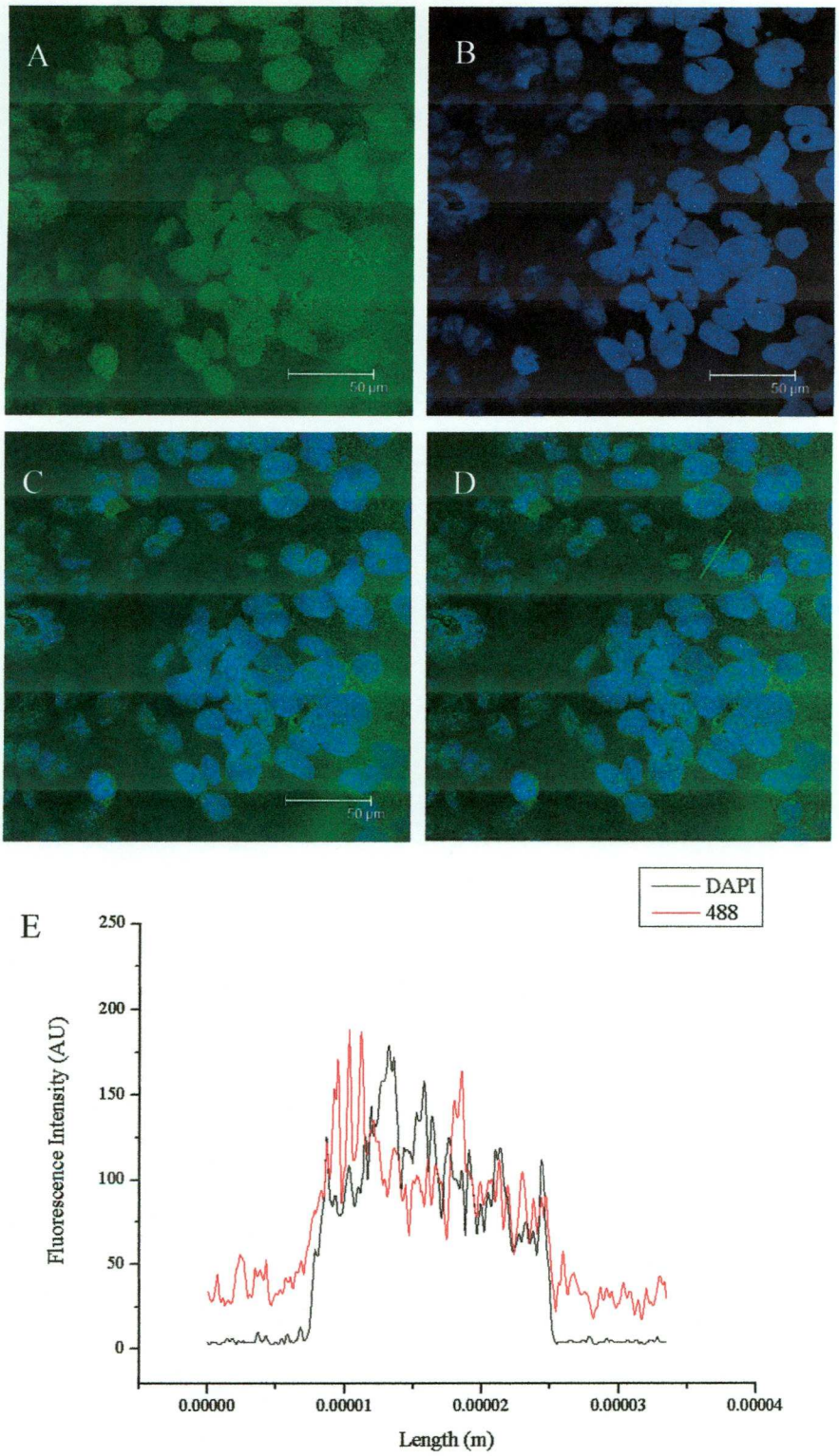

Figure 4.9. MA16 cells stained with primary antibodies against TWIK-2. A) Alexa Fluor-488. B) DAPI. C) Overlaid image of Alexa Fluor-488 & DAPI. D) Sample taken for image analysis. E) Graph showing the intensity of staining along the sample line through the cell selected in D.

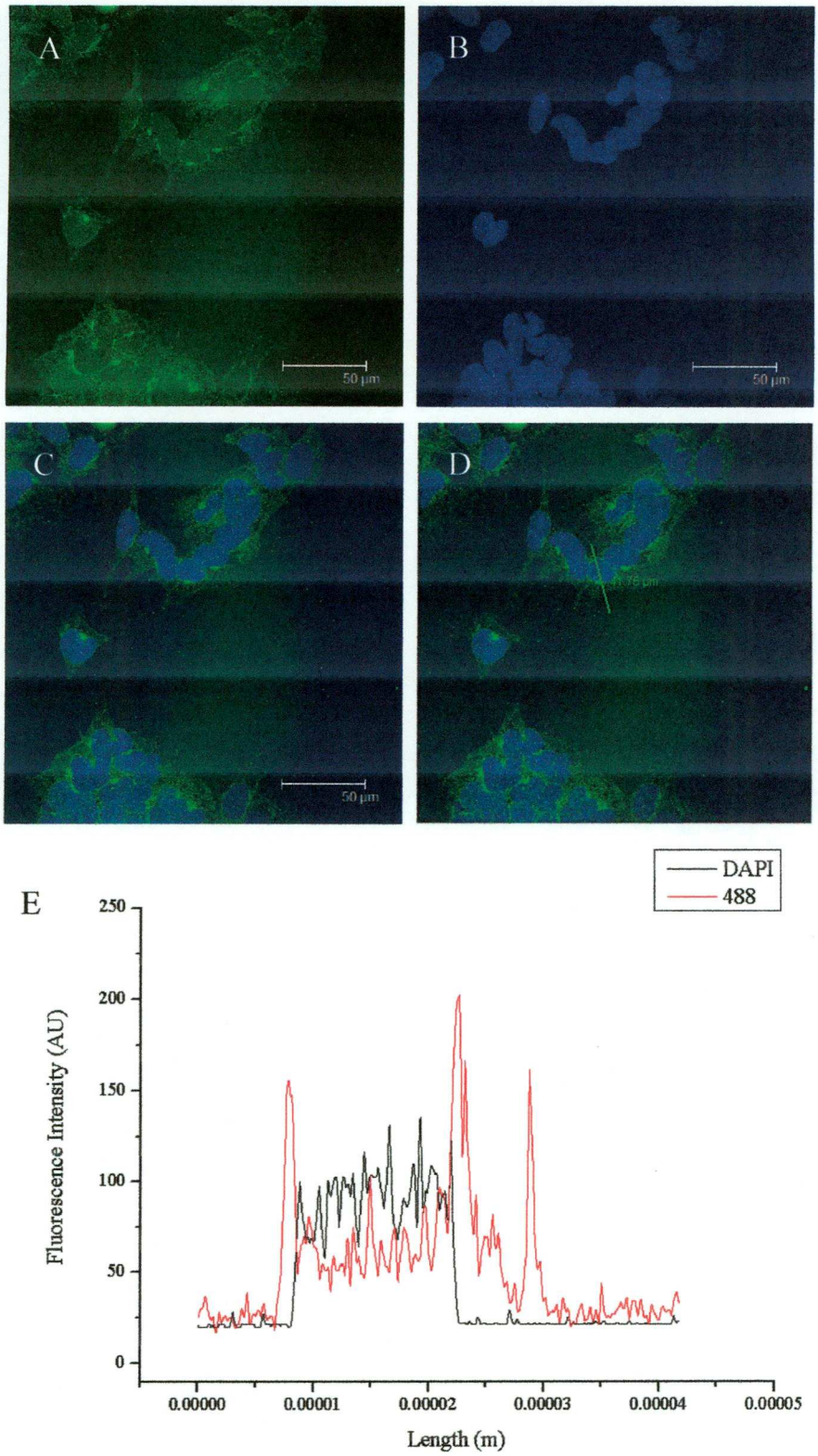

Figure 4.10. TE-85 cells stained with primary antibodies against TWIK-2. A) Alexa Fluor-488. B) DAPI. C) Overlaid image of Alexa Fluor-488 & DAPI. D) Sample taken for image analysis. E) Graph showing the intensity of staining along the sample line through the cell selected in D.

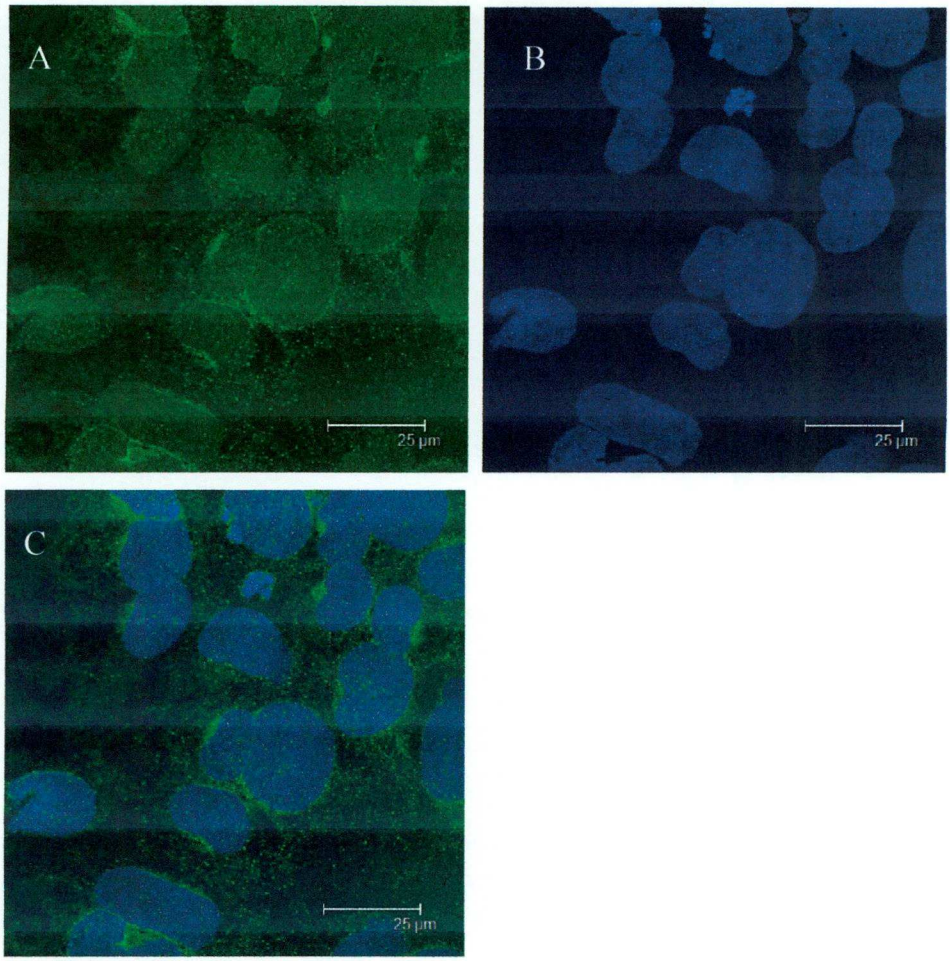

Figure 4.11. TE-85 cells stained with primary antibodies against TWIK-2 (2x zoom). A) Alexa Fluor-488. B) DAPI. C) Overlaid image of Alexa Fluor-488 & DAPI.

In MG-63 cells a clear definition of the cell shape can be seen due to TWIK-2 staining in the membrane. MA16 cells show diffuse perinuclear staining with no apparent membranous signal. TE-85 cells display in interesting punctate pattern of staining close to the nucleus in addition to a more diffuse staining pattern in the region of the cell membrane. In all cell lines stained with TWIK-2 the blue DAPI signal is more clearly seen without association with Alexa Fluor-488.

4.3.4 TRAAK

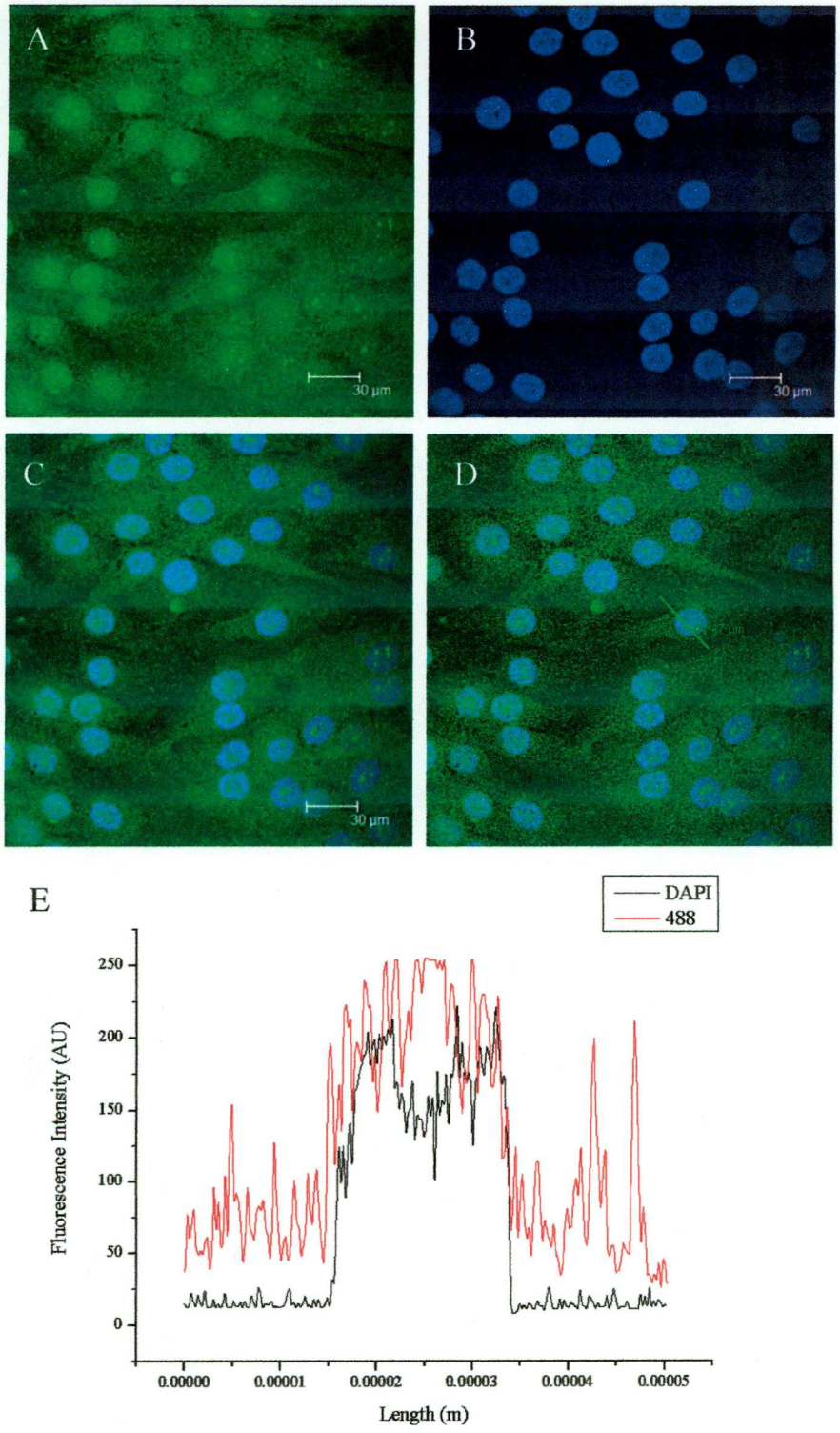

Figure 4.12. MG-63 cells stained with primary antibodies against TRAAK. A) Alexa Fluor-488. B) DAPI. C) Overlaid image of Alexa Fluor-488 & DAPI. D) Sample taken for image analysis. E) Graph showing the intensity of staining along the sample line through the cell selected in D.

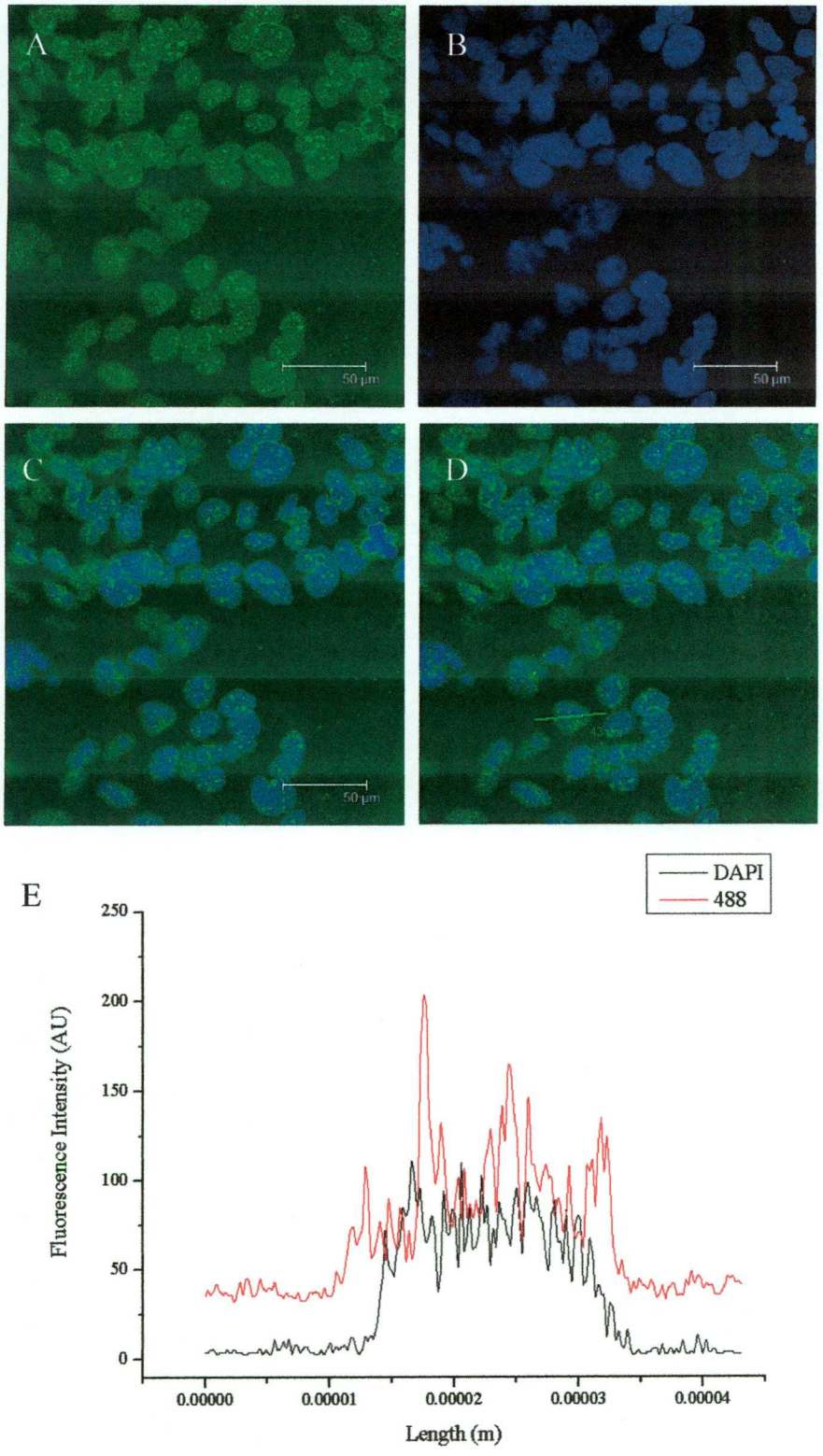

Figure 4.13. MA16 cells stained with primary antibodies against TRAAK. A) Alexa Fluor-488. B) DAPI. C) Overlaid image of Alexa Fluor-488 & DAPI. D) Sample taken for image analysis. E) Graph showing the intensity of staining along the sample line through the cell selected in D.

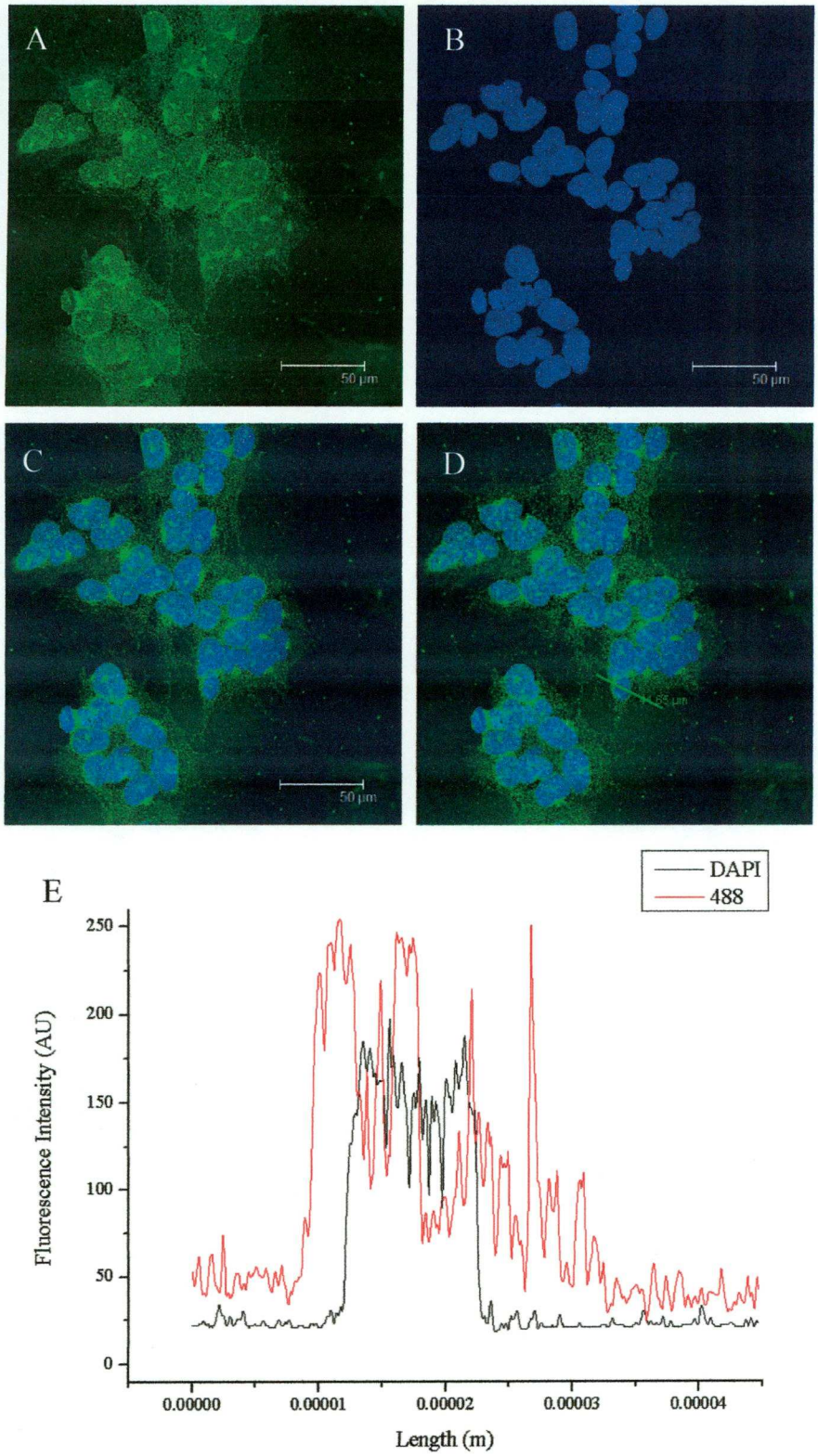

Figure 4.14. TE-85 cells stained with primary antibodies against TRAAK. A) Alexa Fluor-488. B) DAPI. C) Overlaid image of Alexa Fluor-488 & DAPI. D) Sample taken for image analysis. E) Graph showing the intensity of staining along the sample line through the cell selected in D.

All cell lines show a strong punctate perinuclear and nuclear pattern of staining. MG-63 and TE-85 cells also display what appears to be membranous staining which is particularly strong in MG-63 cells. Signal intensity values were strong in all cells stained with anti-TRAAK antibodies.

4.3.5 TREK-1

Anti-TREK-1 antibody gave the strongest indication so far of membranous staining. All cell lines exhibited diffuse staining which clearly defined the shape of the cell membrane and its processes. In the pictures taken with the 2x zoom function, this was evident again on a larger scale.

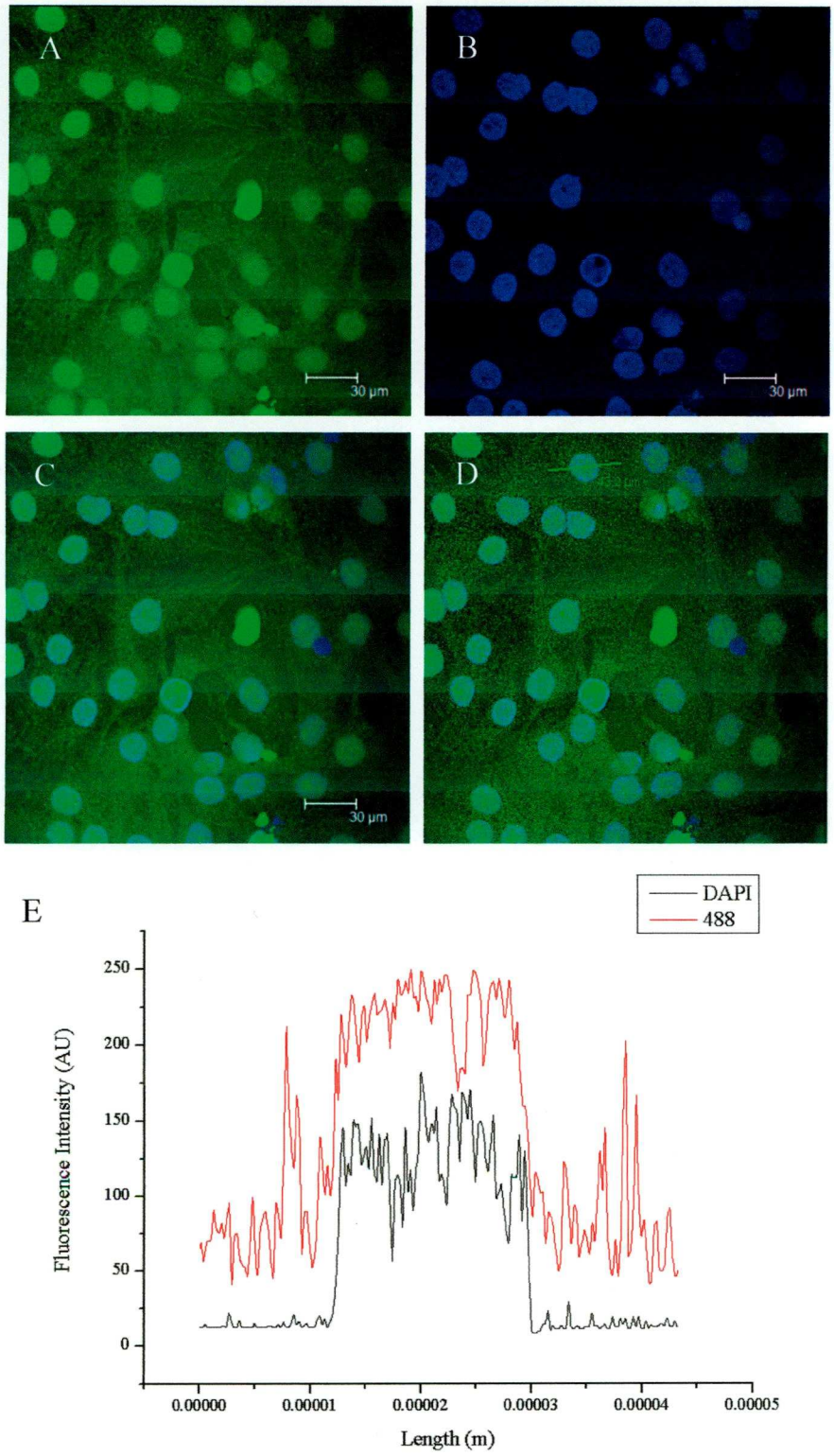

Figure 4.15. MG-63 cells stained with primary antibodies against TREK-1. A) Alexa Fluor-488. B) DAPI. C) Overlaid image of Alexa Fluor-488 & DAPI. D) Sample taken for image analysis. E) Graph showing the intensity of staining along the sample line through the cell selected in D.

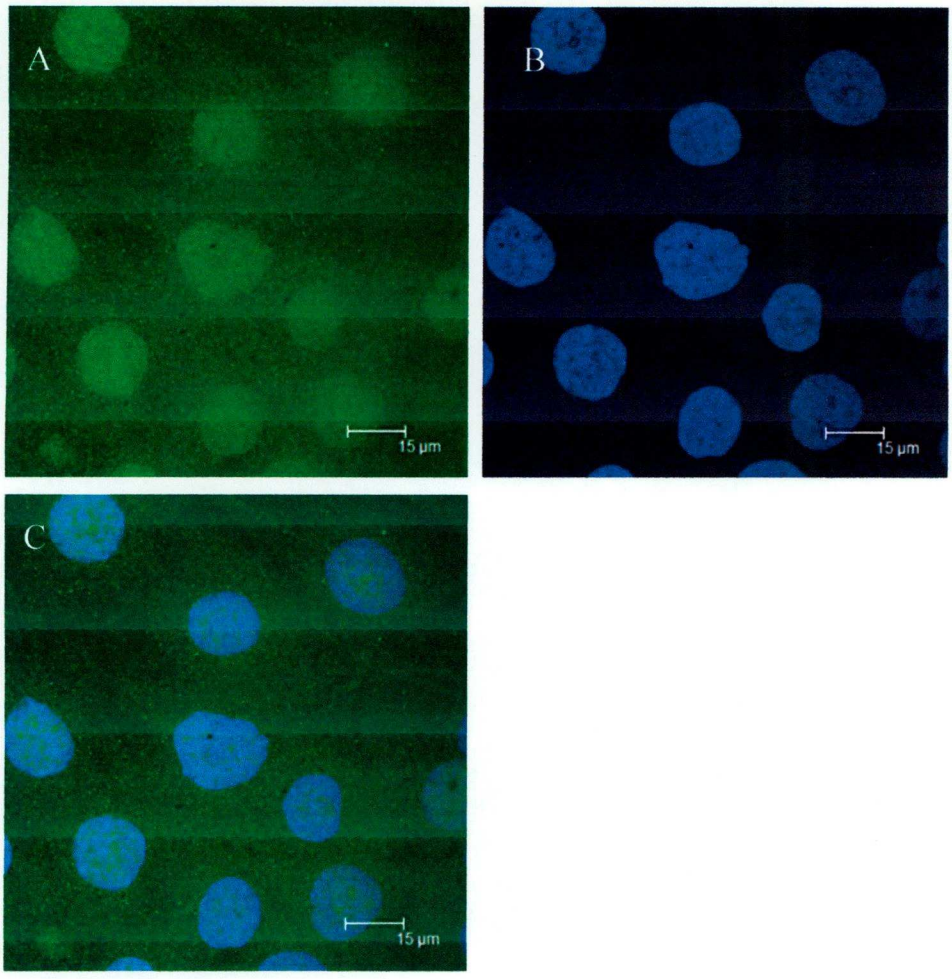

Figure 4.16. MG-63 cells stained with primary antibodies against TREK-1 (2x zoom). A) Alexa Fluor-488. B) DAPI. C) Overlaid image of Alexa Fluor-488 & DAPI.

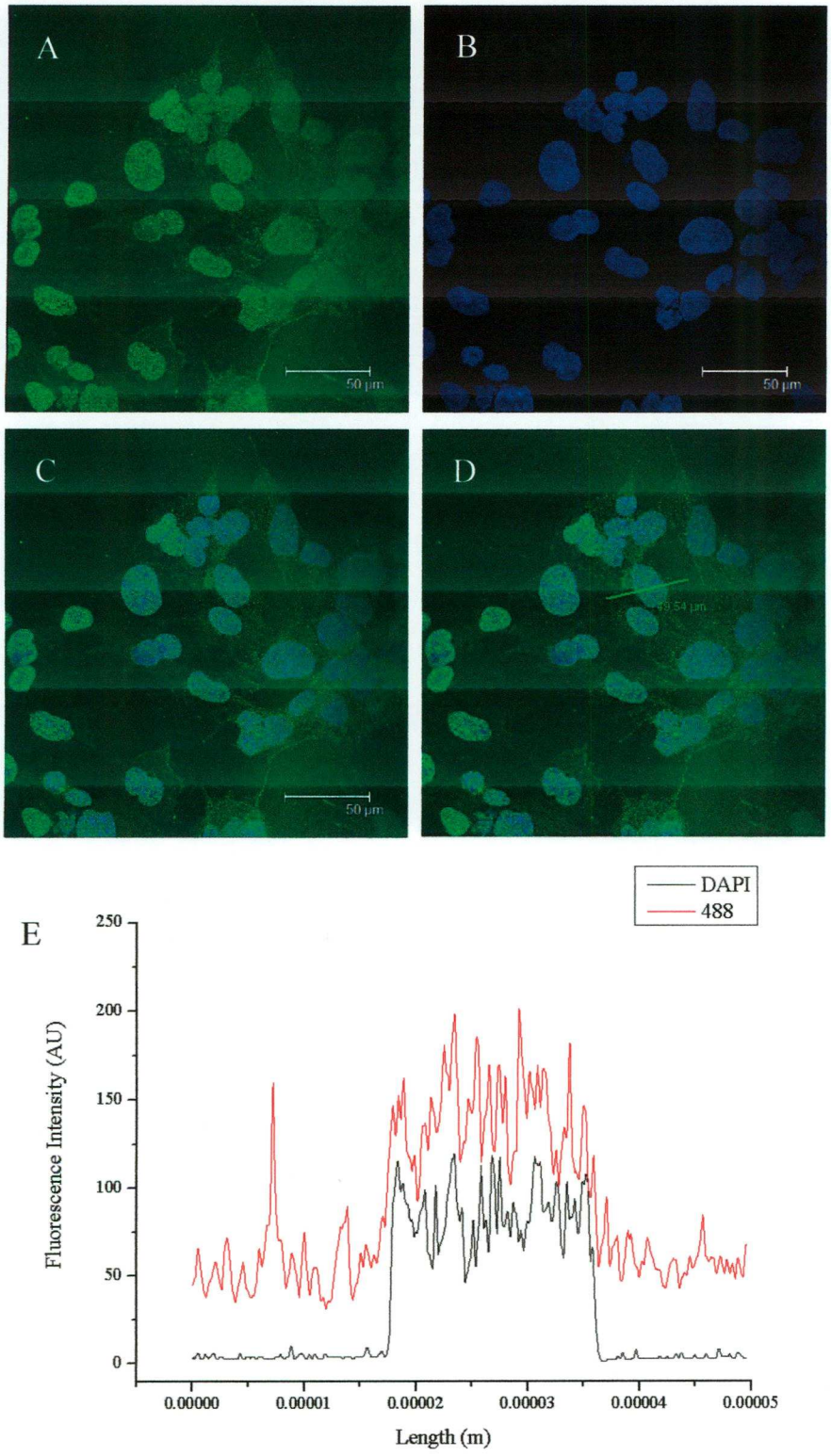

Figure 4.17. MA16 cells stained with primary antibodies against TREK-1. A) Alexa Fluor-488. B) DAPI. C) Overlaid image of Alexa Fluor-488 & DAPI. D) Sample taken for image analysis. E) Graph showing the intensity of staining along the sample line through the cell selected in D.

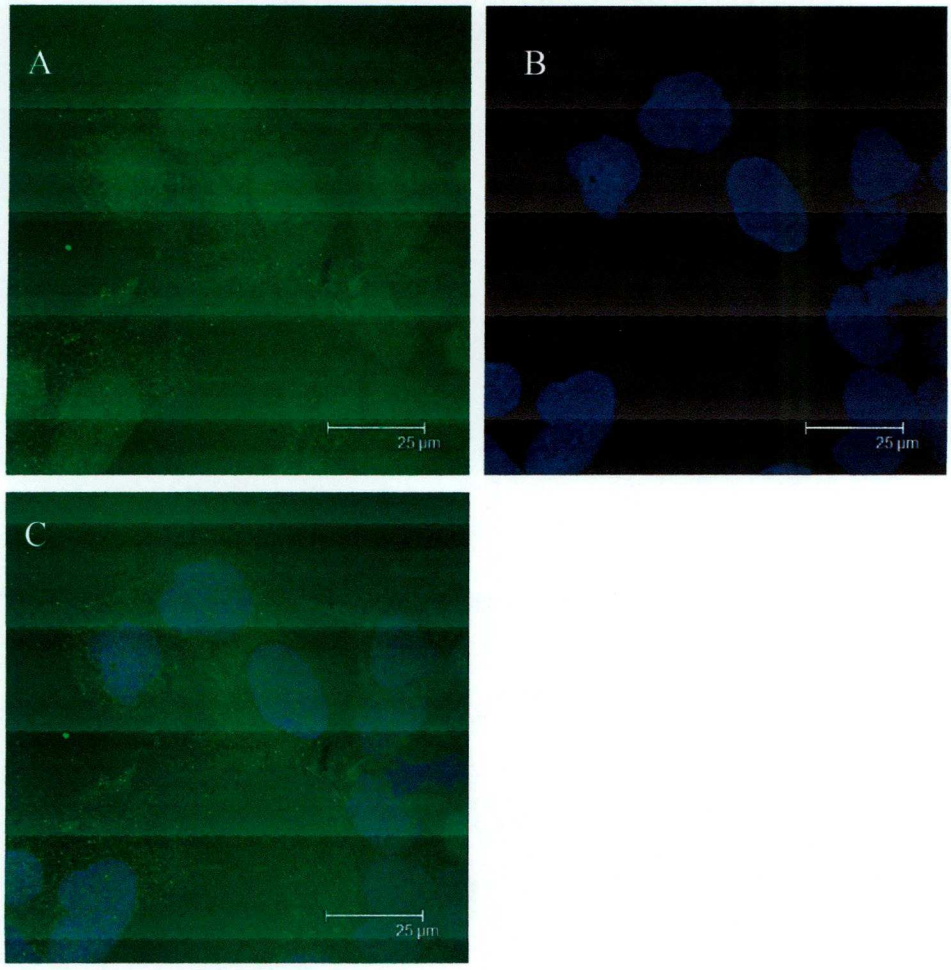

Figure 4.18. MA16 cells stained with primary antibodies against TREK-1 (2x zoom). A) Alexa Fluor-488. B) DAPI. C) Overlaid image of Alexa Fluor-488 & DAPI.

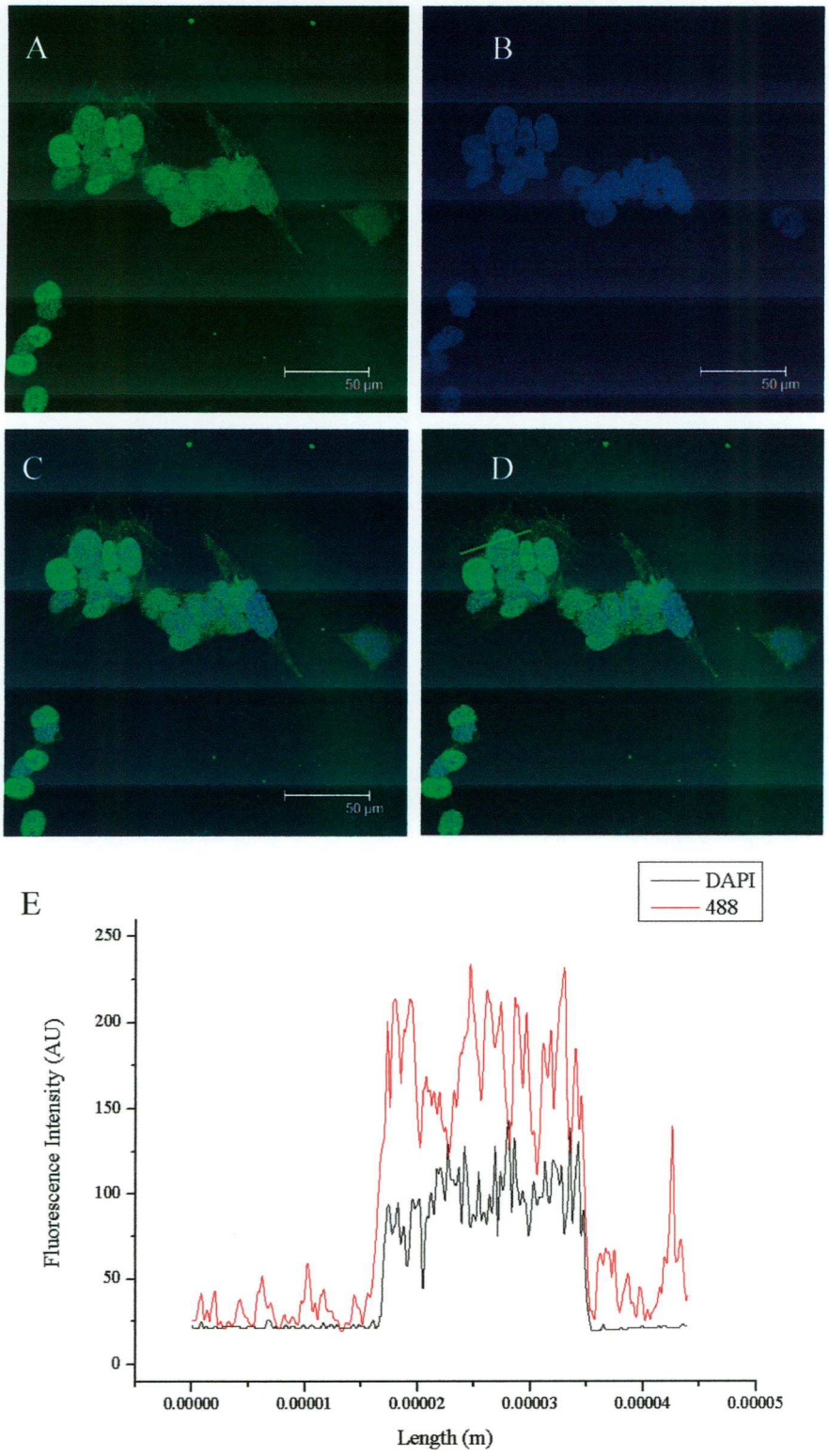

Figure 4.19. TE-85 cells stained with primary antibodies against TREK-1. A) Alexa Fluor-488. B) DAPI. C) Overlaid image of Alexa Fluor-488 & DAPI. D) Sample taken for image analysis. E) Graph showing the intensity of staining along the sample line through the cell selected in D.

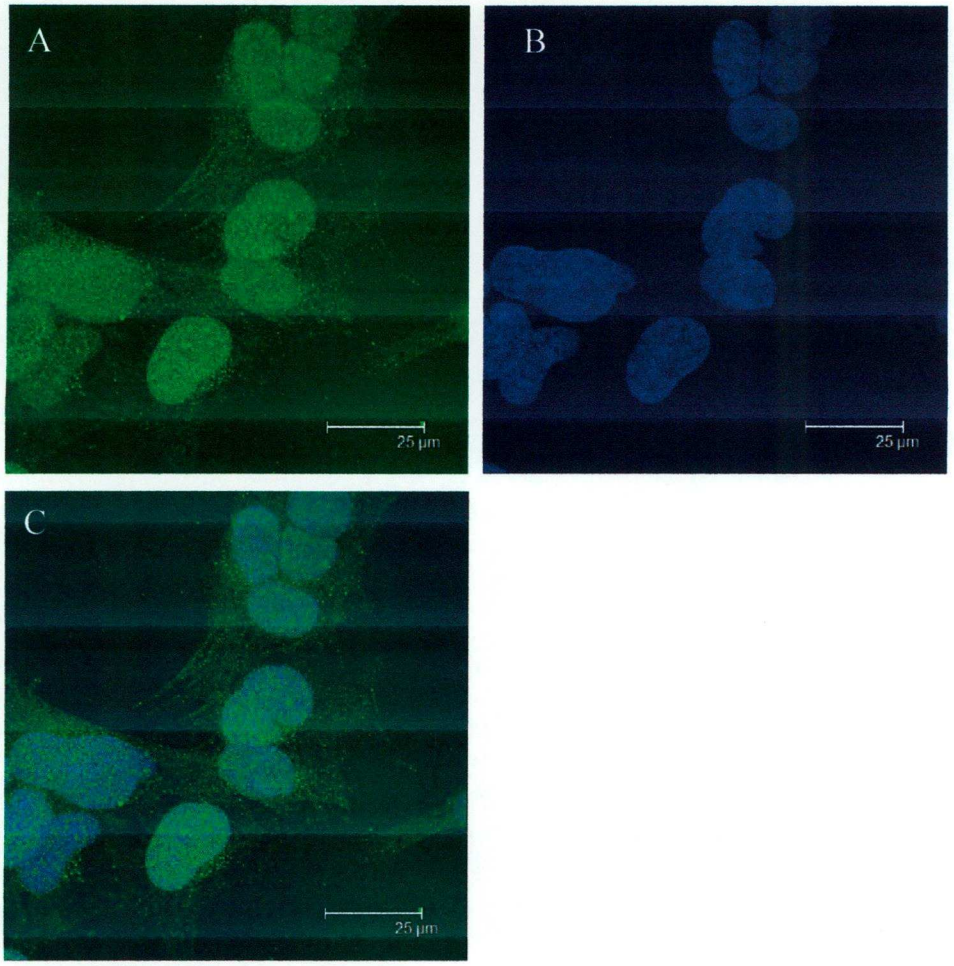

Figure 4.20. TE-85 cells stained with primary antibodies against TREK-1 (2x zoom). A) Alexa Fluor-488. B) DAPI. C) Overlaid image of Alexa Fluor-488 & DAPI.

4.3.6 Negative control

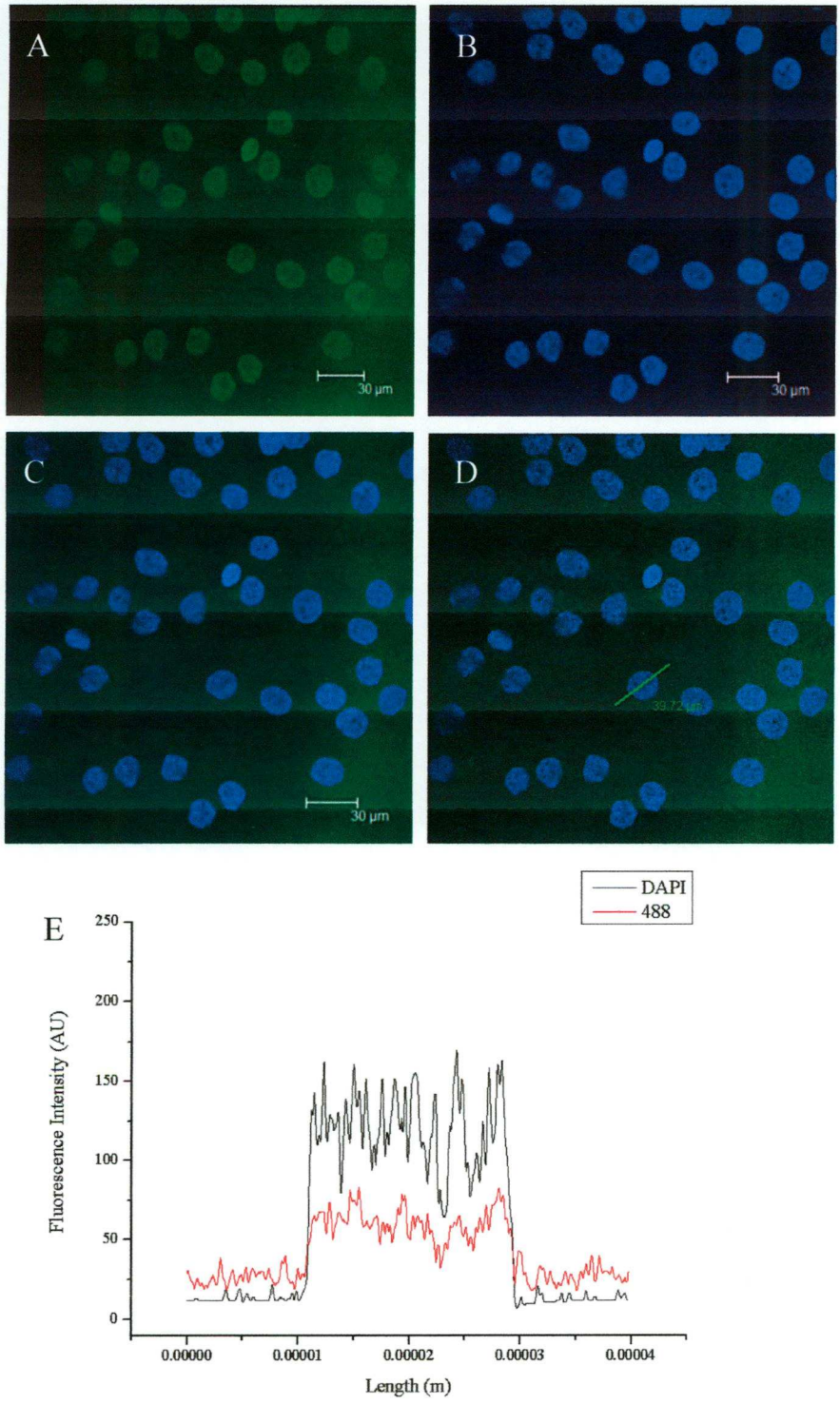

Figure 4.21. MG-63 cells with primary antibody omitted. A) Alexa Fluor-488. B) DAPI. C) Overlaid image of Alexa Fluor-488 & DAPI. D) Sample taken for image analysis. E) Graph showing the intensity of staining along the sample line through the cell selected in D.

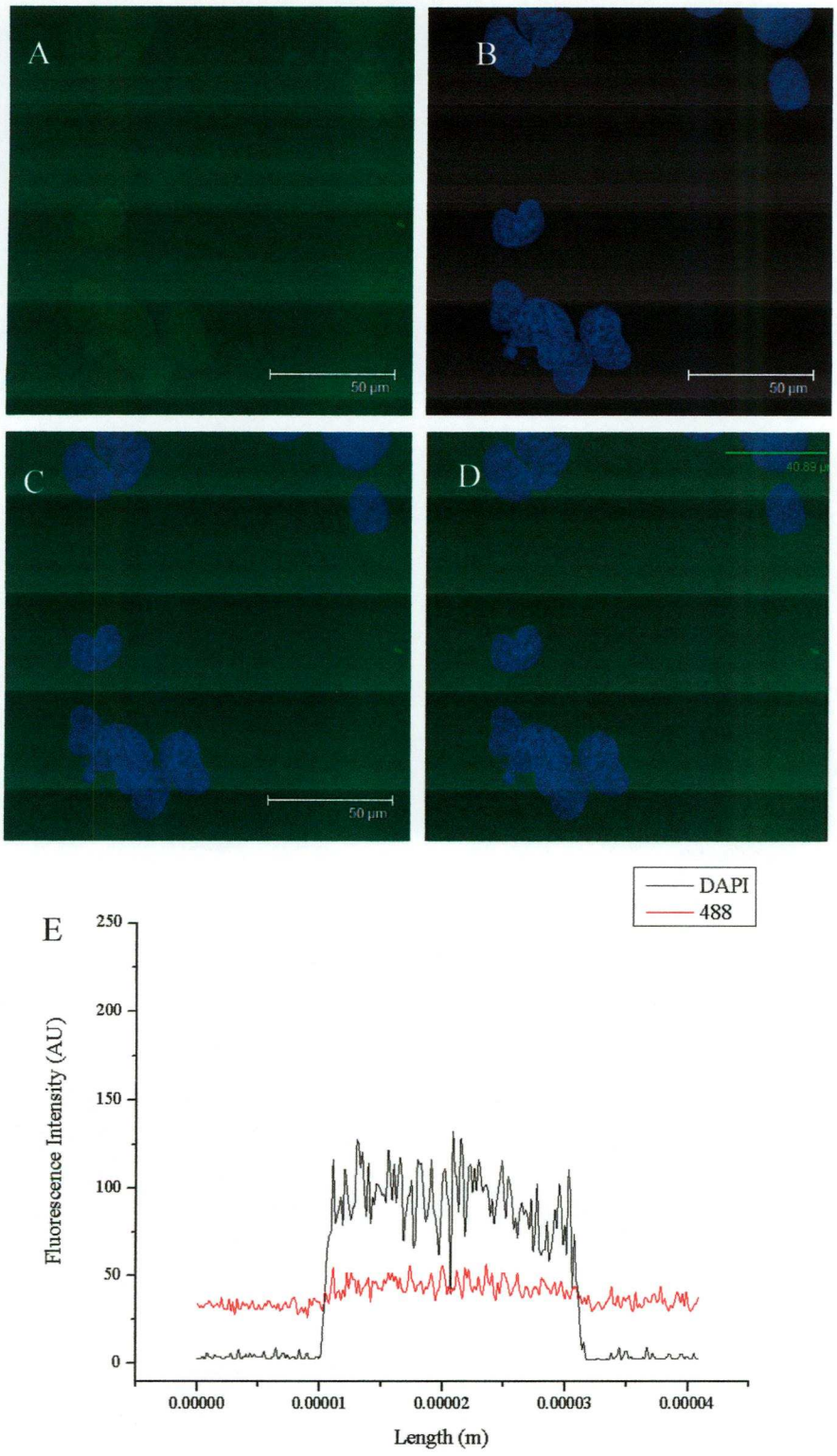

Figure 4.22. MA16 cells with primary antibody omitted. A) Alexa Fluor-488. B) DAPI. C) Overlaid image of Alexa Fluor-488 & DAPI. D) Sample taken for image analysis. E) Graph showing the intensity of staining along the sample line through the cell selected in D.

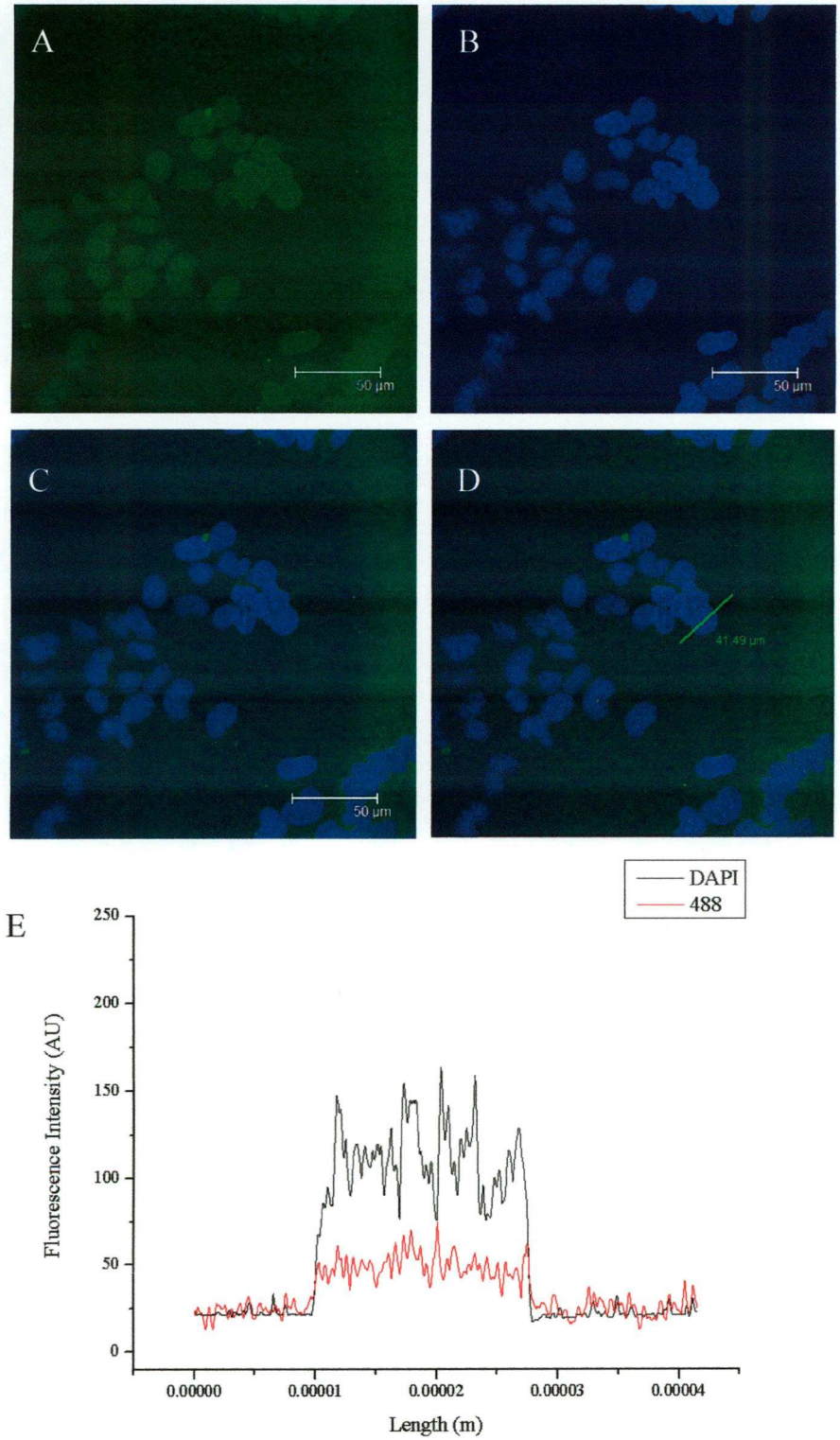

Figure 4.23. TE-85 cells with primary antibody omitted. A) Alexa Fluor-488. B) DAPI. C) Overlaid image of Alexa Fluor-488 & DAPI. D) Sample taken for image analysis. E) Graph showing the intensity of staining along the sample line through the cell selected in D.

No Alexa Fluor-488 staining was observed in any of the cell lines without primary antibody. A small amount of cross-talk between the fluorophores can be seen in the analysis of the staining along the sample lines in each of the three cell types. For brevity, only the images taken from MG-63 cells are shown in the control peptide experiments below. No staining was seen in any of the negative controls or experiments performed with the control peptides.

4.3.7 TASK-1 control peptide

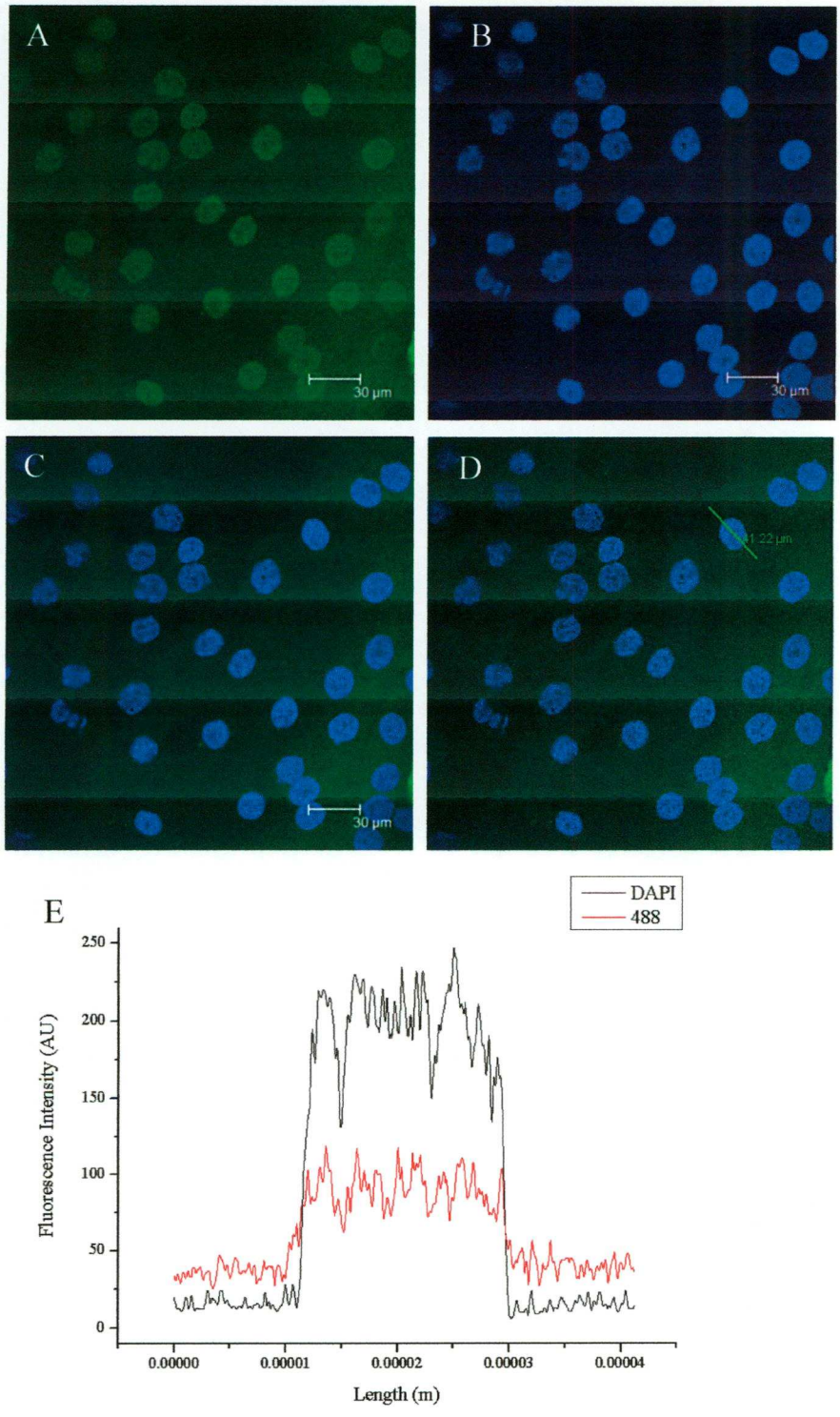

Figure 4.24. MG-63 cells exposed to anti-TASK-1 preincubated with a control peptide. A) Alexa Fluor-488. B) DAPI. C) Overlaid image of Alexa Fluor-488 & DAPI. D) Sample taken for image anaylsis. E) Graph showing the intensity of staining along the sample line through the cell selected in D.

4.3.8 TASK-2 control peptide

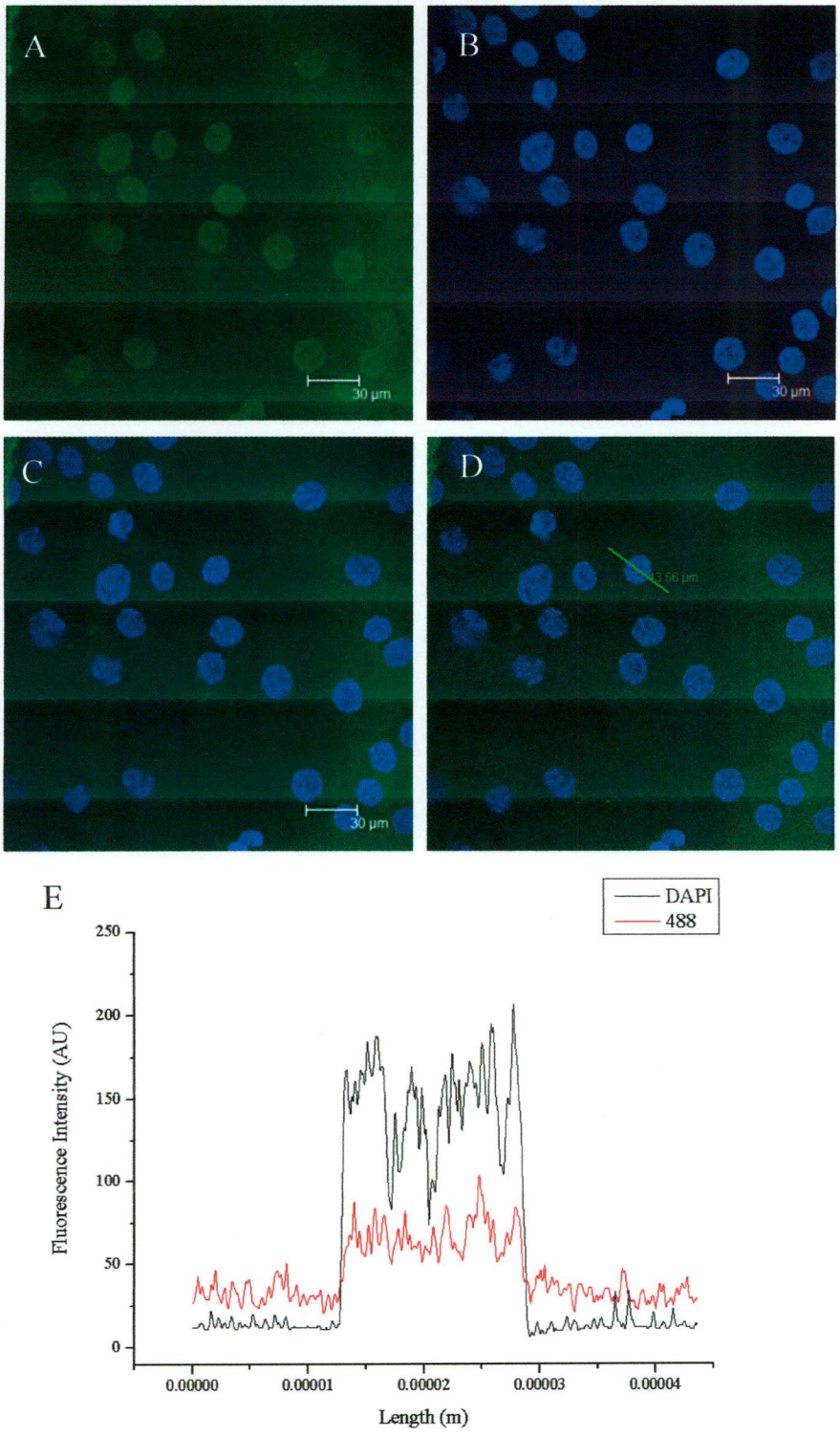

Figure 4.25. MG-63 cells exposed to anti-TASK-2 preincubated with a control peptide. A) Alexa Fluor-488. B) DAPI. C) Overlaid image of Alexa Fluor-488 & DAPI. D) Sample taken for image anaylsis. E) Graph showing the intensity of staining along the sample line through the cell selected in D.

4.3.9 TWIK-2 control peptide

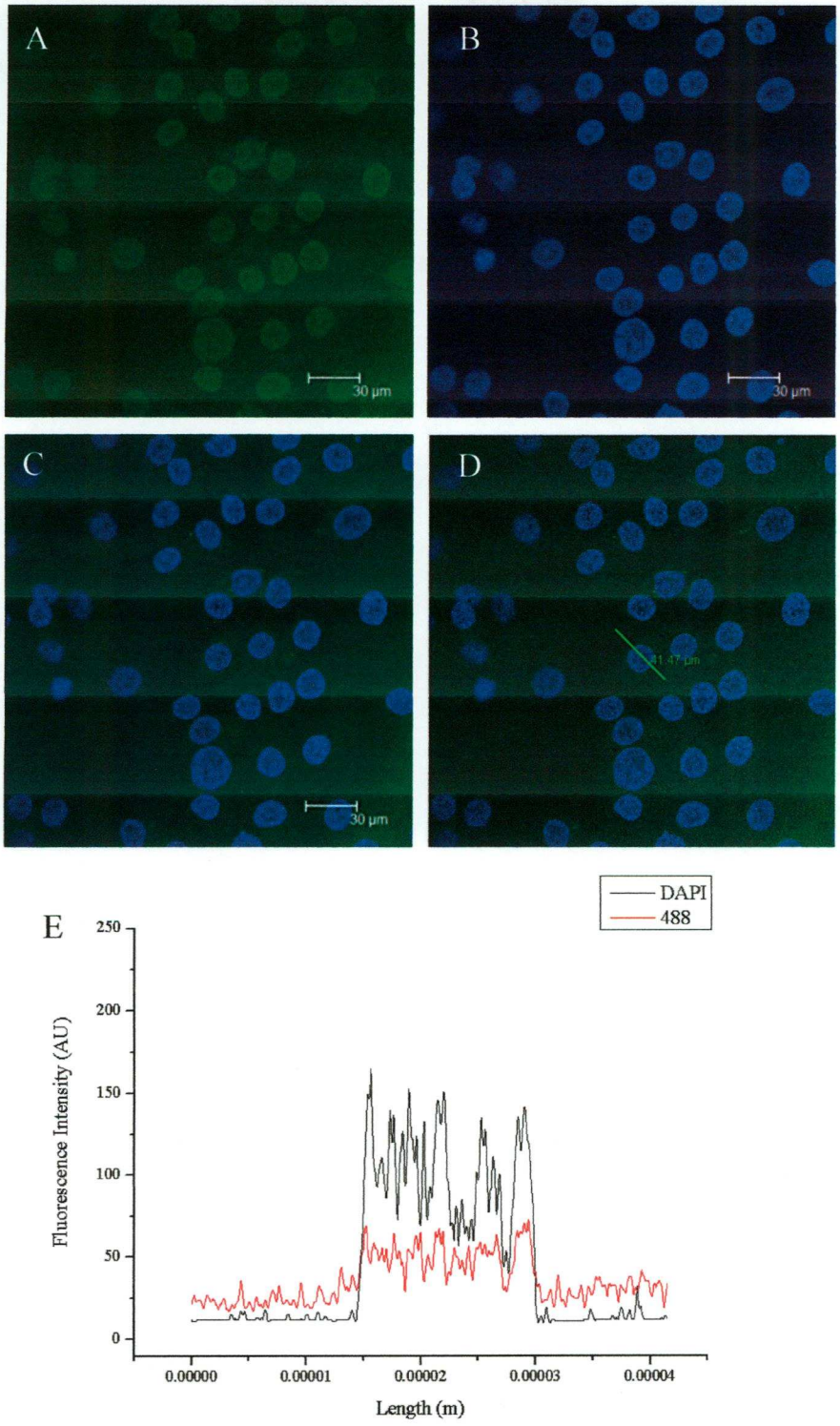

Figure 4.26. MG-63 cells exposed to anti-TWIK-2 preincubated with a control peptide. A) Alexa Fluor-488. B) DAPI. C) Overlaid image of Alexa Fluor-488 & DAPI. D) Sample taken for image anaylsis. E) Graph showing the intensity of staining along the sample line through the cell selected in D.

4.3.10 TRAAK control peptide

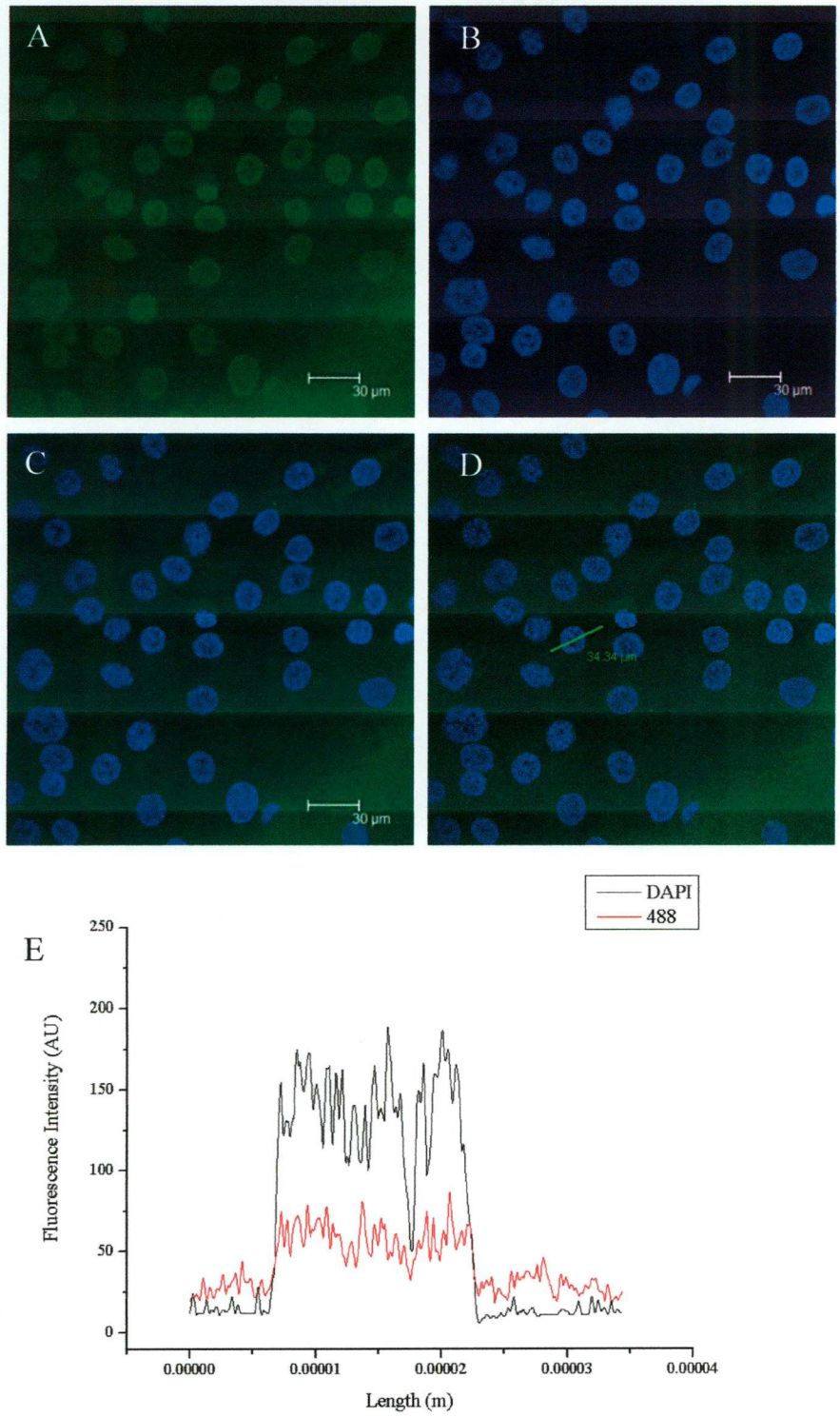

Figure 4.27. MG-63 cells exposed to anti-TRAAK preincubated with a control peptide. A) Alexa Fluor-488. B) DAPI. C) Overlaid image of Alexa Fluor-488 & DAPI. D) Sample taken for image anaylsis. E) Graph showing the intensity of staining along the sample line through the cell selected in D.

4.3.11 TREK-1 control peptide

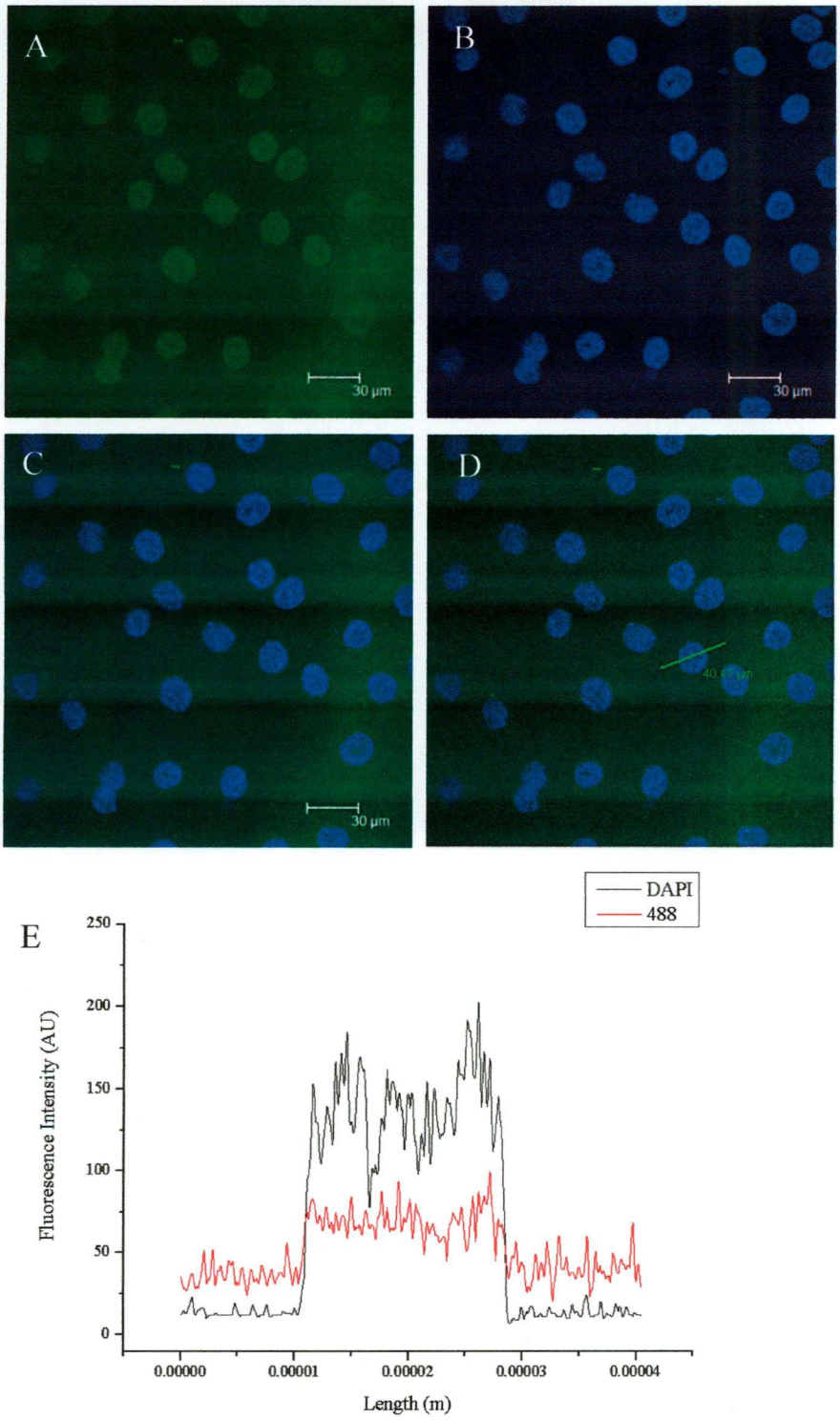

Figure 4.28. MG-63 cells exposed to anti-TREK-1 preincubated with a control peptide. A) Alexa Fluor-488. B) DAPI. C) Overlaid image of Alexa Fluor-488 & DAPI. D) Sample taken for image anaylsis. E) Graph showing the intensity of staining along the sample line through the cell selected in D

Table 4.2. Mean Signal Intensity (SI) and width values for K_{2P} channel staining in the nuclear region of osteoblastic cell-types (n=5). SI values have arbitrary units (Data is expressed ± SEM).

	MG-63	MG-63	TE-85	TE-85	MA16	MA16
Antibody	Mean SI over nuclear region	Mean width over nuclear region (μm)	Mean SI over nuclear region	Mean width of nuclear region (μm)	Mean SI over nuclear region	Mean width over nuclear region (μm)
TASK-1	123.1 ± 3.5	17.0 ± 0.8	62.9 ± 4.5	13.2 ± 1.0	69.1 ± 1.3	16.6 ± 1.2
TASK-2	178.1 ± 7.1	18.3 ± 1.0	90.0 ± 7.1	18.8 ± 0.7	81.0 ± 8.7	17.0 ± 1.5
TWIK-2	146.0 ± 8.7	19.2 ± 0.5	61.0 ± 5.3	22.9 ± 1.2	86.9 ± 6.3	22.7 ± 1.7
TRAAK	199.0 ± 1.8	19.8 ± 0.6	137.1 ± 10.7	19.7 ± 0.9	88.5 ± 3.7	23.9 ± 1.7
TREK-1	220.7 ± 3.1	17.6 ± 0.6	166.4 ± 18.2	20.9 ± 2.1	118.8 ± 5.7	24.8 ± 2.8
NO PRIMARY	69.5 ± 3.8	17.0 ± 0.6	14.5 ± 1.6	16.2 ± 0.9	42.1 ± 0.9	17.5 ± 1.4
TASK-1 CP	84.5 ± 3.3	17.8 ± 0.5	59.3 ± 3.7	18.7 ± 1.2	59.1 ± 3.2	21.6 ± 2.2
TASK-2 CP	66.1 ± 1.6	18.7 ± 0.9	41.4 ± 3.3	18.3 ± 1.0	58.0 ± 2.8	20.5 ± 2.0
TWIK-2 CP	50.9 ± 2.2	16.5 ± 0.7	38.8 ± 1.2	18.7 ± 0.2	54.5 ± 1.3	20.67 ± 0.9
TRAAK CP	55.0 ± 1.5	16.6 ± 0.5	42.9 ± 2.3	19.8 ± 1.1	50.5 ± 1.3	20.2 ± 1.3
TREK-1 CP	65.7 ± 2.8	17.4 ± 0.7	34.8 ± 2.6	21.3 ± 1.1	42.0 ± 0.9	18.9 ± 1.3

Table 4.3. Mean Signal Intensity (SI) and width values for K_{2P} channel staining outside the nuclear region, with the mean distance from the nucleus (Data is expressed ± SEM) (n=5).

Cell Type	Antibody	Mean SI of extranuclear peaks	Mean width of extranuclear peaks (μm)	Mean distance from the nucleus (μm)
TE-85	TASK-2	71.1 ± 12.8	1.4 ± 0.4	8.5 ± 3.8
TE-85	TWIK-2	65.6 ± 6.7	3.5 ± 0.9	3.4 ± 1.0
TE-85	TRAAK	79.6 ± 6.6	2.5 ± 0.4	3.1 ± 0.6
TE-85	TREK-1	66.2 ± 3.6	2.5 ± 0.5	4.9 ± 1.6
MA16	TREK-1	79.3 ± 3.6	3.3 ± 0.7	6.2 ± 1.3
MG-63	TWIK-2	70.9 ± 2.0	1.0 ± 0.1	4.7 ± 0.6
MG-63	TRAAK	108.4 ± 5.6	1.5 ± 0.1	5.2 ± 1.0
MG-63	TREK-1	108.5 ± 2.9	1.1 ± 0.1	8.0 ± 1.5

4.4 Results: Western Blotting

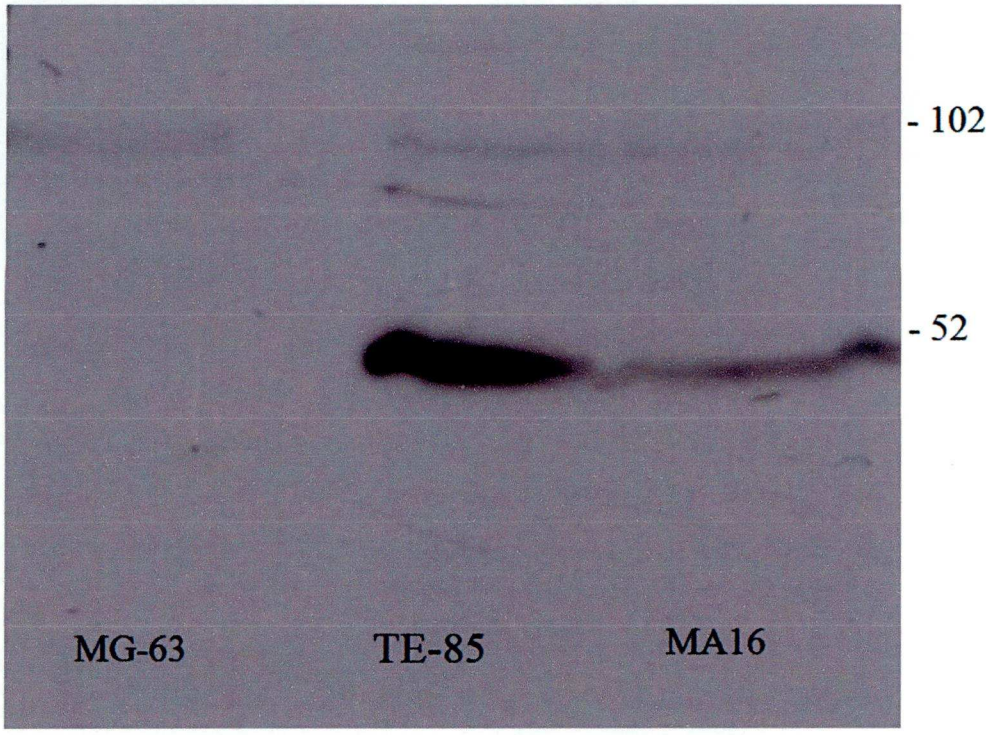

Figure 4.29. Western blot of cell proteins targeted with an antibody against TASK-1. Performed under reducing conditions with 1% skimmed milk powder. The blot was exposed to the photographic film for 1 minute.

Figure 4.29 shows protein extract from MG-63, TE-85 and MA16 cells screened with an antibody against TASK-1. Bands for TASK-1 appear strong in the lanes containing protein extract from TE-85 and MA16 cells at around the level of 50kDa. There appear to be bands at approximately dimer weight in all lanes, including a faint band in the MG-63 extract.

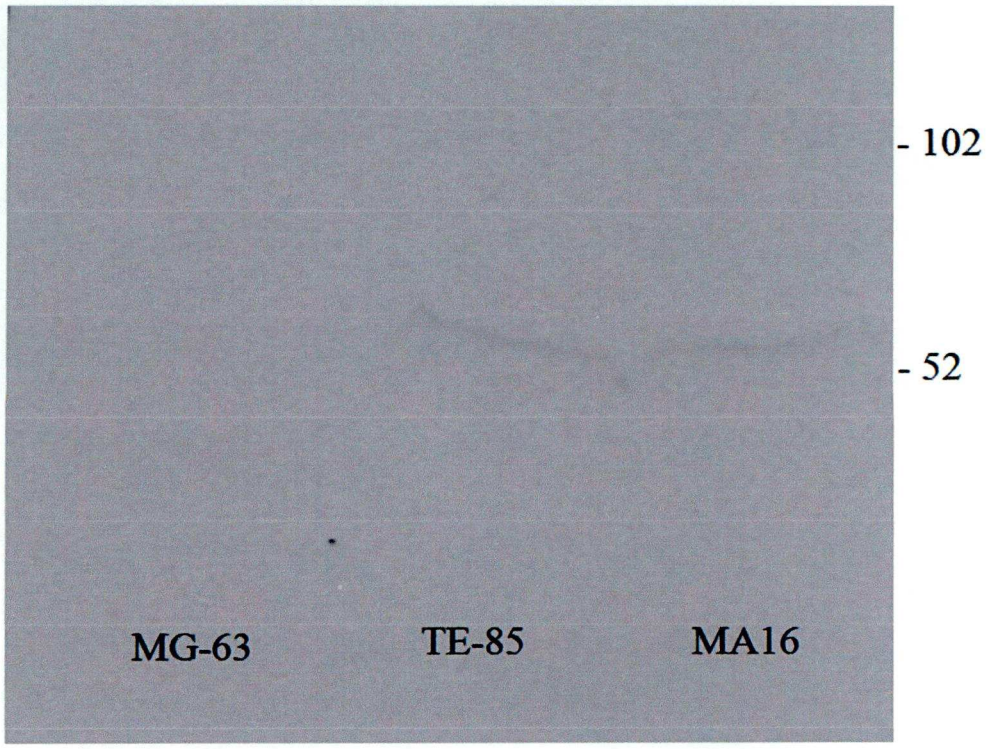

Figure 4.30. Western blot of cell proteins targeted with an antibody against TASK-2. Performed under reducing conditions with 1% skimmed milk powder. The blot was exposed to the photographic film for 5 minutes.

Figure 4.30 shows a western blot performed against the TASK-2 channel protein. The weight of the rather weak bands in MA16 & TE-85 lanes is approximately 57kDa. No bands can be seen in the lane containing MG-63 protein extract, even with a more prolonged exposure period (data not shown).

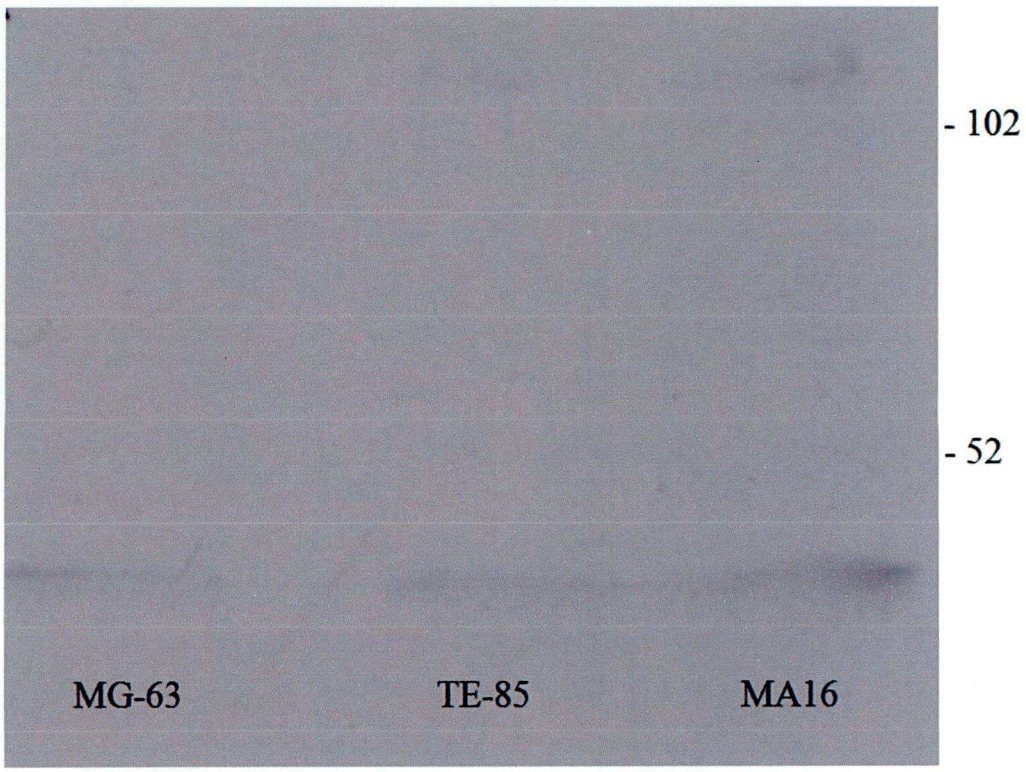

Figure 4.31. Western blot of cell proteins targeted with an antibody against TWIK-2. Performed under non-reducing conditions with 1% skimmed milk powder. The blot was exposed to the photographic film for 5 minutes.

Some very weak staining can be observed in Figure 4.31, which shows protein extract from MG-63, TE-85 and MA16 cells screened with an antibody against TWIK-2. The staining appears to be at the upper and lower extremities of the blot, with two faint bands seen at above the level of 100kDa and a band in each lane below the level of 50kDa.

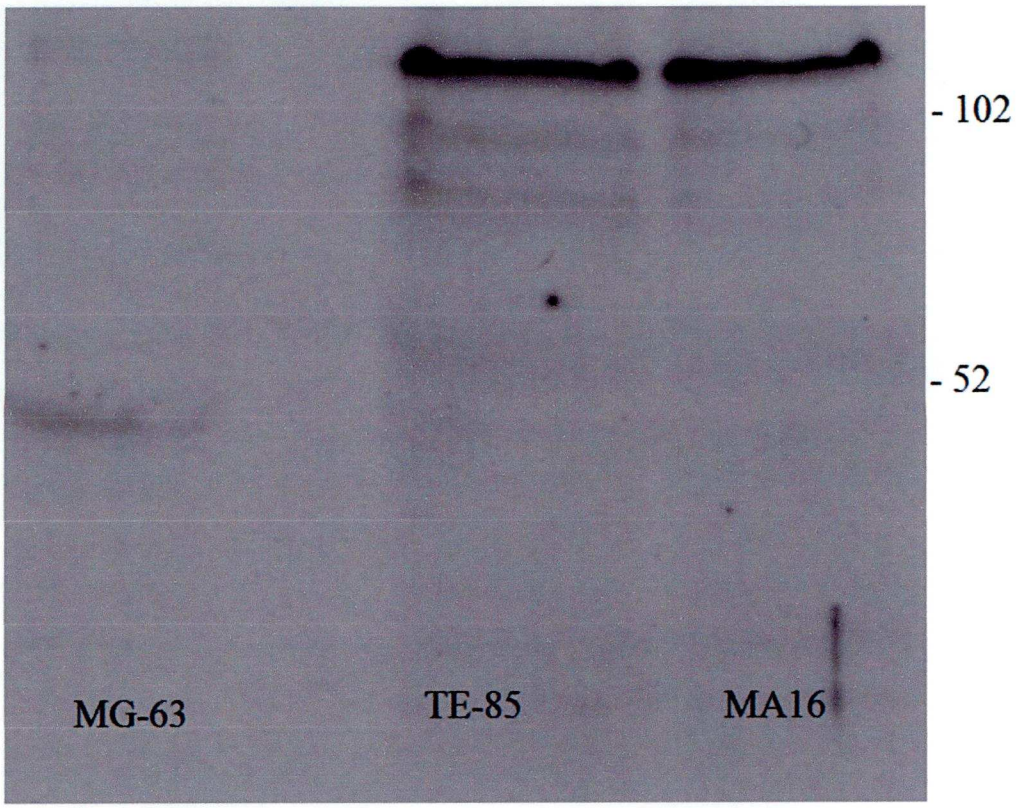

Figure 4.32. Western blot of cell proteins targeted with an antibody against TRAAK. Performed under non-reducing conditions with 1% skimmed milk powder. The blot was exposed to the photographic film for 5 minutes.

Anti-TRAAK targeted against osteoblast cell proteins revealed a band at ~52kDa in MG-63 protein extract. Multiple bands at a variety of weights between 110kDa and 40kDa can be seen in the lanes containing MA16 and TE-85 proteins. However, a band giving very intense staining appears at around 110kDa for TE-85 and MA16.

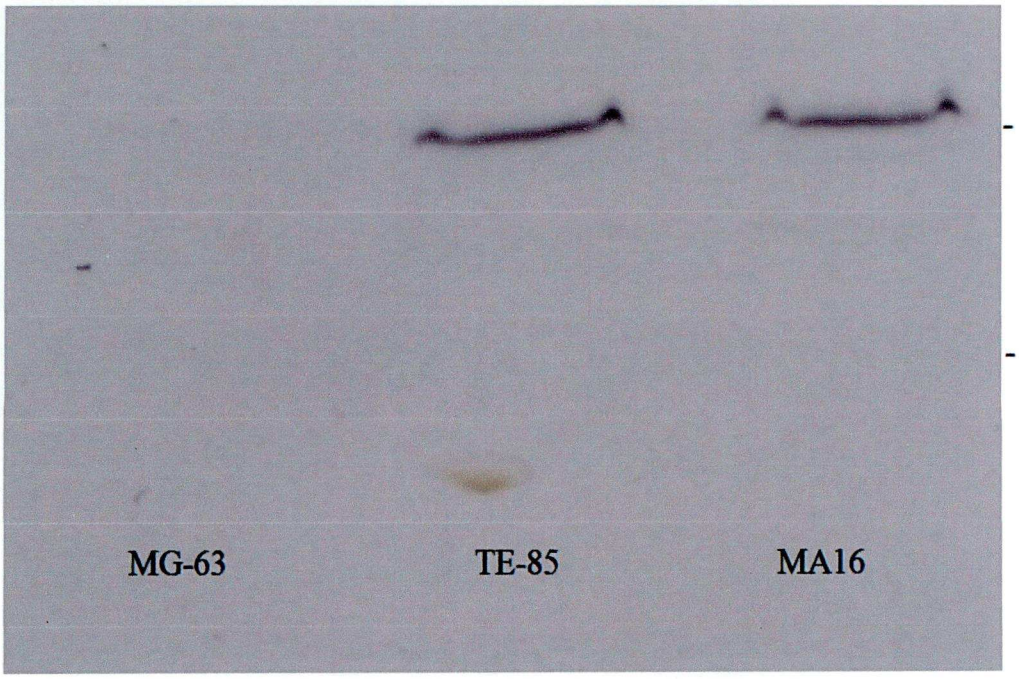

Figure 4.33. Western blot of cell proteins targeted with an antibody against TREK-1. Performed under non-reducing conditions with 1% skimmed milk powder. The blot was exposed to the photographic film for 10 minutes.

Western blotting of osteoblastic cell lysate with anti-TREK-1 revealed two narrow but intense bands at approximately 105kDa for TE-85 and MA16. No other bands can be observed in the lanes containing these protein extracts, and the MG-63 lane appears empty, despite the lengthy exposure of the blot to the film.

4.5 Discussion

The aim of this chapter was to look for protein expression of K_{2P} channels in osteoblastic cells using commercially available antibodies. Immunocytochemistry gave a visual indication of the abundance and localisation of the protein whereas western blotting confirmed the presence of the protein using a different technique. TWIK-2, TRAAK and TREK-1 appeared to reach the plasma membrane and showed strong staining in all three cell lines. TASK-2 stained to a lesser extent and was more variable between cell types. TASK-1 displayed very weak perinuclear staining in all cell lines studied. Negative controls and control peptide staining were clean. However, they did show that there was some cross-over from the nuclear DAPI signal into the Alexa Fluor-488 signal. Western blotting proved helpful for TASK-1 & -2 as these results showed straightforward single bands at the expected weight. Bands for TRAAK & TREK-1 indicated the dimerisation of these proteins. The blot for TWIK-2 was confusing, but immunocytochemistry staining was relatively strong for this channel.

4.5.1 Immunocytochemistry

TASK-1 gave a weak signal that appeared to be in close proximity to the nucleus in all three cell lines observed. In MG-63 cells there did appear to be some weak staining in the cytoplasm. This may suggest that although mRNA and protein may be present in osteoblastic cells, the channel is not trafficked to the plasma membrane, or if it is, it is present in very small amounts. TASK-2 presents a similar story to its relative TASK-1, however in MG-63 and TE-85 cells, there appeared to be some weak staining outside the nuclear region. TWIK-2 staining in MA16 cells is similar to that of TASK-1 in the same cell type, but perhaps slightly stronger and more diffuse. TWIK-2 signal from TE-85 cells shows an intense area of staining in the perinuclear region, but also defines the outline of the cell through what appears to be a signal coming from the membrane. Based on these results, it does seem as though functional activity of TWIK-2 would be likely in TE-85 cells. When stained for TRAAK, all cells displayed concentrated perinuclear staining. In MG-63 and TE-85 cells, the overall shape of the cells was defined due to staining in the cell processes. This gives a good indication

that TRAAK channels are trafficked to the plasma membrane. This was not the case for MA16 cells, where the only staining remained close to the nucleus again. With TREK-1 staining, the cell processes became clearly visible and there did not appear to be any perinuclear staining. The TREK-1 antibody gave what appears to be the clearest indication yet of localising in the plasma membrane, this time in all cell types; supporting the hypothesis that TREK-1 channels are involved with the actin cytoskeleton (Lauritzen *et al.*, 2005). Negative controls and antibodies that were added with control peptides did not show any staining, indicating the absence of false-positives. Hughes *et al.* (2006) only used TREK-1 antibodies in their immunohistochemical study. The pattern of staining they observed was similar to that seen here in section 4.3.5. This is the only comparison available from osteoblastic studies within the current literature.

Looking into the width of a staining pattern should give a reliable guide as to the type of staining i.e. nuclear (broad), organellar (intermediate) or membranous (narrow). Most antibodies screened produced positive signals in the perinuclear region. The width of these signals showed a collection of very narrow peaks towards the higher intensities, and a broad band underneath which roughly corresponded with the DAPI signal. For TREK-1, and to some extent TASK-2, TRAAK and TWIK-2, the staining appeared to be more independent of the nuclear region. A Z-series scan could enable us to prove that the 488 signal is in fact lying in a narrow plane around the nucleus, rather than throughout the nucleus as it might appear on a 2D image. The process of fixing and permeabilisation is bound to affect cellular morphology. For some of the more diffuse staining appearing around the nucleus, it may be possible that the cell membrane is brought into closer proximity to the nucleus through reduced cytoplasmic volume, making it seem as though there is staining in the nucleus itself when assessing a 2D image. As for why the signal might be congregating close to the nuclear area, it is possible that the antibody is binding to a channel still in the protein synthesis pathway. There is no reason why these antibodies could not have the ability to stain the protein present in the rough endoplasmic reticulum (rER) or even in the Golgi apparatus. Both these organelles are situated in close proximity to the nucleus. The issue of staining in the nuclear region is exacerbated by some cross-talk between the two fluorescent stains used. This is

clearly evidenced by the images seen using the control peptides, and by the resulting cross sections taken through stained cells. In the graphs shown corresponding to the control peptide images, a small and even rise in Alexa Fluor-488 signal is observed over the nucleus. Ion channels have been shown to be present within the nuclear membrane, mainly to aid in the transduction of Ca^{2+} signals into the nucleus (Bkaily *et al.*, 2006, Gobeil *et al.*, 2002). Ion channels are also present in organellar cell membranes other than the nucleus (Dêbska *et al.*, 2001). Other types of K^+ channel have been shown to be present in osteoblast intracellular organelles through the use of electron microscopy (Butler *et al.*, 2010). It would be difficult to assign a possible role to K_{2P} channels present inracellularly, given that they mostly seem to be involved in transducing extracellular stimuli into membrane potential changes and in the case of mechanosensitive TREK-1 channels, are involved with the actin cytoskeleton (Lauritzen *et al.*, 2005).

4.5.2 Western Blotting

None of the blots shown in Section 4.4 revealed any strong staining from the MG-63 cells. This could be addressed by either preparing a fresh sample of protein extract then retesting the sample, or from running a positive control antibody such as GAPDH or actin against the MG-63 sample used above. Bands for TASK-1 appear strong in the lanes containing protein extract from TE-85 and MA16 cells at around the level of 50kDa. There appear to be bands at approximately dimer weight for all three extracts. For the western blot performed against TASK-2, the weight of bands in MA16 & TE-85 lanes is ~57kDa. Beckett *et al.*, (2008) recorded bands for TASK-1 & -2 on western blots at around the 50kDa level which agrees with the data shown in Figures 4.29 & 4.30. Staining with the TWIK-2 antibody was faint, and bands did not appear at the expected weight. In their datasheet, Alomone Labs show a western blot of rat brain membranes with 2 distinct molecular weight bands. The smaller weight is approximately 48kDa and the heavier weight band is around 88kDa. The blot for TWIK-2 seen in this chapter does not appear to correspond to the one shown in the antibody datasheet. Anti-TRAAK targeted against osteoblast cell proteins revealed a band at ~52kDa in MG-63 protein extract which corresponds with the

example given in the antibody datasheet. Multiple bands can be seen in the lanes containing MA16 and TE-85 proteins, but the heaviest band appears to be around dimer weight. Because multiple bands were seen for anti-TRAAK, a protein BLAST search was run against the epitope of the antibody (http://blast.ncbi.nlm.nih.gov/Blast.cgi). No obvious result other than the target was revealed. Western blotting of osteoblastic cell lysate with anti-TREK-1 revealed two narrow but intense bands at dimer weight for TE-85 and MA16. Hughes *et al.* (2006) performed immunocytochemistry against TREK-1 channels in osteoblasts using antibodies from Alomone Labs, yet the same paper used antibodies produced by Santa Cruz for western blotting. The authors do not explain their reasons for this, but presumably the respective antibodies gave the best results for the method they were selected for. Since the experiments for this thesis were performed, more antibodies for K_{2P} channels have become available. Alomone Labs now provide a more complete range of antibodies against some of the less well studied proteins such as THIK-1 & TRESK as well as TWIK-1 & TREK-2. Although to date only Hughes *et al.* (2006) have published K_{2P} western blotting data from osteoblasts, others have shown the presence of different members of K^+ channel family in this cell type (Moreau *et al.*, 1997, Hernandez *et al.*, 2007).

4.6 Conclusions

In this Chapter, osteoblastic cells were screened for protein expression of selected K_{2P} channels using immunocytochemistry and western blotting. Protein was observed for all the K_{2P} channels studied in varying quantities. The most striking and promising result is that for TREK-1, which was strongly positive in all cell lines using immunocytochemistry and showed clear evidence of localising to the plasma membrane. The results obtained using the anti-TRAAK antibody were also positive, but western blotting revealed the possibility of non-specific binding: a suspicion that was refuted upon a protein BLAST search using the epitope sequence. TWIK-2 and TASK-2 appeared to be expressed in moderate amounts, particularly in TE-85 and MG-63 cells although the bands for the corresponding western blots were weak in comparison. Anti-TASK-1 gave a small amount of immunochemical staining which did not appear to reach the plasma membrane. There were some discrepancies between the techniques, for example a strong cellular signal for TWIK-2 did not complement the weak staining obtained using western blotting. Conversely, anti-TASK-1 gave strong bands at the correct weight in the western blot but weak staining in the immunocytochemistry. Overall the results supported the data from Chapter 3, which confirmed mRNA expression of members of the TASK, TALK, TWIK and TREK families. This data in the current Chapter shows that the mRNA expression observed previously is successfully translated into protein which is able to reach the plasma membrane.

5.0 Effects of K^+ and Ca^{2+} Channel Agents on Osteoblastic Markers

5.1 Introduction

C-fos is a proto-oncogene found in many cell types. It is an immediate early gene which encodes the transcription factor Fos. Fos heterodimerizes with members of the Jun family of transcription factors to form a complex known as AP-1. C-fos expression can be induced by rises in intracellular Ca^{2+} or cAMP. Upon Ca^{2+} entry into a cell through L-type Ca^{2+} channels, cAMP response element binding protein (CREB) becomes phosphorylated at serine 133. Transactivation of the promoter cAMP response element (CRE) by phosphorylated CREB, results in the initiation and elongation of c-fos transcription (Thompson *et al.*, 1995). The increase in fos subsequently increases AP-1 transactivation which has downstream effects on osteoblast differentiation and function. Fos expression is also important for osteoclast function. Fos -/- mice exhibit osteopetrosis due to impaired osteoclast differentiation (Grigoriadis *et al.*, 1995). In contrast, mice over-expressing the c-fos gene develop osteosarcomas. C-fos measurement is often used in osteoblasts to study the cellular response to PTH. See Chapter 1 for an overview on the effects of PTH on c-fos expression.

Many of the agents used in this Chapter are K^+ channel openers (KCOs) and K^+ channel blockers (KCBs). Opening of K^+ channels results in potassium efflux and subsequent hyperpolarisation. Closure of these channels prevents potassium efflux and may contribute to a depolarization. Calcium channel agents used in these experiments target L-type voltage-gated Ca^{2+} channels. Blockade of these channels prevents Ca^{2+} influx during a depolarization resulting in downstream effects on secretion and gene transcription.

5.2 Methods

The reporter cells described in this chapter were transfected with the full c-fos promoter linked to the luciferase gene. If c-fos expression was induced then there was more luciferase present in the cell with which to catalyse the transformation of luciferin substrate into oxyluciferin. A useful by-product of this reaction is the emission of light. This allows c-fos induction to be determined by the amount of light produced by the cell lysate upon addition of the substrate. The following equation summarizes the reaction (Promega technical bulletin, TB281):

$$\text{Luciferin} + O_2 + \text{ATP} \xrightarrow[Mg^{2+}]{\text{Firefly luciferase}} \text{Oxyluciferin} + \text{AMP} + PP_i + CO_2 + \text{Light}$$

For the assay, cells were seeded in 96-well luminometric plates and left to settle for 24 hours. The following day, the medium was changed to serum-free and the cells were left overnight. On the day of the assay, solutions were freshly prepared and the cells were exposed to the treatments in serum-free medium for 4 hours. Following the treatment time, the medium was removed and the cell layer was washed with 1X PBS. 1X lysis reagent was then added to each well and left at RT for 15 minutes before the plate was stored at -80°C overnight, allowing for a freeze-thaw cycle to aid cell lysis. Plates were fully defrosted at RT before being read in the luminometer (LUCY 1, Labtech Int).

Cells for use in alkaline phosphatase assays were seeded into 24-well plates a day prior to the experiment, and left to settle overnight. The following day, treatments were added to the cells and plates were incubated for 24hrs. Medium was then removed and the cell layer was lysed and frozen. Both samples were assayed using a kit from Pierce. For calcium imaging, cells were grown on glass coverslips and loaded with Fura-2AM. Recordings of intracellular calcium were made in response to the addition of PTH and ATP.

5.3 Results

5.3.1 Traditional and putative potassium channel modulators

The specific aim of the experiments in this Chapter was to see if K^+ channel modulators could in any way affect the expression of the immediate early gene c-fos or ALP levels in osteoblastic cells. In order to answer this query, a preliminary experiment was designed to investigate the effects of several compounds known for their ability to alter K^+ channel function. Observations were made on both basal and elevated c-fos levels in stably transfected SaOS-2 reporter cells. Generic KCBs barium and TEA were used along with TREK-1 activators BL-1249 ((5,6,7,8-tetrahydro-naphthalen-1-yl)-[2-(1H-tetrazol-5-yl)-phenyl]-amine) and riluzole. Pinacidil opens K_{ATP} channels and relaxes vascular smooth muscle at 10μM (Quayle *et al.*, 1995). BL-1249 was used at 10μM concentration as its EC_{50} was calculated as 1-2μM by Tertyshnikova *et al.*, (2005) and was shown to activate TREK-1 in unpublished observations from this laboratory. 10 - 100μM riluzole also activates TREK-1 channels (Duprat *et al.*, 2000). 0.1mM Barium and 1mM TEA have been used for decades to block various K^+ channels (Hille, 2001).

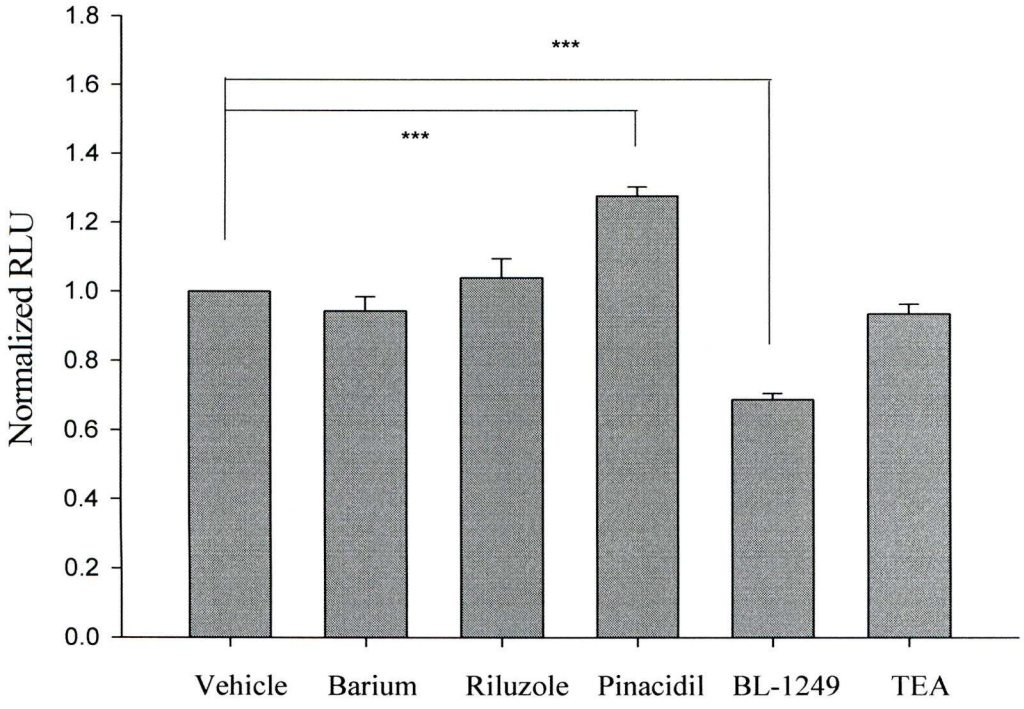

Figure 5.1. Preliminary data which show the effects of various K^+ channel modulators on basal c-fos expression in SaOS-2 cells (n=6-9). Concentrations used were; 0.1mM barium chloride, 10μM riluzole, 10μM pinacidil, 10μM BL-1249 and 1mM TEA. Error bars represent S.D.

The only significant differences compared with vehicle-treated control cells came from the wells treated with 10μM pinacidil and 10μM BL-1249 (both $P<0.001$). Exposure to pinacidil resulted in a 28% increase in c-fos expression over basal levels whereas BL-1249 treatment gave a 31% reduction. To see if BL-1249 could maintain this effect during a physiological elevation of c-fos expression, its effects were then assessed in conjunction with 0.5nM PTH (1 – 34). Evans *et al.* (1996) report that PTH (1 – 34) in the nanomolar to millimolar range activates c-fos gene transcription via PKA-dependent signalling in SaOS-2 cells.

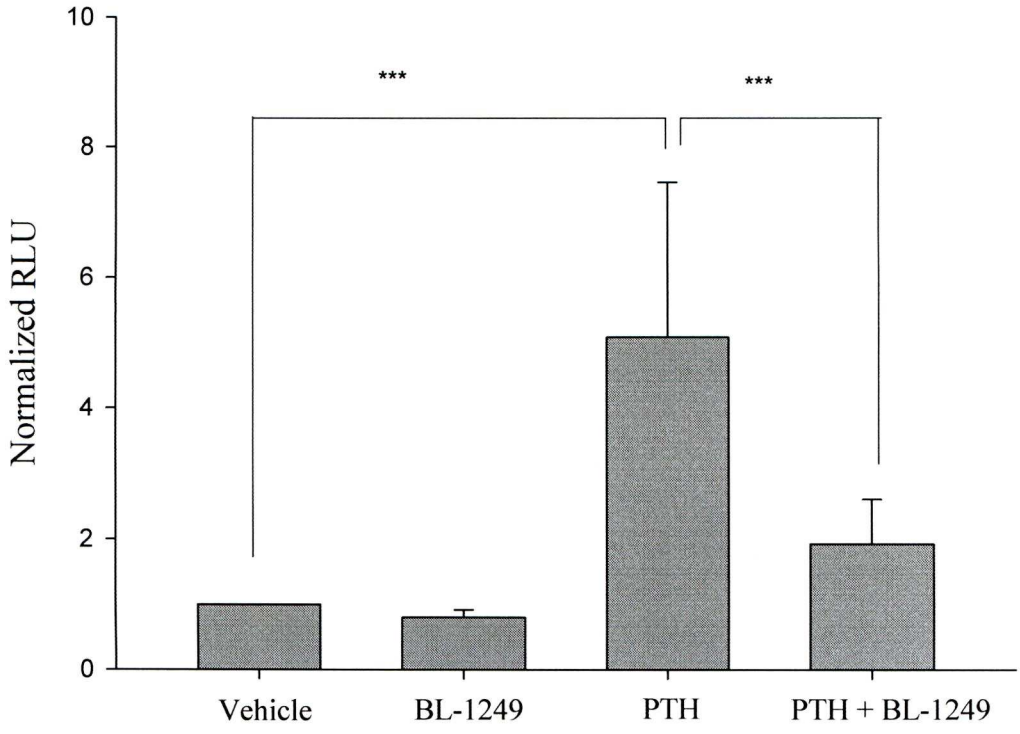

Figure 5.2. The effect of 10μM BL-1249 ± 0.5nM PTH on c-fos expression in SaOS-2 cells (n=17). Each n number represents an average value from between 6-24 wells. Error bars represent S.D.

In this experiment 10μM BL-1249 treatment did not produce a statistically significant reduction in basal c-fos levels, although a 20% reduction suggests that the trend is reproducible given the high n value for this data set. Exposure to 0.5nM PTH gave a 5.1-fold increase over basal levels of c-fos expression ($P<0.001$). 10μM BL-1249 reduced the c-fos induction by PTH down to 1.9-fold above basal expression levels. When compared with PTH treatment alone the difference was significant ($P<0.001$). To test for the dose-dependency of this effect a concentration-response experiment was performed.

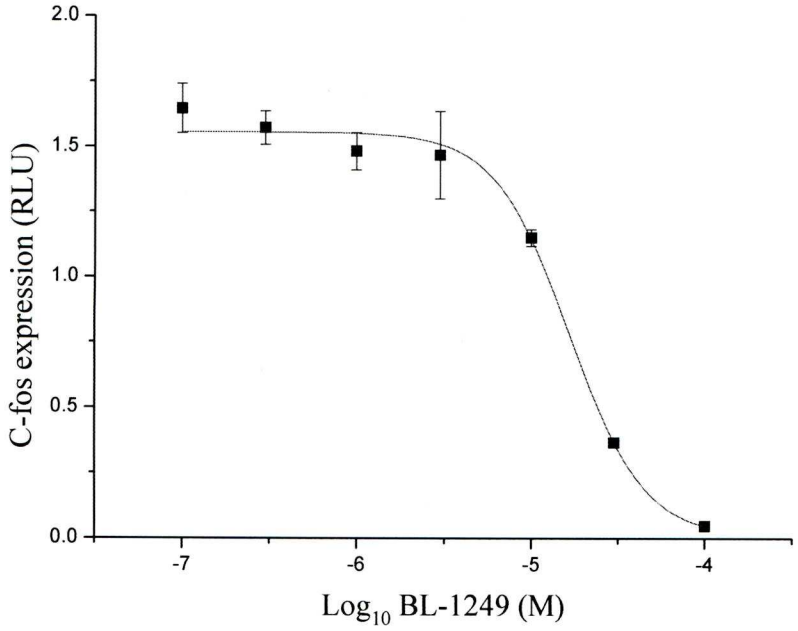

Figure 5.3. Concentration-response curve showing 0.5nM PTH-induced c-fos expression with 0.1 - 100μM BL-1249 (n=6-9). A sigmoidal curve was fitted to the data. The IC_{50} value calculated from this fit is 16.6μM BL-1249. Error bars represent S.E.M.

The reduction in elevated c-fos levels by BL-1249 is shown in Figure 5.3 to be dose-dependent. The IC_{50} value against 0.5nM PTH is 16.6μM BL-1249. Given the measurable effects of the putative TREK-1 activator BL-1249 on c-fos expression, the next candidate compound for screening was another TREK-1 activator; the anti-convulsant and neuroprotective drug riluzole.

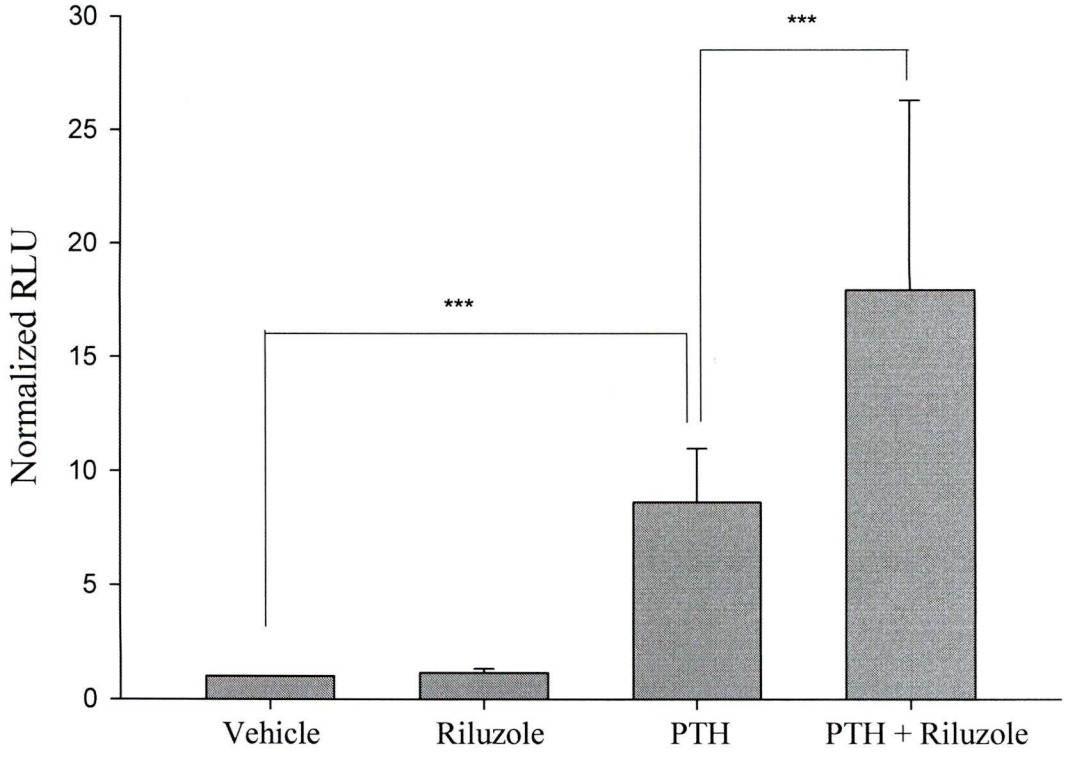

Figure 5.4. The effect of 10μM riluzole ± 0.5nM PTH on c-fos expression in SaOS-2 cells (n=12-24). Error bars represent S.D.

10μM Riluzole was chosen as this was used effectively in a study done on human skeletal muscle (Wang *et al.*, 2008). Treatment with 10μM riluzole induced a modest 17% increase in c-fos expression over basal levels, which was not significant. As seen previously, the induction of c-fos by 0.5nM PTH proved to be significant versus vehicle-treated control cells ($P<0.001$). When combined with PTH treatment riluzole produced a synergistic increase in c-fos expression, doubling the amount of c-fos present compared with PTH treatment alone ($P<0.001$). As investigations into K_{2P} channel openers had shown effects on basal and PTH-induced c-fos expression, the next stage was to look at generic K^+ channel inhibitors. Barium was used in the preliminary experiment to no effect and so tetraethylammonium (TEA) was used as it is another commonly used K^+ channel inhibitor.

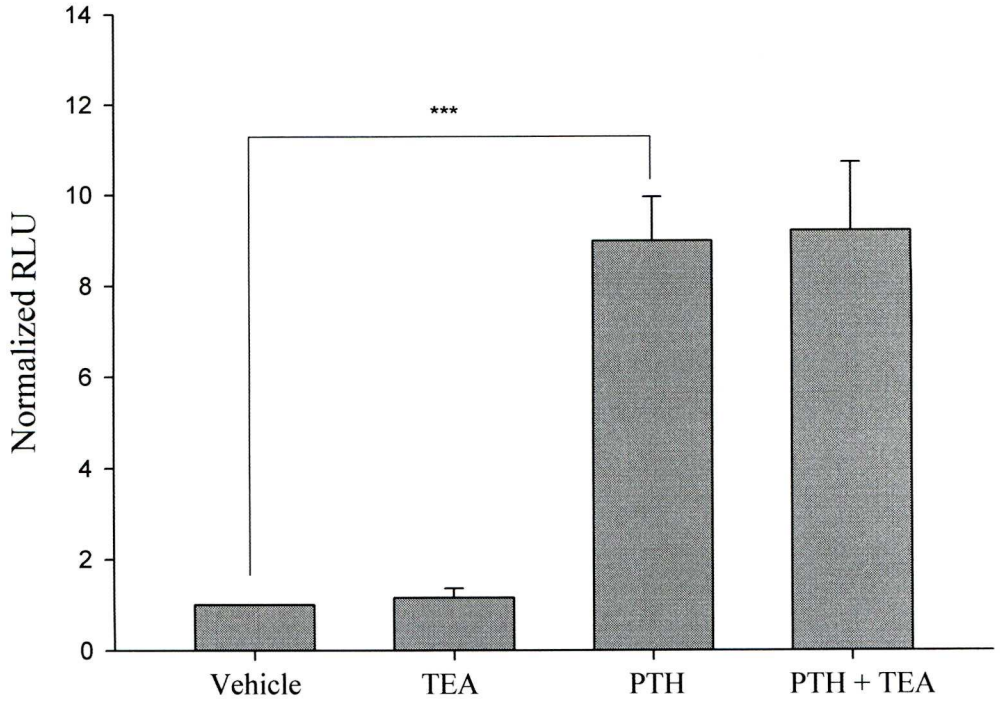

Figure 5.5. The effect of 10mM TEA ± 0.5nM PTH on c-fos expression in SaOS-2 cells (n=5-8). Error bars represent S.D.

The use of 1mM TEA in the preliminary experiment yielded no change in the basal c-fos response and so it was decided to increase the concentration used. Treatment with 10mM TEA gave an increase of 16% in c-fos compared with vehicle-treated control cells. This was not statistically significant. 0.5nM PTH gave a 9-fold increase over basal expression ($P<0.001$). When combined with PTH, TEA gave an almost identical value to that of PTH alone.

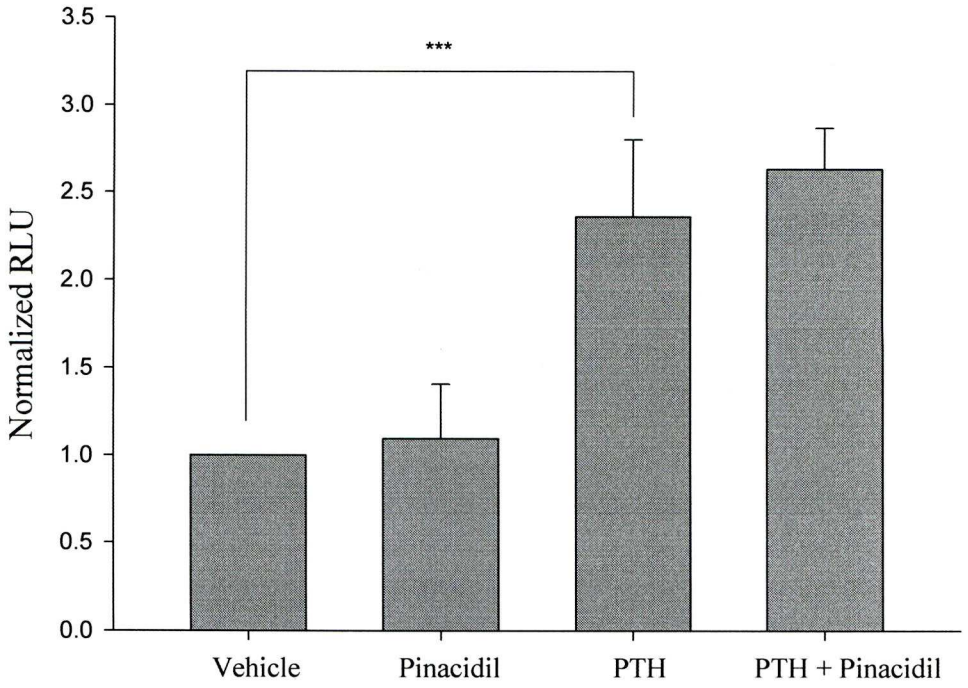

Figure 5.6. The effect of 10μM pinacidil ± 0.5nM PTH on c-fos expression in SaOS-2 cells (n=9-18). Error bars represent S.D.

As in the preliminary experiment (see Figure 5.1), 10μM of the K_{ATP} opener pinacidil increased basal c-fos expression although this time only by a non-significant 9%. 0.5nM PTH gave a 2.4-fold increase over vehicle-treated control cells ($P<0.001$). PTH and pinacidil together did not produce a significant change compared with PTH alone.

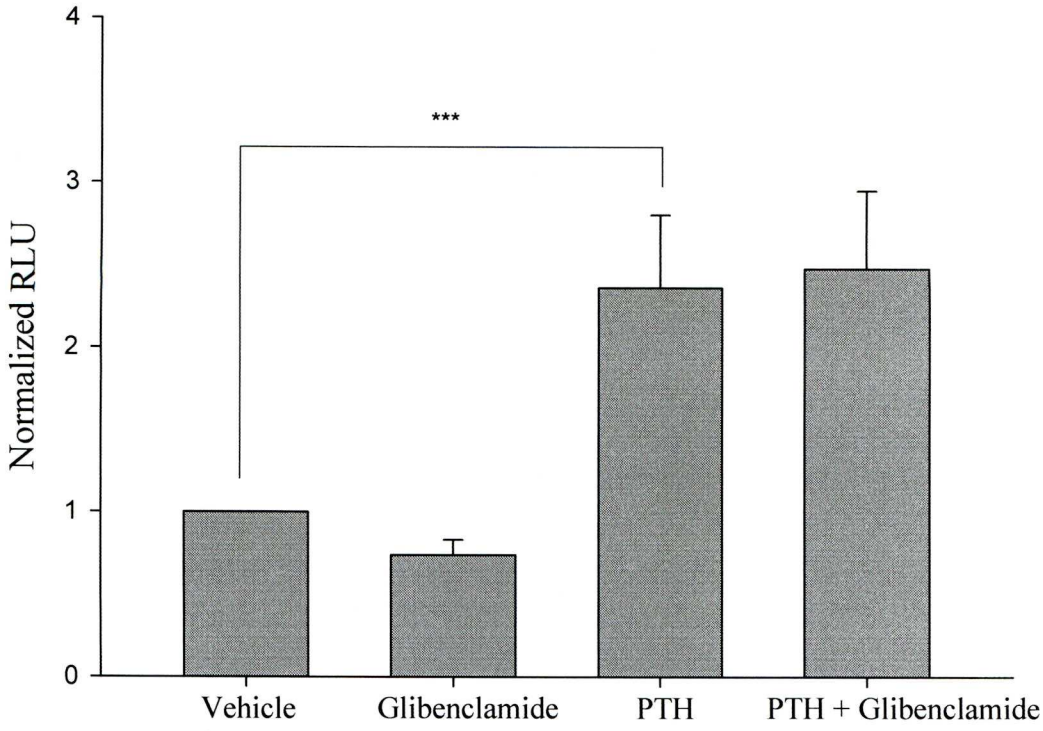

Figure 5.7. The effect of 10μM glibenclamide ± 0.5nM PTH on c-fos expression in SaOS-2 cells (n=9-18). Error bars represent S.D.

Glibenclamide blocks K_{ATP} channels at concentrations less than 10μM (Quayle *et al.*, 1995). Glibenclamide is a sulphonylurea prescribed to diabetics as its depolarizing action assists insulin secretion from pancreatic β-cells (Rendell, 2004). It reduced basal c-fos levels by 26% but this was not significant. A 2.4-fold induction by PTH was significant compared with the vehicle-treated control ($P<0.001$). Glibenclamide and PTH in combination did not produce a significant change when compared to PTH alone.

Table 5.1. Data from repeated experiments using traditional and putative K^+ channel modulators. Data represents normalized c-fos expression following treatment. Data displayed in the figures above are shown in bold.

	Vehicle	Treatment	PTH	PTH + Treatment	n
Riluzole	**1**	**1.17**	**8.6**	**17.9 (***)**	**17**
	1	1.06	4.0	10.3 (***)	9-18
	1	1.32	6.1	12.7 (***)	9-24
TEA	**1**	**1.16**	**9.0**	**9.2**	**5-8**
	1	1.13	6.6	5.1 (**)	9-12
	1	1.37	5.1	6.4 (**)	9-12
Pinacidil	**1**	**1.09**	**2.4**	**2.6**	**9-18**
	1	1.14	7.9	7.7	9-18
Glibenclamide	**1**	**0.74**	**2.4**	**2.4**	**9-18**
	1	0.89	7.9	6.2 (*)	9-18

5.3.2 Depolarization and Calcium Entry

Activators of TREK-1 showed variable but significant changes in c-fos induction. TREK-1 activation would likely cause V_m hyperpolarisation (see also Chapter 6). One of the possible mechanisms of ΔV_m on c-fos expression is via changes in intracellular calcium concentration mediated by L-type VDCCs. In order to test this hypothesis, high external potassium was used to activate VDCCs via depolarization. The dihydropyridines BAY K 8644 and nimodipine were used to directly open and inhibit voltage-gated Ca^{2+} channels respectively (De Vry *et al.*, 1999).

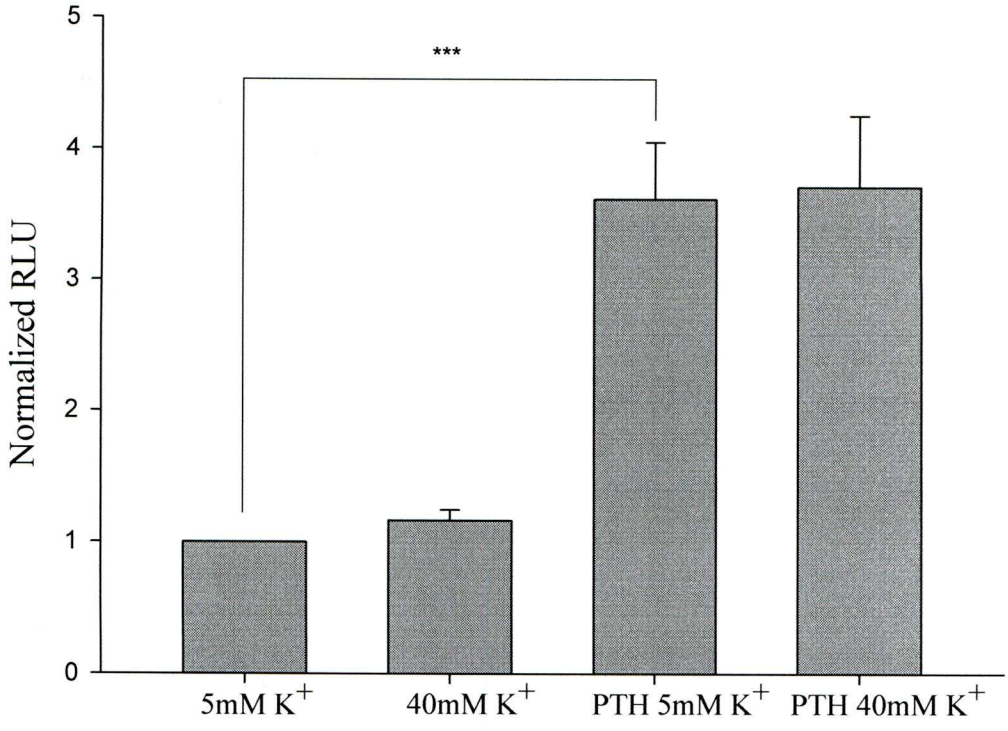

Figure 5.8. The effect of elevated extracellular potassium ± 0.5nM PTH on c-fos expression in SaOS-2 cells (n=12). Error bars represent S.D.

Elevation of extracellular potassium is often used as a simple method of producing depolarization (Hille, 2001). The driving force on potassium ions to leave the cell is lowered by increasing external K^+, therefore K^+ efflux and subsequent hyperpolarisation produced by K^+ channel opening is less likely. As is evident from Figure 5.8, this had little effect on c-fos expression. 40mM K^+ did not produce a statistically significant effect when compared with the 5mM K^+ control. PTH elevated the response basal response ($P<0.001$), yet there was no discernible difference between 5mM and 40mM K^+.

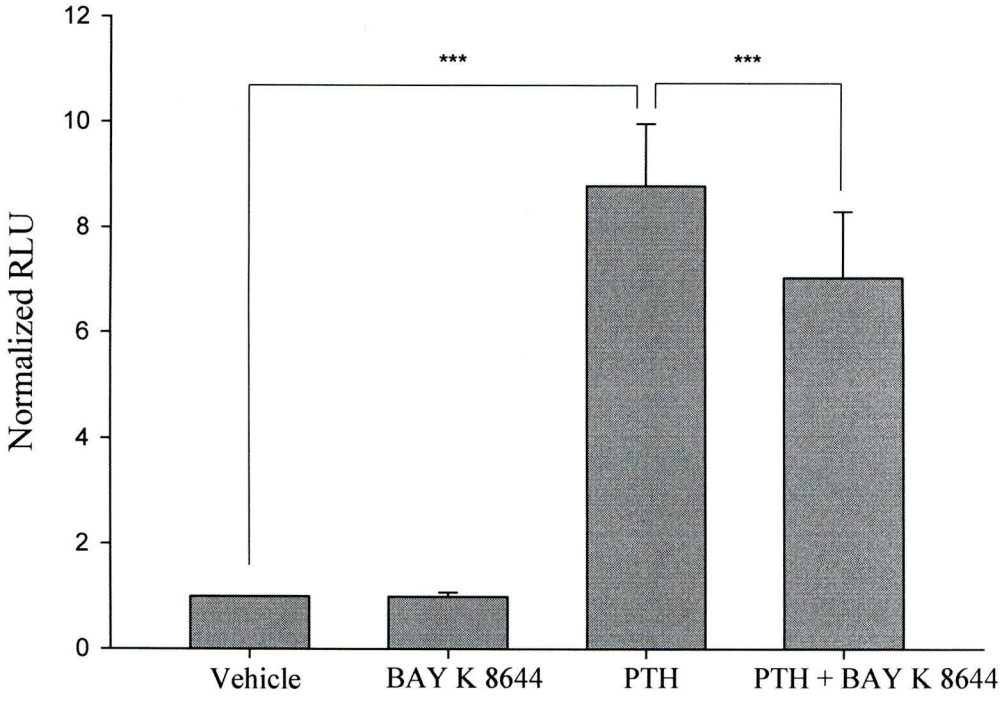

Figure 5.9. The effect of 0.5μM BAY K 8644 ± 0.5nM PTH on c-fos expression in SaOS-2 cells (n=12). Error bars represent S.D.

0.5μM BAY K 8644 had no effect on basal c-fos expression. Treatment with PTH resulted in an 8.8-fold increase over vehicle-treated control cells ($P<0.001$). BAY K 8644 reduced the PTH response to 7-fold over vehicle-treated control cells which amounts to a 17% reduction of the PTH response ($P<0.001$).

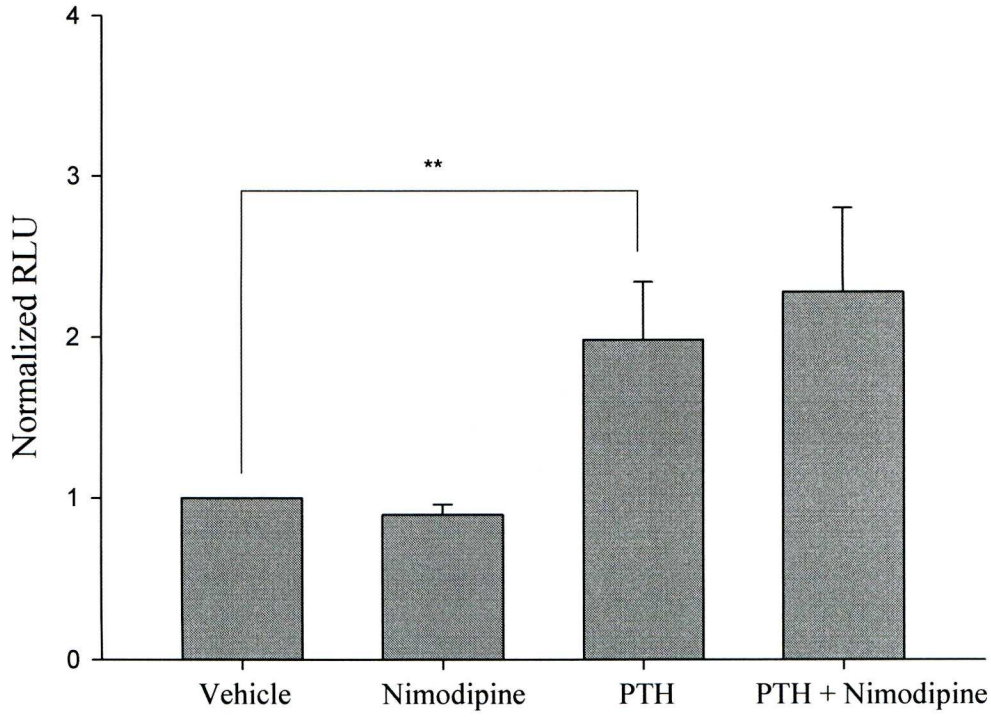

Figure 5.10. The effect of 1μM nimodipine ± 0.5nM PTH on c-fos expression in SaOS-2 cells (n=6-12). Error bars represent S.D.

1μM of the calcium channel blocker (CCB) nimodipine gave a non-significant effect on basal c-fos response. This time PTH treatment gave a 2-fold increase over vehicle-treated control cells ($P<0.01$). In contrast to its action on basal levels, nimodipine elevated the PTH-induced rise by a further 15% yet this did not prove significant.

Table 5.2. Data from repeated experiments observing the effects of depolarization and calcium entry. Data represents normalized c-fos expression following treatment. Data displayed in the figures above are shown in bold.

	Vehicle	Treatment	PTH	PTH + Treatment	n
High K^+	**1**	**1.17**	**3.6**	**3.7**	**12**
	1	0.90	1.4	1.6	6-9
	1	1.01	2.0	4.2 (***)	4-7
BAY K 8644	**1**	**1.00**	**8.8**	**7.0 (***)**	**9-12**
	1	0.85	4.0	2.8 (***)	12-15
	1	0.88	3.2	2.8	12-19
Nimodipine	**1**	**0.90**	**2.0**	**2.3**	**6-12**
	1	1.07	5.1	6.5 (**)	12
	1	0.90	4.0	3.2	9-12

5.3.3 PTH signal transduction

The signal transduction pathway for PTH needed further investigation in order to better understand the effects of K^+ channel modulators on c-fos expression. This series of experiments began with observations on the effects of ATP on PTH-induced c-fos expression. Experiments done previously in the laboratory showed that ATP synergises with PTH to produce a large increase in c-fos (Buckley *et al.*, 2001). It has since been demonstrated that this effect is mediated through the proximal CRE binding site on the c-fos promoter (Murrills *et al.*, 2009). Looking at the effects of ATP should give a positive control and provide a foundation for further studies. After this experiment, the effects of PKA inhibition (H-89 & KT5720) and stimulation (forskolin) were the primary target of investigation. Following this, 8-pCPT-2'-O-Me-cAMP (8-pCPT) was used to test for an exchange protein activated by cAMP (Epac)-mediated component of the PTH response after recent literature suggested a role for this signalling molecule in the osteoblastic response to PTH (Fujita *et al.*, 2002).

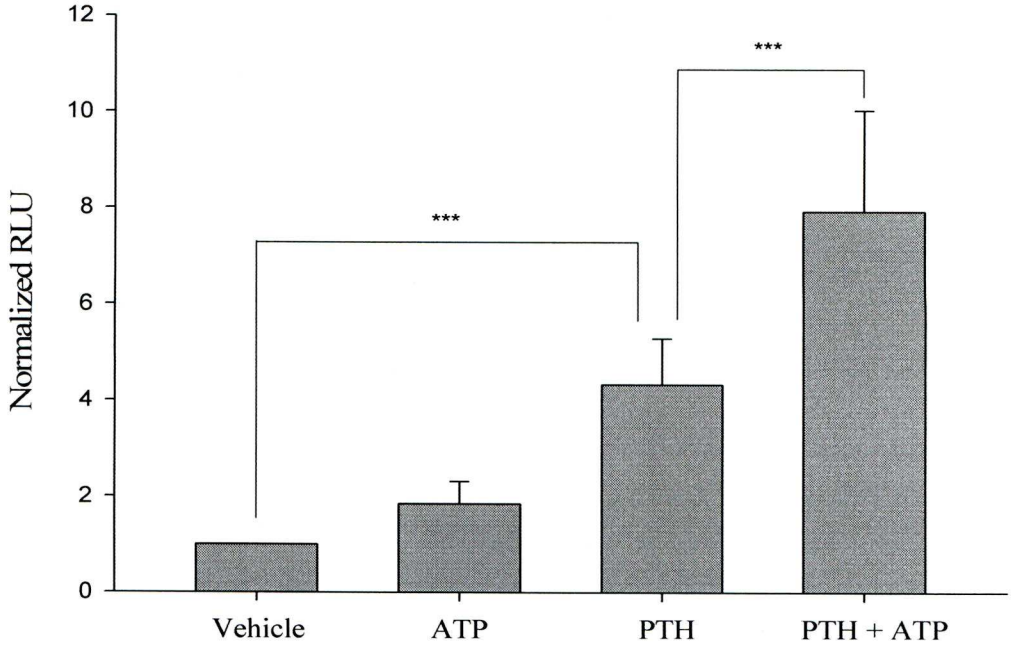

Figure 5.11. The effect of 10μM ATP ± 0.5nM PTH on c-fos expression in SaOS-2 cells (n=9-12). Error bars represent S.D.

The concentration of ATP used here has previously demonstrated an effective calcium response in this cell line (Bowler *et al.*, 1999). 10μM ATP produced an 84% rise in c-fos levels compared to vehicle-treated control cells. Despite this large increase the results were not significantly different. PTH produced a 4.3-fold increase over basal levels ($P<0.001$). As predicted, the PTH response was enhanced by ATP which almost doubled the PTH response alone ($P<0.001$).

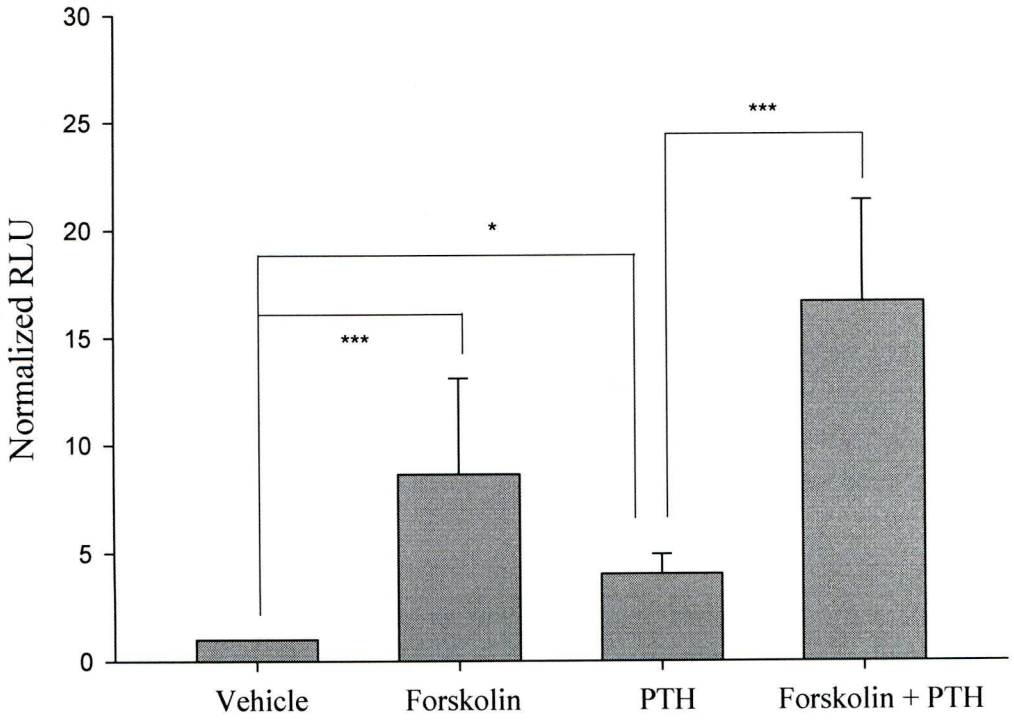

Figure 5.12. The effect of 10μM forskolin ± 0.5nM PTH on c-fos expression in SaOS-2 cells (n=9-18). Error bars represent S.D.

Forskolin acts indirectly on PKA by activating AC and increasing intracellular cAMP levels. 10μM forskolin gave an 8.6-fold increase over vehicle-treated control cells ($P<0.001$). On this occasion, 0.5nM PTH treatment led to a 4-fold increase in c-fos expression over basal levels ($P<0.05$). Forskolin acted synergistically with PTH to give a response which was twice that of forskolin alone, and 8-times that of PTH alone ($P<0.001$). In order to test the effects of the compound BL-1249 further, a concentration-response experiment was performed against 10μM forskolin.

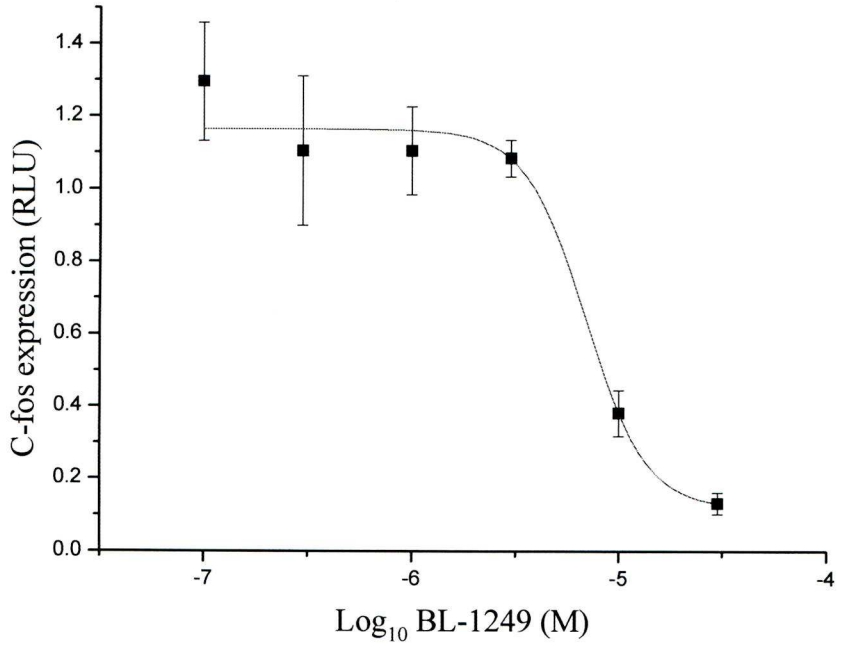

Figure 5.13. Concentration-response curve showing 10μM forskolin-induced c-fos expression with 0.1 - 100μM BL-1249 (n=6-9). A sigmoidal curve was fitted to the data. The IC_{50} value calculated from this fit is 6.9μM BL-1249.Error bars represent S.E.M.

The reduction in forskolin-elevated c-fos levels by BL-1249 is shown in Figure 5.13 to be dose-dependent. The IC_{50} value for BL-1249 against 10μM forskolin is 6.9μM, which is approximately half the amount of BL-1249 needed to produce the same effect against 0.5nM PTH (see Figure 5.3).

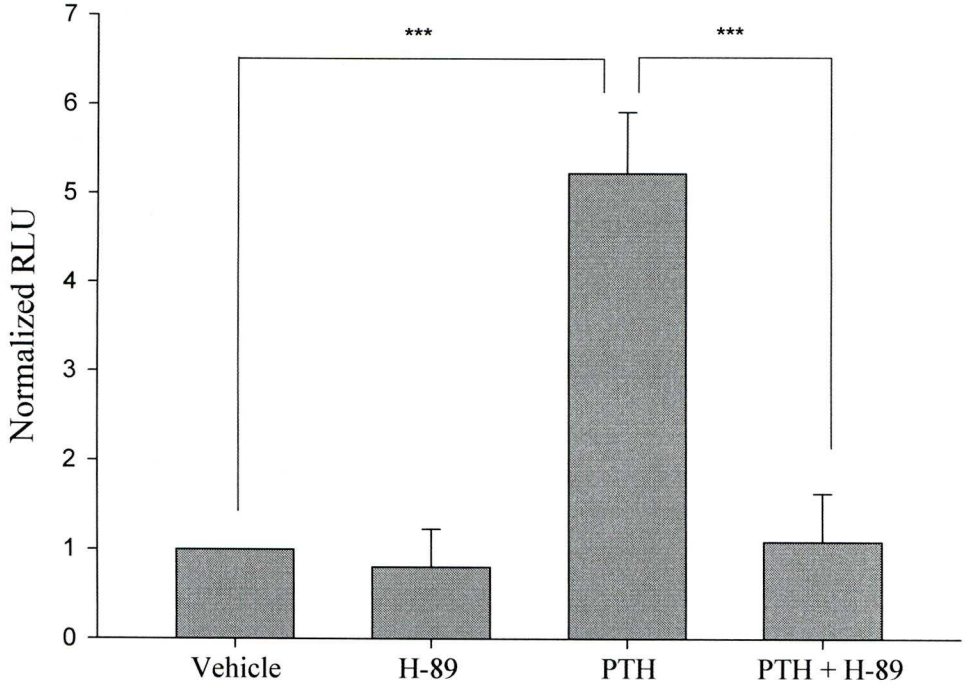

Figure 5.14. The effect of 10μM H-89 ± 0.5nM PTH on c-fos expression in SaOS-2 cells (n=9-12). Error bars represent S.D.

H-89 is a commonly used non-selective PKA inhibitor (Lochner & Moolman, 2006). The concentration of H-89 was decided upon because 10μM had been used previously in this cell line to block the effects of PTH on the CRE (Murrills *et al.*, 2009). H-89 did not significantly affect c-fos expression when compared to the control. On this occasion 0.5nM PTH treatment produced a 5.2-fold increase in expression which proved significant ($P<0.001$). H-89 administered alongside PTH brought c-fos expression back down to just 9% above basal level. This was significant when compared with PTH treatment alone ($P<0.001$).

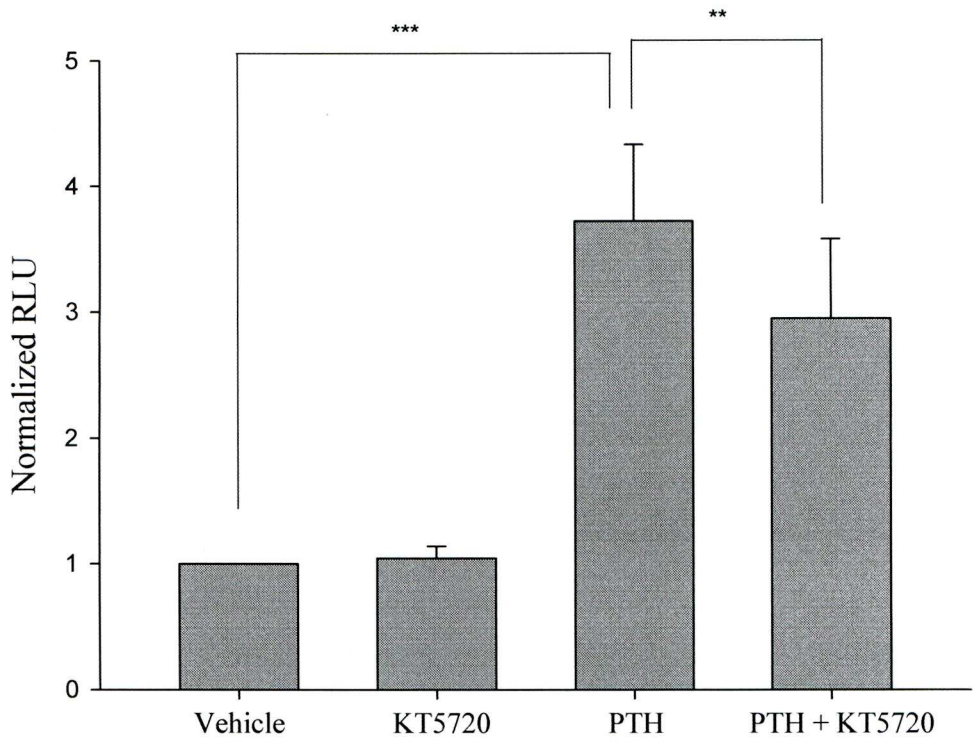

Figure 5.15. The effect of 5μM KT5720 ± 0.5nM PTH on c-fos expression in SaOS-2 cells (n=6-9). Error bars represent S.D.

KT5720 is another PKA inhibitor but is thought to be more selective than H-89 (Lochner & Moolman, 2006). Exposure to KT5720 gave a value close to basal levels of c-fos expression. PTH produced a 3.7-fold increase over vehicle-treated control cells ($P<0.001$). Despite having no effect on basal expression, KT5720 was able to inhibit the PTH-induced elevation by 21% ($P<0.01$). Although H-89 and KT5720 had reduced the PTH response, it seemed prudent to test their effects on a c-fos elevation induced by forskolin.

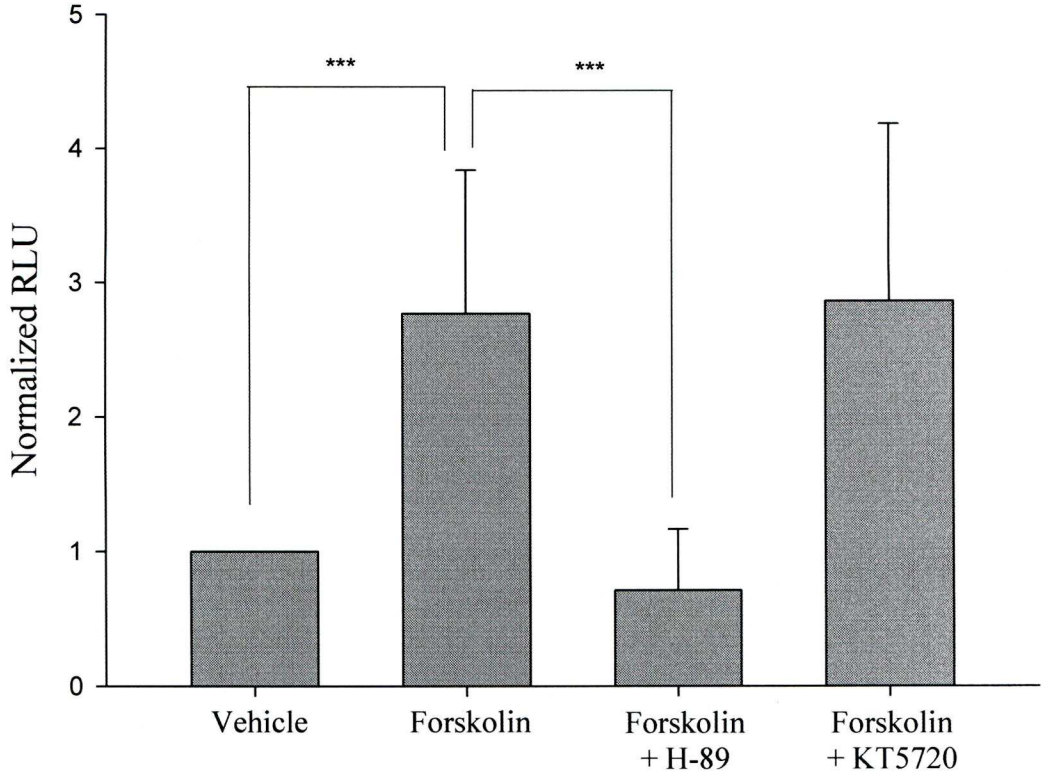

Figure 5.16. The effect of 10μM H-89 and 5μM KT 5720 on forskolin-induced c-fos expression in SaOS-2 cells (n=9). Error bars represent S.D.

10μM forskolin treatment was again significantly different from the vehicle-treated control cells producing a 2.8-fold increase ($P<0.001$). 10μM H-89 again reduced elevated c-fos levels, this time to below that of basal levels ($P<0.001$). KT 5720 was not able to reduce forskolin-induced c-fos.

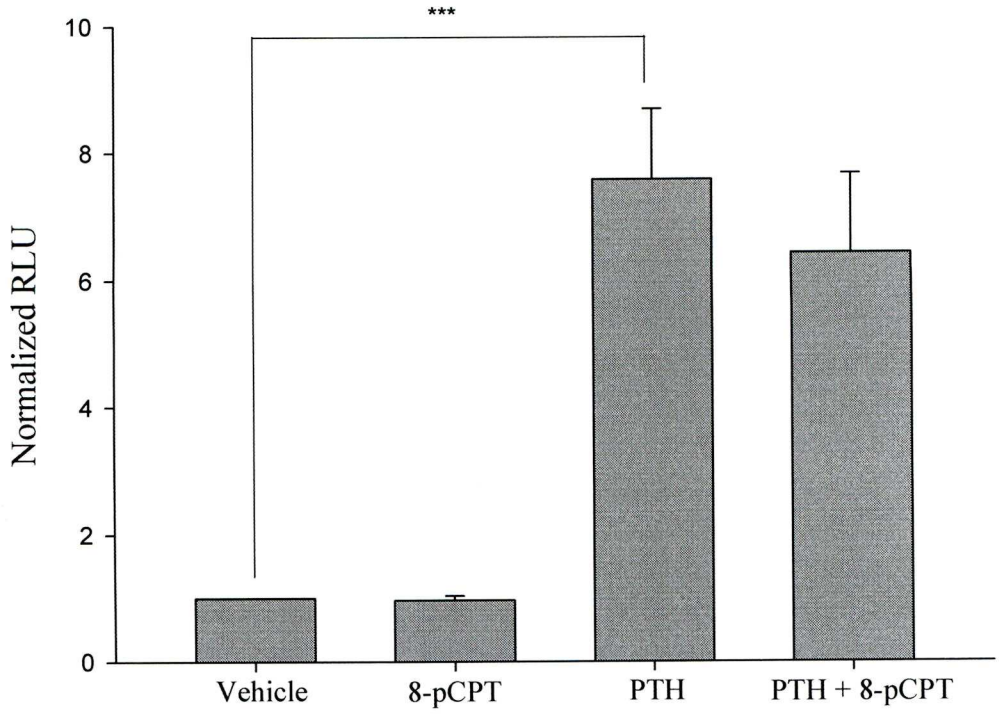

Figure 5.17. The effect of 5μM 8-pCPT ± 0.5nM PTH on c-fos expression in SaOS-2 cells (n=6-9). Error bars represent S.D.

5μM was selected as an appropriate concentration of 8-pCPT as this was used by Purves *et al.* (2009) and Enserink *et al.* (2002) to activate Epac without also activating PKA. Cells treated with 5μM 8-pCPT did not differ from vehicle-treated control cells. 0.5nM PTH gave a 7.6-fold increase over basal c-fos expression ($P<0.001$). 8-pCPT administered with PTH did not prove to significantly affect c-fos levels versus PTH alone.

Table 5.3. Data from repeated experiments observing PTH signal transduction. Data represents normalized c-fos expression following treatment. Data displayed in the figures above are shown in bold.

	Vehicle	Treatment	PTH	PTH + Treatment	n
ATP	**1**	**1.84**	**4.3**	**7.9 (***)**	**9-18**
	1	1.60	4	7.5 (***)	9-18
	1	2.1	6.1	10.4 (***)	9-24
Forskolin	**1**	**8.6 (***)**	**4.0**	**16.6 (***)**	**9-18**
	1	8.0 (***)	6.1	11.3 (***)	9-24
	1	3.4 (***)	1.9	5.1 (***)	6-9
H-89	**1**	**0.80**	**5.2**	**1.1 (***)**	**9-12**
	1	0.62	2.4	1.0 (***)	9-18
KT 5720	**1**	**1.04**	**3.7**	**2.9 (**)**	**6-9**
	1	1.34	7.9	6.6	9-18
	1	1.14	5.2	3.1 (***)	9-12
8-pCPT	**1**	**0.96**	**7.6**	**6.4**	**6-9**
	1	1.01	8.8	8.1	9-12
	1	0.94	4.6	4.0	6-9

5.3.4 Intracellular calcium signalling

The following experiments were performed on wild-type SaOS-2 cells, in a live cell calcium imaging system. Cells were bathed in HEPES buffer solution and incubated at 37°C during recording. Intracellular calcium concentrations were visualised by use of the ratiometric dye fura2-AM.

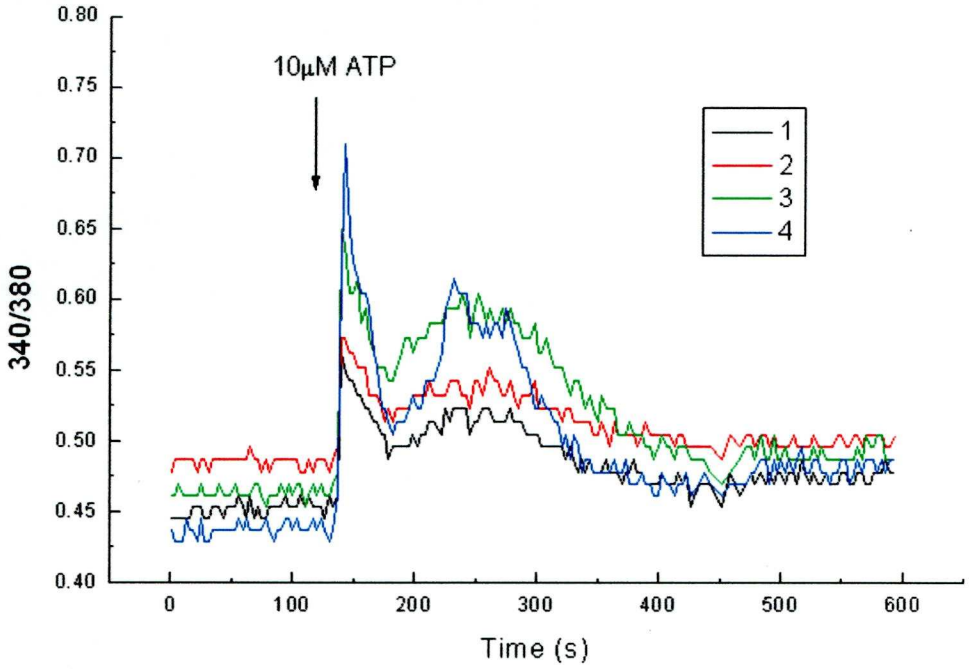

Figure 5.18. The intracellular calcium response to the addition of 10μM ATP to fura2-AM loaded SaOS-2 cells. Recordings were taken simultaneously from 4 cells which were incubated in medium containing calcium.

Figure 5.18 shows that the addition of ATP to the extracellular environment of an osteoblastic cell produces a rapid rise in intracellular calcium levels. Here, the response is biphasic, with a sharp initial peak followed by a smaller, flatter peak.

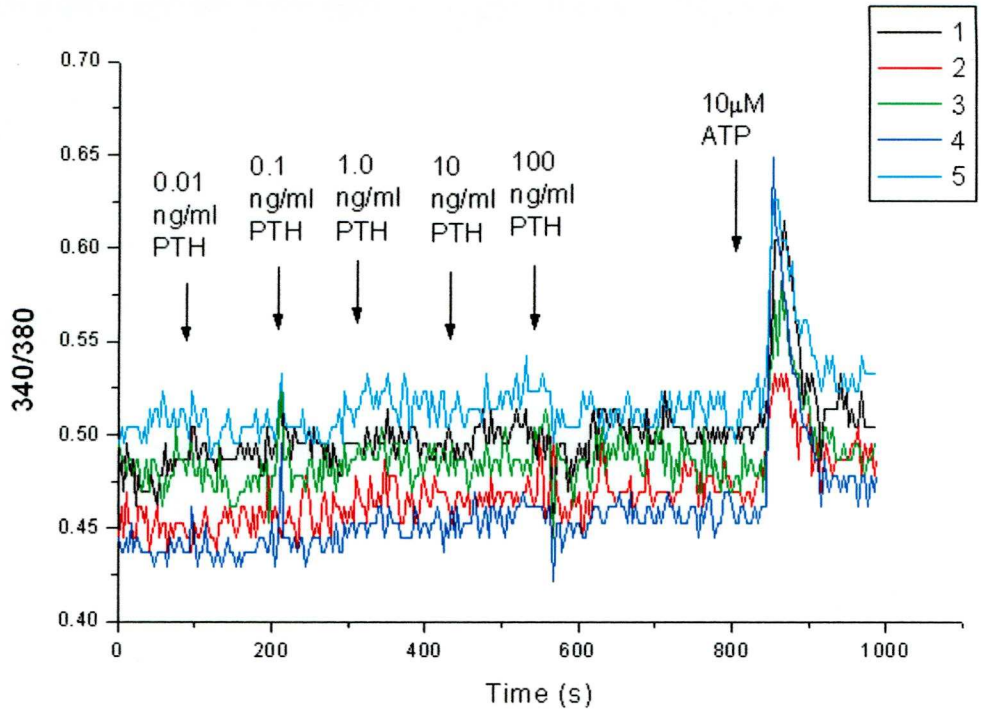

Figure 5.19. Concentration-response experiment measuring intracellular calcium in fura2-AM loaded SaOS-2 cells in response to 0.01 – 100ng PTH. Recordings were taken simultaneously from 5 cells which were incubated in medium containing calcium.

PTH was added in increasing concentrations to the medium covering the cells. No intracellular calcium release or calcium influx was seen. After the concentration-response series was finished, 10µM ATP was added into the medium in the bath to prove that the cells were responsive.

5.3.5 Potassium and calcium channel modulators on alkaline phosphatase expression and secretion

ALP is a marker protein for osteoblast differentiation. C-fos expression can demonstrate early stage responses to various stimuli and is a useful tool, but the measurement of ALP is a late stage effect and can demonstrate a direct effect on protein levels. A dose-response experiment using TEA was performed along with elevated external K^+ and the CCB verapamil to test for a direct effect on an osteoblast marker of differentiation.

A

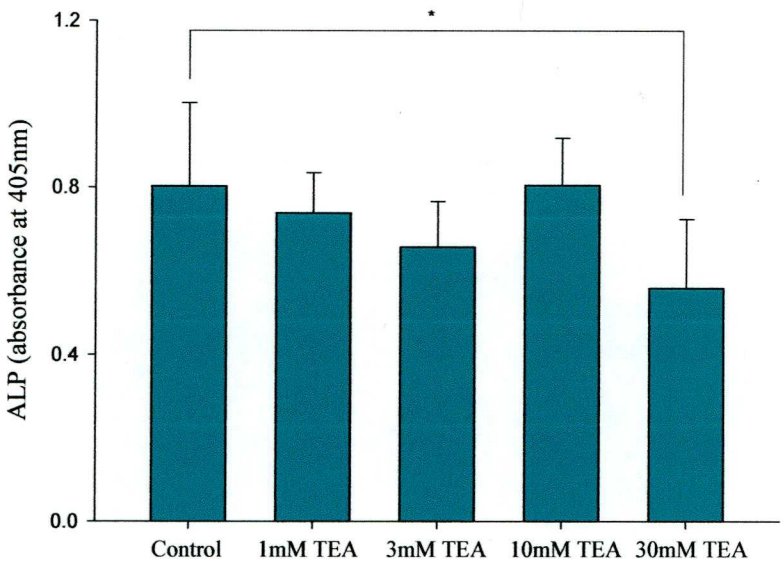

B

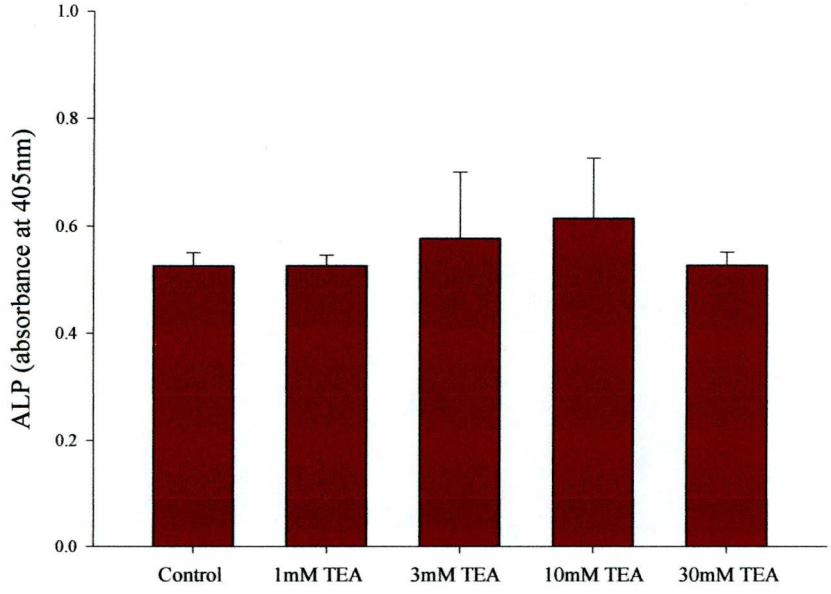

Figure 5.20. Measurement of alkaline phosphate in A) cell lysate and B) conditioned medium from TEA treated wild-type SaOS-2 cells (n=8). Error bars represent S.D.

TEA significantly reduced cell-bound ALP at 30mM ($p<0.05$) but not at lower concentrations. TEA did not appear to affect the amount of ALP found in the medium of cultured SaOS-2 cells.

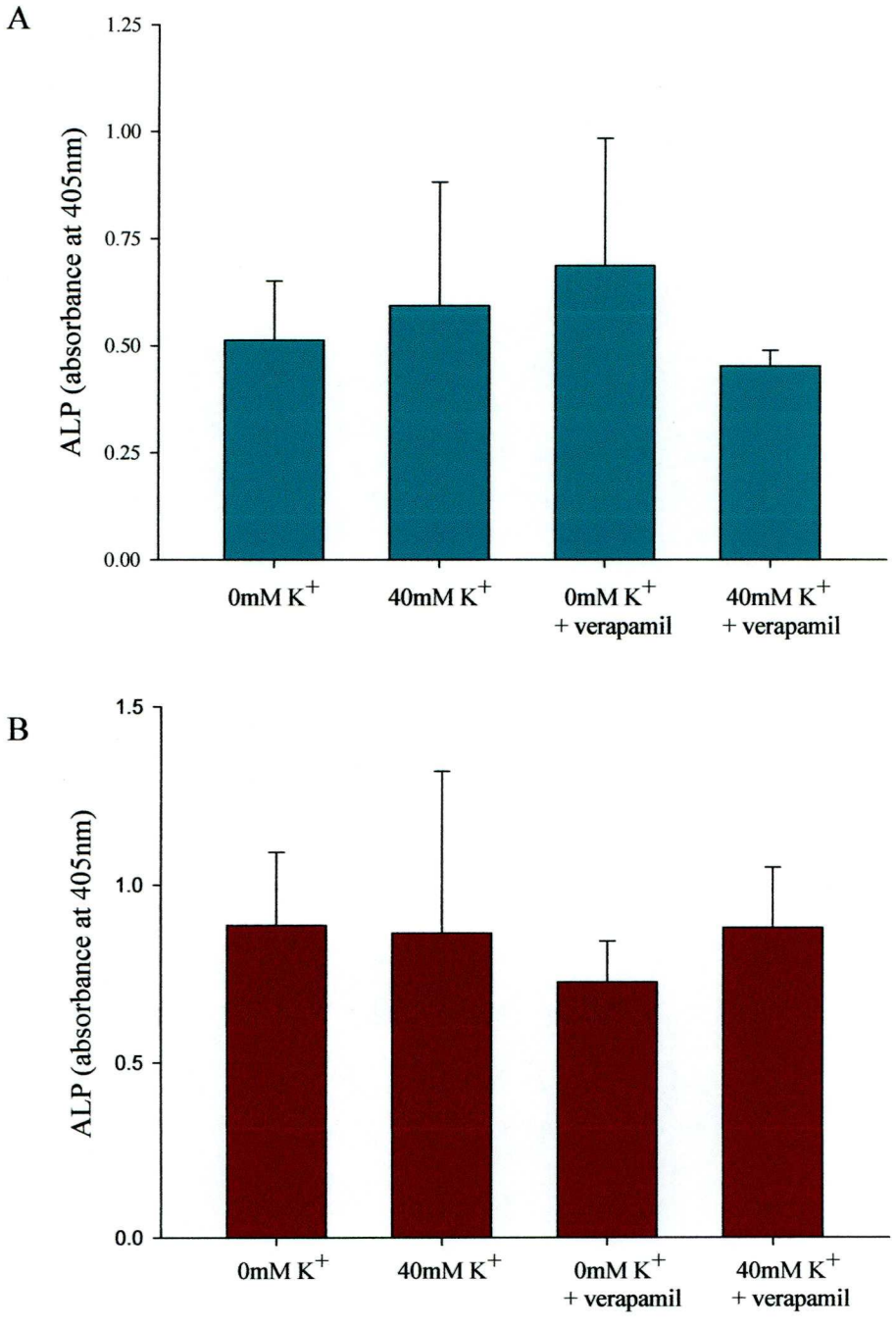

Figure 5.21. Measurement of alkaline phosphate in A) cell lysate and B) conditioned medium from wild-type SaOS-2 cells treated with high external K^+ and 10μM verapamil (n=6). Error bars represent S.D.

Neither elevated external K^+ nor 10μM verapamil gave a statistically significant result in the cell layer or the conditioned medium. In addition to this, no obvious trend was observed from the pattern of results. The standard deviation appeared large in this cohort of SaOS-2 cells.

5.4 Discussion

The experiments in this chapter have generated a large amount of data which requires detailed consideration. The key points are summarised as follows;

1. The putative TREK-1 openers BL-124 and riluzole increase and decrease osteoblastic c-fos expression respectively. This difference must be due to some of the other known and unknown effects of both compounds.
2. Other KCOs and KCBs had little consistent effect on c-fos or ALP.
3. Opening or closure of calcium channels via depolarization or BAY K 8644 treatment and CCBs appeared to have very little effect on basal or PTH-elevated c-fos and ALP.
4. PTH second messenger signalling is not increased by an Epac agonist or decreased by CCBs. Signalling in this system is predominantly through PKA and can be blocked by the non-selective antagonist H-89.

5.4.1 Traditional and putative potassium channel modulators

Riluzole and BL-1249 are two compounds which purport to open TREK-1 channels and yet this study has shown they have contrasting effects on c-fos expression. There is very limited information on BL-1249, which makes a detailed anaylsis rather difficult. In these experiments it reproducibly lowers basal and PTH-elevated c-fos in a dose-dependent manner ($P<0.001$ in PTH treated cells). Riluzole produced a small increase basal c-fos levels and significantly increased the response of PTH alone ($P<0.001$ in PTH treated cells). This discussion aims to relate the current literature on these compounds to explain the results shown above.

The compound BL-1249 is marketed as an activator of TREK-1 channels by Sigma. It was found to produce membrane hyperpolarisation in human bladder myocytes and evoked relaxation of pre-contracted bladder strips but not aortic strips, provoking the possibility that it may be a potential therapy for overactive bladder (Tertyshnikova *et al.,* 2005). Because TREK-1 was shown to be expressed at 12 times the level in bladder compared with aorta, the affects of BL-1249 were attributed to activation of TREK-1 (Tertyshnikova *et al.,* 2005). We know through electrophysiology experiments done in this laboratory on transfected *Xenopus laevis* oocytes that BL-1249 directly activates TREK-1 channels (personal communication, Quayle & Goonetilleke).

Riluzole is a neuroprotective, anticonvulsant and sedative agent used in the treatment of amyotropic lateral sclerosis (ALS) (Van Damme *et al.*, 2005). Its many *in vivo* actions hint at its complex pharmacology. Riluzole inhibits glutamatergic signalling via inhibition of glutamate release and indirect blockade of excitatory amino-acid receptors (Doble, 1996). Riluzole activates TRAAK and TREK-1 channels dose-dependently, although TREK-1 is only activated transiently (Duprat *et al.*, 2000). Exposure to riluzole increases cell cAMP levels and the subsequent PKA activation results in the phosphorylation and closure of TREK-1 which can be reversed during metabolic stress (Duprat *et al.*, 2000). The reactivation of TREK-1 is likely to occur through its sensitivity to intracellular acidosis and the decreased production of cAMP under these conditions (Maingret *et al.*, 1999). Riluzole is thought to interact directly with the channels, given the time course of effects demonstrated by electrophysiology data. The rise in cAMP is an indirect effect that is due to an inhibition of phosphodiesterases (PDEs) (Duprat *et al.*, 2000). Riluzole activates BK currents and inhibits voltage-gated Na^{2+} currents in skeletal muscle cells contributing to muscle relaxation (Wang *et al.*, 2008).

Riluzole is increasing c-fos expression through one or both of the following mechanisms in this model.

1. PDE inhibition leading to PKA activation and CREB phosphorylation.
2. Inhibition of TREK-1 following its phosphorylation by PKA, resulting in depolarization or a less negative V_m.

Barium and TEA showed no significant differences compared with control cells, indicating that blockade of K^+ channels sensitive to these inhibitors do not affect c-fos expression. Studies of these KCBs are extremely limited in osteoblastic cells, perhaps because others have observed negative results such as those seen in Figures 5.1 & 5.5 which have not been published.

Pinacidil is a KCO that acts specifically to open K_{ATP} channels whereas glibenclamide inhibits the currents produced by these channels (Quayle *et al.*, 1995). K_{ATP} channels have been observed in osteoblasts and have been shown to have a role in the response to calcitonin gene-related peptide (CGRP) and $1,25(OH)_2D_3$ (Kawase *et al.*, 1996, Burns et al., 2004, Moreau *et al.*, 1997). K_{ATP} modulators appeared to show more promise than barium and TEA but did not prove significantly different apart from in the initial experiment where pinacidil elevated basal c-fos ($P<0.001$) and in one out of two experiments, glibenclamide reduced the PTH response ($p<0.05$). In subsequent experiments, pinacidil continued to elevate c-fos but not to significant levels. In support of this observation, glibenclamide treatment non-significantly reduced basal c-fos. Closure of K_{ATP} channels by glibenclamide would predictably cause a depolarization and indeed this is related to its clinical applications (Rendell, 2004).

In summary, the effects of TREK-1 openers in this system cannot be entirely explained by their action on K_{2P} channels. The pharmacology of riluzole has been fairly well documented but it will take considerable time and requires a multitude of experiments to map any additional effects of BL-1249. Generic KCBs barium and TEA showed no significant effects on c-fos expression and very limited effects on ALP expression. K_{ATP} modulators pinacidil and glibenclamide showed little consistent effect.

5.4.2 Depolarization and Calcium Entry

Depolarization using high external [K^+] gave no significant responses and neither did treatment with the CCB nimodipine. It was therefore surprising to see that BAY K 8644 significantly reduced the response to PTH on more than one occasion ($P<0.001$ twice, ns once). Others have previously studied the blockade of calcium influx through L-type channels in osteoblasts and the overriding conclusion seems to be that they do not affect proliferation or differentiation (Labelle *et al.* 2007, Zahanich *et al.*, 2005). Labelle *et al.* (2007) found no significant effects of verapamil or nifedipine on osteoblast proliferation. They propose that TRPC channels are involved in CCE and L-type VDCCs are more likely to be involved in secretory functions (Moreau *et al.*, 1997, Bergh *et al* 2003). L- & T-type calcium channels are expressed in human MSCs. L-type currents were recorded from differentiating and non-differentiating MSCs. Nifedipine had no effect on ALP activity in hMSCs undergoing osteogenic differentiation (Zahanich *et al.*, 2005). The authors propose that another type of Ca^{2+} channel mediates the entry of calcium into the cell. In contrast to the studies mentioned previously, Nishiya & Sugimoto (2002) suggest that the dihydropyridine Ca^{2+} channel blocker benidipine promotes ALP activity and mineralization. The same study reported no effects of nifedipine. The evidence from the literature suggests that further studies involving calcium channels in osteoblasts should include TRP modulators alongside more traditional Ca^{2+} channel modulators. This data shows an inhibitory effect of BAY K 8644 on c-fos expression which we believe has not been reported to date.

5.4.3 PTH signal transduction

As predicted, ATP increased both basal and PTH-induced c-fos expression repeatedly although only elevation of the PTH response proved significant ($P<0.001$). This gave a positive control for an attempt to dissect some of the second messengers implicated in the PTH response. It is generally accepted that PTH acts to increase osteoblastic c-fos through the PKA pathway (Evans *et al.*, 1996, Bowler et al., 1999). The AC activator forskolin shows that activation of the PKA pathway via accumulation of cAMP does induce c-fos expression in our

model. The known PKA inhibitors H-89 and KT5720 both significantly reduced the PTH-induced elevation ($P<0.001$ & $P<0.01$), again pointing to PKA as a major signalling pathway.

H-89 effectively reduced both PTH- & forskolin-induced c-fos expression. Although this compound features often in studies to negate the effects of PKA, it has other known effects which may have influenced these results. A review by Lochner & Moolman (2006) states that H-89 inhibits K_v currents through direct blockade of the channel pore. It also inhibits K_{ATP} and K_{ir} currents at micromolar concentrations in arterial smooth muscle (Sun Park *et al.*, 2006). H-89s collection of alternative effects are not limited to K^+ channels, with PKG inhibition being among the others (Satake *et al.*, 1996). H-89 binds to PKA on its ATP binding site which is highly conserved among kinases, thus helping to explain its non-specific effects among the kinase family (Breitenlechner *et al.*, 2005). Possession of this knowledge led to the inclusion of another commonly used and more selective PKA inhibitor KT5720 (Lochner & Moolman, 2006). This alternative to H-89 did not prove as effective at preventing c-fos induction although it did reduce PTH-induced c-fos expression in 3 out of 3 experiments (ns, $P<0.05$, $P<0.001$). When tested against forskolin there was no discernible effect, although H-89 inhibited the response back down to beyond basal levels ($P<0.001$). If the experiments were to be performed again (Rp)-8-Br-cAMPS would perhaps be a better choice as a comparison against H-89. (Rp)-8-Br-cAMPS prevents the dissociation of the catalytic subunit of PKA from the regulatory subunit and therefore acts a step earlier than H-89 (Gjertsen *et al.*, 1995).

8-pCPT is a cAMP analogue that selectively activates Epac (Enserink *et al.*, 2002). Used alone it did not elevate c-fos and when combined with PTH treatment a small and non-significant decrease was observed in all three experiments. Fujita *et al.*, (2002) demonstrate the presence of Epac 1 & 2 in several osteoblastic cells. They propose that activation of PTHR1 increases cAMP which induces Epac signalling and activation of the ERK pathway. The activation of ERKs increases proliferation which may help to explain the dual effects of PTH on osteoblast proliferation. Our model is perhaps not best suited

to confirming these effects in SaOS-2 cells, as c-fos expression is most often associated with differentiation (Ionescu *et al.*, 2001).

5.4.4 Intracellular calcium signalling

The elevation in $[Ca^{2+}]_i$ produced by 10μM ATP in osteoblastic cells has been observed by our group and by others (Bowler *et al.*, 1999, Nishii *et al.*, 2009). Bowler *et al.*, (1999) showed that ATP increases $[Ca^{2+}]_i$ and stimulates c-fos expression in SaOS-2 cells via its activation of P2Y receptors. The second part of the biphasic response to ATP seen in figure 5.18 is likely to be the replenishment of intracellular stores via CCE as described by Berridge, (1995). P2 receptors undergo desensitization making a secondary activation by a nucleotide agonist unlikely (Sistare *et al.*, 1994). Figure 5.19 shows PTH failing to elicit a rise in $[Ca^{2+}]_i$. This is also an observation which has been made previously in our laboratory (Buckley *et al.*, 2001). Others have noted calcium increases to PTH (Reid *et al.*, 1987, Yamaguchi *et al.*, 1987). Resolution concerning the mechanism behind this difference may lie in the regulation of $G\alpha_s$ and $G\alpha_q$ coupling to the PTHR1. Distinction between opening of Ca^{2+} channels and store-operated Ca^{2+} release can be made by repeating an experiment performed with Ca^{2+} in the extracellular solution to one using no Ca^{2+} and Ethylene glycol tetraacetic acid (EGTA).

5.4.5 Potassium and calcium channel modulators on alkaline phosphatase expression and secretion

The ALP measurements showed a greater standard deviation compared to the data from the c-fos experiments and the data were not normally distributed. A Kruskal-Wallis Test (non-parametric ANOVA) had to be performed to test for significance. A dose-response experiment using 1–30mM TEA showed a decrease in ALP protein present in the cell lysate ($P<0.05$ at 30mM TEA). No effect was observed on ALP levels outside the cell even at 30mM TEA. At high doses, TEA appears to inhibit the production but not the secretion of ALP. The spread of the data and large standard deviation in the depolarisation and calcium entry experiment could indicate a large experimental error or more interestingly,

a heterogeneous response. This could occur if there was a difference in Ca^{2+} channel expression among the population. Despite differences in the spread of the c-fos and ALP data, the ALP results do agree with the c-fos results obtained with TEA, depolarization and CCBs. It appears that generic KCBs and Ca^{2+} entry are not able to modulate osteoblast differentiation (Labelle *et al.*, 2007, Zahanich *et al.*, 2005). In order to determine more fully the effects of K^+ and Ca^{2+} channel agents on osteoblasts, further experiments could be performed to measure the levels of other osteoblastic markers such as collagen I, osteocalcin, OPG and ntelopeptide of type 1 collagen (P1NP).

5.5 Conclusions

Both TREK-1 modulators used in combination with PTH showed marked differences when compared to PTH treatment alone. The more traditional voltage-gated and K_{ATP} modulators failed to show such dramatic effects. As the myriad actions of riluzole presented difficulties in this model and undoubtedly influenced these results, it would appear that activation of TREK-1 by BL-1249 may give a better idea of the effects of TREK-1 activation on c-fos expression. If BL-1249 simply activates TREK-1 channels, then an increase in TREK-1 currents inhibits stimulatory events following PTH administration in SaOS-2 cells. Further experiments would be needed in order to conclude that BL-1249 exerts its effects solely via activation of TREK-1 channels. These may include cAMP measurements and electrophysiological studies. The data given in this chapter appear to add support to the hypotheses that PTH-induced gene expression is mediated by PKA and L-type Ca^{2+} channels are not involved in osteoblast differentiation.

6.0 Electrophysiological Observations Made Using Arachidonic Acid & BL-1249

6.1 Introduction

The aim of these experiments was to characterise the electrophysiological response of osteoblastic cells to the putative TREK-1 activator BL-1249. Responses to AA were also recorded to provide a comparison with a known activator of TREK channels. In addition to current-voltage (IV) recordings, the response of the membrane potential was also observed following the addition of BL-1249. The electrophysiological effects of BL-1249 have been documented by Tertyshnikova *et al.* (2005). Because it is a putative TREK-1 activator it is one of the few pharmacological tools available to study the currents produced by these channels. Also, the results in Chapter 5 warrant further investigation into the actions of BL-1249 in osteoblast-like cells.

BL-1249 caused hyperpolarization of human bladder myocytes and induced a non-inactivating and instantaneous outward current which reversed around E_K (Tertyshnikova *et al.*, 2005). The current and the relaxation were inhibited by 10mM Ba^{2+} but not by other commonly used KCBs. Added to the evidence pointing towards activation of a K_{2P} channel were the results of real-time PCR on bladder myocytes and aorta showing TREK-1 expression was over 12 times higher in bladder myocytes than in aorta (Tertyshnikova *et al.*, 2005). TASK-1 & -2 channels have been observed by another group in bladder smooth muscle, suggesting that K_{2P} channels have a functional role in bladder tissue (Beckett *et al.*, 2008).

One of the features of K_{2P} channels are the effects of various intracellular and extracellular stimuli on channel kinetics. Members of the K_{2P} channel family show various degrees of voltage-dependence. A number of recent studies have pointed to the ability of K_{2P} channels to modulate their voltage-dependence upon interaction with signalling molecules (Bockenhauer *et al.*, 2001, Lopes *et al.*, 2005, Chemin *et al.*, 2003). This phenomenon is not exclusive: K_{ir} channels have previously demonstrated variation in their response to voltage when exposed to PIP_2. PIP_2 hydrolysis via activation of PKC has been shown to inhibit TASK & TREK channel activity and cause a shift in voltage-dependence towards more depolarized potentials (Lopes *et al.*, 2005, Chemin *et al.*, 2003). Phosphorylation

of TREK-1 at serine 348 by PKA similarly transforms the channel from a leak to a voltage-dependent phenotype (Bockenhauer *et al.*, 2001). A component of TREK-1 current activates instantaneously, is outwardly-rectifying and non-inactivating. Another component of a typical TREK-1 current shows an increase during the first few milliseconds of membrane depolarization (Fink *et al.*, 1996).

Membrane potential recordings in osteoblasts are infrequent among electrophysiological studies in this cell type. Ferrier *et al.* (1987) recorded an average membrane potential of -24mV in ROS 17/2.8 cells measured within 80ms of microelectode entry. This figure was based on observations from 29 different cells. Hughes *et al.* (2006) recorded a resting membrane potential of -21.5mV in MG-63 cells based on recordings from 8 cells. The same paper reported the resting membrane potential of primary human osteoblasts as -38.1mV (n=11), considerably more negative than the recording from MG-63 cells.

6.2 Methods

A cell suspension was obtained through a routine passage. Recordings were made from single cells in suspension. Extracellular solution contained (mM): 6 KCl, 134 NaCl, 1 MgCl2, 2 CaCl2, 10 HEPES, 10 glucose (pH adjusted to 7.4 with NaOH). The standard pipette (intracellular) solution contained (mM): 107 KCl, 33 KOH, 10 HEPES, 10 EGTA, 3 MgCl2, 3 Na2ATP, pH 7.2. Membrane current and voltage were amplified using an EPC-8 amplifier (List Instruments), digitised via a Digidata 1200 analogue to digital interface (Axon Instruments), and recorded on computer using pCLAMP8 software (Axon Instruments). Data were analysed using pCLAMP8 and SigmaPlot. Experiments were conducted at room temperature (18-22°C). Stock solutions were added to the extracellular solution via a perfusion system to give the desired final concentration. A fresh glass microelectrode was used for each cell patch. After the cells were patched, a voltage-step protocol was performed which recorded current at voltages between -120mV and +100mV in 10mV increments. Two control recording were taken from a single cell whilst cells were perfused in the extracellular solution described above. Then either 20μM AA or 10μM BL-1249 was perfused through the recording chamber and after three minutes, two further recordings were taken from the cell. Immediately after the second recording with the treatment, the recording chamber was washed out. After a further three minutes two washout recordings were taken to determine if the response was reversible. For recordings of membrane potential, current was clamped and voltage was recorded continuously over a period of approximately 10 minutes. Initially, the cell was perfused with the extracellular solution, and after a suitable baseline was recorded 10μM BL-1249 was circulated through the recording chamber. After several minutes, BL-1249 was washed out and the recovery of the membrane potential was observed.

6.3 Results

6.3.1 Current-voltage recordings in osteoblastic cells exposed to AA

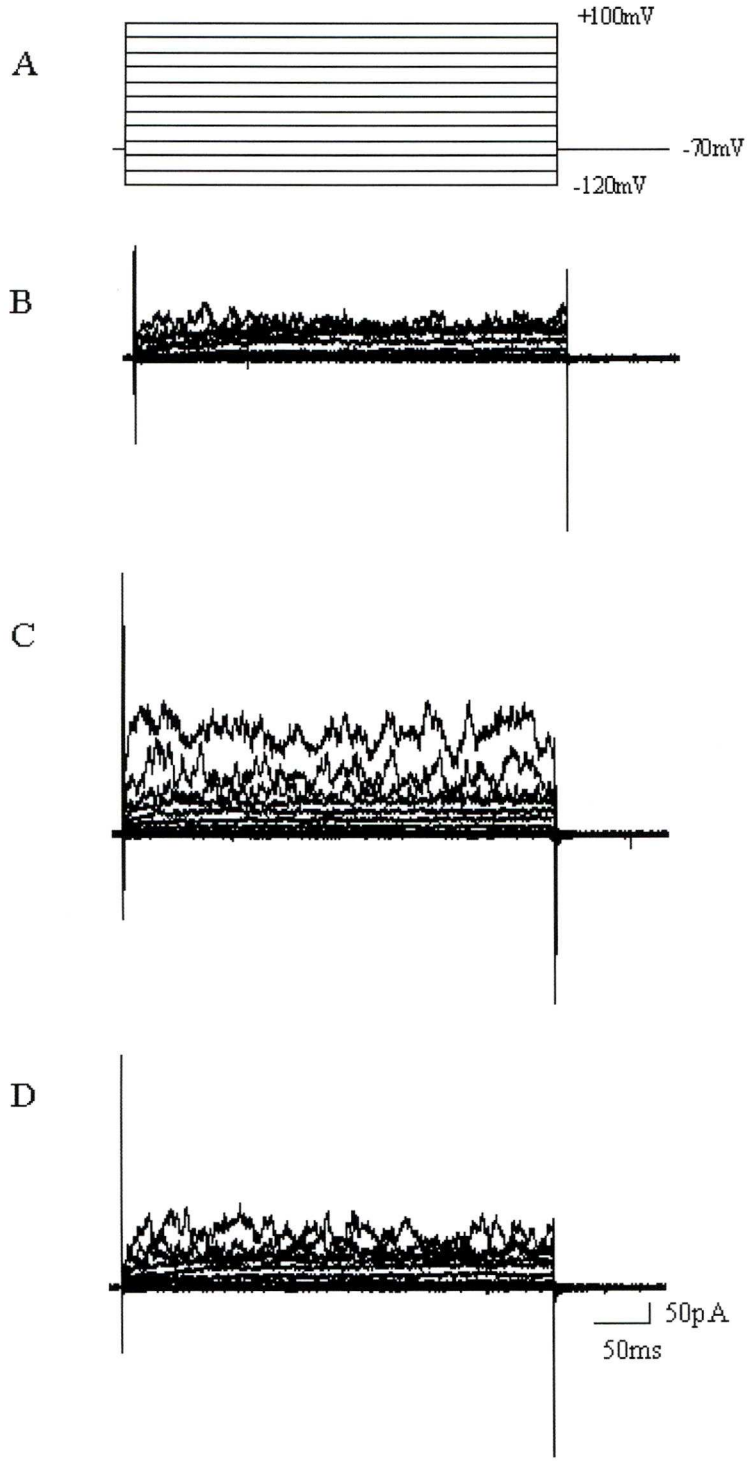

Figure 6.1. Typical whole cell current-voltage recording from a single SaOS-2 cell made using a voltage clamp protocol which made 10mV step changes from -120mV to +100mV, shown in A). Control current recording is shown in B). C) Cell was exposed to 20μM AA. D) Wash-out.

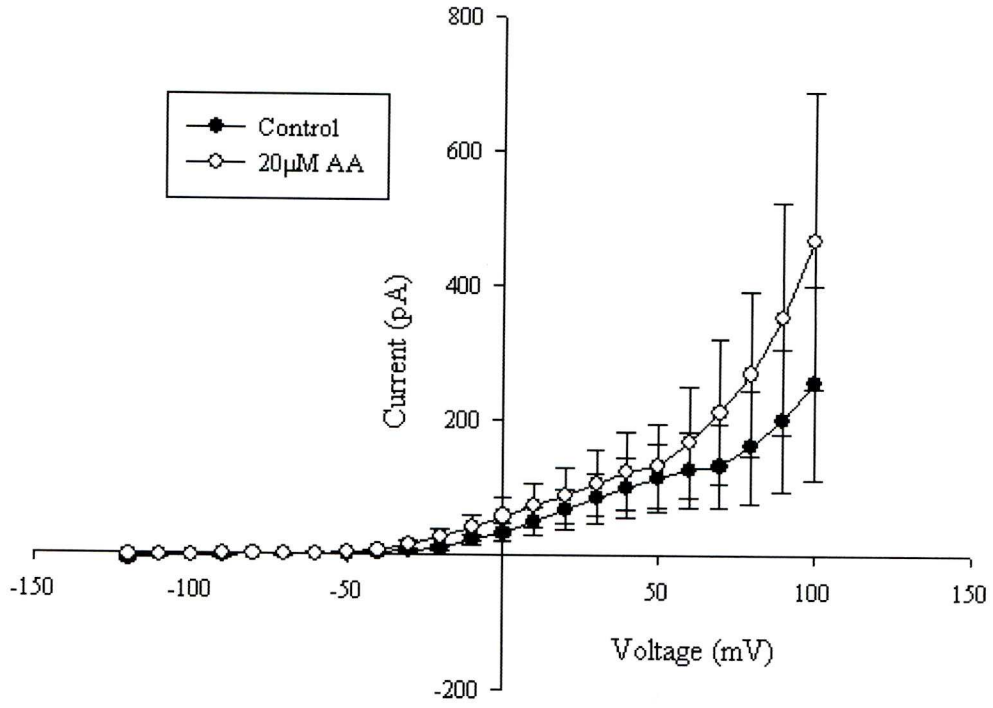

Figure 6.2. Mean IV curve obtained from SaOS-2 cells exposed to 20μM AA (n=5). Error bars represent S.E.M.

Figures 6.1 & 6.2 show a clear increase in whole-cell current upon application of 20μM AA. The effect is reversible as seen in part D of Figure 6.1. The increase in current starts to be become discernable at around -20mV, prior to this there is no difference between the AA-treated and control cells. At +100mV, cells exposed to 20μM AA display currents almost twice those of control cells.

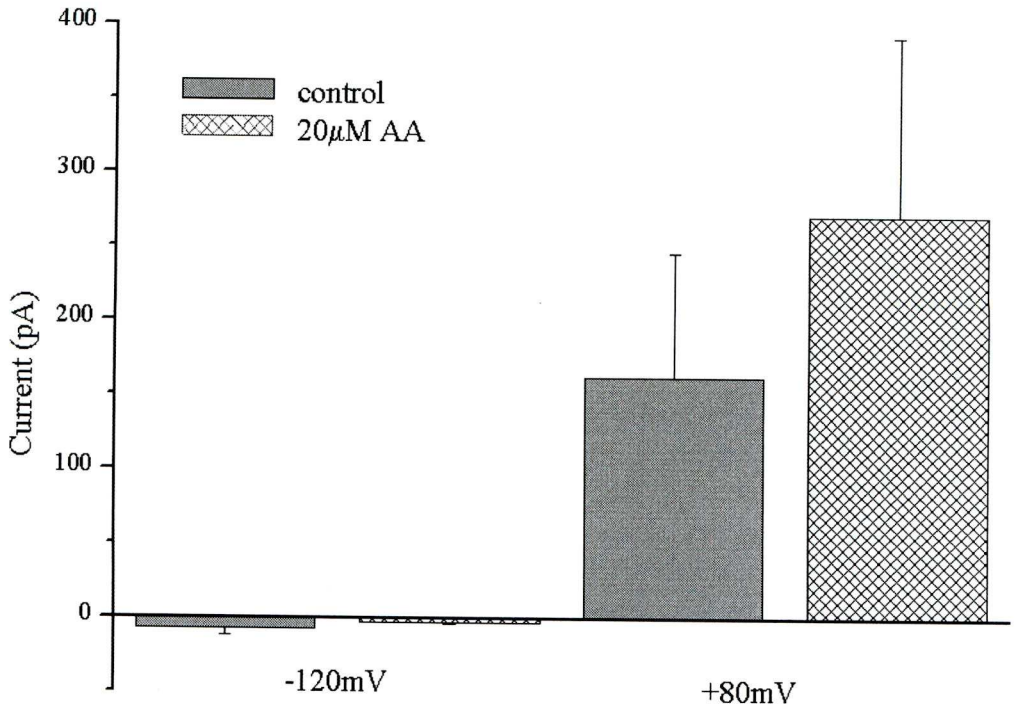

Figure 6.3. Mean current for SaOS-2 cells ± 20μM AA at -120 and +80mV (n=5).

Current values were very small at -120mV in both treated and non-treated cells. At +80mV, control current measured approximately 150pA but in cells exposed to AA the value was around 260pA. Due to the variability between the samples the standard error was high and the increase, although large, did not prove to be significant ($P>0.05$).

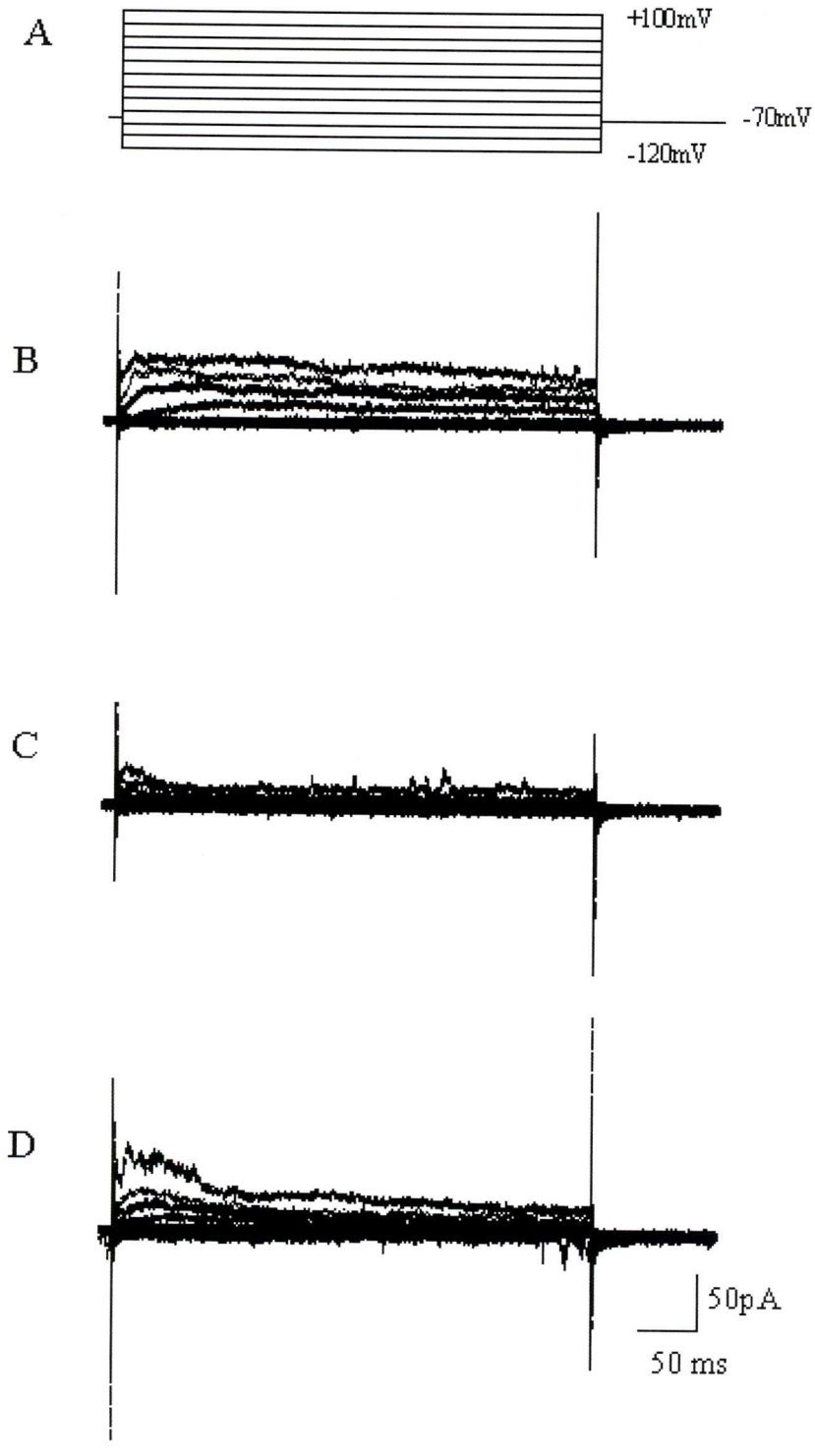

Figure 6.4. Typical whole cell current-voltage recording from a single TE-85 cell made using a voltage clamp protocol which made 10mV step changes from -120mV to +100mV, shown in A). Control current recording is shown in B). C) Cell was exposed to 20μM AA. D) Wash-out.

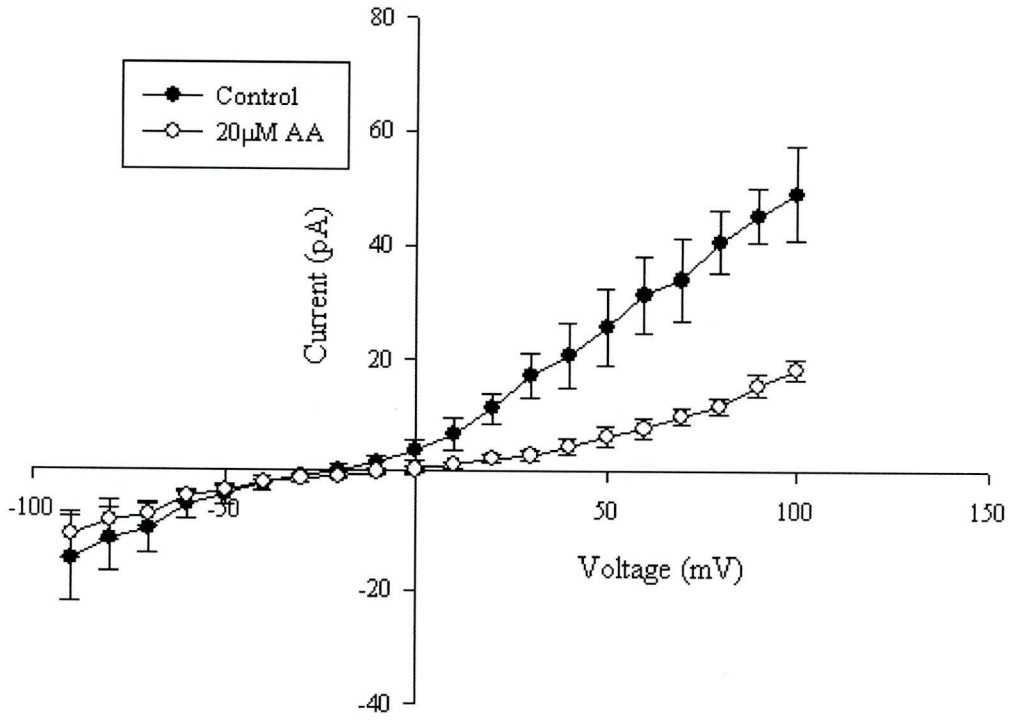

Figure 6.5. Average IV curve obtained from TE-85 cells exposed to 20μM AA (n=9). Error bars represent S.E.M.

Whole-cell currents decrease in TE-85 cells exposed to 20μM AA at more depolarized potentials. There appears to be a small reduction in inward current towards hyperpolarized potentials. The inhibitory effects of AA can be seen at membrane potentials above -20mV. This is the same point at which AA-induced currents in SaOS-2 cells start to show an increase over the control current (see Figure 6.2). Variability between TE-85 cells appeared to be more constant across the range of voltages than SaOS-2 cells.

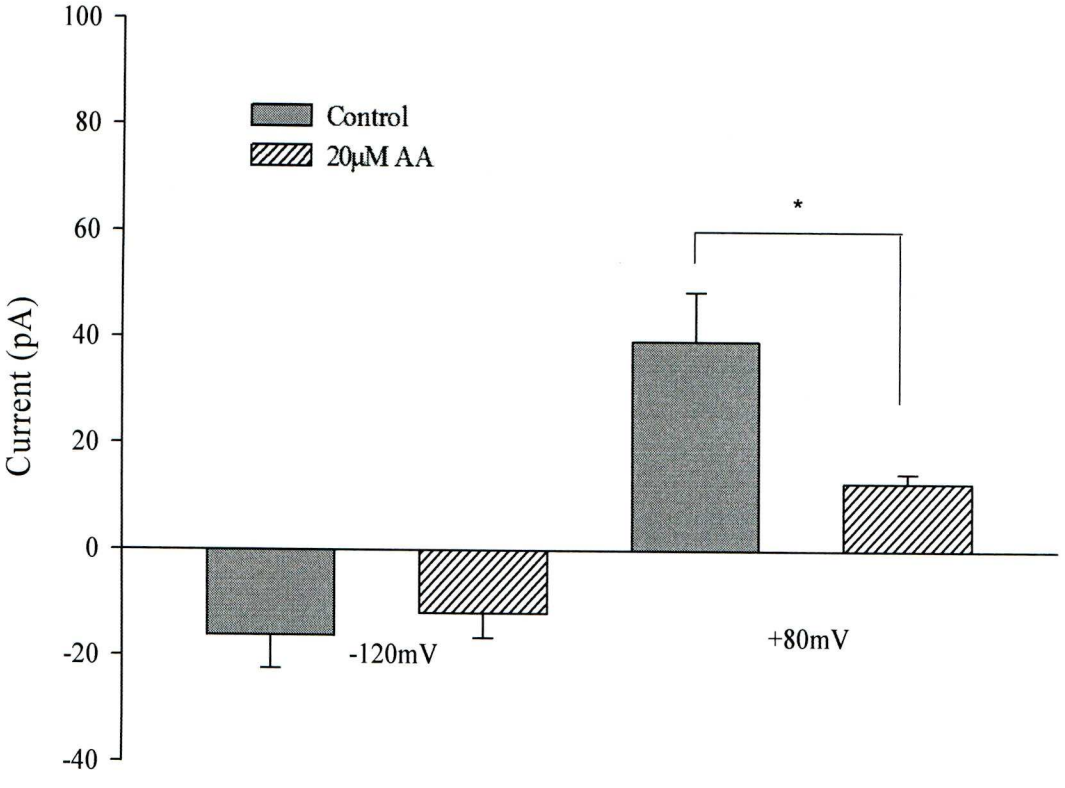

Figure 6.6. Mean current for TE-85 cells ± 20μM AA at -120 and +80mV (n=9).

Control cells showed similar whole-cell current to TE-85 cells treated with 20μM AA at the more negative membrane potentials. As the membrane potential became more positive, whole-cell currents were greater in control cells compared with treated cells. This difference proved to be significant at a membrane potential of +80mV ($p<0.5$).

6.3.2 Current-voltage recordings in osteoblastic cells exposed to BL-1249

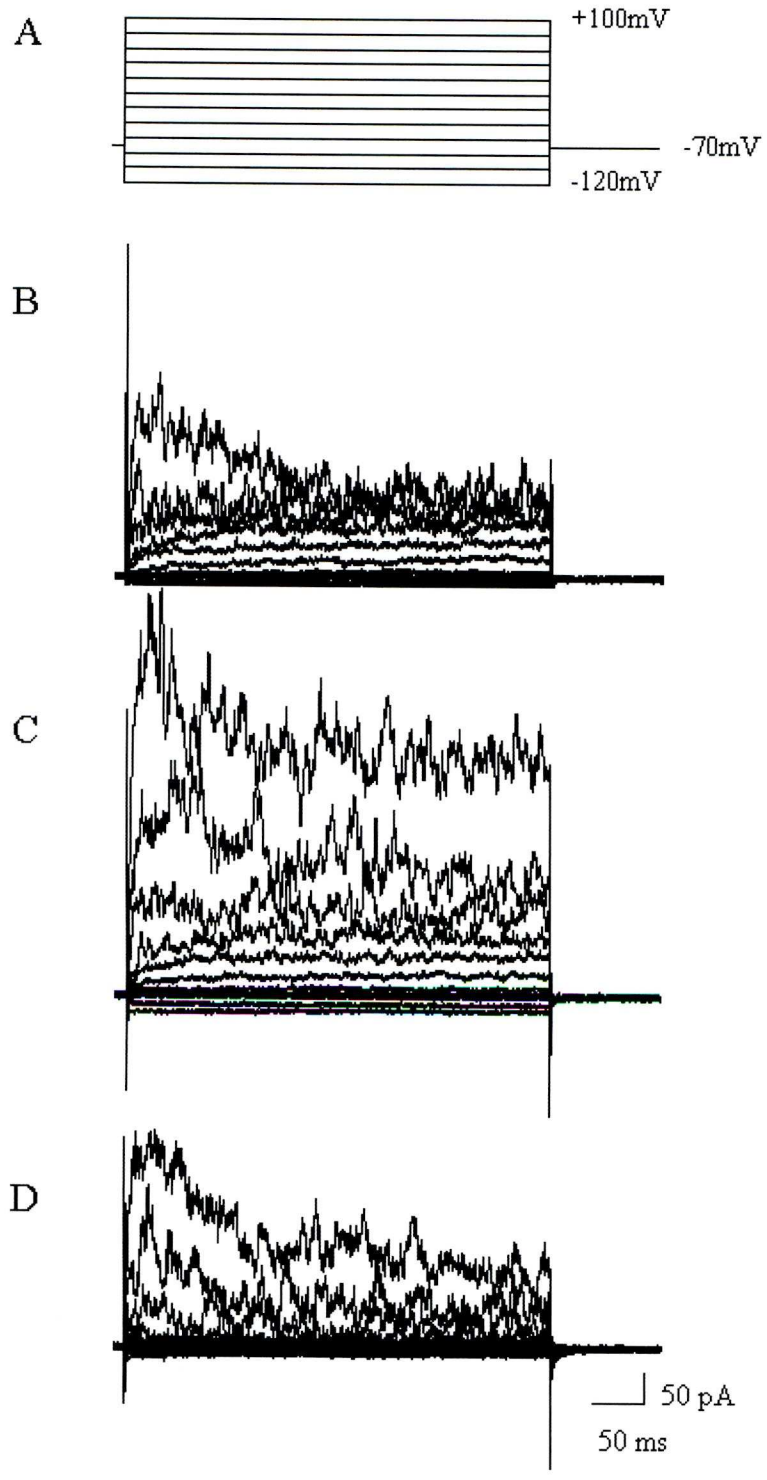

Figure 6.7. Typical whole cell current-voltage recording from a single SaOS-2 cell made using a voltage clamp protocol which made 10mV step changes from -120mV to

+100mV, shown in A). Control current recording is shown in B). C) Cell was exposed to 10μM BL-1249. D) Wash-out.

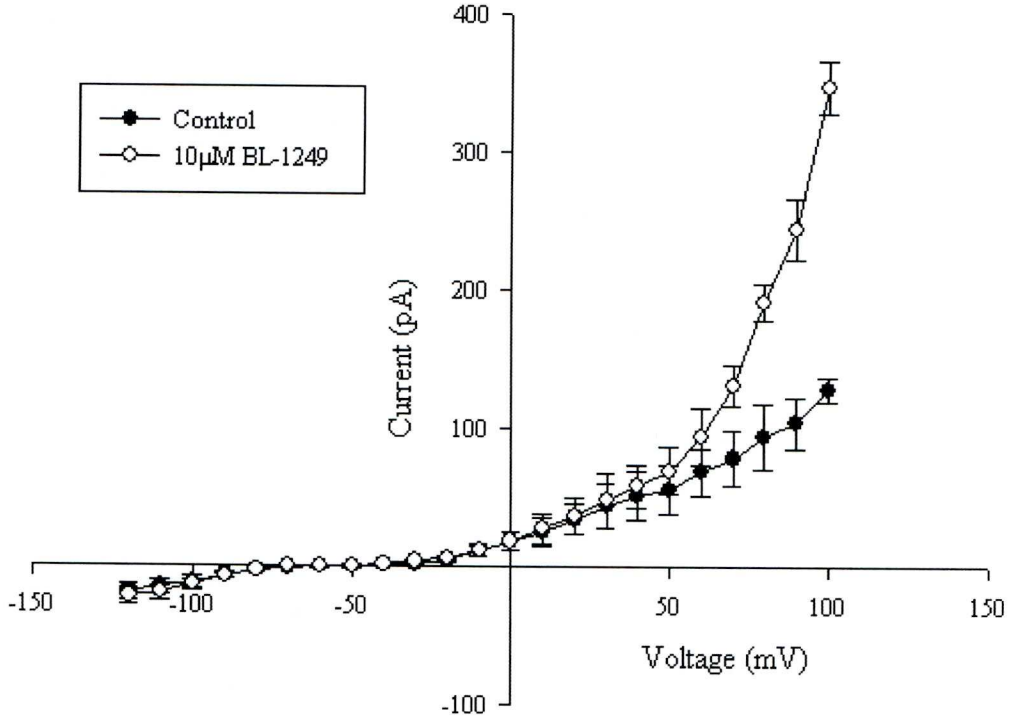

Figure 6.8. Mean IV curve obtained from SaOS-2 cells exposed to 10μM BL-1249 (n=6). Error bars represent S.E.M.

Administration of 10μM BL-1249 to SaOS-2 cells results in a large increase in whole-cell current at depolarized values, seen in Figures 6.6 & 6.7. Treated cells begin to show an increase in current compared to controls at around +40mV. Currents are roughly 3 times larger at +100mV in BL-1249 treated cells when compared with non-treated cells. Cell currents decrease after wash-out, showing that the effects of BL-1249 are reversible.

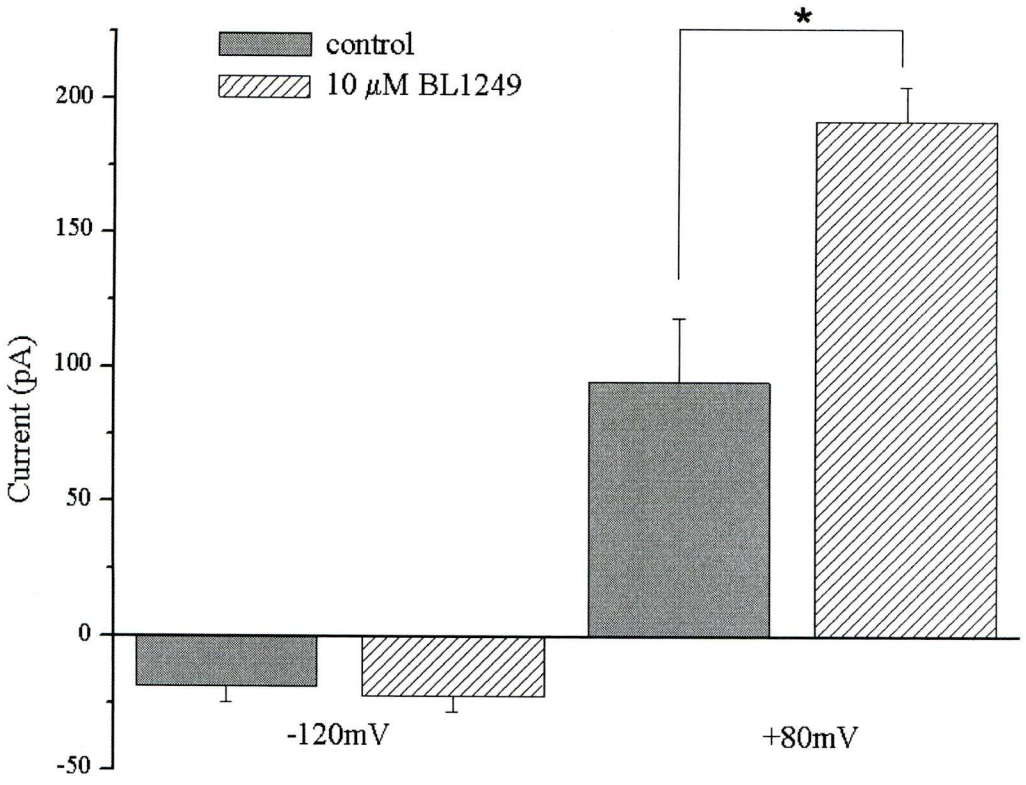

Figure 6.9. Mean current for SaOS-2 cells ± 10μM BL-1249 at -120 and +80mV (n=6).

Prior to BL-1249 administration, current values were around -20pA at -120mV. This value did not noticeably change upon exposure of the cells to 10μM BL-1249. The difference between the treatment and the control did prove significant at the more depolarized potentials, with the current being twice as large in BL-1249 treated cells at +80mV than in the control experiment ($P<0.05$).

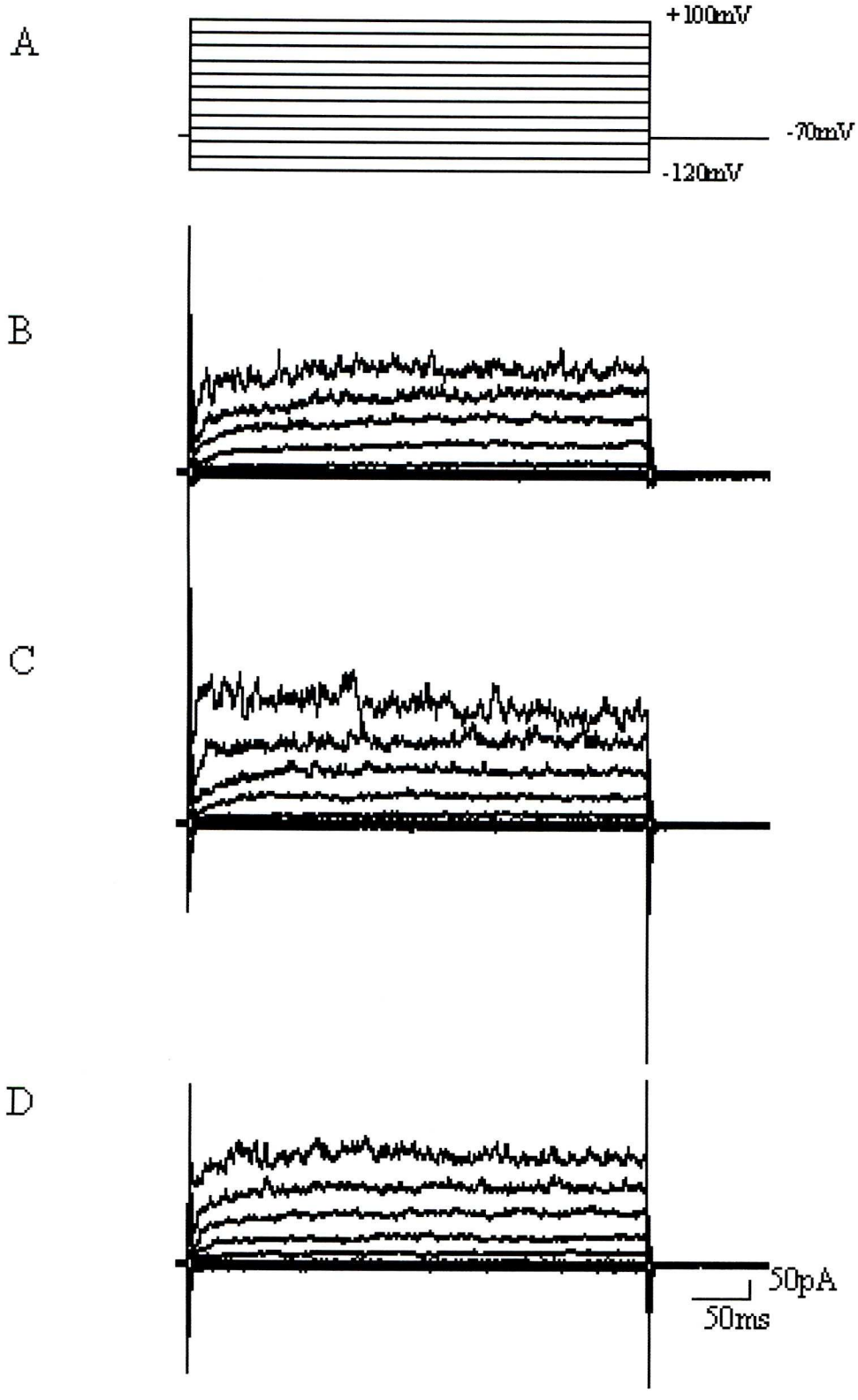

Figure 6.10. Whole cell current-voltage recording from a single TE-85 cell made using a voltage clamp protocol which made 10mV step changes from -120mV to +100mV, shown in A). Control current recording is shown in B). C) Cell was exposed to 10μM BL-1249. D) Wash-out.

The group of eight TE-85 cells exposed to BL-1249 produced five different outcomes. Three cells showed no change in current following BL-1249 administration. One cells showed a small increase in whole-cell current. One cell showed the activation of a small current in the first 100ms of the recording and none thereafter. Two cells displayed a more pronounced activation of this brief current at the start of the trace. One cell followed initial activation of this current followed by a small increase in overall whole-cell current. Because the results for BL-1249 were so variable and displayed no consistent pattern in TE-85 cells, it was decided not to construct a mean IV curve.

6.3.3 Membrane potential recordings

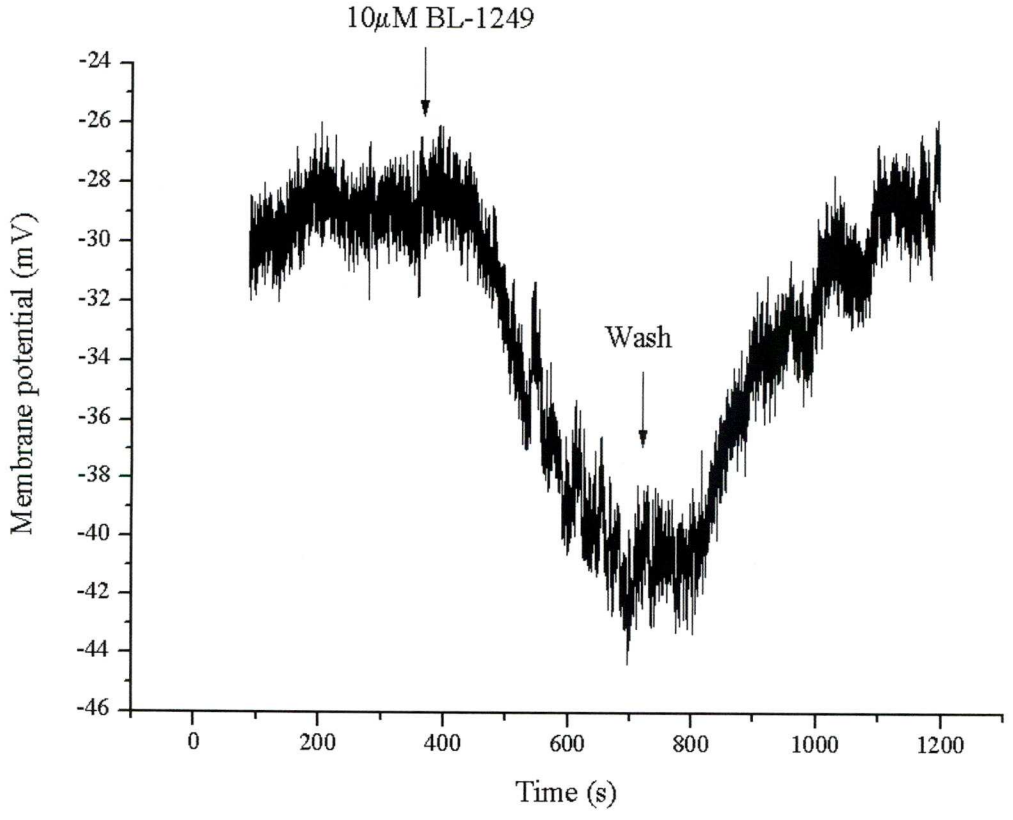

Figure 6.11. Membrane potential recording obtained from a single SaOS-2 cell exposed to 10μM BL-1249.

Recordings of membrane potential were made from six different SaOS-2 cells exposed to 10μM BL-1249. Results from one of these cells are shown above in Figure 6.11. This trace was typical of the six recordings made. A repeated measures analysis of variance test was performed on the three stages of the recording; resting membrane potential, BL-1249 treatment and wash out. The mean resting membrane potential was -22.9mV but following treatment with BL-1249, it became significantly more negative and the average value was -31.6mV ($n=6$, $P<0.001$). The effect of BL-1249 on membrane potential was reversible, and observations made after the wash out showed recovery of the membrane potential back to resting levels (-22.9mV, $n=6$). All six of the cells studied showed the same pattern of hyperpolarization upon exposure to BL-1249, followed by recovery.

6.4 Discussion

The experiments performed in this chapter have shown that BL-1249 directly activates ion channel currents in SaOS-2 cells. Although there is no definitive evidence that this current is caused by the outward flow of K^+, the membrane potential recordings reveal a distinctive hyperpolarization usually attributed to K^+ channel opening. Exposure to AA resulted in an increase in whole-cell current for SaOS-2 cells but a decrease in TE-85 cells. The difference in response to TREK activators continued upon the administration of BL-1249 to SaOS-2 and TE-85 cells. TE-85 cells displayed a large variability within the group studied whereas the response from SaOS-2 cells was consistent and proved significant when compared to the control ($P<0.05$ for +80mV recordings in the absence and presence of BL-1249).

The effects of BL-1249 reported in this Chapter wholly support the data presented by Tertyshnikova *et al.*, (2005), who reported an increase in whole cell current and membrane hyperpolarization in response to BL-1249 administration. Although the experiments by Tertyshnikova and colleagues were done on human bladder smooth muscle cells, they agree with the results shown here for SaOS-2 cells. The published study by Tertyshnikova *et al.*, (2005) represents the only item of literature documenting the effects of BL-1249. Soon after the publication

of the paper, Sigma began selling the compound as a putative TREK-1 activator. The scarce data on the pharmacology of BL-1249 places limitations on the depth of analysis applied to these results. Until further studies are performed on the compound and are subsequently published, it will remain a putative TREK-1 activator. The currents activated by BL-1249 in the study by Tertyshnikova *et al.*, (2005) appear to show voltage-independence, but the results shown in this chapter seem to implicate a voltage-dependent channel. As mentioned in the introduction to this Chapter, TREK-1 channels have the ability to display different voltage phenotypes depending on the levels of intracellular PIP_2 or its phosphorylation state. It is possible that BL-1249 may have the ability to activate other members of the TREK sub-family. TRAAK is a voltage-dependent channel that shows increased currents at depolarized potentials (Lesage *et al.*, 2000). In order to test for specificity against TREK channels an experiment could be designed using oocytes transfected with a particular channel and exposed to BL-1249. This would clearly demonstrate any activation of current or a hyperpolarizing effect.

The results obtained for AA in SaOS-2 cells are clear despite being non-significant. AA causes a considerable increase in current towards the more depolarised potentials. In TE-85 cells the data shows an opposing trend. Whole-cell currents appear to decrease upon administration of AA. The precise reason behind this difference cannot be determined from the results shown here. The difference may come from the expression of other ion channels beyond the scope of this study. It is probable that the inhibitory effect of AA on K_v channels is causing a reduction in whole-cell currents in this cell type (Meves, 2008). Another possibility is that the regulation of certain ion channels is somehow under alternative control in one of the cell lines studied.

The data for AA in SaOS-2 cells shows similarity to the results for BL-1249. Perhaps the most interesting difference is the voltage at which currents start to increase for the two compounds. In SaOS-2 cells treated with 10μM BL-1249, currents start to increase over control values at around +40mV. The same point in cells treated with AA is much lower at approximately -20mV. Although the differences do not become significant at these points in the IV curve, it is the

start of a divergence between the control and treated groups. Relatively few K^+ channels are activated by AA, and in fact most are inhibited by the polyunsaturated fatty acid (Meves, 2008). TASK-1 & -3 currents are inhibited by AA whereas TRAAK, TREK-1 & -2 currents increase rapidly following its application (Patel & Honoré, 2001). TWIK-2 channels are weakly activated by AA (Patel *et al.*, 2000). This supports the idea that functional K_{2P} currents in osteoblasts can be observed by adding AA, given that in previous chapters the expression of TRAAK, TREK-1 and TWIK-2 have all been noted.

The value of the resting membrane potential in SaOS-2 cells was found to be -22.9mV in this study (n=6). This was comparable to the values given by Ferrier *et al.* (1987) and Hughes *et al.* (2006) of -24 and -21.5mV made from rat osteoblastic cells and MG-63 cells respectively. Hyperpolarization induced by 10μM BL-1249 brought the membrane potential down to 31.6mV, which proved to be a significant change ($P<0.001$, n=6). Membrane potential recovered back to resting levels upon the removal of BL-1249 from the bathing solution. If the reversal potentials for Cl^-, Na^+ and non-selective cation channels are calculated using the Nernst equation, then it becomes clear that activation of any of these channels would lead to depolarization. Whole-cell IV recordings in SaOS-2 cells show the activation of a current in response to BL-1249 treatment. It is therefore likely that the hyperpolarization seen in Figures 6.10 & 6.11 is caused by the activation of a K^+ channel and not the inhibition of a depolarizing current.

In hindsight, it may have been wise to run a third compound alongside BL-1249 and AA in these studies. LPC is a known TREK activator and it has a much more stable half-life in solution than AA. Pharmacological agents that block these channels are still scarce and usually require very high doses, meaning that other K^+ channels are also inhibited. Also, to confirm the identity of the ion movement responsible for the increased current in SaOS-2 cells, different concentrations of extracellular K^+ could be used. Comparison of these mean IV curves would enable an accurate conclusion to be formed about the ion involved in creating the outward current seen here.

6.5 Conclusions

In SaOS-2 cells the administration of 10μM BL-1249 results in an increase in whole cell current at depolarized membrane potentials ($P<0.05$ at +80mV). It also produces a significant hyperpolarization during current clamp protocols in the same cell type ($P<0.001$). These data strongly agree with the single study detailing the effects of BL-1249 in the literature (Tertyshnikova *et al.*, (2005). The results for TE-85 cells were not so clear, but because the experiments done in Chapter 6 had incorporated BL-1249 treatment on SaOS-2 reporter cells, it was decided to focus on results from this cell type. Further electrophysiological characterization of the currents enhanced by BL-1249 is required so that any future use of the compound by others can be carefully considered. Due to the lack of commercially available K_{2P} activators, BL-1249 could represent an important tool in the further study of TREK channels.

7.0 General Discussion

7.1 Discussion of results in the context of the current literature

The experiments detailed within this thesis have demonstrated mRNA and protein expression of various K_{2P} channels in primary osteoblasts and osteoblastic cells. Various methods pointed to the presence of members of the TASK, TWIK, TALK & TREK families in osteoblastic cells. Functional expression did not prove as straightforward to characterise, due to the limited range of pharmacological agents that are able to target this group of channels and variations in the responses from different cell lines. The use of the putative TREK-1 activator BL-1249 posed a number of questions in addition to the answers it provided, due to the relatively unknown pharmacology of the compound. BL-1249 significantly reduced the expression of c-fos induced by PTH in SaOS-2 reporter cells in a dose-dependent manner ($P<0.001$, IC_{50} value was calculated as 16.6μM). It also increased whole-cell current and hyperpolarized the membrane potential in the same cell type.

In the most part, the expression profile of K_{2P} channel mRNA shown in Chapter 3 agreed with the limited data published in the literature. Perhaps the most anomalous finding was the lack of TREK-1 mRNA in MG-63 cells (see Figure 3.18) despite Hughes *et al.,* (2006) claiming it was strongly expressed in their study. There were no obvious reasons for this discrepancy, as successful sequencing showed that the primers were correctly targeting TREK-1 mRNA and the same batch of cDNA yielded positive results for other members of the K_{2P} channel family. Also, immunocytochemical staining of this cell type revealed TREK-1 protein to be present at the plasma membrane. Other than for this result, the expression profile of the TREK channels was not dissimilar, with TRAAK channels being strongly expressed throughout samples and a lack of TREK-2 mRNA. Rat osteoblastic cells observed by Chen *et al.*, (2005) were shown to express TREK-2 and that the channel was necessary for the majority of the upregulation of PTHrP expression following mechanical stimulation. This prompts speculation that there may be species-variation of TREK channel expression in osteoblasts. Species-specific differences have already been reported for TWIK and TRESK channels (Patel *et al.* 2000, Keshavaprasad *et al.*, 2005). The profile of mRNA expression in osteoblasts shows great similarity to

that reported for human periodontal ligament (PDL) fibroblasts (Saeki *et al.*, 2007). The PDL acts as a cushion between bone and tooth. It is exposed to large forces during mastication and therefore may require protection through K_{2P} channels. High performance liquid chromotography (HPLC) analysis showed almost a two-fold increase in cyclically stretched PDL fibroblast AA levels over control conditions (Saeki *et al.*, 2007). Autocrine release of AA would provide another mechanism of activating TREK channels to bring the membrane potential back down to resting levels after a mechanical excitation, thus preventing cell damage.

Data from the immunocytochemistry and western blotting experiments provided evidence that the mRNA expression described in Chapter 3 translated into protein expression. Immunocytochemistry also gave an indication that for at least some of the channels, protein was trafficked to the plasma membrane. This was particularly the case with the results obtained using the anti-TREK-1 antibody, although expression of TRAAK, TWIK-2 and TASK-2 appeared strong in some of the cell lines studied. TASK-1 expression seemed weak and mainly perinuclear, although western blotting for this channel gave intense bands. Western blotting appeared to reveal dimerization of TRAAK & TREK-1 channels.

Experiments using SaOS-2 cells stably transfected with a c-fos reporter gene, proved useful in characterizing osteoblastic responses to various ion channel agents. Riluzole demonstrated a significant increase in c-fos in cells treated with PTH, but showed no effect on its own ($P<0.001$ for PTH-treated cells). The fellow TREK-1 activator, BL-1249, produced contrasting effects by significantly reducing the PTH-induced elevation of c-fos ($P<0.001$). The explanation of these results must lie in the alternative pharmacology of both drugs. Riluzole is known to have effects on many other cellular proteins whereas little is known about the actions of BL-1249. Other interesting points from this set of experiments include the apparent lack of c-fos modulation by voltage-gated K^+ & Ca^{2+} channels. The experiments designed to reveal PTHR1 second messengers in the reporter cells supported the study by Evans *et al.*, (1996) who found that PKA was solely responsible for the effects of PTH in SaOS-2 cells. Data shown in this thesis

suggests that H-89 totally inhibited the c-fos response to PTH, although the supposedly more selective PKA inhibitor KT5720 displayed limited effects on PTH-induced c-fos expression. Live cell Ca^{2+} imaging also indirectly supported the involvement of PKA, as no elevation of $[Ca^{2+}]_i$ was observed upon addition of PTH to SaOS-2 cells.

Whole-cell patch clamp recording from SaOS-2 cells revealed an increase in current in response to both AA and BL-1249 ($P<0.05$ for +80mV recordings in the absence and presence of BL-1249). These compounds activate TREK channels although the experimental protocols used did not allow the specific identification of the channel or channels responsible for this effect. Results from TE-85 cells differed greatly from those obtained with SaOS-2 cells. TE-85 cells displayed a decrease in overall current upon the addition of AA whereas the response to BL-1249 was highly variable, making comparison difficult. Membrane potential recordings from SaOS-2 cells gave an average resting value of -22.9mV (n=6). When treated with 10μM BL-1249 there was a significant hyperpolarization which brought the membrane potential down to -31.6mV (n=6, $P<0.001$). Hyperpolarization and an increase in whole cell current have previously been reported following the administration of BL-1249 in bladder smooth muscle (Tertyshnikova *et al.*, 2005).

Two immediate questions are raised by this body of work. Firstly, what is the functional significance of K_{2P} channels in osteoblasts, and secondly what is the specific pharmacology of BL-1249? The second question is one that further experimental work should answer over time. Electrophysiological characterization is needed in the first instance, but effects on proteins other than ion channels also need to be investigated. In order to address the first question it is necessary to look again at the basic properties of K_{2P} channels, which include setting the resting membrane potential and transducing intracellular and extracellular stimuli. Both of these functions would serve to help an osteoblast perform its role as a secretory cell which is tightly regulated by several factors in its immediate environment. Maintenance of resting membrane potential is crucial to many cells but this is particularly the case for excitable or secretory cells. This simple observation explains why the potassium channel superfamily is so large

and widely expressed in mammals and even lower organisms. The emerging properties assigned to K_{2P} channels mean that this versatile group of proteins are likely to have a large profile of expression and it should come as no surprise that they are present in bone. The external environment of an osteoblast varies greatly according to the stage of the remodelling process. During resorption the surrounding pH can become low, whereas cells which are actively involved in bone formation can be exposed to high pH during to the deposition of hydroxyapatite. Extracellular Ca^{2+} can be high in both scenarios. Acidosis is known to inhibit the mineralization of the collagenous matrix (Arnett, 2008). It is conceivable that the presence of one or more TASK channels would be a useful addition to an osteoblasts repertoire of proteins during remodelling. The role of TWIK channels in osteoblasts has yet to be uncovered. The consistent expression of this sub-family across the cell lines studied here points towards a functional role for these channels in skeletal tissue. Characterization of the properties of these channels in other cell lines may help us in understanding the presence of these proteins in osteoblasts. The relevance of TREK channels in bone has obviously been spotted by others, and this sub-family would seem the most obvious candidate to screen for. It is interesting that no studies have yet focussed on the expression of TREK-1 in osteocytes. As a terminally differentiated osteoblast whose primary function is mechanosensing, it would seem that the expression of TREK-1 is likely in these cells. Figure 7.1 demonstrates some of the potential functions K_{2P} channels could usefully serve in an osteoblast.

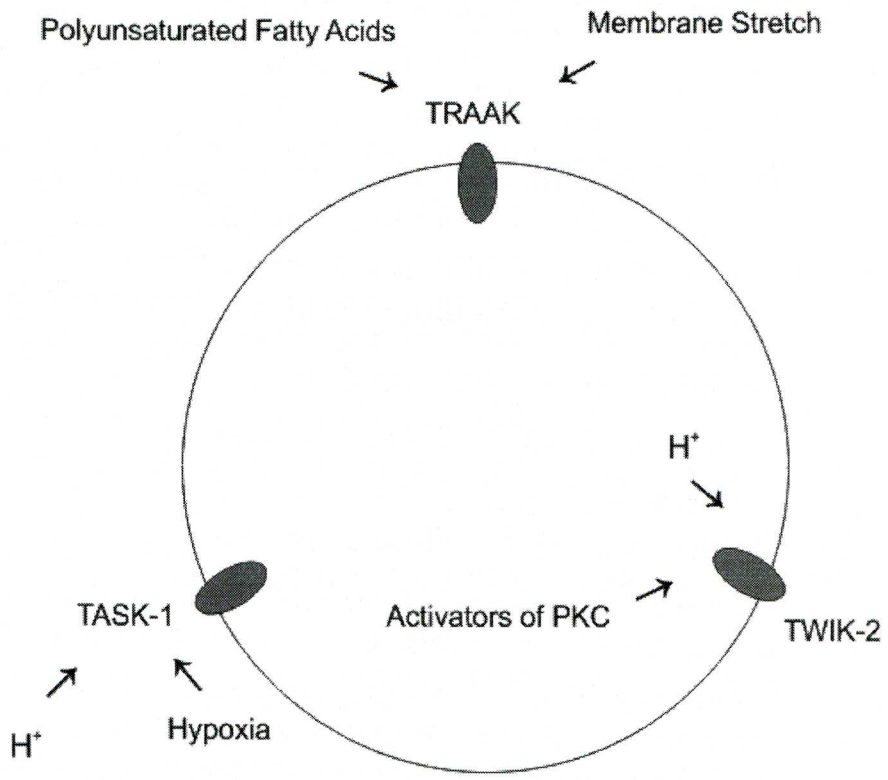

Figure 7.1. A schematic representation of the potential roles K_{2P} channels may perform in osteoblasts.

This thesis has provided a thorough examination of K_{2P} channel expression in osteoblastic cells and provides unequivocal evidence that exposes the presence of TASK, TWIK, TALK & TREK channels. The knowledge that TREK channels are not the only K_{2P} sub-family to be expressed in osteoblasts will hopefully influence the scope of future studies. This interesting family of proteins certainly deserves some attention from scientists working in the field of skeletal biology. The data obtained using BL-1249 also warrants further investigation, by electrophysiologists in particular. It may prove to be a potentially useful compound for the study of TREK-1 channels.

7.2 Further experiments

If time had allowed, experiments would have continued using more detailed electrophysiological studies. Experiments to confirm the identity of the channel or channels involved in the response to BL-1249 would provide much-needed information on the definitive pharmacology of BL-1249. Characterization of the currents seen during voltage clamp protocols using pharmacological compounds would have been useful in profiling the functional expression of other K^+ channels expressed in osteoblasts and in eliminating them as potential targets of BL-1249. Membrane potential recordings from MA16 cells could be taken to compare with the values found from SaOS-2 cells, given that Hughes *et al.*, (2006) found primary osteoblasts to have a more negative resting membrane potential. Membrane potential recordings for TE-85 cells exposed to BL-1249 would perhaps give more clues as to the actions of this compound given the variation seen between this cell type and SaOS-2 cells during the voltage clamp experiments. Although there is no direct evidence to suggest effects of BL-1249 on cAMP levels, it would be wise to rule this out before any further c-fos reporter experiments. cAMP measurements following the addition of BL-1249 could be compared with non-treated cells. Riluzole could also be added to provide a positive control. It would have been interesting to compare the results obtained in Chapter 4 using antibodies from Alamone Labs, to experiments performed with ones produced by Santa Cruz. This is particularly the case for western blotting, given that the results gained would be more comparable with those obtained by Hughes *et al.*, (2006). The use of Santa Cruz antibodies may also give a clearer indication of protein expression for TRAAK when taking into account the potential for non-specific binding exposed in during the western blot for this particular antibody. Had time allowed, sequencing reactions would have been carried out on PCR product from TASK-3 & -5 and TREK-2 primer sets run with MA16 or SK-N-AS cDNA. A tissue sample from human spinal cord would perhaps validate the primer set for TRESK, although this would not be easy to obtain.

For more complex experiments involving a longer time frame, K_{2P} knockout animals could be observed for bone phenotypes. To the authors' knowledge, no effects on bone have been reported in K_{2P} knockout mice at the present time. However, given the possible role of the TREK subfamily in mechanotransduction, it might seem possible that effects of K_{2P} channels could be observed upon mechanical loading of bones in wild-type, heterogeneous and homogeneous animals. Another series of experiments on similar lines could involve the use of siRNA (small interfering RNA) to observe the effects of temporary abolition of K_{2P} gene products on bone structure and function, as seen in the paper by Chen *et al.*, (2005).

Bibliography

- Abed, E., D. Labelle, et al. (2009). "Expression of transient receptor potential (TRP) channels in human and murine osteoblast-like cells." Mol Membr Biol 26(3): 146-58.

- Abou-Samra, A. B., H. Juppner, et al. (1992). "Expression cloning of a common receptor for parathyroid hormone and parathyroid hormone-related peptide from rat osteoblast-like cells: a single receptor stimulates intracellular accumulation of both cAMP and inositol trisphosphates and increases intracellular free calcium." Proc Natl Acad Sci U S A 89(7): 2732-6.

- Alesci, S., M. U. De Martino, et al. (2005). "Glucocorticoid-induced osteoporosis: from basic mechanisms to clinical aspects." Neuroimmunomodulation 12(1): 1-19.

- Allen, M. R., J. M. Hock, et al. (2004). "Periosteum: biology, regulation, and response to osteoporosis therapies." Bone 35(5): 1003-12.

- Amoroso, S., H. Schmid-Antomarchi, et al. (1990). "Glucose, sulfonylureas, and neurotransmitter release: role of ATP-sensitive K+ channels." Science 247(4944): 852-4.

- Arnett, T. R. (2008). "Extracellular pH regulates bone cell function." J Nutr 138(2): 415S-418S.

- Bakker, A. D., M. Joldersma, et al. (2003). "Interactive effects of PTH and mechanical stress on nitric oxide and PGE2 production by primary mouse osteoblastic cells." Am J Physiol Endocrinol Metab 285(3): E608-13.

- Baldi, C., G. Vazquez, et al. (2003). "TRPC3-like protein is involved in the capacitative cation entry induced by 1alpha,25-dihydroxy-vitamin D3 in ROS 17/2.8 osteoblastic cells." J Cell Biochem 90(1): 197-205.

- Balemans, W. and W. Van Hul (2007). "The genetics of low-density lipoprotein receptor-related protein 5 in bone: a story of extremes." Endocrinology 148(6): 2622-9.

- Bayliss, D. A., E. M. Talley, et al. (2001). "TASK-1 is a highly modulated pH-sensitive 'leak' K(+) channel expressed in brainstem respiratory neurons." Respir Physiol 129(1-2): 159-74.

- Beckett, E. A., I. Han, et al. (2008). "Functional and molecular identification of pH-sensitive K+ channels in murine urinary bladder smooth muscle." BJU Int 102(1): 113-24.

- Beresford, J. N., J. A. Gallagher, et al. (1986). "1,25-Dihydroxyvitamin D3 and human bone-derived cells in vitro: effects on alkaline phosphatase, type I collagen and proliferation." Endocrinology 119(4): 1776-85.

- Bergh, J. J., Y. Shao, et al. (2003). "Rodent osteoblastic cells express voltage-sensitive calcium channels lacking a gamma subunit." Calcif Tissue Int 73(5): 502-10.

- Bergh, J. J., Y. Shao, et al. (2006). "Osteoblast Ca(2+) permeability and voltage-sensitive Ca(2+) channel expression is temporally regulated by 1,25-dihydroxyvitamin D(3)." Am J Physiol Cell Physiol 290(3): C822-31.

- Berridge, M. J. (1995). "Capacitative calcium entry." Biochem J 312 (Pt 1): 1-11.

- Bizzarri, C. and R. Civitelli (1994). "Activation of the Ca2+ message system by parathyroid hormone is dependent on the cell cycle." Endocrinology 134(1): 133-40.

- Bkaily, G., M. Nader, et al. (2006). "G-protein-coupled receptors, channels, and Na+-H+ exchanger in nuclear membranes of heart, hepatic, vascular endothelial, and smooth muscle cells." Can J Physiol Pharmacol 84(3-4): 431-41.

- Bockenhauer, D., N. Zilberberg, et al. (2001). "KCNK2: reversible conversion of a hippocampal potassium leak into a voltage-dependent channel." Nat Neurosci 4(5): 486-91.

- Boland, C. J., R. M. Fried, et al. (1986). "Measurement of cytosolic free Ca2+ concentrations in human and rat osteosarcoma cells: actions of bone resorption-stimulating hormones." Endocrinology 118(3): 980-9.

- Bowler, W. B., C. J. Dixon, et al. (1999). "Signaling in human osteoblasts by extracellular nucleotides. Their weak induction of the c-fos proto-oncogene via Ca2+ mobilization is strongly potentiated by a parathyroid hormone/cAMP-dependent protein kinase pathway independently of mitogen-activated protein kinase." J Biol Chem 274(20): 14315-24.

- Boyce, B. F. and L. Xing (2008). "Functions of RANKL/RANK/OPG in bone modeling and remodeling." Arch Biochem Biophys 473(2): 139-46.

- Brazier, S. P., H. S. Mason, et al. (2005). "Cloning of the human TASK-2 (KCNK5) promoter and its regulation by chronic hypoxia." Biochem Biophys Res Commun 336(4): 1251-8.

- Breitenlechner, C. B., D. Bossemeyer, et al. (2005). "Crystallography for protein kinase drug design: PKA and SRC case studies." Biochim Biophys Acta 1754(1-2): 38-49.

- Buckler, K. J. (2007). "TASK-like potassium channels and oxygen sensing in the carotid body." Respir Physiol Neurobiol 157(1): 55-64.

- Buckler, K. J., B. A. Williams, et al. (2000). "An oxygen-, acid- and anaesthetic-sensitive TASK-like background potassium channel in rat arterial chemoreceptor cells." J Physiol 525 Pt 1: 135-42.

- Buckley, K. A., S. C. Wagstaff, et al. (2001). "Parathyroid hormone potentiates nucleotide-induced [Ca2+]i release in rat osteoblasts independently of Gq activation or cyclic monophosphate accumulation. A mechanism for localizing systemic responses in bone." J Biol Chem 276(12): 9565-71.

- Burns, D. M., L. Stehno-Bittel, et al. (2004). "Calcitonin gene-related peptide elevates calcium and polarizes membrane potential in MG-63 cells by both cAMP-independent and -dependent mechanisms." Am J Physiol Cell Physiol 287(2): C457-67.

- Butler, J., A. Warley, et al. (2010). "Immunolocalization of mitoKATP subunits in human osteoblast-like cells." Front Biosci 2: 739-51.

- Caffrey, J. M. and M. C. Farach-Carson (1989). "Vitamin D3 metabolites modulate dihydropyridine-sensitive calcium currents in clonal rat osteosarcoma cells." J Biol Chem 264(34): 20265-74.

- Chavez, R. A., A. T. Gray, et al. (1999). "TWIK-2, a new weak inward rectifying member of the tandem pore domain potassium channel family." J Biol Chem 274(12): 7887-92.

- Chemin, J., C. Girard, et al. (2003). "Mechanisms underlying excitatory effects of group I metabotropic glutamate receptors via inhibition of 2P domain K+ channels." EMBO J 22(20): 5403-11.

- Chen, X., C. M. Macica, et al. (2005). "Stretch-induced PTH-related protein gene expression in osteoblasts." J Bone Miner Res 20(8): 1454-61.

- Chesnoy-Marchais, D. and J. Fritsch (1994). "Concentration-dependent modulations of potassium and calcium currents of rat osteoblastic cells by arachidonic acid." J Membr Biol 138(2): 159-70.

- Chow, J. W., S. Fox, et al. (1998). "Role for parathyroid hormone in mechanical responsiveness of rat bone." Am J Physiol 274(1 Pt 1): E146-54.

- Civitelli, R., Y. S. Kim, et al. (1990). "Nongenomic activation of the calcium message system by vitamin D metabolites in osteoblast-like cells." Endocrinology 127(5): 2253-62.

- Cole, J. A. (1999). "Parathyroid hormone activates mitogen-activated protein kinase in opossum kidney cells." Endocrinology 140(12): 5771-9.

- Damsky, C. H. (1999). "Extracellular matrix-integrin interactions in osteoblast function and tissue remodeling." Bone 25(1): 95-6.

- De Vry, J., R. Schreiber, et al. (1999). "Discriminative and affective stimulus effects of dihydropyridine calcium channel modulators: relationship to antialcohol effects." Pharmacol Biochem Behav 64(2): 203-11.
- Debska, G., A. Kicinska, et al. (2001). "Intracellular potassium and chloride channels: an update." Acta Biochim Pol 48(1): 137-44.
- Doble, A. (1996). "The pharmacology and mechanism of action of riluzole." Neurology 47(6 Suppl 4): S233-41.
- Dobnig, H. and R. T. Turner (1995). "Evidence that intermittent treatment with parathyroid hormone increases bone formation in adult rats by activation of bone lining cells." Endocrinology 136(8): 3632-8.
- Doyle, D. A., J. Morais Cabral, et al. (1998). "The structure of the potassium channel: molecular basis of K+ conduction and selectivity." Science 280(5360): 69-77.
- Ducy, P. (2000). "Cbfa1: a molecular switch in osteoblast biology." Dev Dyn 219(4): 461-71.
- Ducy, P., M. Amling, et al. (2000). "Leptin inhibits bone formation through a hypothalamic relay: a central control of bone mass." Cell 100(2): 197-207.
- Ducy, P., T. Schinke, et al. (2000). "The osteoblast: a sophisticated fibroblast under central surveillance." Science 289(5484): 1501-4.
- Duprat, F., C. Girard, et al. (2005). "Pancreatic two P domain K+ channels TALK-1 and TALK-2 are activated by nitric oxide and reactive oxygen species." J Physiol 562(Pt 1): 235-44.
- Duprat, F., I. Lauritzen, et al. (2007). "The TASK background K2P channels: chemo- and nutrient sensors." Trends Neurosci 30(11): 573-80.
- Duprat, F., F. Lesage, et al. (2000). "The neuroprotective agent riluzole activates the two P domain K(+) channels TREK-1 and TRAAK." Mol Pharmacol 57(5): 906-12.
- Dworetzky, S. I., E. G. Fey, et al. (1990). "Progressive changes in the protein composition of the nuclear matrix during rat osteoblast differentiation." Proc Natl Acad Sci U S A 87(12): 4605-9.
- Enserink, J. M., A. E. Christensen, et al. (2002). "A novel Epac-specific cAMP analogue demonstrates independent regulation of Rap1 and ERK." Nat Cell Biol 4(11): 901-6.
- Evans, D. B., R. A. Hipskind, et al. (1996). "Analysis of signaling pathways used by parathyroid hormone to activate the c-fos gene in human SaOS2 osteoblast-like cells." J Bone Miner Res 11(8): 1066-74.

- Ferrier, J., A. Ward-Kesthely, et al. (1987). "Further analysis of spontaneous membrane potential activity and the hyperpolarizing response to parathyroid hormone in osteoblastlike cells." J Cell Physiol 130(3): 344-51.

- Fink, M., F. Duprat, et al. (1996). "Cloning, functional expression and brain localization of a novel unconventional outward rectifier K+ channel." EMBO J 15(24): 6854-62.

- Franceschi, R. T. (1999). "The developmental control of osteoblast-specific gene expression: role of specific transcription factors and the extracellular matrix environment." Crit Rev Oral Biol Med 10(1): 40-57.

- Fujita, T., T. Meguro, et al. (2002). "New signaling pathway for parathyroid hormone and cyclic AMP action on extracellular-regulated kinase and cell proliferation in bone cells. Checkpoint of modulation by cyclic AMP." J Biol Chem 277(25): 22191-200.

- Fukayama, S., A. H. Tashjian, Jr., et al. (1992). "Mechanisms of desensitization to parathyroid hormone in human osteoblast-like SaOS-2 cells." Endocrinology 131(4): 1757-69.

- Gallagher, J. A. (2004). "ATP P2 receptors and regulation of bone effector cells." J Musculoskelet Neuronal Interact 4(2): 125-7.

- Gesty-Palmer, D., M. Chen, et al. (2006). "Distinct beta-arrestin- and G protein-dependent pathways for parathyroid hormone receptor-stimulated ERK1/2 activation." J Biol Chem 281(16): 10856-64.

- Gjertsen, B. T., G. Mellgren, et al. (1995). "Novel (Rp)-cAMPS analogs as tools for inhibition of cAMP-kinase in cell culture. Basal cAMP-kinase activity modulates interleukin-1 beta action." J Biol Chem 270(35): 20599-607.

- Gobeil, F., Jr., I. Dumont, et al. (2002). "Regulation of eNOS expression in brain endothelial cells by perinuclear EP(3) receptors." Circ Res 90(6): 682-9.

- Goldstein, S. A., D. A. Bayliss, et al. (2005). "International Union of Pharmacology. LV. Nomenclature and molecular relationships of two-P potassium channels." Pharmacol Rev 57(4): 527-40.

- Goltzman, D. (1999). "Interactions of PTH and PTHrP with the PTH/PTHrP receptor and with downstream signaling pathways: exceptions that provide the rules." J Bone Miner Res 14(2): 173-7.

- Gray, A. T., B. B. Zhao, et al. (2000). "Volatile anesthetics activate the human tandem pore domain baseline K+ channel KCNK5." Anesthesiology 92(6): 1722-30.

- Gu, Y., P. G. Genever, et al. (2002). "The NMDA type glutamate receptors expressed by primary rat osteoblasts have the same electrophysiological characteristics as neuronal receptors." Calcif Tissue Int 70(3): 194-203.

- Gu , Y., M. R. Preston, et al. (2001). "Three types of K(+) currents in murine osteocyte-like cells (MLO-Y4)." Bone 28(1): 29-37.

- Harada, S. and G. A. Rodan (2003). "Control of osteoblast function and regulation of bone mass." Nature 423(6937): 349-55.

- Heberden, C., I. Denis, et al. (1998). "TGF-beta and calcitriol." Gen Pharmacol 30(2): 145-51.

- Heitzmann, D., R. Derand, et al. (2008). "Invalidation of TASK1 potassium channels disrupts adrenal gland zonation and mineralocorticoid homeostasis." EMBO J 27: 179-87.

- Henney, N. C., B. Li, et al. (2009). "A large-conductance (BK) potassium channel subtype affects both growth and mineralization of human osteoblasts." Am J Physiol Cell Physiol 297(6): 1397-408.

- Hernandez, L., K. H. Park et al. (2007). "The antiproliferative role of ERG K+ channels in rat osteoblastic cells." Cell Biochem Biophys.;47(2): 199-208.

- Heurteaux, C., N. Guy, et al (2006). "TREK-1, a K^+ channel involved in neuroprotection and general anaesthesia." EMBO J 23: 2684-95.

- Hille, B. (2001). "Ion Channels of Excitable Membranes." Sinauer Associates, 3rd edition.

- Hodgkin, A. L. and A. F. Huxley (1952). "A quantitative description of membrane current and its application to conduction and excitation in nerve." J Physiol 117(4): 500-44.

- Honore, E., F. Maingret, et al. (2002). "An intracellular proton sensor commands lipid- and mechano-gating of the K(+) channel TREK-1." EMBO J 21(12): 2968-76.

- Honore, E., A. J. Patel, et al. (2006). "Desensitization of mechano-gated K2P channels." Proc Natl Acad Sci U S A 103(18): 6859-64.

- Huang, J. C., T. Sakata, et al. (2004). "PTH differentially regulates expression of RANKL and OPG." J Bone Miner Res 19(2): 235-44.

- Hughes, S., J. Magnay, et al. (2006). "Expression of the mechanosensitive 2PK+ channel TREK-1 in human osteoblasts." J Cell Physiol 206(3): 738-48.

- Ionescu, A. M., E. M. Schwarz, et al. (2001). "PTHrP modulates chondrocyte differentiation through AP-1 and CREB signaling." J Biol Chem 276(15): 11639-47.

- Kang, D., C. Choe, et al. (2004). "Functional expression of TREK-2 in insulin-secreting MIN6 cells." Biochem Biophys Res Commun 323(1): 323-31.

- Kang, D. and D. Kim (2004). "Single-channel properties and pH sensitivity of two-pore domain K+ channels of the TALK family." Biochem Biophys Res Commun 315(4): 836-44.

- Kano, J., T. Sugimoto, et al. (1994). "Direct involvement of cAMP-dependent protein kinase in the regulation of alkaline phosphatase activity by parathyroid hormone (PTH) and PTH-related peptide in osteoblastic UMR-106 cells." Biochem Biophys Res Commun 199(1): 271-6.

- Kano, J., T. Sugimoto, et al. (1994). "Second messenger signaling of c-fos gene induction by parathyroid hormone (PTH) and PTH-related peptide in osteoblastic osteosarcoma cells: its role in osteoblast proliferation and osteoclast-like cell formation." J Cell Physiol 161(2): 358-66.

- Karsenty, G. (2001). "Minireview: transcriptional control of osteoblast differentiation." Endocrinology 142(7): 2731-3.
- Karsenty, G. (2003). "The complexities of skeletal biology." Nature 423(6937): 316-8.

- Kawase, T., G. A. Howard, et al. (1996). "Calcitonin gene-related peptide rapidly inhibits calcium uptake in osteoblastic cell lines via activation of adenosine triphosphate-sensitive potassium channels." Endocrinology 137(3): 984-90.

- Keshavaprasad, B., C. Liu, et al. (2005). "Species-specific differences in response to anesthetics and other modulators by the K2P channel TRESK." Anesth Analg 101(4): 1042-9, table of contents.

- Kindler, C. H. and C. S. Yost (2005). "Two-pore domain potassium channels: new sites of local anesthetic action and toxicity." Reg Anesth Pain Med 30(3): 260-74.

- Krishnan, V., H. U. Bryant, et al. (2006). "Regulation of bone mass by Wnt signaling." J Clin Invest 116(5): 1202-9.

- Komarova, S.V., S. J. Dixon and S. M. Sims. (2001). "Osteoclast ion channels: potential targets for antiresorptive drugs." Curr Pharm Des 7(8): 637-54.

- Kubo, Y., J. P. Adelman, et al. (2005). "International Union of Pharmacology. LIV. Nomenclature and molecular relationships of inwardly rectifying potassium channels." Pharmacol Rev 57(4): 509-26.

- Labelle, D., C. Jumarie, et al. (2007). "Capacitative calcium entry and proliferation of human osteoblast-like MG-63 cells." Cell Prolif 40(6): 866-84.

- Lauritzen, I., J. Chemin, et al. (2005). "Cross-talk between the mechano-gated K2P channel TREK-1 and the actin cytoskeleton." EMBO Rep 6(7): 642-8.

- Lefebvre, V., R. R. Behringer, et al. (2001). "L-Sox5, Sox6 and Sox9 control essential steps of the chondrocyte differentiation pathway." Osteoarthritis Cartilage 9 Suppl A: S69-75.

- Lesage, F. (2003). "Pharmacology of neuronal background potassium channels." Neuropharmacology 44(1): 1-7.

- Lesage, F., E. Guillemare, et al. (1996). "TWIK-1, a ubiquitous human weakly inward rectifying K+ channel with a novel structure." EMBO J 15(5): 1004-11.

- Lesage, F., F. Maingret, et al. (2000). "Cloning and expression of human TRAAK, a polyunsaturated fatty acids-activated and mechano-sensitive K(+) channel." FEBS Lett 471(2-3): 137-40.

- Lesage, F., R. Reyes, et al. (1996). "Dimerization of TWIK-1 K+ channel subunits via a disulfide bridge." EMBO J 15(23): 6400-7.

- Lewiecki, E. M. (2008). "Denosumab: an investigational drug for the management of postmenopausal osteoporosis." Biologics 2(4): 645-53.

- Lieberherr, M. (1987). "Effects of vitamin D3 metabolites on cytosolic free calcium in confluent mouse osteoblasts." J Biol Chem 262(27): 13168-73.

- Lips, P. (2006). "Vitamin D physiology." Prog Biophys Mol Biol 92(1): 4-8.

- Liu, C., J. F. Cotten, et al. (2005). "Protective effects of TASK-3 (KCNK9) and related 2P K channels during cellular stress." Brain Res 1031(2): 164-73.

- Liu, P., B. O. Oyajobi, et al. (1999). "Regulation of osteogenic differentiation of human bone marrow stromal cells: interaction between transforming growth factor-beta and 1,25(OH)(2) vitamin D(3) In vitro." Calcif Tissue Int 65(2): 173-80.

- Lochner, A. and J. A. Moolman (2006). "The many faces of H89: a review." Cardiovasc Drug Rev 24(3-4): 261-74.

- Lopes, C. M., T. Rohacs, et al. (2005). "PIP2 hydrolysis underlies agonist-induced inhibition and regulates voltage gating of two-pore domain K+ channels." J Physiol 564(Pt 1): 117-29.

- Lotinun, S., J. D. Sibonga, et al. (2002). "Differential effects of intermittent and continuous administration of parathyroid hormone on bone histomorphometry and gene expression." Endocrine 17(1): 29-36.

- Lu, Z., J. Gao, et al. (2007). "Two-pore K+ channels, NO and metabolic inhibition." Biochem Biophys Res Commun 363(1): 194-6.

- MacDonald, B. R., J. A. Gallagher, et al. (1986). "Parathyroid hormone stimulates the proliferation of cells derived from human bone." Endocrinology 118(6): 2445-9.

- Magra, M., S. Hughes, et al. (2007). "VOCCs and TREK-1 ion channel expression in human tenocytes." Am J Physiol Cell Physiol 292(3): C1053-60.

- Maingret, F., M. Fosset, et al. (1999). "TRAAK is a mammalian neuronal mechano-gated K+ channel." J Biol Chem 274(3): 1381-7.

- Mancini, L., N. Moradi-Bidhendi, et al. (1998). "Nitric oxide superoxide and peroxynitrite modulate osteoclast activity." Biochem Biophys Res Commun 243(3): 785-90.

- Manolagas, S. C., D. C. Anderson, et al. (1979). "Glucocorticoids regulate the concentration of 1,25-dihydroxycholecalciferol receptors in bone." Nature 277(5694): 314-5.

- Mathie, A. (2007). "Neuronal two-pore-domain potassium channels and their regulation by G protein-coupled receptors." J Physiol 578(Pt 2): 377-85.

- Medhurst, A. D., G. Rennie, et al. (2001). "Distribution analysis of human two pore domain potassium channels in tissues of the central nervous system and periphery." Brain Res Mol Brain Res 86(1-2): 101-14.

- Meszaros, J. G., N. J. Karin, et al. (1996). "Down-regulation of L-type Ca2+ channel transcript levels by 1,25-dihyroxyvitamin D3. Osteoblastic cells express L-type alpha1C Ca2+ channel isoforms." J Biol Chem 271(51): 32981-5.

- Meves, H. (2008). "Arachidonic acid and ion channels: an update." Br J Pharmacol 155(1): 4-16.

- Miller, P. D. (2008). "Anti-resorptives in the management of osteoporosis." Best Pract Res Clin Endocrinol Metab 22(5): 849-68.

- Moreau, R., R. Aubin, et al. (1997). "Pharmacological and biochemical evidence for the regulation of osteocalcin secretion by potassium channels in human osteoblast-like MG-63 cells." J Bone Miner Res 12(12): 1984-92.

- Mulkey, D. K., E. M. Talley, et al. (2007). "TASK channels determine pH sensitivity in select respiratory neurons but do not contribute to central respiratory chemosensitivity." J Neurosci 27: 14049-58.

- Mulkins, M. A., S. C. Manolagas, et al. (1983). "1,25-Dihydroxyvitamin D3 increases bone alkaline phosphatase isoenzyme levels in human osteogenic sarcoma cells." J Biol Chem 258(10): 6219-25.

- Murrills, R. J., J. L. Andrews, et al. (2009). "Parathyroid hormone synergizes with non-cyclic AMP pathways to activate the cyclic AMP response element." J Cell Biochem 106(5): 887-95.

- Nakashima, K., X. Zhou, et al. (2002). "The novel zinc finger-containing transcription factor osterix is required for osteoblast differentiation and bone formation." Cell 108(1): 17-29.

- Nishii, N., N. Nejime, et al. (2009). "Effects of ATP on the intracellular calcium level in the osteoblastic TBR31-2 cell line." Biol Pharm Bull 32(1): 18-23.

- Nishiya, Y., N. Kosaka, et al. (2002). "A potent 1,4-dihydropyridine L-type calcium channel blocker, benidipine, promotes osteoblast differentiation." Calcif Tissue Int 70(1): 30-9.

- Nomura, S. and T. Takano-Yamamoto (2000). "Molecular events caused by mechanical stress in bone." Matrix Biol 19(2): 91-6.

- Novak, A. and S. Dedhar (1999). "Signaling through beta-catenin and Lef/Tcf." Cell Mol Life Sci 56(5-6): 523-37.

- O'Connell, A. D., M. J. Morton, et al. (2002). "Two-pore domain K+ channels-molecular sensors." Biochim Biophys Acta 1566(1-2): 152-61.
- Ohnaka, K., M. Tanabe, et al. (2005). "Glucocorticoid suppresses the canonical Wnt signal in cultured human osteoblasts." Biochem Biophys Res Commun 329(1): 177-81.

- Otto, F., A. P. Thornell, et al. (1997). "Cbfa1, a candidate gene for cleidocranial dysplasia syndrome, is essential for osteoblast differentiation and bone development." Cell 89(5): 765-71.

- Owen, T. A., M. S. Aronow, et al. (1991). "Pleiotropic effects of vitamin D on osteoblast gene expression are related to the proliferative and differentiated state of the bone cell phenotype: dependency upon basal levels of gene expression, duration of exposure, and bone matrix competency in normal rat osteoblast cultures." Endocrinology 128(3): 1496-504.

- Pardo, L. A. (2004). "Voltage-gated potassium channels in cell proliferation." Physiology (Bethesda) 19: 285-92.

- Partridge, N. C., A. L. Opie, et al. (1985). "Inhibitory effects of parathyroid hormone on growth of osteogenic sarcoma cells." Calcif Tissue Int 37(5): 519-25.

- Patel, A. and E. Honore (2002). "The TREK two P domain K+ channels." J Physiol 539(Pt 3): 647.

- Patel, A. J. and E. Honore (2001). "Anesthetic-sensitive 2P domain K+ channels." Anesthesiology 95(4): 1013-21.

- Patel, A. J. and E. Honore (2001). "Properties and modulation of mammalian 2P domain K+ channels." Trends Neurosci 24(6): 339-46.

- Patel, A. J., F. Maingret, et al. (2000). "TWIK-2, an inactivating 2P domain K+ channel." J Biol Chem 275(37): 28722-30.

- Plant, L. D., S. Rajan, et al. (2005). "K2P channels and their protein partners." Curr Opin Neurobiol 15(3): 326-33.

- Purves, G. I., T. Kamishima, et al. (2009). "Exchange protein activated by cAMP (Epac) mediates cAMP-dependent but protein kinase A-insensitive modulation of vascular ATP-sensitive potassium channels." J Physiol 587(Pt 14): 3639-50.

- Qin, L., X. Li, et al. (2005). "Parathyroid hormone uses multiple mechanisms to arrest the cell cycle progression of osteoblastic cells from G1 to S phase." J Biol Chem 280(4): 3104-11.

- Quayle, J. M., A. D. Bonev, et al. (1995). "Pharmacology of ATP-sensitive K+ currents in smooth muscle cells from rabbit mesenteric artery." Am J Physiol 269(5 Pt 1): C1112-8.

- Quinn, C. O., R. A. Rajakumar, et al. (2000). "Parathyroid hormone induces rat interstitial collagenase mRNA through Ets-1 facilitated by cyclic AMP response element-binding protein and Ca(2+)/calmodulin-dependent protein kinase II in osteoblastic cells." J Mol Endocrinol 25(1): 73-84.

- Rajan, S., E. Wischmeyer, et al. (2001). "THIK-1 and THIK-2, a novel subfamily of tandem pore domain K+ channels." J Biol Chem 276(10): 7302-11.

- Ravesloot, J. H., R. J. van Houten, et al. (1990). "Identification of Ca(2+)-activated K+ channels in cells of embryonic chick osteoblast cultures." J Bone Miner Res 5(12): 1201-10.

- Rawlinson, S. C., A. A. Pitsillides, et al. (1996). "Involvement of different ion channels in osteoblasts' and osteocytes' early responses to mechanical strain." Bone 19(6): 609-14.

- Reid, I. R., R. Civitelli, et al. (1987). "Parathyroid hormone acutely elevates intracellular calcium in osteoblastlike cells." Am J Physiol 253(1 Pt 1): E45-51.

- Reimann, F. and F. M. Ashcroft (1999). "Inwardly rectifying potassium channels." Curr Opin Cell Biol 11(4): 503-8.

- Rendell, M. (2004). "The role of sulphonylureas in the management of type 2 diabetes mellitus." Drugs 64(12): 1339-58.

- Rodan, G. A. (1997). "Bone mass homeostasis and bisphosphonate action." Bone 20(1): 1-4.

- Rodan, S. B., Y. Imai, et al. (1987). "Characterization of a human osteosarcoma cell line (Saos-2) with osteoblastic properties." Cancer Res 47(18): 4961-6.

- Sabbadini, M. and C. S Yost (2009). "Molecular biology of background K channels: Insights from K_{2P} knockout mice." J Mol Biol 385: 1331-44.

- Saeki, Y., A. Ohara, et al. (2007). "The presence of arachidonic acid-activated K+ channel, TREK-1, in human periodontal ligament fibroblasts." Drug Metab Rev 39(2-3): 457-65.

- Sano, Y., K. Inamura, et al. (2003). "A novel two-pore domain K+ channel, TRESK, is localized in the spinal cord." J Biol Chem 278(30): 27406-12.

- Satake, N., S. Fujimoto, et al. (1996). "The potentiation of nitroglycerin-induced relaxation by PKG inhibition in rat aortic rings." Gen Pharmacol 27(4): 701-5.

- Shieh, C. C., M. Coghlan, et al. (2000). "Potassium channels: molecular defects, diseases, and therapeutic opportunities." Pharmacol Rev 52(4): 557-94.

- Sistare, F. D., B. A. Rosenzweig, et al. (1994). "Separate P2T and P2U purinergic receptors with similar second messenger signaling pathways in UMR-106 osteoblasts." J Pharmacol Exp Ther 269(3): 1049-61.

- Sommer, B., M. Bickel, et al. (1996). "Expression of matrix proteins during the development of mineralized tissues." Bone 19(4): 371-80.

- St-Arnaud, R. (2008). "The direct role of vitamin D on bone homeostasis." Arch Biochem Biophys 473(2): 225-30.

- Sun Park, W., Y. Kyoung Son, et al. (2006). "The protein kinase A inhibitor, H-89, directly inhibits KATP and Kir channels in rabbit coronary arterial smooth muscle cells." Biochem Biophys Res Commun 340(4): 1104-10.

- Tertyshnikova, S., R. J. Knox, et al. (2005). "BL-1249 [(5,6,7,8-tetrahydro-naphthalen-1-yl)-[2-(1H-tetrazol-5-yl)-phenyl]-amine] : a putative potassium channel opener with bladder-relaxant properties." J Pharmacol Exp Ther 313(1): 250-9.

- Van Damme, P., M. Dewil, et al. (2005). "Excitotoxicity and amyotrophic lateral sclerosis." Neurodegener Dis 2(3-4): 147-59.

- Vezeridis, P. S., C. M. Semeins, et al. (2006). "Osteocytes subjected to pulsating fluid flow regulate osteoblast proliferation and differentiation." Biochem Biophys Res Commun 348(3): 1082-8.

- Wagner, E. F. and G. Karsenty (2001). "Genetic control of skeletal development." Curr Opin Genet Dev 11(5): 527-32.

- Walsh, C. A., W. B. Bowler, et al. (1997). "Effects of PTH on PTHrP gene expression in human osteoblasts: up-regulation with the kinetics of an immediate early gene." Biochem Biophys Res Commun 239(1): 155-9.

- Wang, L. L. (2005). "Biology of osteogenic sarcoma." Cancer J 11(4): 294-305.

- Wang, Y. J., M. W. Lin, et al. (2008). "Riluzole-induced block of voltage-gated Na+ current and activation of BKCa channels in cultured differentiated human skeletal muscle cells." Life Sci 82(1-2): 11-20.

- Weidema, A. F., J. Barbera, et al. (1997). "Extracellular nucleotides activate non-selective cation and Ca(2+)-dependent K+ channels in rat Osteoclasts." J Physiol 503(2): 303-15.

- Wilson, J.R., N. A. Duncan, et al. (2004) "A voltage-dependent K^+ current contributes to membrane potential of acutely isolated canine articular chondrocytes." J Physiol 557.1: 93-104.

- Wonderlin, W. F. and J. S. Strobl (1996). "Potassium channels, proliferation and G1 progression." J Membr Biol 154(2): 91-107.

- Xiao, G., D. Wang, et al. (1998). "Role of the alpha2-integrin in osteoblast-specific gene expression and activation of the Osf2 transcription factor." J Biol Chem 273(49): 32988-94.

- Yamaguchi, D. T., T. J. Hahn, et al. (1987). "Parathyroid hormone-activated calcium channels in an osteoblast-like clonal osteosarcoma cell line. cAMP-dependent and cAMP-independent calcium channels." J Biol Chem 262(16): 7711-8.

- Yellowley, C. E., J. C. Hancox, et al. (1998). "Whole-cell membrane currents from human osteoblast-like cells." Calcif Tissue Int 62(2): 122-32.

- Ypey, D. L., A.F. Weidema, et al. (1992). "Voltage, calcium, and stretch activated ionic channels and intracellular calcium in bone cells." J Bone Min Res 7(2): S377-87.

- Zahanich, I., E. M. Graf, et al. (2005). "Molecular and functional expression of voltage-operated calcium channels during osteogenic differentiation of human mesenchymal stem cells." J Bone Miner Res 20(9): 1637-46.

- Zallone, A. (2006). "Direct and indirect estrogen actions on osteoblasts and osteoclasts." Ann N Y Acad Sci 1068: 173-9.

- Zanello, L. P. and A. W. Norman (2003). "Multiple molecular mechanisms of 1 alpha,25(OH)2-vitamin D3 rapid modulation of three ion channel activities in osteoblasts." Bone 33(1): 71-9.

- Zhong, N., R. P. Gersch, et al. (2006). "Wnt signaling activation during bone regeneration and the role of Dishevelled in chondrocyte proliferation and differentiation." Bone 39(1): 5-16.